EXPERIMENTAL AND FINITE ELEMENT INVESTIGATION OF ULTRASONIC METAL FORMING APPLICATIONS

by

MOHD YUSOF MD DAUD

UNIVERSITY
of
GLASGOW

Thesis submitted in fulfilment of the requirements for the Degree of Doctor of Philosophy to the Faculty of Engineering University of Glasgow

JUNE 2006

This thesis is produced under the accordance of British Standards BS 4821:1990

TO MY PARENTS: SANIAH JAAFAR & MD DAUD ABD JALIL al-haj

ABSTRACT

The research reported in this thesis demonstrates the effects of applying longitudinal and radial ultrasonic vibration to forming tools in metal forming processes using aluminium. In the study of ultrasonic vibration assisted tension tests, and ring and cylindrical specimen compression tests, finite element (FE) models under quasi-static loading were first developed to gain insight into material and interface mechanisms. FE simulations of the metal material included the effects of elasticity, plasticity, large deformation and a Coulombic interface friction boundary condition in the presence and absence of lubricants. Agreement was achieved between the FE results and those obtained from tension and compression experiments with respect to the stress-strain relationships and deformed configurations for a range of friction coefficients.

The coefficients of friction for static and ultrasonic ring compressions were estimated for dry and lubricated surfaces by matching the experimental data with the FE results for quasi-static deformation in the form of friction calibration curves. Analysis of the surfaces of deformed ring specimens was conducted using two techniques; profilometry and scanning electron microscopy, and the experimental results were compared with the estimated friction condition.

By measuring the oscillatory force response of the longitudinal mode ultrasonic loading as well as the static force, it was shown that the experimentally derived stress-strain data from tension and compression tests do not satisfy the description of a simple oscillatory stress superposition model. Subsequently FE models of tension and compression tests were developed, and a description of the contact friction condition was included for the compression test model. For ultrasonic tension tests, it was found that by superimposing ultrasonic excitation for an interval during plastic deformation, the measured stress-strain relationship could be closely matched by finite element model data where the model was adjusted to a softer material during the interval. For ultrasonic compression tests, by combining a softer material model description with a change in the coefficient

of friction at the contact surface, only during the interval of ultrasonic excitation, the FE model predicted stress-strain data matched the experimentally derived stress-strain data. By superimposing a radial mode ultrasonic vibration on static compression tests, the experimental and FE results suggest that the stress-strain relationship is dominated by a reduction in interface friction, with little effect due to material softening.

Finite element models of two metal forming processes were subsequently developed; extrusion of an aluminium solid cylinder and die necking of an aluminium hollow thin cylinder. The models were validated against experimental data reported in the literature. By developing the FE models it was possible to show how a reduction in the extrusion force can be achieved if ultrasonic excitation of the die results in a reduction in the coefficient of friction at the die-material interface. For the die necking operation, the FE model showed how a diameter reduction could be achieved without buckling of the hollow cylindrical body if a reduction in the coefficient of friction was modelled under ultrasonic excitation of the die. However, by comparing with the published experimental data, the calculated extrusion force reduction achieved by a change in coefficient of friction estimated from the FE model is not sufficient alone to explain the effects of ultrasonic excitation in extrusion.

The experimental and FE models developed in this study have provided some insights into the contribution of reduced friction to measured reductions in forming force in ultrasonic forming processes. The evidence suggests that, as well as changes in the interface friction condition, material properties are also affected by ultrasonic excitation applied to forming aluminium.

ACKNOWLEGDEMENTS

I would like to express my sincere gratitude to my dedicated supervisor, Professor Margaret Lucas for her supervision, advice, guidance and encouragement throughout the research work. Her continuous support and encouragement both launched and sustained me in the study and the writing of this thesis.

I would also like to thank Dr Zhihong Huang at the University of Dundee for her advice and assistance. Thanks are also due to Professor John W. Hancock, Dean of the Engineering Faculty, Professor Matthew Cartmell, Head of the Mechanical Engineering Department, for the use of departmental facilities and for their professional advice and the technical staff of the Department of Mechanical Engineering, in particular Mr Alex Torry (retired) and Mr Brian Robb, for their help, preparation of specimens, setting up the test-rig, and assistance in experimental work.

Also, I would like to convey my thanks and appreciation to the Government of Malaysia and the Universiti Teknologi Malaysia, for funding me throughout the study.

Unforgettable, my special thanks to the members of the Dynamics Group, in particular Andrea (Dr A. Cardoni), Alan (Dr A. MacBeath), Graham and Euan, for their helpful support and warmest friendship throughout my studies.

The work was carried out in the Department of Mechanical Engineering at the University of Glasgow, where the support of secretarial staff and computing service staff is gratefully acknowledged.

Finally, I am very indebted to my beloved wife, Eda, and children, Alesha and Danial, for their support, patience, and encouragement throughout the research.

CONTENTS

LIST OF FIGURES

LIST OF TABLES

CHAPTER 1

INTRODUCTION

1.1 Research Background

Metals are used in many engineering applications because of their unique physical and mechanical properties and versatility in fabrication. The increase in demand for products with complex designs, and high reliability and quality have led engineers and researchers to investigate optimised operations for this competitive environment.

Research into the application of ultrasonic vibration in metalworking processes has become well-established, and has focused on metal forming in applications such as forging, drawing, extrusion and sheet-metal operations. It has been demonstrated that significant benefits can be achieved by the application of ultrasonics to such processes. These benefits include reduced forming forces, improved surface finish and increased processing rates. The attributable mechanisms are recognised to include oscillatory stress superposition, ultrasonic energy absorption, thermal and friction effects. However, precise characterisation of these mechanisms has not been fully explained and understood.

In an early study, an attempt to clarify the mechanism of the modification of the stress-strain characteristic was carried out by Blaha and Langenecker [1], who explained that the change in mechanical properties during tension tests of pure zinc crystal and polycrystalline materials where ultrasonic excitation was applied to the specimen, was due to activation of dislocations. However, since this study, it has not been explained how ultrasonic oscillations in the 15 – 80 kHz frequency range transmit energy into the dislocation structure. The natural frequency of dislocations is estimated to be at about 100 MHz [2], therefore the energy transmission cannot be explained in terms of resonance.

Nevill and Brotzen [3] proposed a realistic model of oscillatory stress superposition to explain the resulting stress-strain relationship when an ultrasonic oscillation is superimposed onto a static load. This was later clarified by Kirchner [4] for low frequency tests. The model showed that the path of the maximum oscillatory stress during superimposed ultrasonic excitation follows the path of the static stress-strain curve and the path of the mean stress will be lower than and parallel to the static curve. However, for some cases, the reduction of the mean oscillatory stress is equal to or considerably larger than the oscillatory stress amplitude. Therefore, to explain the stress reduction as solely due to oscillatory stress superposition is not adequate. Accordingly, investigations began into contact friction mechanisms in order to provide a better understanding of the measured oscillatory stress-strain.

Friction effects play an important role in many ultrasonic applications and the influence of ultrasonic oscillation on friction was examined in several fundamental studies [2, 5-12]. It was reported that reduced interface friction could be obtained when the oscillation direction was parallel or perpendicular to the direction of motion of the workpiece or die. One explanation of the largely unsubstantiated claims of friction reduction that was proposed was that surface heating resulted in loss of strength of asperities resulting in a reduction in the friction force. However, there is also evidence in the literature that no significant temperature increases occur. Another explanation that has been proposed to explain the measured reduction in forming force is periodic changing of the line of action of the friction vector. Tangential oscillation in the direction of sliding may produce a periodic reversal of the friction force, and normal to the sliding direction a swinging of the friction force vector about its equilibrium position [13, 14].

The published attempts to clarify the material and surface factors seem to be inconclusive. It is proposed here that a major contributing factor has been that only the mean oscillatory stress has been measured in all previous studies. This has meant that no experimental data has been reported which allows the oscillatory stress to be characterised and models have therefore not been validated. Another significant contributing factor has been that previous studies have been limited to a single friction condition and the effect of different lubricants has not been investigated. Previous studies have attempted to analyse the interface friction using a special test-rig to

measure a reduction in the coefficient of friction [9, 10]. However, a detailed and quantitative experimental analysis has not been reported due to the difficulties of real-time measurement of the forming process during the application of ultrasonic excitation.

This present study aims, for the first time, to address these issues and investigate the effects of ultrasonic excitation on the oscillatory stress-strain behaviour of aluminium specimens during tension and compression tests under different friction conditions. The knowledge and insights gained from these investigations are subsequently used to develop finite element models of two ultrasonic forming operations.

1.2 Objectives

The purpose of this research programme is to investigate the application of ultrasonic excitation in the forming of aluminium.

The investigation, using both experimental and finite element modelling techniques, is divided into four parts. In order to eliminate the friction effects and concentrate on material effects due to ultrasonic excitation, in the first part static and ultrasonic deformations under tensile loading are carried out. By comparing conventional static tension test data with the oscillatory data, the oscillatory stress-strain relationship is characterised.

The second part is a study of ring compression tests, in which a ring specimen is compressed with and without longitudinal and radial ultrasonic excitation. This is an investigation into the interface mechanism. The coefficients of friction for different interface conditions are estimated from the ring data for static compressions and longitudinal and radial ultrasonic compressions, by matching with data calculated from FE models. The deformed specimen surfaces are analysed with a 2D-profilometer and surface topographies are scanned and magnified. The correlation between ring test data and surface evaluation data is studied to achieve a better understanding into the effects of ultrasonics on deformation under different interface conditions. The estimated coefficient of friction under a specific interface conditions is subsequently used as a numerical friction coefficient value for other finite element models.

The third part is a study of compression of cylindrical specimens with and without ultrasonic excitation. This investigation focuses on characterising the combination of material and surface effects due to the application of longitudinal and radial ultrasonic excitation.

The fourth part is a study of finite element simulations for static and ultrasonic extrusion and thin cylinder necking operations. The models are developed based on previous experimental studies. The models are used to calculate the numerical oscillatory forces for a given set of process parameters. An investigation of interface friction during ultrasonic thin cylinder necking uses a prediction of the buckling profile of the cylinder body when constant and reduced interface friction are included in the models.

1.3 Introduction to Ultrasonics

1.3.1 Ultrasound

In general, the term ultrasound refers to sounds which are too high in frequency to be heard by the human ear [15-17]. The range of ultrasonic frequencies is not definitive, but the study and application of high frequency sound waves is usually in excess of 20 kHz.

The practicalities of employing ultrasonics for any application are largely subject to the feasibility of the ultrasonic technology for generation and transmission of acoustic energy at the required intensity and frequency. In many ultrasonic applications, the main components of the ultrasonic system are a power supply or generator, transducer, output device, cooling system equipment and various systems for providing measurement and control of acoustic parameters [16, 18].

Ultrasonic waves can be generated using mechanical, electromagnetic and thermal energy sources. The waves can be produced in gasses, liquids and solids. There are two common types of transducer used in ultrasonic applications, magnetostrictive and piezoelectric. The magnetostrictive transducer uses the inverse magnetostrictive effect to convert magnetic energy into ultrasonic energy. This is accomplished by applying a strong alternating magnetic field to certain metals, alloys and ferrites. Piezoelectric

transducers employ the inverse piezoelectric effect using natural or synthetic single crystals such as quartz, or ceramics such as barium titanate which has a strong piezoelectric behaviour. The advantage of ceramic over crystal is that ceramic can easily be shaped by casting, pressing and extruding. Modern ultrasonic transducers can produce frequencies as high as several gigahertz by transforming alternating electric currents into mechanical oscillations.

1.3.2 Brief history of ultrasound

The roots of ultrasonics can be traced back to research on the piezoelectric effect conducted by Pierre Curie around 1880. Curie found that asymmetrical crystals such as quartz and Rochelle salt (or *potassium sodium tartrate*) generate an electric charge when mechanical pressure is applied. Conversely, mechanical vibrations are obtained by applying electrical oscillations to the same crystals.

The early application of ultrasound was sonar (an acronym for sound navigation ranging). Sonar operates by bouncing a series of high frequency, concentrated sound waves off a target and then recording the echo. Because the speed of sound in water is known, it is easy to calculate the distance of the target.

Researchers were inspired by sonar to develop analogous techniques for qualitative inspection. For example, the use of ultrasonic waves in detecting metal objects began in the late 1920's and in 1931 a patent was obtained for using ultrasonic waves to detect flaws in solids.

In the late 1940's researchers in Japan began to explore the medical diagnostic capabilities of ultrasonics. Japan was also the first country to apply Doppler ultrasound, which detects internal moving objects such as blood flowing through the heart. In the 1950's researchers in the United States and Europe advanced ultrasonics into a wide range of applications and ultrasonic technology is now employed in many applications in research, industry and medicine [15, 16].

1.3.3 Applications of ultrasonics

Ultrasonic vibrations have been widely used in many industrial areas as well as in medicine. The application of ultrasonic vibrations is based on the exploitation of the physical properties and mechanical nature of the sound waves. Ultrasonic waves are used in a variety of ways such as the establishment of ultrasonic standing waves, acoustic emission, the Doppler effect, and the use of the transit time of a transmitted and reflected ultrasonic pulse, which is commonly called the pulse-echo technique. Ultrasonic waves can also be applied mechanically by exploiting the high frequency mechanical vibrations to generate heat on a contact surface, fluid cavitation, agitation effects and energy absorption in forming processes [17]. Some common applications of ultrasonics are described below.

Cleaning

One of the most common ultrasonic applications is cleaning. This includes the removal of grease, dirt, rust, and paint from metal, ceramic, glass, and crystal surfaces from parts used in the electronic, automotive, aircraft, and precision instrument industries. This cleaning is accomplished through the use of the cavitation effect. Cavitation is the rapid formation and collapse of tiny gas and vapour filled bubbles or cavities in a solution that is irradiated with ultrasonic vibrations. The repeated collapsing of the bubbles produces tiny shock waves that remove the contaminants from the surfaces of the parts. A variety of cleaning solutions can be used, including water, detergents and organic solvents. Ultrasonic cleaning can be highly efficient for applications in which extreme cleanliness is required. It is also well suited for cleaning parts with very complex shapes. Examples of specific applications are optical glass for lenses, quartz crystals, small ball bearings and dental bridges.

Non-destructive testing

Non-destructive testing has been practiced for many decades, with initial rapid developments in instrumentation spurred by the technological advances that occurred during World War II and the subsequent defence effort. Among the techniques that have been developed are eddy currents, x-rays, dye penetrant, magnetic particles and ultrasound.

Ultrasound is particularly attractive for non-destructive testing because it can be used with most types of materials, and it can be used to investigate both material surfaces and interior.

The attenuation of ultrasonic waves is very low in solids and liquids, thus allowing solids more than 20 feet thick to be penetrated by both continuous and pulsed waves. Ultrasonic testing uses sound waves to detect flaws in materials and to measure material properties. The most common ultrasonic testing technique used is pulse-echo, where sound is introduced into a test object and reflections or echoes returned to a receiver from internal flaws or from the part's geometrical surfaces are analyzed. Defects and other internal irregularities result in changes in the echo pattern from the waves.

Sonochemistry

Most applications of ultrasound use low power waves which pass through materials without affecting their physical or chemical structure. On the other hand, very high intensity ultrasonic vibrations can cause chemical and physical changes in materials. In sonochemistry, this is accomplished by violent cavitation which creates stress and intense localised heating. Among the chemical processes which can be produced are acceleration of chemical reactions, oxidation, hydrolysis, polymerisation, depolymerisation and the production of emulsions.

Medicine

The use of ultrasonics in medicine has progressed rapidly. The most common ultrasonic technique used in medicine is imaging, which requires a high ultrasonic frequency. Other medical applications of ultrasonics include sterilisation of surgical instruments, surgical blades, and high intensity focussed ultrasound for tumour ablation.

Metalworking

Another industrial application of ultrasonics is in the machining of materials. Ultrasonic machining can allow machining of complex shapes or cutting of hard materials such as glass and ceramics that cannot be performed by conventional machining.

Ultrasonic vibrations have also proved to be very useful for joining materials and can be used for both soldering and welding. In the case of soldering, the cavitation produced by high intensity ultrasonic waves destroys the oxide layer on aluminium, thus permitting parts to be joined with tin soldering materials without the use of flux. In ultrasonic welding, pressure and heat are generated by the intense vibratory action of the material to be welded. Ultrasonics can be used to weld pieces of similar or dissimilar plastic to each other and can also be used in metal welding processes.

In metal forming processes, the application of high frequency vibrations on dies is used to assist the deformation process in order to reduce the forming load and to improve the finished part quality [15-18]. A detailed review regarding the application of ultrasonics to metal forming is presented in the following chapter.

CHAPTER 2

LITERATURE REVIEW

2.1 The Application of Low Frequency and Ultrasonic Vibrations in Metal Forming Processes

Since the mid 1950's the application of power ultrasonics to metal forming processes has been reported by numerous researchers [1-3, 12, 19-21]. Many early investigations reported that by superimposing an ultrasonic excitation on the static load during plastic deformation the flow stress was significantly reduced [1-3, 12, 19, 20] and the surface quality and the metallurgical properties of some deformed metals were improved [5, 6, 19, 20, 22]. The effectiveness of applying ultrasonic vibration during deformation processes was related to the type of deformations, process speed, ultrasonic frequency and amplitude, mode of vibration, material properties and the interface friction condition [7, 10, 12, 22].

The investigation of the phenomenon of a superimposed ultrasonic vibration on a steady static stress was reported first by Blaha and Langenecker in 1955 [1]. In their experiment, a tension test was performed on a single crystal of zinc. Ultrasonic vibration at a frequency of 800 kHz was superimposed in an axial mode during plastic deformation. A significant stress reduction was achieved for the oscillatory tension test compared with the non-oscillatory test. In other series of tension tests, for single crystals of aluminium, cadmium, beryllium and polycrystalline zinc, similar results were obtained when axial mode ultrasonic vibration was applied continuously or intermittently through the test [19, 21]. Blaha and Langenecker further observed that the magnitude of stress reduction was independent of the excitation frequency for the ultrasonic range, but dependent on the amplitude of vibration.

A reduction in forming load due to the influence of ultrasonics was not only reported for tension test results. Many subsequent studies of superimposing ultrasonics on the plastic compressive stress of metals in the upsetting process were also investigated [7, 12, 20, 23]. Similarly, a reduction in flow stress during ultrasonic excitation was reported. A series of cold forging tests was conducted by Kristoffy [7] for aluminium and lead specimens. The forming load dropped as the specimen's height reduction increased when the punch was axially vibrated at a frequency of 20 kHz. Using the same procedure, Izumi et al [12] performed ultrasonic compression tests on aluminium, silver, copper-zinc alloy, mild steel, lead, and magnesium specimens. Izumi observed that the flow stress of compressive deformation was considerably lowered by the ultrasonic vibration superimposed on the static load. As in the tension tests, in most cases as the vibration amplitude increased, the load decreased remarkably. Unlike the tension test, an additional influence is created in upsetting tests with the introduction of contact effects at the die and specimen interface.

In an attempt to explain the claims that oscillations reduce process stress, much research has been concerned not only with the fundamental effects of oscillations on metal plasticity and surface friction, but also with the application of ultrasonics to many industrial metal-forming processes [2, 9, 24, 25]. This revealed the generally accepted dual role of oscillations, namely; surface effects and volume effects. It was believed that the vibration energy was preferentially absorbed at dislocation sites, enabling deformation to proceed with very much reduced forces. The effect of adding the vibration was believed to be characterised by a reduction in the rate of work-hardening and an increase in the strain to fracture [26]. These effects were initially introduced by Dawson et al [13, 26] in their review of the volume effect. In the same review, it was reported that the reduction in forming force for some oscillatory tests was not fully accounted for by a change in metallurgical properties of the metal, in particular for the deformations which involved a contact surface between die and specimen. Later, it was proposed that the interface friction was changed in such a way as to reduce the forming force. This came to be known as the surface effect. Generally, the volume effect deals with the influence of oscillations on the internal stresses during plastic deformation, whereas the surface effect deals with the interfacial contact friction.

2.1.1 Energy absorption and heating mechanism

Since the reduction of the forming force has been accepted as a substantial result when a metal is subjected to a high frequency vibration during a forming process, many reports and reviews have been published in an attempt to explain the fundamental effects of the reduced oscillatory stress [5, 14, 19, 21, 22]. Langenecker [19] suggested that the reduction of the forming force was due to the reduction of barriers in front of moving dislocations, which subsequently induced acoustic softening and acoustic hardening. Further, Langenecker suggested that the shear stress, τ, required to produce continuous plastic flow is the stress needed for migration of dislocations in the slip plane. When ultrasonic vibration reduces the shear stress of a crystal to a certain value, it is predicted that the acoustic field has to supply a stress equal to the shear stress, τ. Therefore the acoustic stress, X, produced by an ultrasonic wave travelling through a solid medium can be calculated from

$$X = \xi\rho\omega c = \rho U c = \sqrt{\frac{2}{\nu}} I E , \tag{2.1}$$

where ξ is the particle displacement, ρ is the density, ω angular frequency, c the sound velocity, U the particle velocity, I the intensity, ν is Poisson's ratio, and E is elastic modulus.

Langenecker's theory was expanded later by Winsper et al [21]. According to Winsper, the strength of a given metal depended on obstacles to the movement of dislocations and any reduction in yield stress would have to involve some mechanism in which these obstacles could be overcome. Hence, the application of a cyclic stress supplied the energy to impart dynamic mobility to the dislocations, enabling them to overcome the obstacles, which were not readily surmounted by a static stress alone.

Schmid [22] combined the conclusion of his works with Langenecker and other previous studies and suggested that the superposition of oscillatory and static stress is probably responsible for the major part of the softening of the material. Schmid also suggested that a specimen could be hardened if the ultrasonic vibration was applied

prior to a deformation process, and the amount of hardening depended on the ultrasonic intensity, temperature rise, and the amount of pre-strain.

Once it was claimed that resonance of dislocations could only occur at a minimum frequency of 100 MHz [2], much higher than the 15-800 kHz range of the reported studies, many researchers changed their focus from the study of energy absorption to the mechanisms of internal friction [2], stress superposition effects [3, 4, 27], and the effects of interface friction [2, 7, 10]. For example, in a study of ultrasonic wire drawing of copper, Pohlman and Lehfeldt [2] suggested that the measured reduction in the drawing force was related to a reduction of internal friction. However, there was no detailed explanation provided in their report with which to clarify how internal friction was reduced by ultrasonic vibration.

Research into the effects of ultrasonics on a microstructural level for metals was recently conducted by Smirnov et al [28]. In this study a thin-foil annealed iron was qualitatively observed using transmission electron microscopy. It was reported that the configurations of local dislocations and the movement of dislocations under ultrasonic excitation were qualitatively different from those observed under a static load. Although it was previously claimed that dislocations could not be resonated by a low ultrasonic frequency, this paper tends to suggest that ultrasonic excitation can modify the microstructural configuration of an ultrasonically deformed specimen.

The influence of ultrasonic oscillation on temperature was examined in a few fundamental studies [3, 12, 19]. It was reported that an increase in bulk specimen temperature was measured when the ultrasonic amplitude used was above a specific value, also known as the threshold or critical value. At a higher ultrasonic intensity, it was reported that a copper specimen was heated up to 300°C during superimposed ultrasonic excitation in tension [3] and compression tests [12]. However, there was no significant temperature rise recorded at low ultrasonic intensities for copper, and also at any range of the ultrasonic amplitude for steel and magnesium [3, 12]. Accordingly, Langenecker [19] suggested that the rise in specimen temperature was due to conversion of ultrasonic energy into heat. Apart from the Langenecker study, there has not been found a conclusive reason why ultrasonic excitation increased the temperature for copper but none of the other metals. However, it has been suggested that other factors,

such as specific heat of the material and duration of the ultrasonic excitation, could explain heat generation in the material [5, 11, 20].

Non-uniformity of material structure, such as grain boundaries, inclusions and lattice defects, has been suggested to impart a strong effect on the flow resistance of a forming process [5, 19, 20]. When a specimen is subjected to ultrasonic excitation during a deformation process it is believed that the ultrasonic waves propagated, scattered and absorbed at the sites of non-uniformity in the material, result in energy loss due to hysteresis or heat generation, thus contributing to the lowering of flow resistance. Although generated heat has some effect on the deformation behaviour, it is not considered to be a main factor causing the lowering of flow stress. Figure 2.1 shows the experimental result of static, intermittent ultrasonic, and ultrasonic upsetting of aluminium by Izumi et al [20]. As can be as in Figure 2.1, when ultrasonic vibration was suddenly superimposed on static compression during the course of deformation, the flow stress dropped immediately at the onset of ultrasonic excitation, and at that moment any immediate significant rise in temperature could not be expected [20].

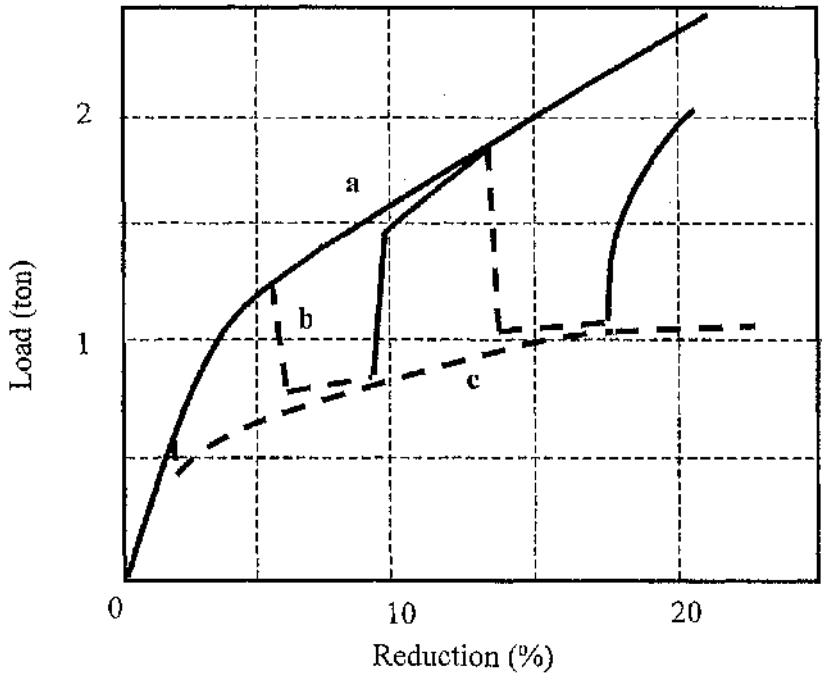

Figure 2.1: Measured compressive load due to superimposed ultrasonic vibration, (a) without ultrasonic vibration, (b) intermittently superimposed ultrasonic vibration, (c) continuous ultrasonic vibration [20].

2.1.2 Oscillatory stress superposition

Although Blaha and Langenecker's energy absorption theory [1] has been generally accepted to explain the reduction in flow stress during superimposed ultrasonic excitation on a static deformation process, there have been no other investigations attempting to clarify the mechanism by which the dislocations absorb the energy. Various hypotheses for the energy absorption were studied by Nevill and Brotzen [3] in terms of resonance, relaxation and hysteresis, however they were unable to find any correlation between experimental and theoretical results. Nevertheless, Nevill and Brotzen attributed the reduced yield strength to the superposition of steady and oscillatory stress. This later theory was supported by Kristofy [7], Winsper et al [5] and more recently by Huang et al [11], and this is universally accepted as a mechanism to describe stress behaviour under applied ultrasonic excitation having amplitudes of less than some threshold value.

As previously discussed in a review [21], the stress superposition effect for ideal oscillatory plastic deformation of metals occurs when an oscillatory stress is superimposed on a non-oscillatory stress, and the peak of each cyclic stress variation is coincident with the corresponding steady-state or non-oscillatory stress. It should be noted that this ideally expressed mechanism rarely occurs alone, in particular for a process which involves a contact surface, and therefore this mechanism could be modified by frictional effects.

An ideal oscillatory stress superposition definition can only be achieved in the absence of interface friction and a temperature rise [12]. For applied low frequency ultrasonic oscillations during a wire drawing process, the superposition effect could be demonstrated by elastic straining and non-straining due to the oscillatory load [27]. This is analogous to swaging which occurs [26] when an increase in the lateral stresses (often compression) produces a consequential reduction in stress. Consideration of either of the yield criteria, Tresca and von Mises criterion, applicable to ductile materials, leads to the conclusion that since the yield stress of a metal remains constant, if either of the lateral principle stresses is increased, the remaining principle stress must be reduced.

The mechanics of oscillatory metalworking was introduced by Winsper et al [5]. To exclude friction effects, this analytical study employed a tension model to predict stress reduction due to pure oscillatory stress superposition. According to Winsper, if a specimen of uniform cross section A and length l, is fixed at one end and at the other end is subjected to an oscillatory force of $X_0 \sin\omega t$, and if the specimen is made of homogenous and isotropic material and obeys Hooke's law, then at any instant the vibratory force acting on an element length, dx, must be equal to a longitudinal inertia force acting on that element, which is given by

$$-(\sigma_x + d\sigma_x)A + \sigma_x A = -\rho A dx \frac{\partial^2 u}{\partial t^2}, \tag{2.2}$$

where u is the displacement of any cross section, ρ is the density of the material, and σ_x is the normal stress of the cross section. The vibratory strain in the specimen is given by $\partial u/\partial x$, and therefore σ_x can be expressed by Hooke's law re-written in the form of $\sigma_x = E\frac{\partial u}{\partial x}$. Using this relationship, equation (2.2) can be re-expressed as,

$$\frac{\partial^2 u}{\partial x^2} = \frac{\rho}{E}\frac{\partial^2 u}{\partial t^2} = \frac{1}{c^2}\frac{\partial^2 u}{\partial t^2}, \tag{2.3}$$

where E is the Young's modulus and $c = \sqrt{E/\rho}$ is the velocity of sound in the material. Let,

$$u(x, t) = X(x) \sin \omega t, \tag{2.4}$$

which is the general solution for steady-state forced vibration in a uniform specimen. Therefore, by partially differentially differentiating equation (2.4) with respect to t and x respectively and replacing $\frac{\partial^2 u}{\partial x^2}$ and $\frac{\partial^2 u}{\partial t^2}$ in the equation of motion (2.2),

$$\frac{d^2 X(x)}{dx^2} + \frac{\omega^2 X(x)}{c^2} = 0.$$

The solution is then given by

$$X(x) = A_1 \cos\frac{\omega x}{c} + A_2 \sin\frac{\omega x}{c},$$

where, A_1, A_2 are constants. By substituting into equation (2.4)

$$u(x,t) = \left(A_1 \cos\frac{\omega x}{c} + A_2 \sin\frac{\omega x}{c} \right) \sin \omega t. \tag{2.5}$$

Now, when x = 0, u(0,t) = 0, therefore $A_1 = 0$. Also when x = l, u(l,t) = $X_o \sin \omega t$, and hence $A_2 = X_o \operatorname{cosec}(\omega l / c)$ therefore equation (2.5) becomes

$$u(x,t) = X_o \operatorname{cosec}\frac{\omega l}{c} \sin\frac{\omega x}{c} \sin \omega t. \tag{2.6}$$

The dynamic stress, σ_D, variation induced in the specimen can be calculated by differentiating equation (2.6) with respect to x and substituting with Hooke's law,

$$\sigma_D = \frac{\omega E X_o}{c} \operatorname{cosec}\frac{\omega l}{c} \cos\frac{\omega x}{c} \sin \omega t. \tag{2.7}$$

From the above, it is clear that the reduction of stress modelled by stress superposition is only represented by a mean stress of the maximum and minimum oscillatory stress amplitude. For non-strain-rate dependent materials the mean stress is always lower than the static stress. However, for strain-rate dependent materials the mean stress could be lower than or coincident or higher than the static stress, depending on the oscillatory stress amplitude [4]. Therefore, for a strain-rate dependent material there may be no benefit of applied ultrasonic vibration from oscillatory stress superposition.

Previous investigators measured only the mean stress rather than the maximum and minimum oscillatory stress [14]. This led to difficulties in identifying if the reduction in flow stress was due to oscillatory stress superposition or real changes in the interface friction or metallurgical properties of the metals.

2.1.3 Effects on mechanical and metallurgical properties

A considerable number of investigations into mechanical and material properties of an ultrasonically deformed specimen have been carried out [12, 22, 27, 29]. An initial series of experiments was conducted using uniaxial tests, tension and compression. Various metals were tested with different ultrasonic amplitudes and various qualities were measured. The general observations were that mechanical properties during plastic deformation and specimen hardness were considerably reduced. Under a compression test, the specimen was highly strain-hardened at the central part compared with the both end parts in which the specimen was in contact with the dies [12].

In an attempt to clarify the mechanism of the reduced mechanical properties of the deformed metal, Nerubai [29] explained this in terms of dislocation theory. It was suggested that a reduction of limiting plastic deformation under the action of ultrasonic vibration in a tension test was associated with formation of the increased concentration of dislocations and vacancies in a local volume of the specimen. As a result discontinuities and disintegration of crystal structure were developed and this led to the initiation of micro-cracks, then failure.

Winsper et al [27] conducted a low oscillatory frequency test on wire drawing process. In their experiments, stainless steel, aluminium and copper wire were drawn using an oscillating die at the range of 50 to 500 Hz. By observing the stress-strain relationships, this study concluded that there was no apparent reduction of mechanical and metallurgical properties of the materials due to the oscillatory loading. Consequently, these observations would tend to suggest that there was no such mechanism including diffusion or energy absorption occurred for low frequency oscillatory load applied on a static deformation process.

2.1.4 Contact surface effects

Most of the early attempts to apply oscillations to metalworking processes were impeded by a lack of understanding of the nature of ultrasonic stress waves and the lack of ability to measure their magnitude accurately. Consequently, under ultrasonic excitation only mean oscillatory forces were measured. Any assessment of the validity

of the various mechanisms reported to be involved in the apparent force reduction is hampered by insufficient detail of equipment, technique or results presented. As discussed previously, one of the major factors, generally proposed, which led to an apparent reduction in flow stress during an applied ultrasonic load was due to a reduction in interface friction [5, 13]. However, this claim was not fully substantiated by the experimental evidence and, therefore, in an attempt to clarify how the ultrasonic excitation could reduce the interface friction, investigators suggested several postulates including effects of surface separation, friction vector reversal, and heating of asperities [5].

In an early investigation into the effects on friction of ultrasonic vibration, Fridman and Levesque [30] designed a simple friction experiment by sliding a metal block on a vibrating inclined plane. Although in this test the block was not deformed, some fundamental ideas regarding a metallic interface subjected to an oscillatory load were presented. The coefficient of friction during the ultrasonic excitation applied to the plane, was reduced almost to zero. Fridman related the reduced friction coefficient to the breaking of the formed welded junction between the asperities of the surfaces due to the vibrations. Similar results were later published by Skare et al [31] when they continued Fridman's study. To explain their result of a reduction in the coefficient of friction, Skare added more factors, including resonance of contacting asperities, reversal of the friction vector, superposition of static and oscillatory loads, and localised transformation of vibration energy into heat which resulted in a lowering of the yield point of the surface asperities.

In metal forming processes, particularly involving contact between a die and specimen such as upsetting, drawing and extrusion, it was accepted that the reduction in the mean force during superimposed ultrasonic excitation of the die could be substantially accounted for by a reduction in friction at the die-specimen interface. As was previously reported by Perotti [8] in an experimental study of ultrasonic upsetting of copper, lead and aluminium, the reduction in measured forming force under applied ultrasonic excitation during static upsetting was due to a reduction in the interface friction between die and specimen.

Many research studies have been conducted to investigate the effects of ultrasonic excitation on contact friction and most of the investigations have been concerned with strip and wire drawing processes [9, 10, 24, 32]. In general, these studies agreed that the flow stress was significantly reduced during applied ultrasonic excitation and that a reduction in friction substantially accounted for stress reduction. In later investigations [9, 10], the coefficient of friction was directly estimated from the experimental data in ultrasonic drawing experiments. By comparing ultrasonic and conventional drawing, it was reported that the friction coefficient in ultrasonic drawing was approximately reduced by 30% to 40 %.

The reduction in contact friction could be explained by the friction force vector reversal and, for some cases, the loss of die-specimen contact due to the vibrations [27]. Studies have also concluded that the effectiveness of ultrasonic excitation to reduce interface friction relies on the ratio of the process speed to the vibration velocity [7, 10, 27].

Recently, an investigation of the effects of ultrasonic excitation of the die in compression tests on soft solids was reported by Huang et al [11]. By interpreting the experimental data with finite element model results, this study concluded that for short intervals of applied ultrasonic excitation the reduction in mean forming force could be explained by oscillatory stress superposition. A further reduction in the forming force when the interval of ultrasonic excitation of the die was increased during the compression test, was due to a thermal reduction of the interface friction. A recent study by Hung et al [33] reported an experimental investigation into the influence of ultrasonic vibration on hot upsetting of aluminium. Hung concluded that the magnitude of the reduction in forming stress decreased as the temperature increased and that the effects of ultrasonic vibration on hot upsetting could not be explained simply by mechanisms such as interface friction, superposition of stress, or absorption by dislocations of the ultrasonic vibration energy.

Previous studies have reported that the initial interface condition greatly influences the effectiveness of ultrasonic excitation to reduce interface friction. For example, under a dry surface condition the reduction in friction obtained for ultrasonic assisted forming was higher than the reduction obtained under a lubricated condition [7, 10]. For a lubricated interface, one explanation of the action of ultrasonic excitation on the

lubricant was the lubricant being sucked in and out through surface micro cracks which open and close due to the vibration [34]. Also, it was suggested that the effectiveness of using lubricant in ultrasonic forming depended on the ultrasonic amplitude, type of forming operation and the chemical reactivity of the lubricant used [7, 23]. Although many explanations have been put forward, there have been no conclusive explanations reported regarding the beneficial effects of lubricants in ultrasonic forming processes. An understanding of the effects of lubricants would be helpful in maximising the beneficial effects and allowing an optimisation of the forming process.

2.2 Ultrasonics in Metalworking and Finite Element (FE) Simulations

Many studies have been concerned not only with fundamental effects of oscillation on elastic-plastic deformation of metal and friction at the contact surface, but also with a wide variety of industrial metalworking operations in order to obtain an optimum manufacturing design and commercial opportunities. Many studies have been published in metalworking processes such as machining [35, 36], forging and upsetting [4, 7, 8, 11], drawing and extrusion [9, 10, 18, 24, 27], and welding [37]. The investigators have adopted experimental and analytical approaches to investigate issues of force reduction, process optimisation, finished product quality and process design.

2.2.1 Machining

Ultrasonic machining originated more than 50 years ago and this technique is widely accepted in many metalworking industries. Ultrasonics is commonly applied in machining, including milling, turning, and threading. Other methods of material removal that utilise ultrasonic vibrations are electrolytic and spark erosion machining, and abrasive machining. The use of ultrasonics in turning processes has demonstrated a noticeable decrease in cutting forces, improvement in surface finish, increase in tool life (up to 20 times), noise reduction and has been successfully implemented for machining brittle materials such as plastics and glass [35, 36].

The basic difficulty of using conventional spark erosion or electrolytic machining is that the machining rates are rapid at the beginning then the erosion slows owing to a layer of oxide forming on the anode. By applying ultrasonic vibration on the cathode, this oxide

layer is easily broken up. Furthermore, the cutting rate can be increased by combining conventional and ultrasonic machining. Ultrasonic vibration is also used successfully in abrasive machining, and can be adopted for very brittle materials. The final cut shape is easily obtained and tool wear can be reduced [35].

2.2.2 Forging and upsetting

A considerable number of investigations into the application of ultrasonic excitation to compressive deformation of metals has been carried out [4, 7, 8, 20, 23, 27, 34]. Various materials were forged, hot and cold, with and without lubricant, in both open and closed dies. Tests were carried out in a specially constructed hydraulic or mechanical press machine equipped with a vibrating mechanism, which is normally located on the top or bottom platen or on both platens. General observations were made during the operation regarding stress-strain behaviour, temperature, hardness distribution, deformation configuration and surface properties.

The greatest benefits were obtained in the reduction of forming force, increased degree of deformation and improved quality of deformed parts. These beneficial effects were largely attributed to improvements in interface friction [7, 8, 11], stress superposition [7, 12, 20] and softening effects [19].

Although many previous studies attempted to provide explanations of how friction at the die and specimen interface can be reduced, they were not verified by conclusive experimental evidence or analytical models [7, 8]. In Kristoffy's study [7], the reduction in friction in oscillatory cold forging for aluminium was suggested to be a result of the periodic change in the direction of the friction force vector, but again this idea was not validated by analytical model or experimental evidence.

In all these previous studies, investigators tended to measure the mean overall stress rather than the actual oscillatory stress amplitude, due to the lack of measurement transducers that could simultaneously measure the static and oscillatory forming force. Kirchner et al [4] tried to resolve this problem by adopting low and medium frequencies in an upsetting test. Low frequency test results were related to an analytical model of oscillatory stress superposition for elastic-plastic strain-rate independent and strain-rate

dependent materials in compression. The model showed that the path of maximum stress during superimposed low frequency vibration excitation will follow the path of the static stress-strain curve for a strain-rate dependent specimen and the mean stress will therefore be lower than the static stress. For a strain-rate dependent specimen, the path of the maximum oscillatory stress will be parallel to, but can be higher than, the static stress. This analytical model was thoroughly validated for a low frequency experimental test and therefore the paper concluded that the mechanism of mean flow stress reduction in ultrasonic upsetting would similarly be a result of oscillatory stress superposition, although this was not verified by experimental measurements.

2.2.3 Drawing and extrusion processes

The application of ultrasonic vibration to drawing processes offers many advantages. The ultrasonic vibration can be either applied to the workpiece or to the dies. In most cases ultrasonic drawing is carried out using axial or radial vibration mode dies. The studies have been concerned with drawing force, interface friction, process speed, the applicability of vibration mode being used, and quality of the finished product [9, 24, 27, 32].

An early investigation into the application of ultrasonic vibration in wire drawing was conducted by Pohlman [2]. A pure copper wire was drawn through a die which was subjected to an axial ultrasonic vibration at 20 kHz. By superimposing an ultrasonic excitation on the wire drawing process, an apparent reduction in the drawing force was measured during plastic deformation. Also, Pohlman suggested that the force reduction was due to a reduction in internal friction. In later investigations, it was suggested that the beneficial effects, of reduced drawing force and improved surface finish, can only be obtained when the drawing speed is lower than the ultrasonic vibration velocity. [6, 24].

More recently, Murakawa [32] compared radial mode and axial mode ultrasonic vibration on the wire drawing process. Murakawa introduced a critical speed of ultrasonic drawing, which was defined in term of ultrasonic vibration velocity, mode of vibration and die angle. The experimental results showed that the effectiveness of ultrasonic excitation to reduce drawing force seemed to be dependent on the drawing

velocity. Also, the paper concluded that the application of radial ultrasonic vibration effectively extended the drawing critical speed compared with axial ultrasonic vibration.

There are a limited number of investigations of ultrasonic extrusion, mainly due to the relative complexity of the experimental test rigs. However, Petukhow et al [25] reported an experimental investigation into the effects of ultrasonic excitation on the extrusion of aluminium. In an attempt to optimise the benefits of ultrasonic excitation, Petukhow individually and simultaneously applied ultrasonic excitation to three parts of the extrusion test rig; die, punch and container. For all cases, it was reported that the extrusion force decreased as the ultrasonic amplitude increased. However the most effective reduction in the extrusion force was recorded by applying ultrasonic excitation to the punch and die simultaneously. Also it was concluded that the extrusion force was dependent on extrusion rate and specimen length, but was not affected by degree of deformation, die angle and lubricant properties.

2.2.4 Finite element modelling in oscillatory and ultrasonic forming processes

A rapid increase in the use and application of finite element modelling (FE) to metalworking simulation has occurred due to the increase in capability of computers. The flexibility of the commercial packages available allows the input of numerous material parameters in complex calculations. Updated Lagrangian implicit and explicit formulations have been used in the majority of publications since the mid 1980's. In this approach, elements move with the workpiece thus experiencing large plastic deformations in a forming process [38]. Various criteria for large material deformation, failure and mechanical contact are introduced into modelling schemes in order to describe non-linear deformation and contact mechanics. In an attempt to tackle complex contact and large deformation problems, several algorithms have been used to define the contact parting line between two or more surfaces, movement of elements, and re-mesh of the elements.

The effective application of FE simulation procedures depends on the availability of a set of governing equations which provide the inputs for a simulation process. Bulk metal forming process simulation allows a realistic prediction of the workpiece response during the forming process. FE simulations can also eliminate the need for experimental

investigations although there is usually a requirement for experimentally derived material and contact definitions.

Finite element modelling has been usefully employed in a number of commercial areas and has become a normal part of design and improvement of many industrial processes. Examples include extrusion [39-42], sheet forming [42-44] and rolling [45]. The results obtained from such methods have proved to be in agreement with those obtained in experimental studies and from analytical models.

Apart from FE models used to simulate conventional processes, models have been developed for more complex processes such as oscillatory assisted forming [11, 46, 47], ultrasonic turning [36], and also to predict the effects of human body response to a vibratory load [48]. In most cases, the calculated FE data can be verified by experimental data or vice-versa. Also, in many investigations, a better insight into a phenomenon can be achieved by using a combination of an FE model and experimental studies [11, 12, 47].

Although the application of FE modelling to ultrasonic forming can be considered as a new field of study, several reports and papers have published on this subject [11, 32, 46, 47]. Previously, many investigations used FE modelling to design the ultrasonic horn, as geometry and dynamic characteristics of the horn could be predicted prior to fabrication [49-53]. FE models have been successfully used to predict an accurate geometry for an ultrasonic horn with a specific operating frequency and vibration mode shape. However, practically, the fabricated horn is subsequently tuned and characterised using an experimental analysis such as experimental modal analysis (EMA).

By employing FE simulation of an ultrasonic forming process, the oscillatory stress can be predicted and an investigation into the material response due to an ultrasonic load can also be performed. Recently, Huang et al [46] carried out experimental and FE model investigations into the effects of static and ultrasonic upsetting of plasticine specimens. For static upsetting, it was reported that an excellent agreement was obtained when comparing the experimental and FE results for the relationships between the forming force and displacement and also for the deformed configurations.

Subsequently, for ultrasonic upsetting, it was also concluded that FE models can accurately predict the effects of a superimposed oscillatory load on the forming force.

The versatility of the finite element method has been demonstrated by displaying detailed information during static and ultrasonic deformation, such as the effective stress, plastic strain, the axial stress and shear stress. By including thermal properties in the models, the distribution of temperature in the specimen can also be predicted throughout the deformation process [11, 54].

Another recent study by Hayashi et al [47], of an FE simulation of ultrasonic wire drawing, reported that the predicted FE results of drawing force closely agreed with a previous experimental study [32] for the dependency of drawing force reduction on the drawing speed when radial or axial ultrasonic excitation was applied. It was also concluded that the FE model could reveal changes in stress distribution in the wire due to changes in the drawing speed.

FE modelling provides an opportunity to investigate many changes in process parameters in ultrasonic forming processes, such as changes to boundary conditions, ultrasonic frequency and amplitude, and process speed, which would be difficult to achieve experimentally.

2.2.5 Conclusion

Following a large number of investigations in many metalworking processes, it is clear that the reported principal effect of superimposing an ultrasonic vibration to a metal forming process is a reduction in the force necessary to deform the metal. However, the claims and explanations offered in the literature are generally inadequate as they fail to include the oscillatory stress or oscillatory force response in the measurements and analysis. This leads to a lack of understanding of how the benefits arise and an inability to quantify their contribution.

Although the stress superposition effect, dislocation movement, and change in interfacial friction are all suggested as major contributions to the measured reduction in

mean forming force in ultrasonic metal forming, it not yet clear how these are effected by ultrasonic vibrations.

2.3 Friction in Metal Forming Processes

Friction and lubrication are of great importance in many industrial forming processes such as forging, sheet metal forming, rolling and extrusion. Friction not only changes the forming load but is directly related to the quality of the deformed workpiece in metal forming processes. Many studies have been carried out to investigate friction in various forming processes [55-58]. In most cases the investigation has been concerned with measurement of the coefficient of friction. In recent years, many computational programs based on the finite element method have been developed and employed in commercial areas of metal forming process. However, the accuracy of such analysis can be seriously limited by lack of knowledge of an exact numerical value of the interface friction coefficient [58]. To estimate a coefficient of friction, many studies have suggested that the characteristic material flow during a deformation process provides significant information of the interface friction. This information subsequently provides knowledge for optimising a process and for designing an accurate die in which to avoid material defects and failure during a deformation process [55, 59, 60, 61].

In an early investigation, Schroeder and Webster [62] conducted a series of compression tests of aluminium and magnesium disc specimens under different surface conditions. Subsequently, Schroeder derived experimental friction curves from the dimensionless ratio of the pressure applied to the flow stress versus the ratio of the compressed radius of the disc to the deformed thickness of the disc. By matching the experimental curves with theoretical curves, the coefficient of friction for different surface conditions can be estimated. Although the authors claimed that their outcomes needed to be verified, this technique successfully provided a useful method for estimating the coefficient of friction for metal forming process.

Schroeder's studies have been continued in many later investigations [55, 56, 63]. Generally the authors agreed that the coefficient of friction could be estimated by utilising the knowledge of material flow characteristics for a large plastic deformation.

However, the applicability of this method was confined by a maximum limit of the coefficient of friction value that could be estimated [63].

This disc compression technique is considered to be a difficult method to conduct in practice, because it requires a direct force measurement, knowledge about material properties, and a specific measurement device if the investigation is performed under elevated temperature. Therefore, in an attempt to estimate the coefficient of friction for metal forming processes, this method was altered [64, 65] by adopting the same principle of material flow characteristic but modifying the specimen from cylindrical to a ring geometry. This experimental technique was later known as the ring compression test.

2.3.1 Theory of friction in metal forming

The most comprehensive contribution to the modern ideas about friction was pioneered back several hundred years by Amontons (1699). Almost a century later, Coulomb (1785) largely established the basic laws of friction and although he recognised that adhesion might play some part in friction he considered that the major factor involved the interaction of surface roughness. The general critical picture of the present understanding of the frictional process was presented by Tabor [66]. Tabor has pointed out three basic elements that are involved in the sliding friction of unlubricated solids, they are: (1) the true area of contact between mating rough surfaces, (2) the type and strength of bond formed at the interface where contact occurs, and (3) the way in which the material in and around the contacting regions is sheared and ruptured during sliding.

The importance of these three elements can be easily understood from the definition of the coefficient of friction,

$$\mu = \frac{Q}{F} \tag{2.8}$$

where Q is the tangential force needed to shear the junctions between the contacting surfaces and F is the external normal force. The actual contact load, P, in the true area of contact is different from F by the amount of the intermolecular forces acting between the surfaces in contact. These forces are referred to as adhesion forces, F_s, and hence,

$$P = F + F_s. \tag{2.9}$$

From equation (2.8) and (2.9), therefore

$$\mu = \frac{Q}{P - F_s}. \tag{2.10}$$

The contact load, P, is related to the true area of contact through the general problem of contacting rough surfaces. The adhesion force, F_s, relates to the strength of the bond formed at the interface [67].

In metalworking theory, types of slip boundary conditions are generally considered. These are referred to as Coulombic and Tresca criteria, also known as constant friction models [60, 68]. For the case of a Coulombic boundary condition, it is assumed that the frictional shear stress, τ, is directly proportional to the normal stress, p. In the presence of sufficient lubricant, the adhesion effects, F_s in equation (2.10), are negligible, therefore,

$$\tau = \mu\, p. \tag{2.11}$$

In the case of uniaxial deformation, both values τ and p would generally be functions of the radial co-ordinate, r, that has its origin at the axis of the cylindrical specimen.

The Tresca boundary condition, in contrast, defines the wall traction as being some function of shear flow stress, τ_f, thus

$$\tau = m\, \tau_f, \tag{2.12}$$

where *m* is known as the interface shear or the friction factor.

The least value in the fully lubricated case where the normal wall stress induces plastic flow is given as the uniaxial yield stress, σ_y or the flow stress, σ_f. Then, the maximum value of the coefficient is given by a ratio of the shear yield stress, τ_y, to the flow stress, σ_f. Hence, using the von Mises criterion, $\mu = \tau_f/\sigma_f = 1.155/2$, where $\mu_{max} = 0.57$ or $m =$

1.0. For the Tresca criterion, $\mu = \tau_f/\sigma_f = 1/2$, where $\mu_{max} = 0.5$. Thus the estimated maximum value of the coefficient of friction for a slip boundary condition will be equal to 0.577 or 0.5 depending on the yield criterion used. It may be assumed for practical estimations of the coefficient of friction, that under a sufficiently lubricated wall boundary condition, the wall shear stress, τ, is given by $\tau = \mu p$. This is only valid provided the value of $\tau < \tau_f$, otherwise, there is a sticking boundary friction condition i.e. $\tau \geq \tau_f$. It is however, quite difficult to achieve a perfectly lubricated condition during the deformation process. This may be simply due to the deterioration of the lubricant as a result of thinning of the film when deformation proceeds. The deterioration of the lubricant exposes fresh and unlubricated material to the tool surfaces, which may lead to a sticking rather than a sliding boundary at the interfaces [69].

The above approximation in the calculation of μ is categorised under the theorem of limit analysis of the theory of plasticity or more specifically known as the lower and the upper bound theorem [70]. This method is relevant to steady-state problems. Therefore when applying the theorem limit, the following assumptions are usually made: (1) the deformation material is isotropic and incompressible, (2) the elastic deformations are neglected, (3) the inertial forces are small and can be neglected, (4) the tangential friction or shear stress, τ, is constant at the die-material interface, (5) the material flow follows von Mises's flow rule and, (6) the shear flow stress, τ_f, is constant [63, 70]. In a real situation Lee et al [63] suggested that the assumption of shear flow stress, τ_f being constant should be avoided and the predictions have to be made by considering, at small deformation steps, (1) the distribution of τ_f and, (2) an average value for τ_f. Therefore, as the deformation proceeds, a new distribution, or a new value for τ_{avg} is calculated at each step according to,

$$\tau_{avg} = \int \tau_f dV / V \tag{2.13}$$

where V is the total volume of deformation material.

The method of the approximation of the friction models has been extended by many investigators to achieve a better estimation of material flow [60, 68, 71]. It has been suggested that the method initiated by Wanheim [68, 71], known as a general friction

law, provides a better solution in finite element analysis. According to this model, the frictional stress, τ is described by;

$$\tau = f\alpha\tau_f. \tag{2.14}$$

Where f is the friction factor, α is the ratio between the real and apparent contact areas and, τ_f is defined by $\tau_f = \sigma_y / \sqrt{3}$. The frictional, τ, and normal, p, stresses at the die-workpiece interface are proportional for $p / \sigma_y < 1.5$, whilst for $p / \sigma_y > 3$ the relative frictional stress, $\tau/\tau_f = f\alpha$, approaches a constant value which is equal to f. In order to eliminate the sudden changes of the frictional stress at the neutral point, the following approximation is defined [72];

$$\tau = jf\alpha\,\tau_y \frac{2}{\pi}\tan^{-1}\left(\frac{|u_r|}{u_o}\right). \tag{2.15}$$

Where j is the unit vector in the direction opposite to the velocity, u_r, of the frictional shear stress relative to the die, and u_o is an arbitrary constant much smaller than the velocity.

In practice the friction factor f is determined experimentally and the term α is determined by the equation as follow [68],

$$\frac{\tau}{\tau_f} = \frac{\tau^*}{\tau_f}\left(\frac{p / \sigma_f}{p^* / \sigma_f}\right)$$

for $p/\sigma_f \le p^*/\sigma_f$, and

$$\frac{\tau}{\tau_f} = \frac{\tau^*}{\tau_f} + \left(f - \frac{\tau^*}{\tau_f}\right)\left[1 - \exp\frac{(p^*/\sigma_f - p/\sigma_f)(\tau^*/\tau_f)}{(1-\tau^*/\tau_f)(p^*/\sigma_f)}\right] \tag{2.16}$$

for $p/\sigma_f \ge p^*/\sigma_f$, where τ^* is the limit friction stress, p^* the limit normal stress while τ/τ_f and p/σ_f are called the dimensionless friction and dimensionless normal pressure,

respectively. The limit of proportionality between friction stress and normal stress (τ^*, p^*) is defined by [60, 68];

$$\frac{\tau^*}{\tau_y} = 1 - \sqrt{1-f}\,, \tag{2.17}$$

and

$$\frac{p^*}{\sigma_f} = \frac{1 + \frac{\pi}{2} + \cos^{-1} f + \sqrt{1-f^2}}{\sqrt{3}(1+\sqrt{1-f})}. \tag{2.18}$$

The implementation of this model requires knowledge of the normal stress, p at contact surface between tool and workpiece. The normal stress, p, for a two-dimensional model, can be obtained from

$$p = (S_{ij} \cdot \vec{n}) \cdot \vec{n}. \tag{2.19}$$

Where S_{ij} is the state of stress at the boundary and $\vec{n}$ is the unit normal to the surface [68].

2.3.2 Lubrication in metal forming

The importance of tribological considerations in bulk metal forming has been generally recognised as affecting tool life, metal flow during forming, applied load, relationship of lubricant to the machine elements and quality of surface finish. Many lubricants have been developed for metal forming operations. For light press-working, low-viscosity mineral oil, synthetic oils, or water-based lubricants are suitable. For severe forming operations in which extreme pressures are applied, additive and low-friction coatings such as phosphate are often employed [73]. The effectiveness of using lubricants in forging and other metal forming processes has been studied by many previous investigators [55, 73, 74, 75]. Apart from the investigations into the effectiveness of the lubricants applied, these authors also observed the other deformation parameters including specimen configuration throughout the process, normal and shear stresses, modification in material properties and coefficient of friction.

Many types of lubricants have been developed and tested for various industrial purposes. The most common lubricants such as mineral oil, oleic acid, sodium stearate soap, Teflon and lead have been widely used in many previous studies [73, 74, 76]. A wide variety of lubricants used in the investigations provided different interface lubricated conditions, providing different interface friction coefficients.

Efforts have been made in the development of new lubricant formulations and lubrication technology. The conventional lubricants have been modified by adding additives of compounds to reduce the concentrations of active elements or even replace them in order to adapt their application in a metal working process. Rao et al [73] investigated the applicability of a new lubricant, boric acid, for deep-drawing of aluminium sheet. By comparing with other lubricants, Teflon (PTFE), oleic acid, molybdenum disulfide, and graphite, it was concluded that boric acid was comparable with commonly used lubricants over a wide range of forming parameters.

It has been recognised that the effectiveness of lubricants applied in metal forming is dependent on many variables including viscosity, thickness of lubricant layer, original contact surface profile, process speed, physical and chemical reaction between contact surfaces, and magnitude of the applied force [76-79].

The action of a lubricant during a plastic deformation that accounts for a lowering of the friction coefficient is defined as hydrodynamic action [73]. This action is developed when the lubricant is trapped in micro and macro surface pockets, interrupting the metal to metal contact. The mechanism of the action of a lubricant during a metal forming process was described in two practical approaches [78]: (1) the trapped lubricant may serve as a reservoir for the boundary film which is being continuously destroyed by mechanical rubbing, generated heat, or through enlargement of the surface area of the workpiece, (2) the trapped lubricant would sustain a part of the die pressure and prevent the inter-metallic contact from increasing.

The observation of surface texture of a deformed specimen can provide useful knowledge regarding how the lubricant influences the effect of friction of the contact surface. It was reported that by applying a relatively high-viscosity lubricant, the

interface friction was significantly reduced due to hydrodynamic action of the trapped lubricant in the surface asperities, however this action also deteriorated the deformed surface and produced a dull surface texture [76, 79, 80].

2.3.3 Ring compression test

Among the methods to measure the coefficient of friction, the ring compression test has gained wide acceptance in the last two decades. This method was originated by Kunogi [64] and later improved and presented in a usable way by Male and Cockcroft [65]. The technique introduced by Konugi did not provide a quantitative evaluation of friction, whereas Male and Cockcroft defined a quantitative coefficient of friction value.

Male and Cockcroft adapted Konugi's principle by producing a set of specific friction curves based on the hollow cylinder compression test which later became known as the ring compression test. This technique utilises the dimensional changes of a test specimen to arrive at the magnitude of the coefficient of friction. For a given percentage of height reduction during compression tests, the corresponding measurement of the internal diameter of the test specimen provides a quantitative measure of the magnitude of the friction coefficient at the die-specimen interface. If the specimen's internal diameter increases during deformation, friction is low, whereas if the specimen's internal diameter decreases during deformation, friction is high. The profile of the deformed ring is illustrated in Figure 2.2.

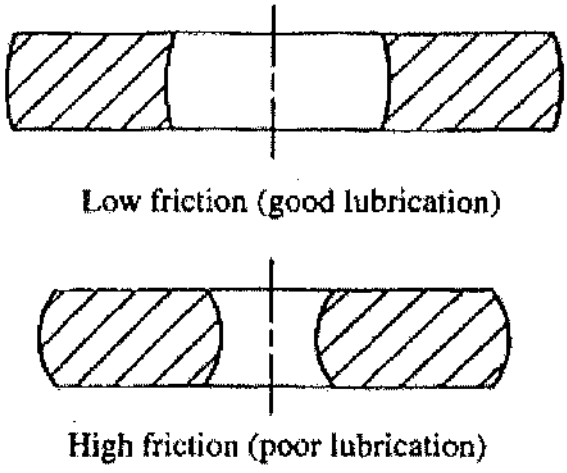

Figure 2.2: Effect of friction on metal flow during a ring compression test.

Using this relationship, the specific friction curves, later called friction calibration curves (FCC) were generated by Male and Cockcroft [65]. Initially Male and Cockcroft generated the two most extreme friction conditions. In their first test, it was assumed that sticking friction occurred when the aluminium ring specimens were compressed at 600°C. According to the von Mises yield criterion, the coefficient of friction $\mu \geq 0.57$ for sticking friction. Secondly, zero friction, $\mu = 0$, was achieved by using a wax ring specimen which melted during compression on hot platens. This melting of an extremely thin surface layer provided an almost perfect lubricant. For intermediate values of friction coefficient, Male and Cockcroft performed upsetting tests of disc shape specimens for various deformation amounts, and μ was calculated from the results using the analysis of Schroeder and Webster [62]. By using the same material as used for the disc, the ring specimens were produced and treated in the same manner and compressed under identical condition. Then, the friction coefficient values were checked and calibrated for the relatively lower friction coefficient values of 0.07 to 0.1 by using an experimental technique of thin foils and a calculation of μ which was suggested by Hill [65]. By relating the percentage reduction in internal diameter of the ring specimen to its reduction in height, Male and Cockcroft generated a set of friction calibration curves for the coefficients of friction as shown in Figure 2.3.

Since the friction calibration curves generated by Male and Cockcroft have not accounted for material properties and test parameters, it has been claimed in recent investigations that these curves need to be improved. These parameters, including material properties of the specimen, deformation speed, strain hardening and barrelling were included in later studies [63, 76, 81, 82].

The theoretical analyses such as the slip-line field approach, upper bound method, and limit theorem, are only applicable where the forces and material flow are in a steady-state condition. With recent advancements in computer technology, the study of friction using the ring compression technique has shifted from using experiment and classical plasticity theory to the application of the finite element (FE) method. The capability to solve non-steady-state conditions and the flexibility of the FE method to include material parameters, deformation speed, and interface properties, has enabled the solution of many complex friction problems in many forming processes [83-87].

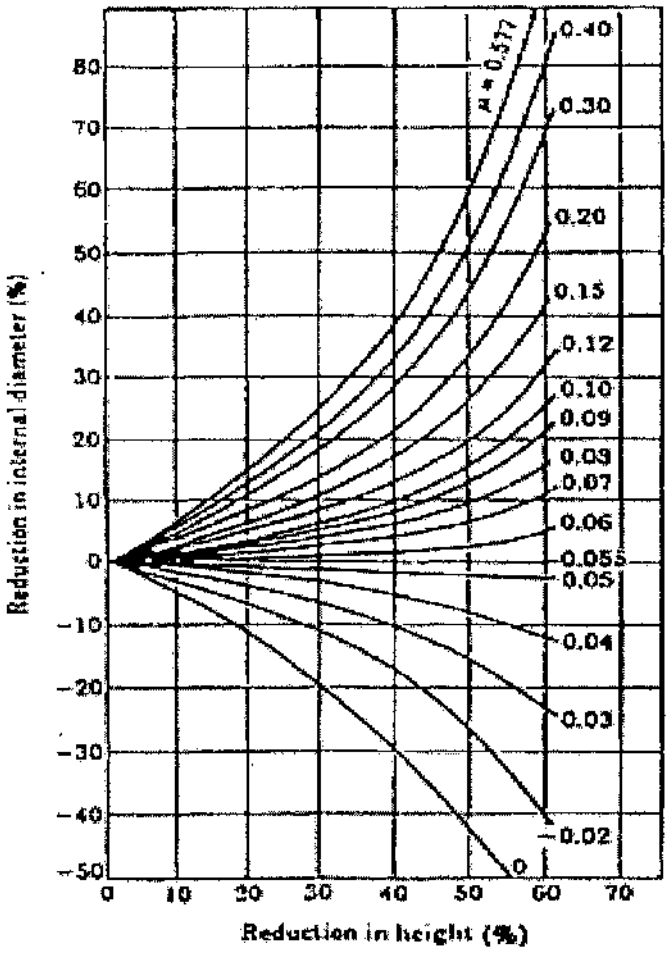

Figure 2.3: Friction calibration curves in term of μ [65].

Hartley [83] successfully developed the finite element method for axial compression of rings. Hartley introduced the β-stiffness method in his FE formulation so that the yield stress of the surface layer is a function of both bulk material properties and applied forces. Hartley suggested that for the interface friction factor $m = 0.1$ and deformation up to 50%, excellent agreement was obtained between FE results and experimental data. For the observation of the internal surface profile of the ring, for $m = 0.1$, the FE model predicted a perfect concave inner diameter profile, however the experimental study measured an unsymmetrical concave profile, which Hartley clarified as due to the unsymmetrical nature of experimental deformation.

In 1985 Carter and Lee [88] simulated the ring compression test by employing the ADINA finite element code and generated the FCC for aluminium 6061-T6. They reported a disagreement with the calibration curves obtained by Male and Cockcroft, which was attributed to assumptions of no barrelling of the deforming specimen and a constant friction coefficient across the interface in Male and Cockcroft's work. Later, a study of hot ring compression tests using FE simulation was carried out by several authors [85, 87, 89] and it was shown that strain rate and temperature significantly influenced the frictional shear factor, m, at the interface of die and specimen. A further study of the dependency of the friction curves on material properties, strain rate sensitivity, and barrelling by using soft material was carried out by Sofuoglu and Rasty [84], and Sofuoglu and Gedikli [87]. It was concluded that although the ring compression test is an effective method for determining the coefficient of friction during large deformation processes, the use of generalised friction calibration curves (FCC) regardless of the material properties and test condition must be avoided.

Although the ring compression technique employs upsetting deformation, this does not mean that the estimated friction coefficient value is only applicable for upsetting or forging processes, and the friction values can be also be applied in many other analytical or experimental studies of forming processes such as rolling, drawing, and extrusion [57, 85, 90, 91]. Male [90] investigated the relationship between the coefficient of friction obtained using the ring compression technique with the coefficient of friction estimated for actual metal forming processes, namely; rolling, drawing, and extrusion. It was concluded that, in most cases, the friction coefficient values measured for the three metal forming operations agreed with the values obtained using ring compression tests, as the tests were carried out under similar conditions. This would suggest that the ring compression technique can be adopted effectively as a simple method for estimating the coefficient of friction value for a range of complex metal forming processes, which avoids the need to take friction measurements from a full-scale metal forming operation, which is extremely difficult, time consuming, expensive, and often inaccurate.

CHAPTER 3

STATIC AND ULTRASONIC TENSION TESTS

3.1 Introduction

The engineering tension test is widely used to provide basic design information on the strength of materials and as an acceptance test for the specification of materials. In a tension test procedure, a specimen is subjected to continually increasing uniaxial force while simultaneous observations are made of the elongation of the specimen. Investigations in ultrasonic forming, which have concentrated on tension deformation [1, 19, 28, 29] have demonstrated that significant tension force reduction can be achieved by superimposing ultrasonic excitation on this process. This force reduction can be equal to or larger than the oscillatory force amplitude [1]. According to Langenecker [19], the force reduction is due to the removal of barriers in front of moving dislocations. In a later investigation, this dislocation theory was expanded, and it was proposed that the dislocations may absorb energy from vibrations in three ways: (1) a resonant mechanism, (2) a relaxation mechanism, and (3) a mechanism of simple hysteresis [92].

However, within the frequency range of 15 to 80 kHz, resonance of dislocations is reported not to be possible [2]. Therefore, in an attempt to clarify the reduction of flow stress under applied ultrasonic excitation during a tension test of carbon steel wire, Nevill and Brotzen [3] introduced a model by considering a superposition of static and oscillatory stress. As illustrated in Figure 3.1, Nevill and Brotzen explained that to induce yield, a minimum stress, S_y is required. For the case of $S_y > S + A$, where S is static stress and A is stress amplitude, the specimen would not yield. For the case of $S_y < S + A$, the specimen for a portion of the vibration cycle, is subjected to a total stress greater than that required to induce plastic deformation. This model was later known as the superposition effect.

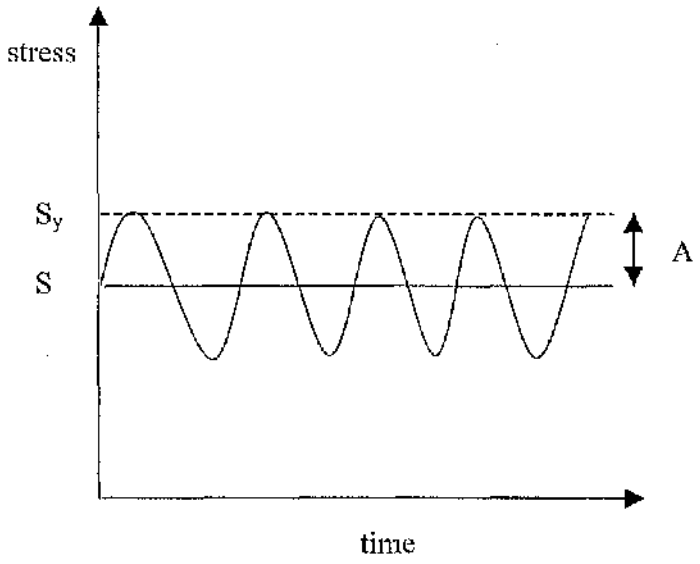

Figure 3.1: Model of superposition of steady-state and alternating stresses to cause yielding [3].

The principle of stress superposition (superimposing an oscillatory stress on a static stress) that was modelled by Nevill and Brotzen was clarified by Kirchner et al [4] for low frequency oscillation applied in a series of compression tests. In this work, a low frequency excitation force was applied to a static compression test during plastic deformation, in order to validate an analytical model of oscillatory stress superposition effects for elastic-plastic strain-rate independent and strain-rate dependent compression. Figure 3.2(a) shows a typical stress-strain curve for static compression of an elastic-plastic work hardened material model. If an oscillatory stress is superimposed for an interval during plastic deformation, Figure 3.2(b) illustrates that the path of the maximum oscillatory stress will follow the path of the static stress-strain curve and that the path of the mean stress will be lower than and parallel to the static stress-strain curve. For a strain-rate dependent specimen, Figure 3.2(c) shows that the path of the maximum oscillatory stress will be parallel to, but can be higher than the static stress, referred to as overshoot. The two descriptions, for rate independent and rate dependent materials, define the superposition of an oscillatory stress on a static stress for oscillatory compression tests of elastic-plastic materials, and therefore any deviation from these descriptions is attributable to other mechanisms of interface or bulk

specimen effects during ultrasonic compression. In Kirchner's study, the analytical model was well validated for low frequency experimental tests and therefore the paper concluded that the mechanism of mean flow stress reduction at ultrasonic frequencies would similarly be a result of oscillatory stress superposition, although this was not verified by experimental measurements. This was due to an inability to measure the oscillatory response at the higher frequencies and therefore the study had to draw conclusions from measurements of the mean compression force.

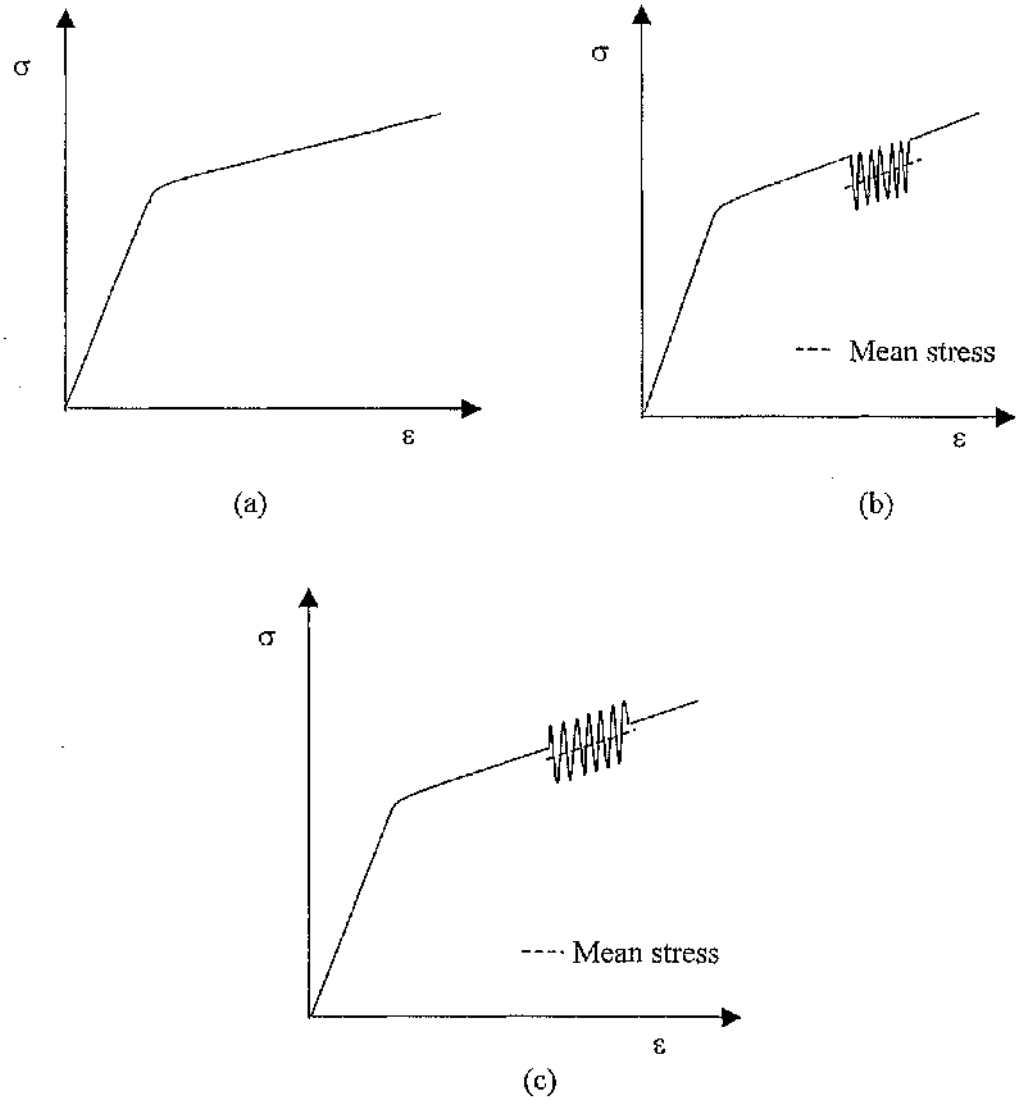

Figure 3.2: Superposition principle where an oscillatory stress is superimposed on a static stress, showing: (a) static stress, (b) static-oscillatory stress for rate independent material and (c) static-oscillatory stress for rate dependent material [4].

This lack of measurement of the oscillatory force response has been a common limiting feature of most of the previous studies of ultrasonic metal forming processes. In previous studies, researchers have argued that in many cases the stress-strain relationship departs from this idealised stress superposition model. Although stress superposition features as part of the explanations [3, 7, 11], measured reductions in the mean forming load have been attributed to several other possible mechanisms, including reduction of internal and contact friction [2], and dynamic effects of high frequency vibrated tools [93].

In order to eliminate friction effects and concentrate on any other material effects due to ultrasonic excitation, this chapter aims to investigate the application of ultrasonic excitation in tension tests. Also, by measuring the oscillatory force response during these tests, rather than merely the mean force response, comparisons between experimental data and finite element calculations can provide a better insight into the response of material under ultrasonic excitation.

3.2 Aluminium Specimens

The properties of aluminium make this metal and its alloys economical and attractive for a wide variety of applications. Aluminium and its alloys are categorised by a relatively low density, high electrical and thermal conductivities and a resistance to corrosion in some common environments. Since aluminium has a face-centred cubic crystal structure, its ductility is retained even at low temperatures. However, a major limitation of aluminium is its low melting temperature of around 660°C, which restricts its application for higher temperatures. Most aluminium alloys are formable materials that can withstand processes ranging from a simple forming operation such as upsetting to a severe forming process, including deep drawing, extrusion, and rolling [94, 95].

Many aluminium alloys are ductile and do not have a clearly defined yield point. In many cases, aluminium shows a low hardening property during plastic deformation. It has been suggested that, under certain process conditions, the thermal properties of aluminium change during deformation; for example a lower flow stress was reported when an aluminium specimen was extruded under high speed [96, 97].

In the present study, a soft wrought aluminium alloy of A1050 composition is used as the metal specimen in all tests. The chemical composition of aluminium A1050 is tabulated as in Table 3.1. Standard tension test specimens [98] were prepared by machining from a cylindrical bar, giving the test section a diameter of 5 mm and test length of 20 mm. Both ends of the specimen were cut into a thread of M12 enabling the specimen to be securely tightened between the ultrasonic horn and the upper sleeve. A photograph of the specimen used in this study is shown in Figure 3.3.

Table 3.1: Chemical composition of aluminium alloy A1050 [94].

Elements	Composition (%)	Limits
Aluminium	99.5	Min
Silicon	0.4	Max
Iron	0.05	Max
Copper	0.05	Max
Manganese	0.05	Max
Magnesium	0.05	Max
Others	0.03	Max

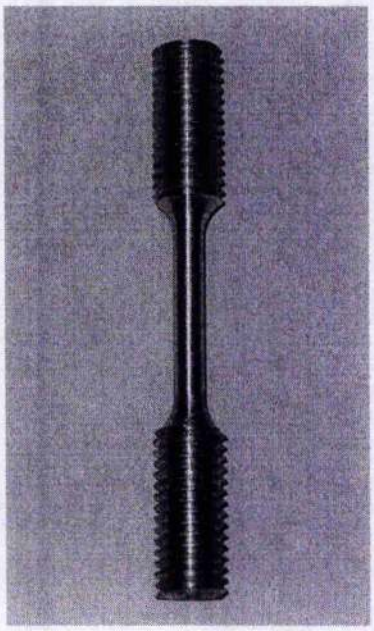

Figure 3.3: Aluminium specimen for tension tests.

3.3 Experimental Rig for Ultrasonic Tension Tests

3.3.1 Design of block horn for ultrasonic tension test

In many applications of high power ultrasonics, horns are used as tools which operate directly on the working surface or as intermediate components to transmit ultrasonic energy from the transducer to another tool element. In the design process for a horn, the main focus is to ensure that the horn operates at the required tuned frequency and has uniform amplitude across its output surface. In order to achieve this, the frequency of operation must be isolated from other modal frequencies in close vicinity [49].

The natural frequencies and mode shapes of the horn are predicted using a finite element (FE) model which is validated using experimental modal analysis, using a 3D laser Doppler vibrometer and LMS data processing software. The combination of FE model and 3D laser measurement has accommodated the need to design an accurate horn with specified vibration mode, uniformity in amplitude on the working surface and excitation frequency.

In the present study, finite element simulations were used to predict the modal frequency and mode shape of the horn. It was reported by Frederick [15] that a conical horn profile can amplify the vibration velocity amplitude on the small cross-section end with minimum stress. Apart from this advantage, this profile is very easy to fabricate, providing a flexible choice in specifying the cross sectional dimensions of both ends of the horn. As a result, this profile has been used as the basic design for FE modelling, and then the horn was fabricated based on the specific dimensions calculated from the FE model, which concentrated on prediction of the horn dimensions so that it can operate in a longitudinal mode with a tuned frequency of 20 kHz.

A three dimensional model was developed to calculate the longitudinal natural frequency and mode shape of the horn using a commercial finite element simulation code, ABAQUS 6.3 (Hibbit, Karlsson & Sorensen, INC). Three dimensional solid quadratic elements were used in the FE model. A natural frequency extraction procedure and steady-state dynamic analysis were applied. The conical horn material, aluminium A6070, is assumed to be homogenous with the following properties;

Young's Modulus 69 GPa, Poisson's ratio 0.33, and density 2700 kg/m^3. An estimate of the horn dimensions was first modelled and then the model was tuned until the longitudinal mode frequency was 20 kHz. Subsequently, to calculate the frequency isolation and the operating vibration velocity amplitude of the tuned horn, steady-state dynamic analysis was applied, and frequency spectrum was derived from the model.

The horn was fabricated from a high grade aluminium cylinder (6070). The predicted conical horn dimensions from the FE model were; length 125 mm, end diameters 70 mm and 45 mm. For experimental validation, the horn was attached to the ultrasonic transducer and mounting structure as shown in Figure 3.4. Experimental modal analysis was carried out using a 3D laser Doppler vibrometer and LMS modal analysis system at an array of points on the surface of the conical horn. The ratio of the vibration velocity to excitation force in the frequency domain is known as the frequency response function (FRF). When the FRF measurements were completed, the LMS software was used to extract the modal parameters. The modal response of the horn at frequencies close to 20 kHz was characterised, as modes appearing at these close frequencies can couple with the tuned longitudinal mode response.

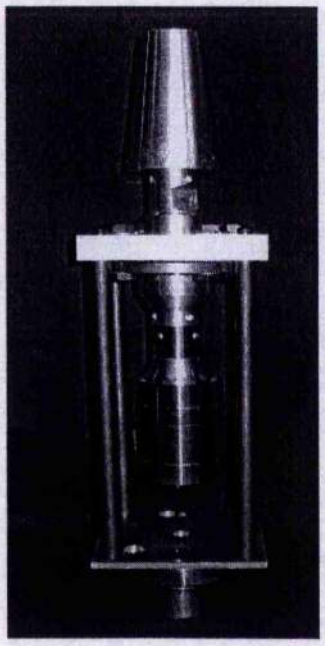

Figure 3.4: Conical horn for ultrasonic tension test attached to ultrasonic system and mounting structure.

The use of numerical method to design the horn was successfully validated when the predicted mode shapes showed a close correlation with modes extracted from the experimental results. Figure 3.5 illustrates the predicted longitudinal mode at the tuned frequency of 20.13 kHz, and the measured mode shape at 20.36 kHz. The mode with the closest frequency to the tuned mode was a flexural mode, which is shown in Figure 3.6. It is worth noting that the experimentally derived response is plotted at the defined measurement points and straight lines are drawn between these points to provide a visual representation of the modal response of the structure.

Figure 3.7 shows the calculated frequency response of a point on the horn top surface. Three components of the response are shown in the figure; y is the longitudinal axis, x and z are orthogonal axes in the plane of the horn top surface. The FE results indicate that the horn has a clear spectrum within 2.5 kHz of the tuned frequency which therefore satisfies the design criterion for an ultrasonic horn to operate with at least 1 kHz frequency isolation of the tuned mode from other non-tuned modes [49].

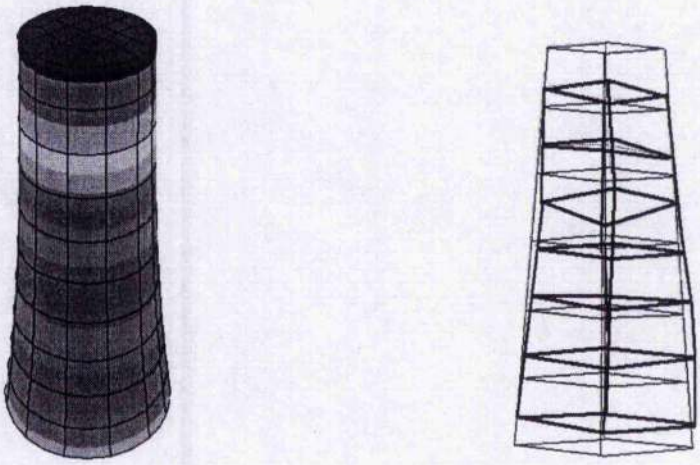

(a) Frequency = 20133 Hz (b) Frequency = 20355 Hz

Figure 3.5: A longitudinal mode shape of conical horn from (a) FE model and (b) experiment.

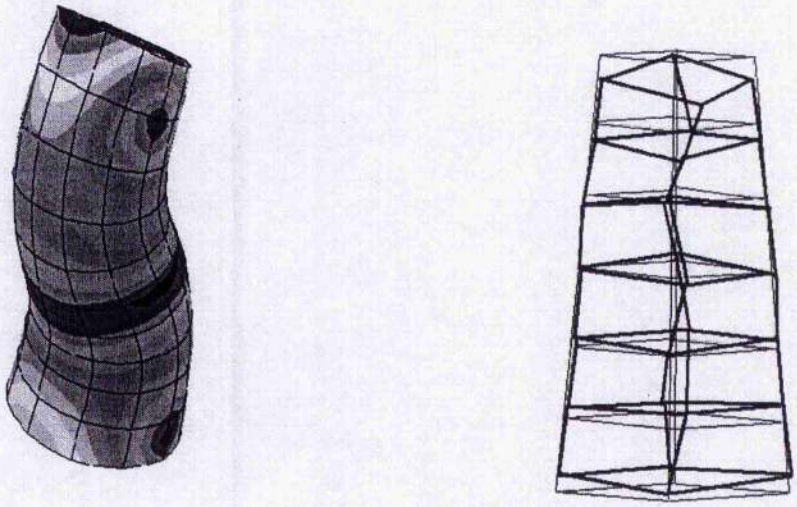

(a) Frequency = 22414 Hz (b) Frequency = 22264 Hz

Figure 3.6: A flexural mode shape of conical horn from (a) FE model and (b) experiment.

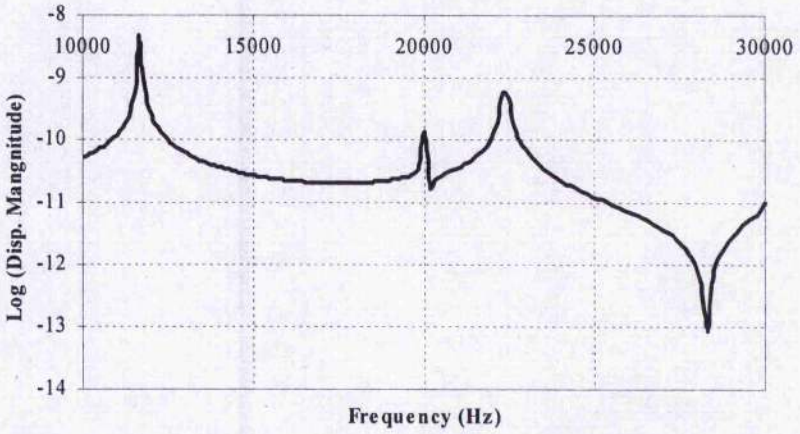

(a) Frequency response in x-direction.

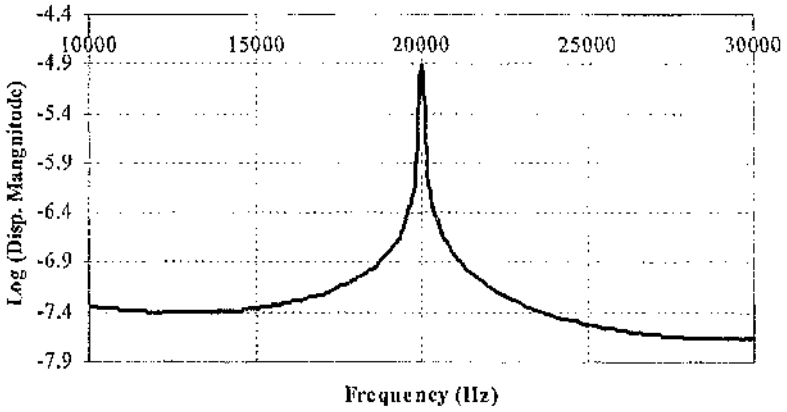

(b) Frequency response in y-direction, longitudinal axis.

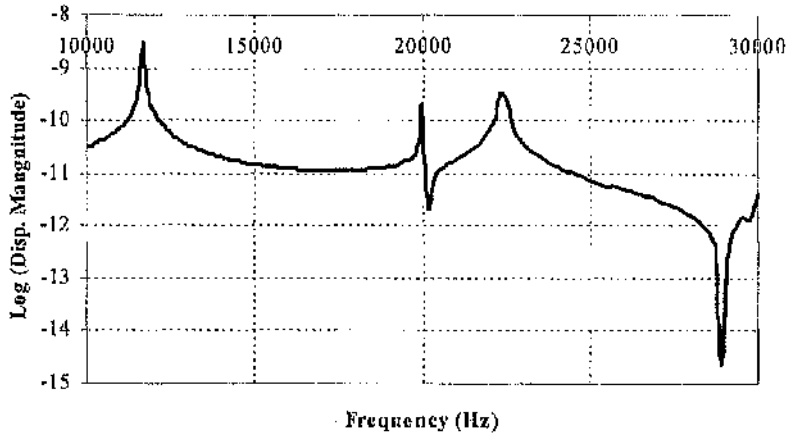

(c) Frequency response in z - direction

Figure 3.7: Calculated frequency response of conical horn working surface.

3.3.2 Ultrasonic system and test equipment

The apparatus for the ultrasonic excitation system for tension testing consists of an ultrasonic generator, transducer, booster and a conical horn. A 1 kW ultrasonic generator was used to deliver a sinusoidal signal of 20 kHz frequency to the piezoelectric transducer, where the electrical signal is converted to mechanical vibration. The mechanical vibration generated by the transducer is then amplified by a booster which is attached between the transducer and the horn. The horn is capable of providing a longitudinal mode vibration with a nominal peak amplitude of 10–12 μm on

the output surface. The ultrasonic system was mounted at the booster via a nodal flange and the flange was supported by four steel columns and clamped on the machine base using bolts, as shown in Figure 3.4.

A piezoelectric transducer was used in the present study. These transducers are widely used in high power ultrasonics applications due to their capability for converting electrical energy into mechanical vibration efficiently and with low losses. The ultrasonic generator operates with a piezoelectric transducer by matching their impedance properties at the 20 kHz operating frequency.

A booster was mounted between the transducer and the conical horn and, in this case, was used as a tuned intermediate component that allows a nodal flange to be mounted for the purpose of structurally mounting the vibrating elements without transmitting vibrations to the mounting structure or damping the horn vibration. Ultrasonic vibrations produced by transducers are usually generated at very low amplitudes and in most cases, the amplitude needs to be amplified to provide operational gain, and this is achieved via a booster. Boosters can also be designed to decrease the vibration amplitude, depending on the requirements of the application and the design of the horn.

The tension experiments were performed using a Lloyds test machine which has a 50 kN loading capability in tension or compression and a maximum cross-head speed of 100 mm/min. The ultrasonic system was set mounted on the base of machine and the tension test specimen was screwed into the horn at one of its ends and into the upper sleeve at its other end. The tests were conducted at a tuned frequency of 20 kHz and a set nominal horn output vibration amplitude of 10 μm. The upper sleeve was connected to the machine cross-head which was set to a constant speed of 5 mm/min. A laser Doppler vibrometer (LDV) was used to measure the vibration response of the working surface of the horn, of the upper sleeve and of the test specimen. A piezoelectric force transducer was attached to the upper sleeve to monitor the static and ultrasonic response of the tension force. The recorded signals were acquired by DataPhysics signal acquisition hardware and software for data processing. A schematic of the ultrasonic tension test set-up is illustrated in Figure 3.8.

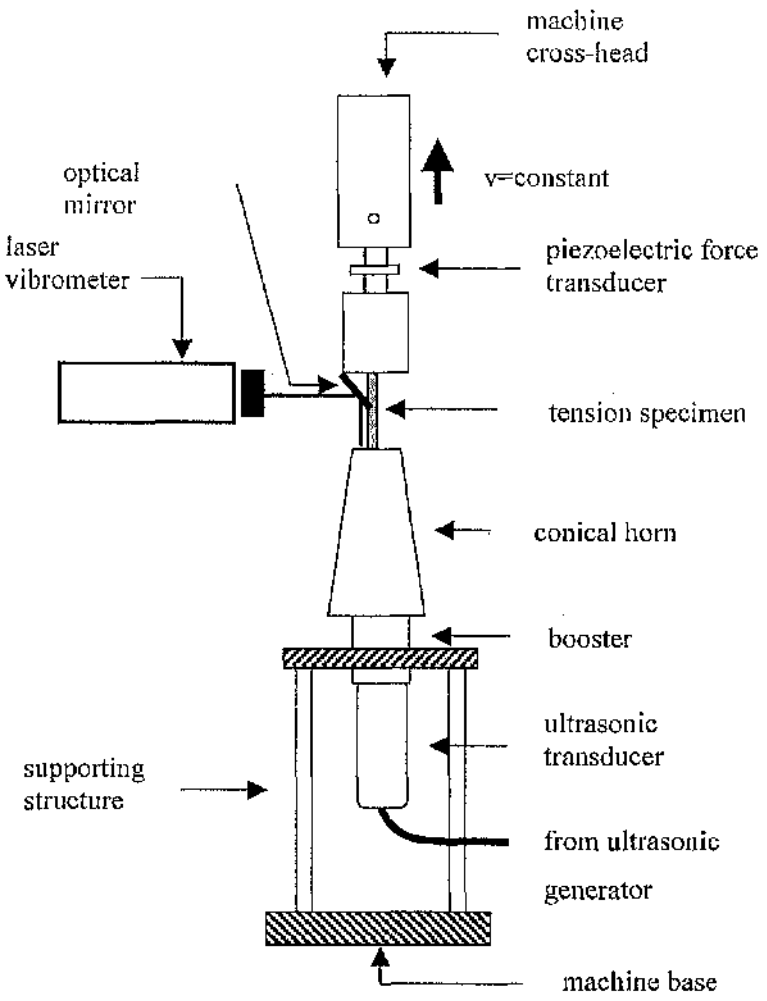

Figure 3.8: Schematic of ultrasonic tension test.

3.3.3 Measurement system

The experimental set-up for the measurements, as shown in Figure 3.9, consists of three main systems which are: (1) amplitude response measurement, provided by a 1D laser Doppler vibrometer (LDV) and 3D LDV, (2) load response measurement for measuring static and ultrasonic load using a Kitsler piezoelectric load cell, and (3) data analysis, provided by DataPhysics data acquisition and dynamic signal processing software, for processing the recorded data from LDV's and load cell.

A 1D-LDV (single beam) consists of an optical head that emits a laser beam and a converter that processes the Doppler frequency of the reflected laser beam. The laser beam is directed onto a vibrating test structure using a focusing device. The back-reflected beam is recombined with the internal reference beam. When the test structure moves, the frequency of the signal beam reflected from the structure is shifted from the original frequency of the emitted laser beam, f_O, due to the Doppler effect. The change in frequency, referred to the Doppler frequency is given by $f_D = 2v / \lambda$, where v is the velocity of the moving structure and λ is the wavelength of the emitted laser beam, $\lambda = 0.633$ μm. The voltage signal converted from recombined beam is proportional to the velocity at which the structure under measurement moves [69].

A 3D-LDV (triple beam) simultaneously measures both in-plane and out-of-plane vibration responses. The system comprises a three channel laser vibrometer controller unit coupled to an optical sensor head containing three independent optical systems, all focused to the same measurement point in front of the lens. The optical head contains the optical components of three independent sensors. Each output laser beam is inclined at a 12° angle with respect to the surface, but from three slightly different directions, separated by 120° in the output plane. The geometry calculation module generates true, v_x, v_y, and v_z (velocity in x-, y- and z-direction respectively) analog outputs in real time.

A single beam LDV can only be used to measure the vibration response normal to the target surface (ie. out-of-plane component) and therefore the beam can be reflected by an optical mirror for measuring vibration at locations where there is no direct line of sight. A 3D-LDV offers simultaneous measurement of the out-of-plane and two orthogonal in-plane components of the target surface vibration response, which can be combined to provide the surface vibration response at each measurement location. The advantages of using laser vibrometer are that the test structure is not affected by the measurement system, due to the non-contact measurement method, and the beam provides a small spot enabling small test structures to be measured. Laser vibrometers offer a high sensitivity and high resolution and preserve accuracy and precision of the measurement data.

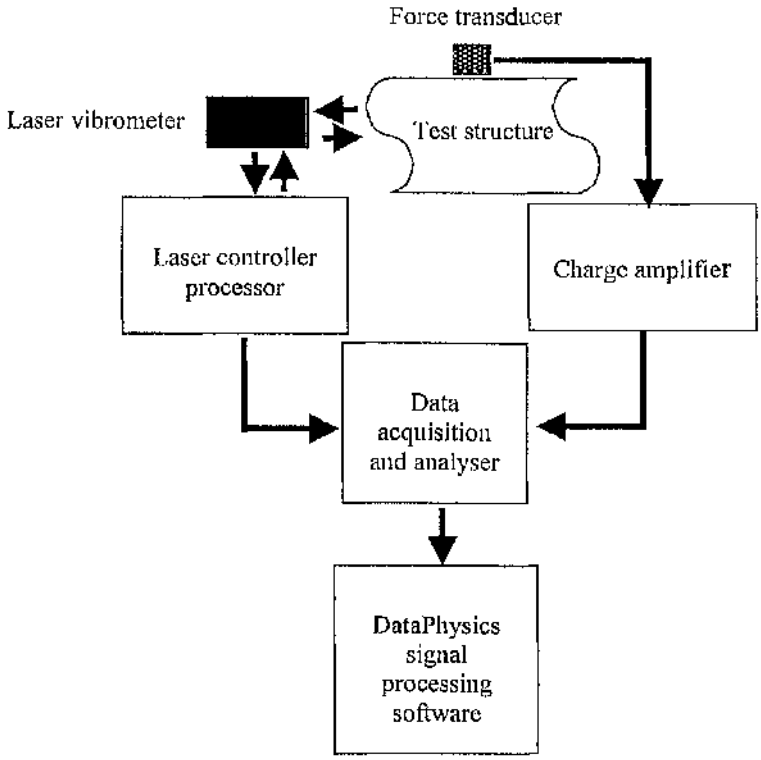

Figure 3.9: Block diagram of experimental measurement system.

A Kistler piezoelectric load cell is used to measure quasi-static and dynamic force responses. The piezoelectric device measuring relies on the crystals produce an electrical output when experiencing a change in force. Quartz transducers, paired with signal conditioners, offer quasi-static and dynamic measuring capability. A charge amplifier is required to convert the charge output to a voltage. The natural frequency of the load cell is 55 kHz, well above the 20 kHz test frequency, and it has a maximum tension or compression load capacity of 10 kN, satisfying the requirements of this study.

DataPhysics (SignalCalc) is a multi-channel dynamic signal analyser which consists of a data acquisition unit accompanied by a portable computer with installed SignalCalc software. The vibration responses from the laser vibrometers and piezoelectric load cell in voltage are channelled into the data acquisition system for processing, analysis and then converting into readable data.

3.4 Static and Ultrasonic Tension Experiments

3.4.1 Test procedure

A series of tension tests was carried out at a constant cross-head speed of 5 mm/min for static and superimposed ultrasonic excitation. In the first test, the specimen was subjected to a static tension force by monitoring the constant cross-head speed, and the test was stopped when the specimen elongated 5 mm. In the ultrasonic tension test, the specimen was initially pulled by a static force. The ultrasonic excitation was applied via the conical horn post-yield during plastic deformation. Two sets of ultrasonic tension tests were conducted. In the first set, the ultrasonic excitation was applied continuously, from the onset of plastic deformation to completion of the test. In the second set, the ultrasonic excitation was applied for 6 seconds and then ultrasonic excitation was discontinued for 6 seconds, continuing to allow the specimen to deform under a static load, and subsequently ultrasonic excitation was applied for a further interval of 12 seconds and then discontinued, with deformation again continuing under a static load. The tension test was completed when the specimen elongated 5 mm. The stress-strain data were then derived from the measured force-displacement data.

3.4.2 Test results

Stress-strain curves from the measured load-displacement data are plotted in Figure 3.10, which compares tension test data from a conventional static test with the data from a test where ultrasonic excitation was applied during plastic deformation. For clarity, during applied ultrasonic excitation the paths of maximum, mean and minimum oscillatory stresses are included in the figure rather than the oscillations. The figure shows that the mean and maximum oscillating stress are significantly reduced from the static stress curve at the onset of ultrasonic excitation and follow a paths nearly parallel to the static stress path.

Figure 3.11 shows the stress-strain curves for a static tension test and for a static-ultrasonic tension test for two intervals of ultrasonic excitation applied during plastic deformation. By comparing Figure 3.10 with Figure 3.11, the two figures can be overlaid, exhibiting exact correspondence between the paths of the maximum, mean and

minimum oscillating stress during the ultrasonic excitation intervals. The figures show the same relationship between oscillating stress amplitude and strain, with maximum, minimum, and mean stress paths parallel to the static stress path. The figures show that mean flow stress is significantly reduced at the onset of ultrasonic excitation and follows an elastic path back to the static stress-strain curve when the ultrasonic excitation ceases. At a strain of 0.087, the mean flow stress is reduced by 23 MPa from the static stress or 27% reduction, and the peak-peak oscillatory stress amplitude is 5 MPa (which depends on the ultrasonic vibration amplitude of the lower platen).

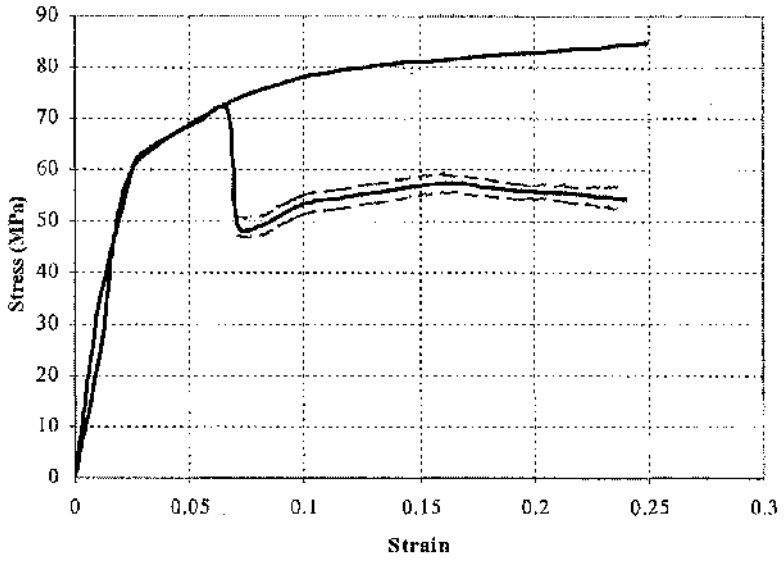

Figure 3.10: Measured static and ultrasonic tension test with ultrasonic excitation applied continuously during plastic deformation, showing: — static and mean stress, ---- path of max. and min. oscillatory stress.

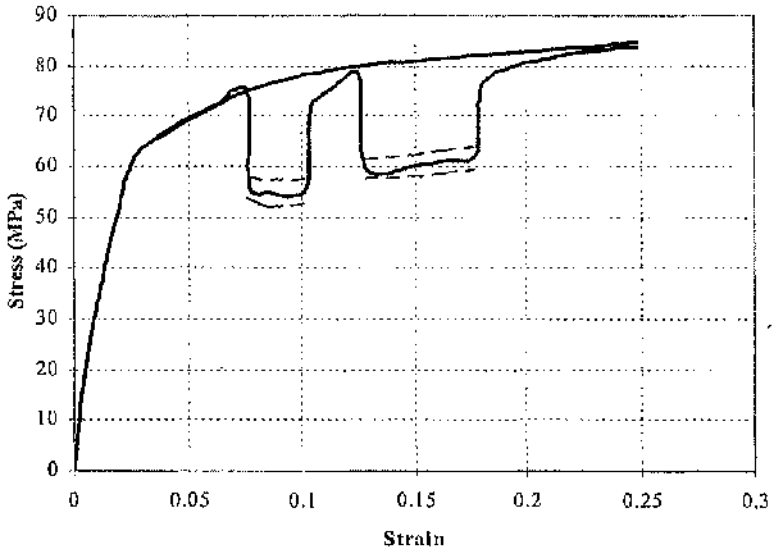

Figure 3.11: Measured static and ultrasonic tension test with two intervals of ultrasonic excitation, showing: — static and mean stress, ----- path of max. and min. oscillatory stress.

In order to assess any response contributions due to machine dynamics, throughout the ultrasonic tension test the displacement amplitude response of the lower horn, upper sleeve and specimen were measured using 1D and 3D LDVs. Figure 3.12 shows the amplitude response of the top surface of the horn, gauge part of the specimen, and the bottom surface of the upper sleeve. For the tension tests reported here, the conical horn was driven at a nominal constant peak amplitude of 10 μm, with the measured response being between 9 and 11 μm during ultrasonic tension. The displacement amplitude response on the upper sleeve and the specimen seem to be consistent with specimen elongation, giving values of 2.5 and 6.5 μm respectively. These measurements confirmed that the ultrasonic system delivered a consistent amplitude throughout the ultrasonic tension experiments.

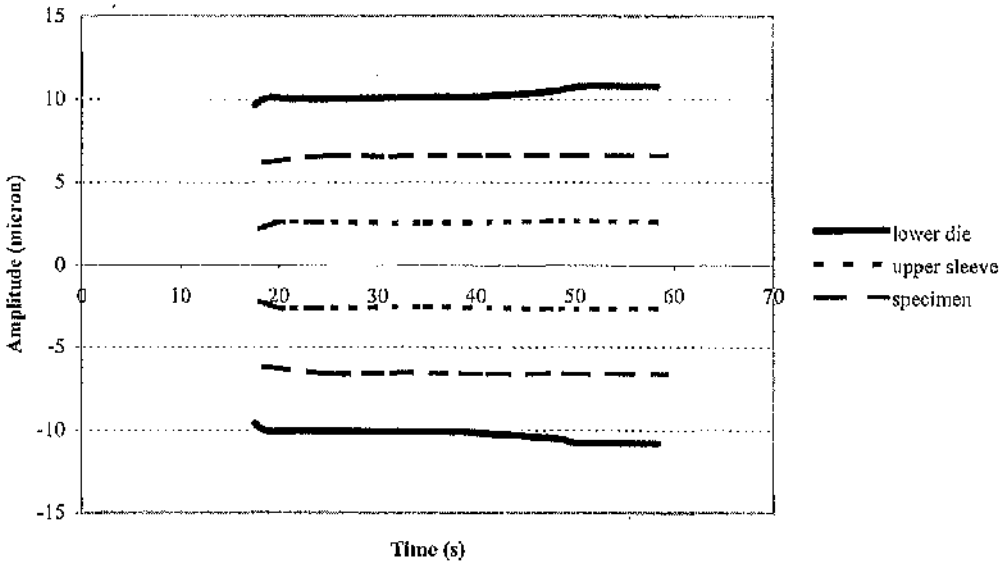

Figure 3.12: Amplitude response measured on lower die, upper sleeve, and specimen during ultrasonic tension test.

The measured stress-strain relationships in part follow the definition of oscillatory stress superposition as described earlier. As in Kirchner's [4] and other studies [3, 69], the path of the mean, maximum, and minimum oscillatory stress is consistent with oscillatory stress superposition in that they are parallel with the static stress curve and the mean stress follows an elastic curve back to the static stress curve when the ultrasonic excitation stops. As the path of the maximum oscillatory stress never exceeds the static stress path, aluminium does not exhibit strain rate dependent material behaviour. However, the data departs from the definition of oscillatory stress superposition in that there is a considerable drop from the static stress curve to the maximum oscillatory stress curve. The experimentally derived stress-strain curves of Figures 3.10 and 3.11 would therefore indicate that the effects of ultrasonic excitation are not only the superposition of an oscillatory stress on a static stress. The advantage of conducting ultrasonic tension tests in this investigation is that the effects of contact, in particular friction effects, are eliminated. Hence, the measured reduction in the maximum oscillatory stress must be attributed to some other phenomenon such as material softening, as suggested in some previous studies [1, 19, 22].

3.4.3 Ultrasonic tension test to failure

In an attempt to investigate the mechanical behaviour of aluminium when a continuous ultrasonic load is applied post-yield until failure, another series of tension tests was conducted. This investigation was concerned with the failure behaviour of specimens subjected to continuous ultrasonic excitation. In the first test, a specimen was subjected to a static tension force until failure. In the second test, a specimen was statically pulled, then during plastic deformation ultrasonic excitation was applied continuously until failure. The stress-strain relationships derived from the measured load-displacement data are shown in Figure 3.13.

By comparing the stress-strain relationships for ultrasonic tension with static tension, there are differences for both the flow stresses and breaking points. As can be seen in Figure 3.13, ultrasonic vibration changes the breaking point, significantly reducing the specimen elongation during plastic deformation. These experimental results agree with some previous investigations [29, 99] which reported that the ultrasonic load reduced the mechanical properties of the tested metals. Nerubai [99] attempted to clarify these reduced mechanical properties using dislocation theory. According to Nerubai, an ultrasonic load induces the formation of a high concentration of dislocations and vacancies in the deforming material, leading to the formation of micro cracks, then failure.

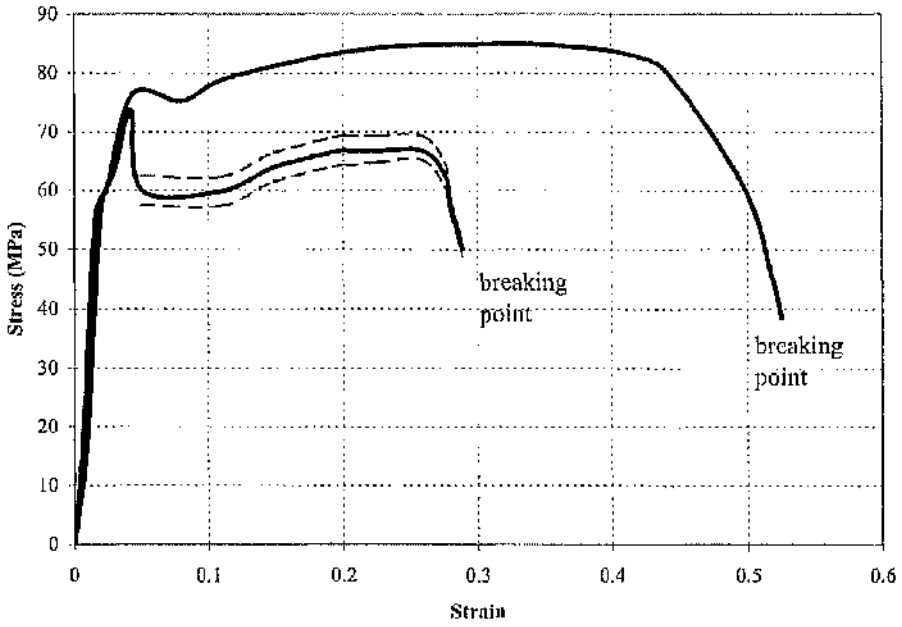

Figure 3.13: Failure of aluminium for static and ultrasonic tension test, showing: — static and mean stress and, ---- paths of max. and min. oscillatory stress.

3.5 Finite Element Modelling

Theoretical models of most metal forming operations are concerned with the prediction of stresses produced during the deformation process and, subsequently, the forces that must be applied to induce plastic flow. In the present study, the numerical method is used to investigate the numerical effect of applied ultrasonic excitation during static tension deformation of aluminium.

In this numerical study, the specimen is deformed by controlling the upper sleeve to a constant velocity, while the lower die, or conical horn, is fixed during intervals of static deformation. A sinusoidal ultrasonic excitation is superimposed on the static load by vibrating the lower die with an amplitude A and frequency ω. The displacement of the lower sleeve is therefore defined by $X_L = A\cos(\omega t)$.

Aluminium is used as the metal specimen. The material properties of aluminium, derived from the previous static tension test, were: Young modulus 69 GPa, yield stress

60 MPa and Poisson's ratio 0.33. Classical metal plasticity was used to define the plastic strain by using the following equation [100],

$$\varepsilon^{pl} = \varepsilon^{t} - \varepsilon^{el} = \varepsilon^{t} - \frac{\sigma}{E} \tag{3.1}$$

where, ε^{pl} is true plastic stress, ε^{t} is true total strain, ε^{el} is true elastic strain, σ is true stress, and E is Young's Modulus. The material is initially isotropic, homogeneous and incompressible such that the volume of each element of the model remains constant. The behaviour of aluminium is treated as elastic-plastic with low strain hardening. The material was deformed under steady-state conditions at room temperature and no temperature effects were induced.

In the numerical analysis, the tension simulation was carried out using a commercial finite element code, ABAQUS, with implicit solution. Half of the specimen was meshed using 2D axi-symmetric 4-node elements. The upper and lower sleeves were assumed to be rigid bodies, modelled as an analytically rigid surface. Figure 3.14 shows the original and deformed meshes of the tension model. The experimental conditions were modelled by setting a constant speed of the upper platen at 5 mm/min. Post-yield, an ultrasonic excitation was applied to the lower sleeve during plastic deformation, in the form of a peak vibration displacement amplitude of 10 μm at a frequency of 20 kHz. To allow for manageable computational time, whilst ensuring that the effects of ultrasonic oscillation could be evaluated, the ultrasonic excitation was applied for much shorter time intervals in the FE models than in the experiments.

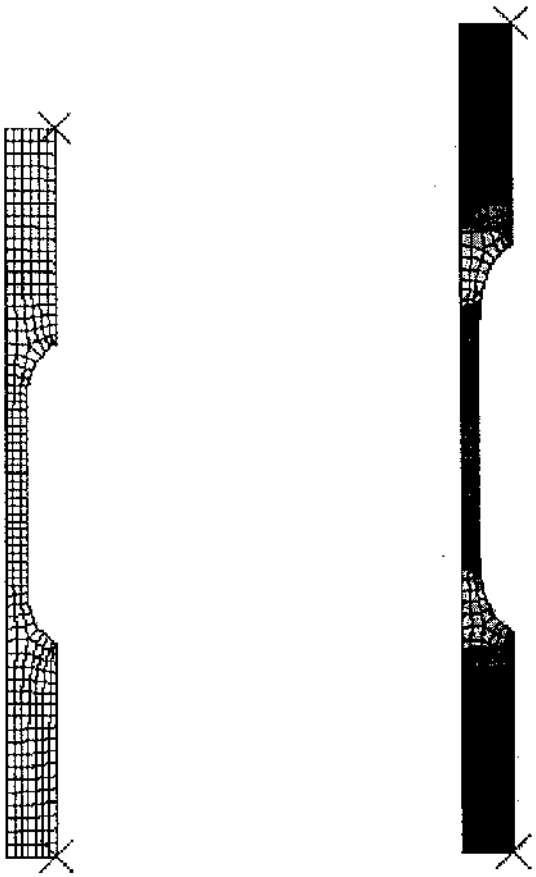

Figure 3.14: Original (left) and deformed mesh profiles for tension specimen FE model.

3.6 Discussion of FE Model Results and Effects of Material Properties

3.6.1 Material verification

First, in order to verify the material properties data used in the tension FE models, stress-strain data were derived from a static tension model, and subsequently included along with the measured stress-strain data from the previous static tension test. Figure 3.15 shows the stress-strain relationships for the static tension model and for the static tension test. For the defined material properties, a close agreement is achieved between experimental and FE stress-strain data.

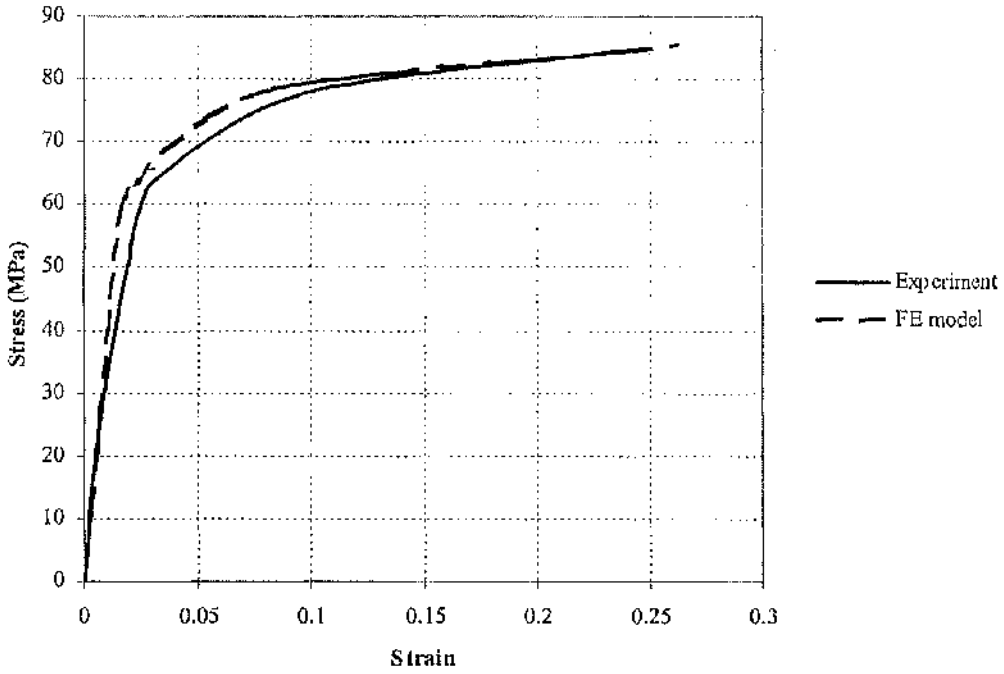

Figure 3.15: Validation of FE model for tension test.

3.6.2 Oscillatory stress-strain data

When an interval of ultrasonic vibration is superimposed on the lower die during plastic deformation, the FE model predicts stress-superposition as shown in Figure 3.16, where the path of the maximum oscillatory stress follows the path of the static stress, with the stress amplitude of the oscillatory stress dependent on the amplitude of the ultrasonic vibration. However, the experimental data departs from this ideal. Although the same oscillatory stress amplitude, of about 5 MPa, is derived from both the experimental and FE data, the experimentally derived stress-strain relationship in Figure 3.11 shows a reduction in the maximum, mean and minimum oscillatory stress such that the path of the maximum stress no longer follows the static stress-strain curve.

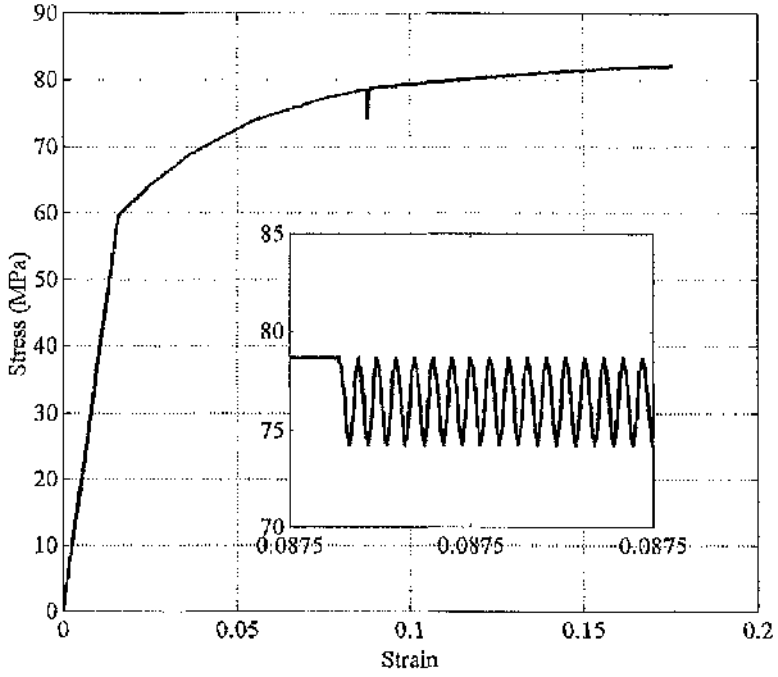

Figure 3.16: FE predicted oscillatory stress superposition in ultrasonic tension modelling, inset shows expanded view of oscillating stress.

3.6.3 Adjusting material properties

By adjusting the finite element model of the tension test, it is possible to conduct a numerical investigation into the effects on the stress-strain relationship of changing material parameters. It is hoped that this can provide some explanations of the significant reductions in measured mean oscillatory stress reported in this and other previous studies.

An explanation, proposed by some authors, is that there is a temporary softening of material properties during ultrasonic excitation of the lower platen [1, 19, 22]. This explanation has largely been rebuffed in the literature [5, 14, 33], partly because it is known that there is no significant increase in specimen bulk temperature during ultrasonic compression tests, and also because it is known that significant absorption of ultrasonic energy at dislocation sites can only occur at 100 MHz frequencies and not in the low kHz ultrasonic range [2]. However, it is clear from the experimental data, that the tension test does not satisfy the description of oscillatory stress superposition and,

since there is no contact friction effect in the tension test data, the effects of a temporary change in materials properties is investigated in the tension test FE simulation.

There is a significant reduction in the maximum, as well as the mean and minimum oscillatory stress during ultrasonic excitation measured in the tension tests and it is clear that this reduction is not explainable in terms of the classic description of oscillatory stress superposition. It is proposed, therefore, that the material is temporarily softened by the ultrasonic excitation, causing a drop in the maximum oscillatory stress and the path of the mean oscillatory stress follows an elastic recovery path back to the static stress path once the ultrasonic excitation is discontinued. It is proposed that the softer plastic properties of the material can be simulated by a stress-strain relationship derived from the path of the measured mean stress path during an ultrasonic tension test. Hence, the softened material properties for input to the FE model have been calculated from this measured mean oscillatory stress data.

Figures 3.17 shows the FE predicted stress-strain relationships for the original and softened material properties. What is observable in the figure is that the oscillatory stress during the interval of ultrasonic excitation of the lower die closely simulates the oscillatory stress measured in the ultrasonic tension tests. Figure 3.18 shows the stress-strain relationship calculated by modelling the static tension test as having the original material properties for aluminium, then adjusting the material properties to the new softened material during superimposed ultrasonic excitation. From this figure, at a strain of 0.0877 the reduction in mean flow stress is 23 MPa and the peak-to-peak oscillatory stress amplitude is 5.5 MPa. This adjustment to the model has allowed close correlation to be achieved with the experimental data, which exhibited a reduction in mean flow stress of 23 MPa and oscillatory stress amplitude of 5 MPa.

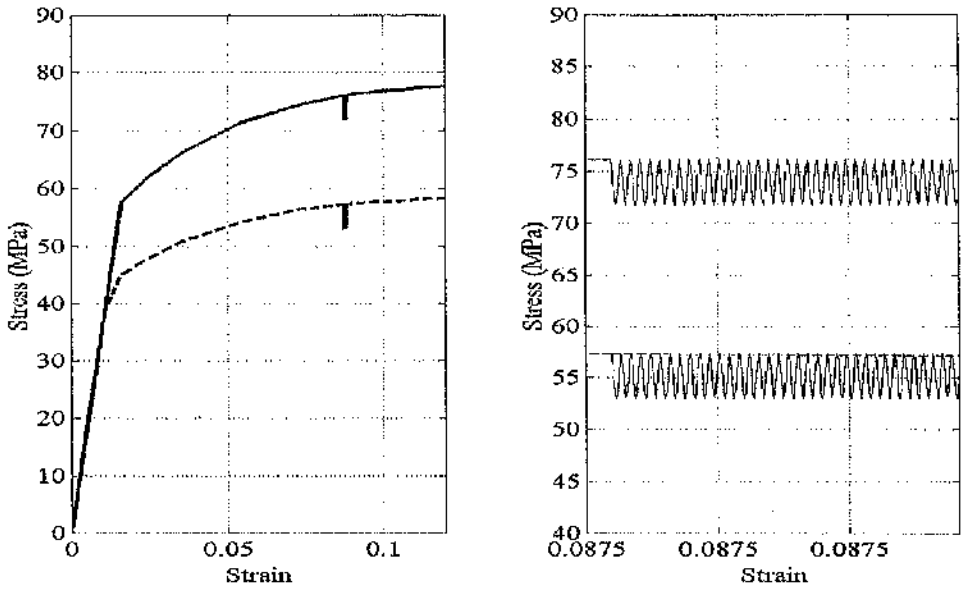

(a) (b)

Figure 3.17: (a) Tension test FE predicted stress-strain relationship showing a short interval of superimposed ultrasonic excitation for: — original material properties, and ----- softened material properties, (b) expanded view of oscillatory stress.

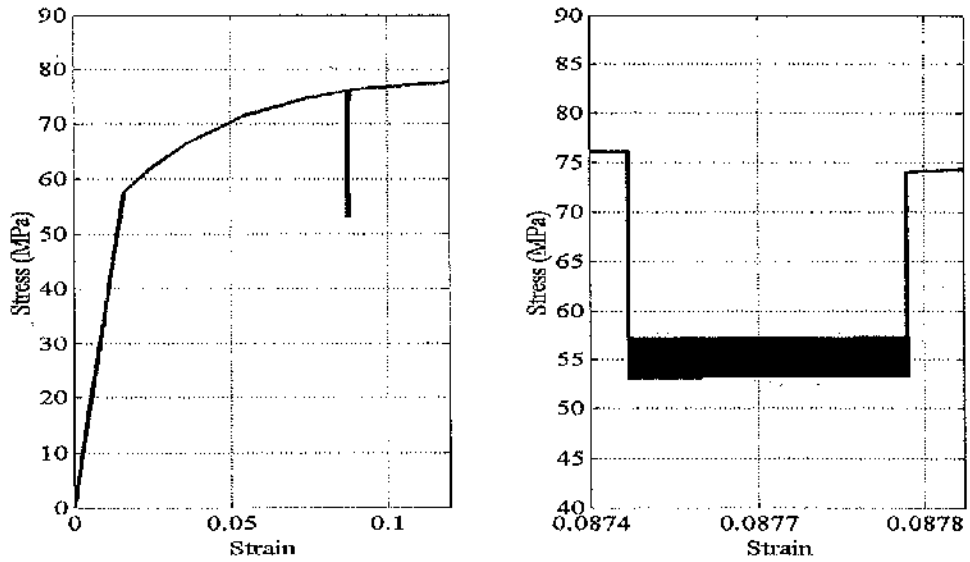

(a) (b)

Figure 3.18: (a) FE predicted stress-strain relationship showing the original material properties during static tension and softened material properties during superimposed ultrasonic vibration, (b) expanded view of oscillatory stress.

3.7 Conclusions

An experimental set-up for static and ultrasonic tension test experiments has been successfully designed, using finite element models to assist with the design and tuning of the customised ultrasonic horn. By Combining FE model predictions of modal parameters with experimental modal analysis, an ultrasonic horn was designed that met the requirements of the experiments to successfully deliver a constant longitudinal mode displacement amplitude of 10 μm at the output surface at a tuned frequency of 20 kHz.

Tension experiments have been carried out using the designed ultrasonic test apparatus. A series of static-ultrasonic tension experiments have been performed to investigate the effects of applied ultrasonic excitation during plastic deformation. Stress-strain relationships were derived from the measured load-displacement data.

By superimposing short intervals of ultrasonic excitation on a static load during steady-state plastic deformation, the flow stress was significantly reduced, both in terms of the mean flow stress and also in terms of a reduction in the path of the maximum oscillatory stress from the static stress path. This signifies a departure from the classical description of oscillatory stress superposition. Subsequently, when the ultrasonic excitation is discontinued, the stress returns on an elastic path to the original static stress-strain curve.

A series of FE models have been developed to predict the numerical effects of applied ultrasonic excitation during plastic deformation in a tension test. The material properties used in the FE models were adjusted in order to simulate the experimental results of an apparent softening of the material properties due to applied ultrasonic excitation during plastic deformation. The numerical data for the adjusted material properties model showed a very close agreement with the results of static-ultrasonic tension experiments.

It is now clear that the measurements presented in this current study require the whole issue of the effects of ultrasonic vibration on bulk properties of metals to be readdressed and that it is not sufficient to explain the effects only in terms of stress superposition. Although it is not a part of this study, the results make it clear that it is necessary to understand the way ultrasonic energy is absorbed by aluminium in terms of its

microstructure in order to fully explain the benefits for a range of metal forming processes.

The advantage of conducting tension tests was that surface effects were not present to influence the stress-strain relationships and therefore surface effects can be eliminated as a complete explanation of ultrasonic vibration effects in metal forming processes. However, it is also possible that surface effects play a role in ultrasonic metal forming. Therefore, compression tests will be performed in an attempt to investigate the surface effects under ultrasonic deformation.

CHAPTER 4

STATIC AND ULTRASONIC RING COMPRESSION TESTS AND SURFACE ANALYSIS

4.1 Introduction

In metal forming processes, frictional forces are generated at the interface between the tool and deforming material by virtue of the workpiece surface extension. Friction affects the deformation load, product surface quality, internal structure, tools and die wear characteristics and material flow. Qualitative and quantitative characterisations of friction phenomena provide an effective method to optimise design and processing parameters in metal forming.

Many previous studies [6, 8, 9] have suggested that the application of ultrasonic excitation in metal forming processes reduces friction at the die-specimen interface. Based on indirect measurements, these reports concluded that the reduction in friction in metal forming is related to the measured reduction in forming force.

The most accepted quantitative model to characterise friction is the Coulomb law of friction, where a constant parameter of coefficient of friction, μ is introduced. In the Coulomb law of friction, μ is defined by the ratio of the frictional shear stress to the normal stress as given in equation 2.11. Among the methods to measure the coefficient of friction in metal forming operations, the ring compression test has the best capability for quantitative measurement of friction under normal deformation processes. Ring compression tests were initially introduced by Kunogi [64] and later improved and presented in a usable way by Male and Cockcroft [65]. The specific curves generated by Male and Cockcroft were later known as friction calibration curves (FCC).

The ring compression test involves a simple forging operation on a flat ring-shaped specimen. The change in ring diameters due to a given amount of compression in the thickness direction is related to the interface friction condition. If there is zero friction, the ring would deform in the same way as a solid disk, with each point flowing radially outwards at a rate proportional to its distance from the centre. For low interface friction, material flows outwards at a lower rate for the same degree of compression, the external and internal diameters of the ring are therefore smaller than for zero friction. If there is high friction at the interface, with the same amount of compression, the material flow inwards towards the centre is higher than the material flow outwards. For a high interface friction, the external and internal diameters of the ring are smaller. Therefore, for a given percentage of height reduction during compression tests, the corresponding measurement of the internal diameter of the test specimen provides quantitative knowledge of the magnitude of the friction coefficient at the interface of the specimen and die.

The advantages of applying a ring compression test to evaluate the friction coefficient are; no direct measurement of force is required and no yield strength value of the deforming material are needed, therefore the difficulties related to the measurement of those parameters can be eliminated. Also, correlation of changes in internal diameter with numerical values of friction can be obtained either by independent calibration, or by the application of available theoretical analysis [82].

In an attempt to correlate the changes in internal diameter of ring specimens during compression, a few theoretical approaches, such as upper bound method, stress analysis approach and finite element (FE) method, have been proposed. Among these approaches, the FE method is the most commonly used to generate friction calibration data because of its ability to include material properties [84] and different temperature conditions [85] which were not accounted for in the classical friction calibration curves generated by Male and Cockroft [65].

The aim of the present study is to estimate coefficients of friction under different lubrication conditions by employing the ring compression test technique. The friction curves are generated by relating the percentage reduction in the internal diameter of the ring specimen to its height reduction. The coefficients of friction can be estimated by

matching the experimental friction curves with the friction calibration curves generated using FE models. The estimated friction coefficient values from the ring compression tests are then used in the FE models of compression tests in the following chapter. Also by using this technique, the coefficients of friction, μ, for specimens being compressed under static, longitudinal and radial ultrasonic excitation under different interface conditions are estimated

It has been established that the friction behaviour of a contact surface significantly depends on its roughness, texture, and integrity. Thus, the characterisation of the deformed specimen surfaces under static and ultrasonic compression provides a useful indicator for friction during static and ultrasonic metal forming.

4.2 Specimens and Lubricants

Soft aluminium grade (A1050) specimens were used in ring compression tests. The properties of aluminium A1050 have been discussed in Chapter 3. The ring specimens were machined from the same batch aluminium bar as previously used in tension experiments (Chapter 3) to provide samples of 12 mm external diameter, 6 mm internal diameter, and 4 mm thickness, which follows the common ring geometry ratio 6:3:2. All specimen surfaces were polished using a high-grade abrasive paper (grit 1200) to provide a uniform surface roughness. Figure 4.1 shows a ring compression test specimen.

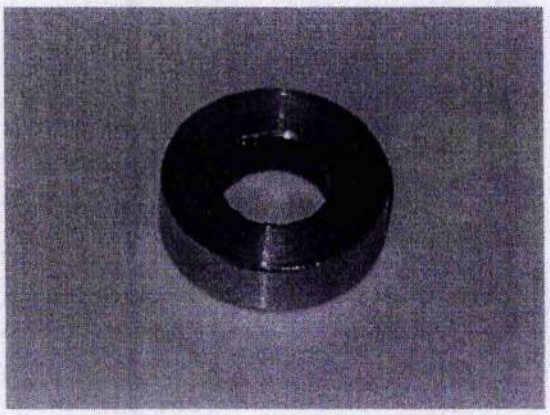

Figure 4.1: Ring compression test specimen.

Lubricants are widely used in metal forming operations. The main purposes of applying lubricants are to separate workpiece and tool surfaces, to reduce interface friction, to ease metal flow into the required shape, and to increase tool life. In the current study, lubricants were used to provide different interface conditions during static and ultrasonic deformation processes. Each lubricant has a specific coefficient of friction and, therefore, various friction coefficients can be obtained by applying a variety of lubricants at the interfaces. Furthermore, the effects of applying ultrasonic excitation during metal forming under different friction coefficients can be experimentally or numerically investigated.

In the present study, five different lubrication conditions were selected to investigate the effects of friction in a ring compression test: dry surface, chemically pure oleic acid, Lubrodal, Molyslip, and a thin soft solid film of PTFE (polytetrafluoroethylene). Prior to each test, the specimen and platen surfaces were cleaned and dried in air. Oleic acid, Lubrodal and Molyslip were brushed onto the surfaces, and a dry film of PTFE was prepared by spraying the suspension onto the surfaces and drying in air. The properties and application methods for the lubricants is shown in Table 4.1.

Table 4.1: Chemical and physical properties of lubricants.

Lubricant	**Content**	**Viscosity $Kgm^{-1}s^{-1}$**	**Application method**	**Nature of lubricant**
Dry	—	—	Polish and clean with methanol	—
Oleic acid	70% pure oleic acid	0.065	Spread with brush	Thick solution
Lubrodal	Polymer and siloxane emulsion	0.05	Spread with brush	Water soluble, thin solution
Molyslip	Lubricating oil, molybdenum disulphide (MoS_2) and graphite	—	Spread with brush	Grease or paste
PTFE (Teflon)	Polytetrafluoroethelene (PTFE)	—	Sprayed from aerosol can	Soft film coating

4.3 Experimental Set-up for Static and Ultrasonic Ring Compression Tests

The design of the experiment for ring compression tests was based on the upsetting of a specimen between two parallel dies. A Lloyds test machine was used for these experiments. The upper die was connected to the machine cross-head which is capable of delivering a constant velocity up to 50 mm/min.

A series of ring compression experiments was conducted. Firstly, aluminium ring specimens were compressed under static load between lower and upper platens with different lubrication conditions. The platens were fabricated from a high grade aluminium plate (H15), giving 50 x 50 mm in square and thickness 12 mm. The working surfaces of the platens were machined to a smooth texture, and polished by fine abrasive paper (grit 1200) to obtain a uniform surface finish.

In the second series of tests, a longitudinal ultrasonic (LU) vibration was applied to the lower platen via a double slotted block horn during the compression process. A longitudinal mode horn is used to deliver vibrations normal to the plane of the ring specimen surface. The block horn was specially designed for compression test applications. The horn is cubic and double slotted in the two transverse axes. It is made of aluminium (grade H15) and is a tuned half-wavelength giving a longitudinal mode of vibration at 20 kHz. The characterisation process of modal behaviour of the horn was carried out previously [11] using experimental modal analysis and FE simulation. Figure 4.2 shows the double slotted block horn attached to the ultrasonic transducer and mounting arrangement used in the LU ring compression tests.

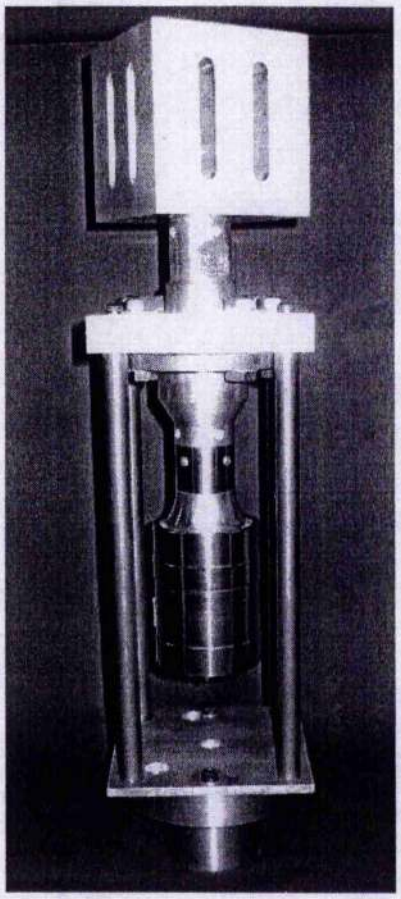

Figure 4.2: Double slotted block horn attached to the ultrasonic transducer.

For the third series of the experiments, a radial-mode ultrasonic (RU) vibration was applied to the lower platen during the compression test. A tuned radial-mode horn is used to deliver oscillations in the plane of the ring surface. The radial-mode horn is a thick cylinder which is tuned to its fundamental radial mode at 20 kHz, with a tuned clamping flange, and is based on the design of Lucas and Chapman [51]. Characterising the modal behaviour of the horn was achieved by validating finite element models by experimental modal analysis. The horn was designed using FE simulations to tune the radial mode at 20 kHz. The fabricated horn was then tested and tuned using experimental modal analysis. Figure 4.3 shows the radial horn, with the ultrasonic transducer attached, and the structural mounting via the tuned clamping flange.

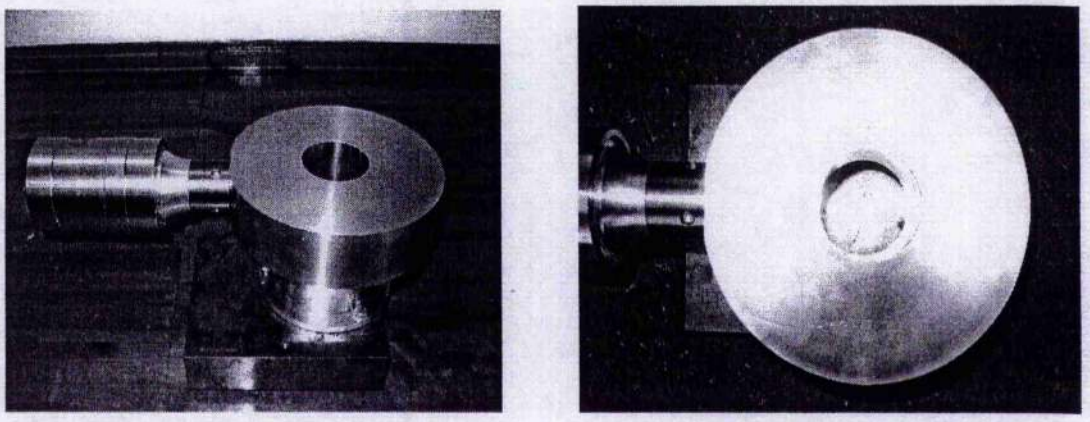

(a) radial horn (b) working surface

Figure 4.3: Radial horn with transducer, attached to a steel plate via a clamping flange.

The whole ultrasonic system consists of an ultrasonic generator, transducer, booster and either the double slotted block horn or the radial-mode horn. The generator delivers a sinusoidal wave of 20 kHz frequency to the transducer where the electrical energy is converted to mechanical vibrations at the same frequency. The working principle of the ultrasonic components comprising the ultrasonic system has been detailed in Chapter 3. For longitudinal ultrasonic excitation, the ultrasonic transducer and the double slotted block horn are attached to a booster through threaded studs. The structural element supporting the ultrasonic system within the Lloyds test machine consists of four steel columns and a plate. The booster is secured to the columns and base plate through a nodal flange to minimise vibration transmission between different parts of the test rig. For radial excitation, the ultrasonic excitation is generated by a transducer which is attached to the thick cylinder using a threaded stud. The horn is secured on a steel plate through a nodal flange on the tuned clamping flange. Figure 4.4 shows a schematic of the experimental set-up for radial ultrasonic ring tests.

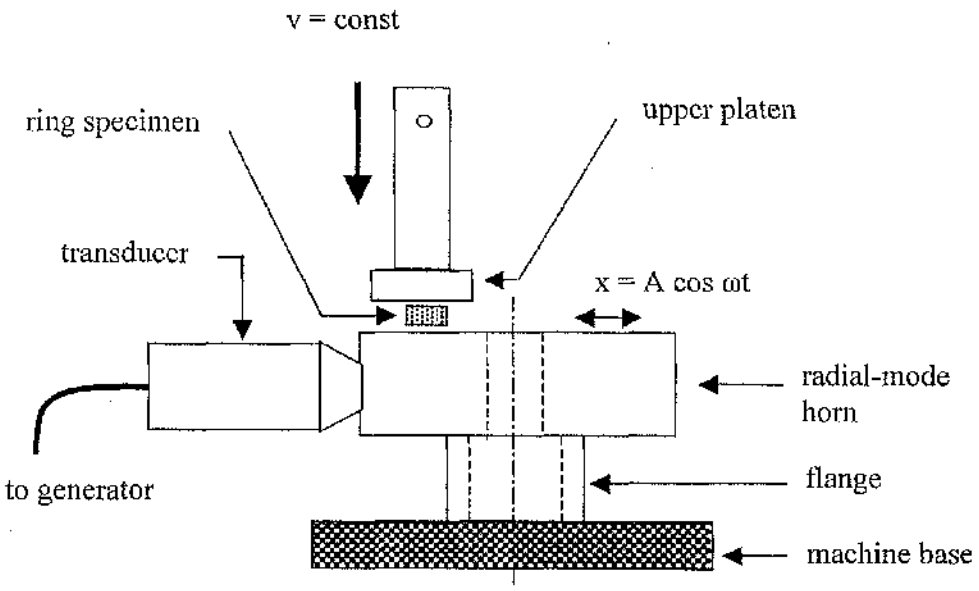

Figure 4.4: Schematic of radial ultrasonic ring compression tests.

Prior to each compression test, the working surface of the ultrasonic horns and upper platen were polished using fine abrasive paper (grit 1200) and cleaned with methanol solution. The surfaces were allowed to dry in air.

4.4 Experimental Procedure

Ring tests were performed at a constant cross-head speed of 5mm/min under dry and lubricated surface conditions. After each specimen reached approximately 0.8 mm reduction in height, the internal diameter of the ring was recorded. The compression was repeated and lubricant was applied to the surfaces prior to each stage of compression. The internal ring diameter and height reduction were recorded in stages until the ring specimen reached approximately 60% of it original height. Measurement of the internal diameter of the compressed ring specimen provided knowledge about the coefficient of friction at the die and specimen interface. The friction curves were generated by relating the percentage of internal diameter reduction to the percentage of reduction in height of the ring specimen.

Longitudinal ultrasonic (LU) ring tests were also performed using the same procedure but, after the specimens reached plastic flow, LU oscillations of the lower platen (via

the double slotted block horn) at 20 kHz and a nominal peak amplitude of 10 μm were superimposed on the static load for the entire interval of each compression stage.

The effects on friction under radial-mode ultrasonic vibration were also investigated. The ring tests were carried out using the same procedure as in the LU ring tests. The radial ultrasonic (RU) excitation was generated by the radial horn giving a peak displacement amplitude of 4 μm at 20 kHz in the plane of the ring surface. The RU oscillations were superimposed on the static load for entire interval of each compression stage.

The coefficients of friction were estimated by comparing the friction curves generated from experimental measurements with the friction calibration curves which were reproduced from FE model data.

4.5 Finite Element Model

Finite element simulations were developed using a commercial finite element code, ABAQUS, with implicit solution. Half of the ring specimen was meshed using 2D axi-symmetric 4-node elements. In this model the platens were assumed to be rigid bodies, modelled by an analytical rigid surface. Figure 4.5 shows the mesh for the ring compression model. The material properties of aluminium, derived from prior compression tests, were; Young's modulus 69 GPa, yield stress 60 MPa, and Poisson's ratio 0.33. The friction calibration curves (FCC) were constructed by relating the percentage of internal diameter reduction to the percentage of height reduction of the ring specimen. Each friction coefficient is represented by a unique friction calibration curve.

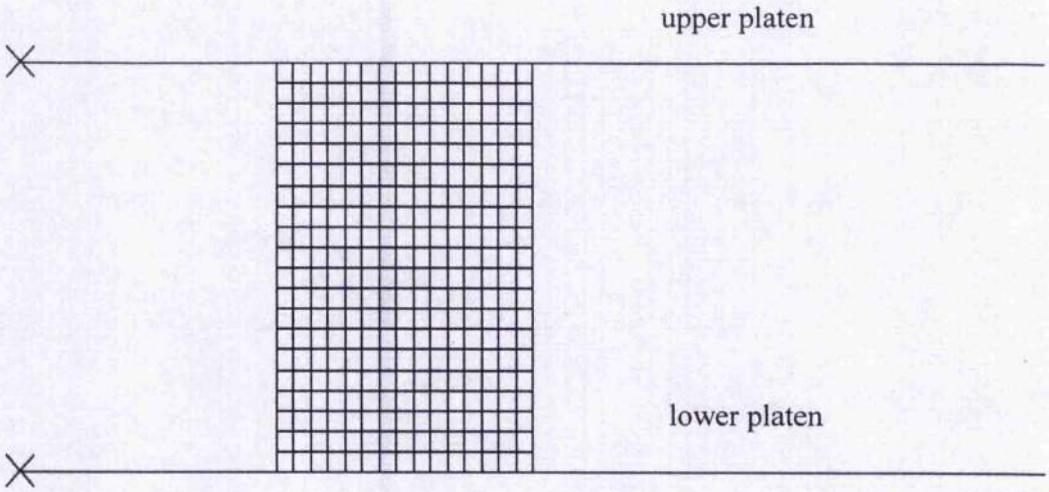

Figure 4.5: Initial mesh for ring compression model.

4.6 Friction Calibration Curves and Discussion

Figure 4.6 shows the deformed ring specimens under different lubrication conditions. For a highly lubricated surface, Figure 4.6 (a), the material flows outwards during the compression process, giving a large internal diameter of the ring specimen. On the other hand, for a higher value of μ, Figure 4.6 (c) shows that the material flows inwards and consequently the internal diameter of the ring decreases.

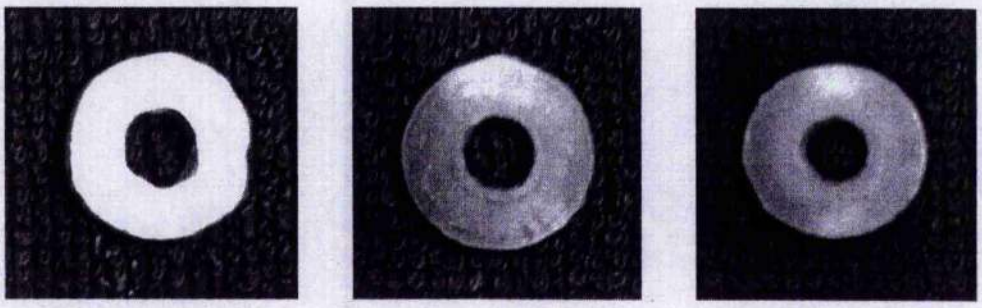

(a) PTFE (b) oleic acid (c) dry surface

Figure 4.6: Ring specimens deformed under different lubrication conditions.

Similar results were also obtained in the FE analysis (Figure 4.7), where the material flow is more towards the centre of the ring as the friction coefficient increases. The phenomenon of ring compression under high friction conditions is complex and the material flow is not obvious during the experiment. However, by implementing FE methods, the flow of material during compression can be modelled. Figure 4.7 shows the simulation results of the bulging process of deformed material under different friction coefficients for ring compression tests. At a high friction coefficient value, the original surfaces in contact with the dies tend to slide and the free surfaces start to bulge when a certain amount of deformation is imposed. When sufficient bulging takes place, material originally at the free surface comes into contact with the dies and adds to the area of the material tending to slide. Stick and slip phenomena during deformation depend on the frictional and geometry conditions.

It is also difficult to determine the diameter of the neutral circle, that separates the material flow inwards to the ring centre, with the material flow outwards, during a compression test [65]. However, by using an FE model, the neutral circle of the ring can be tracked. The FE model predicts that the location of the neutral circle depends on the coefficient of friction, as can be seen in Figure 4.7.

(a) Coefficient of friction, $\mu = 0$

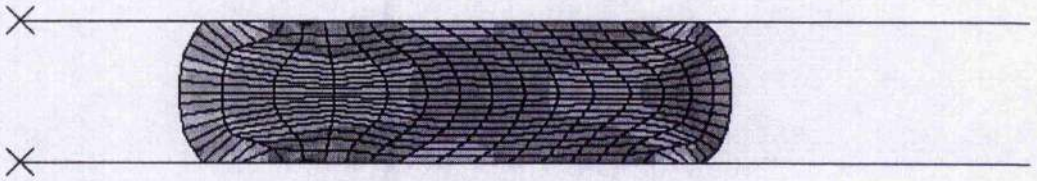

(b) Coefficient of friction, $\mu = 0.15$

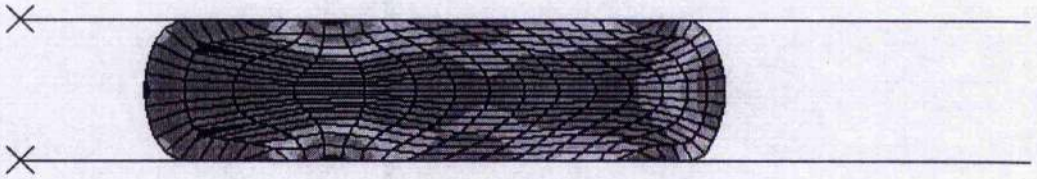

(c) Coefficient of friction, $\mu = 0.20$

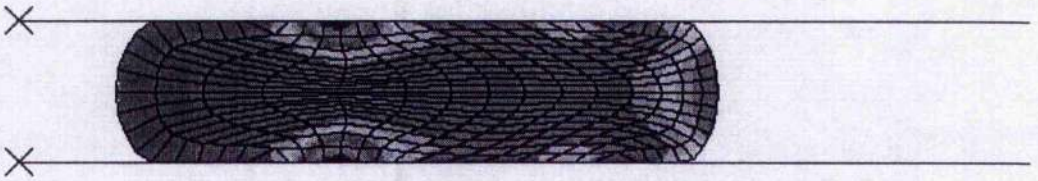

(d) Coefficient of friction, $\mu = 0.25$

Figure 4.7: Deformation profiles of ring specimens using FE models for different interface friction coefficients.

Friction calibration curves were generated from FE model data and data from the ring experiments were incorporated in the FCC, Figure 4.8. For static ring tests, a dry surface provides the highest coefficient of friction of 0.25, followed by oleic acid at 0.13, Lubrodal at 0.1, with PTFE and Molyslip demonstrating the same coefficient value of approximately 0.07.

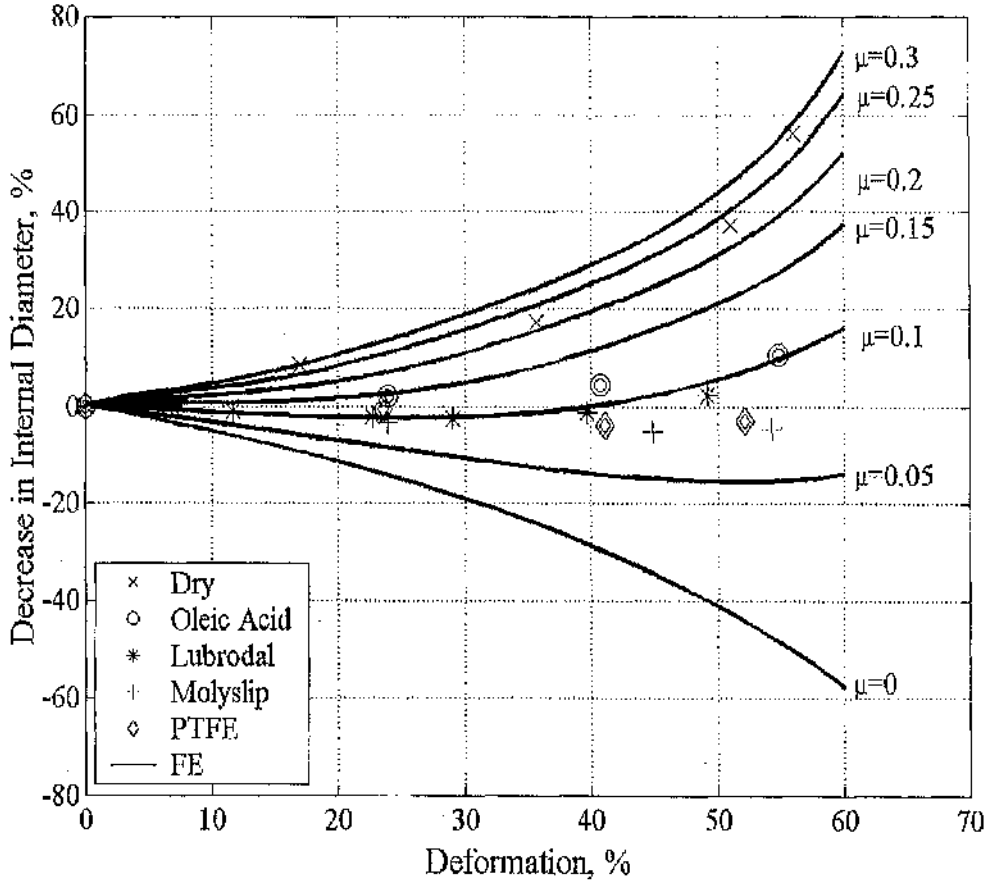

Figure 4.8: Friction calibration curves.

The results of LU ring tests are shown in Figure 4.9, along with data from static ring tests and the FE model for each interface condition. From the friction calibration curves as shown in Figure 4.9, only very small changes in the coefficients of friction were measured as a result of LU excitation of the lower platen during ring tests. For a dry surface there was no measurable change, and for the four lubricated interfaces the change in coefficient was very small but an increase in value was observed. For all the surfaces which were lubricated the coefficients of friction increased by 0.05 or less.

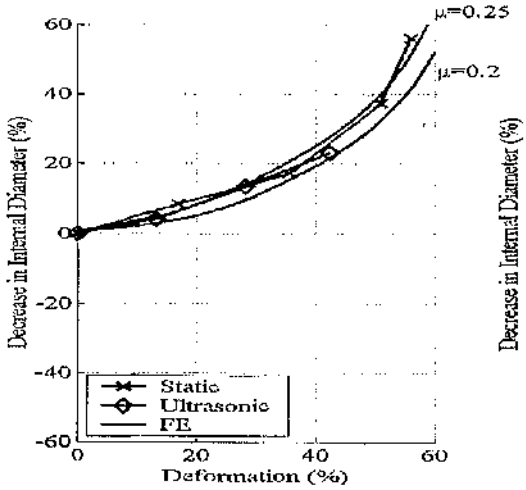

(a) dry surface

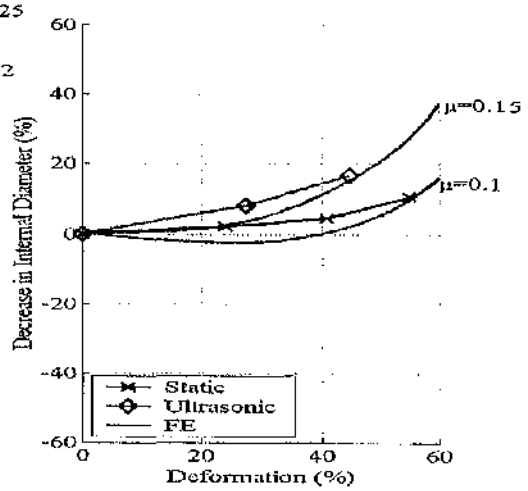

(b) oleic acid

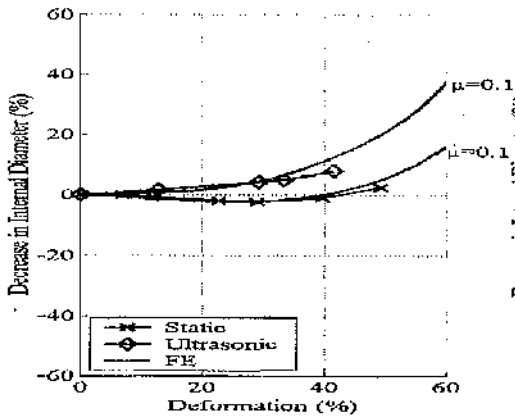

(c) Lubrodal

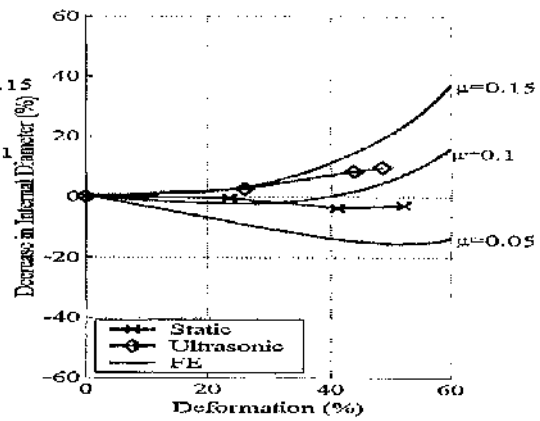

(d) Molyslip

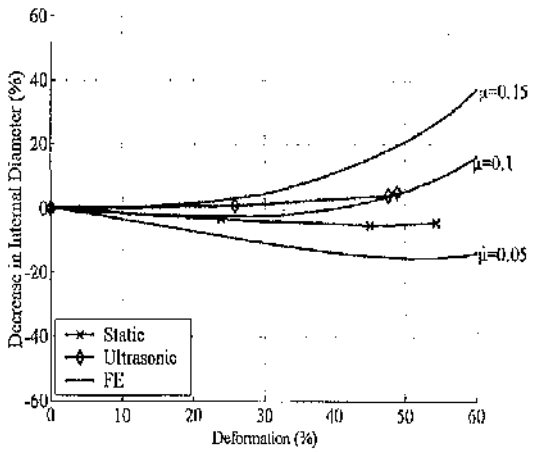

(e) PTFE

Figure 4.9: Static and LU ring test data with FE friction calibration curves.

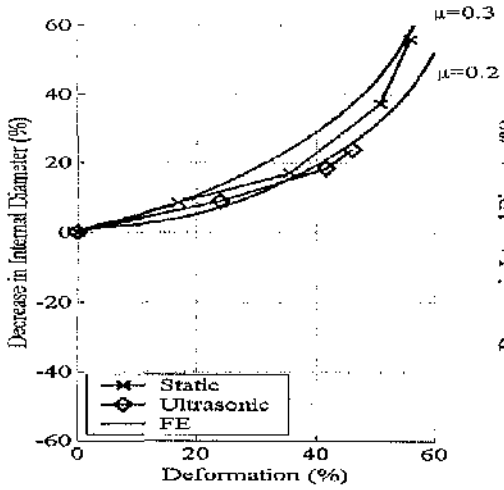

a) dry surface

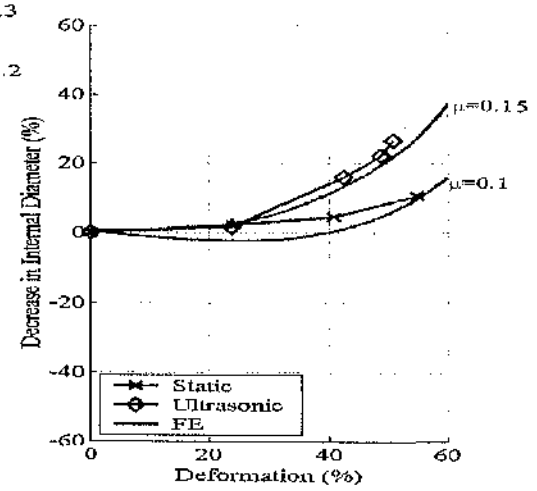

b) oleic acid

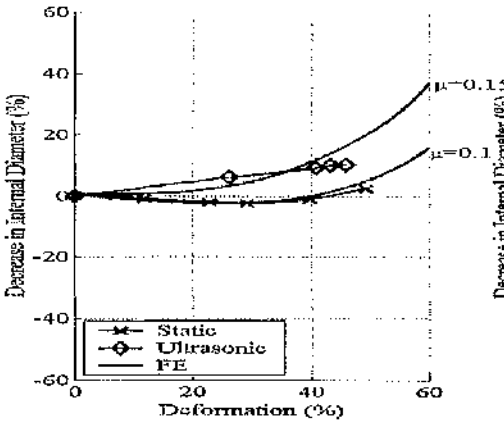

c) Lubrodal

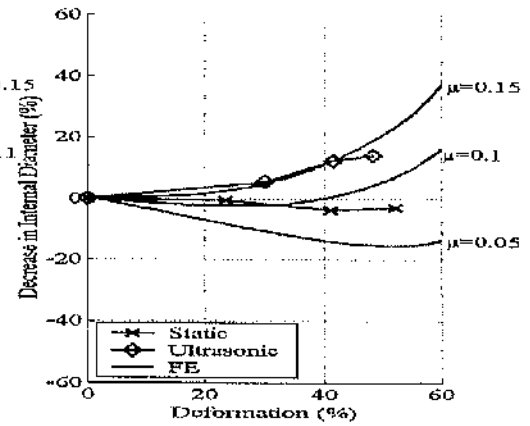

d) Molyslip

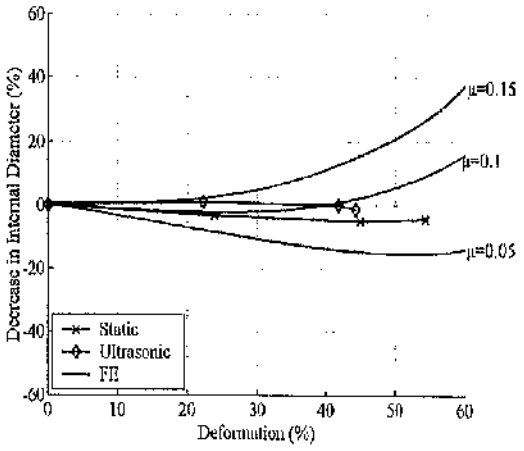

e) PTFE

Figure 4.10: Static and RU ring test data with FE friction calibration curves.

The effect on friction, as determined from FCCs, of superimposed RU excitation during ring compression tests was also investigated. Figure 4.10 shows the results of RU ring tests along with the static ring test data and FE friction calibration curves. As can be seen in Figure 4.10, there was a small deviation in the friction coefficient between static and RU ring tests for all surface conditions. For a dry surface, the coefficient of friction from the RU ring test shows a slightly reduced value than the static ring test. For the lubricated surface with oleic acid, Lubrodal and Molyslip, the coefficient of friction for RU ring tests increases by approximately 0.05 compared with the static ring test. Also, the lubricated surface using a soft solid film of PTFE measured a slightly higher friction coefficient value from the RU ring test compared with the static ring test.

Generally, ring tests show no significant change in friction coefficient between ultrasonic and static ring tests. However, there is some slight different between LU and RU ring tests which show that the RU excitation slightly reduces the coefficient of friction than the LU excitation for dry surface. This may be explainable later by surface analysis.

Although the ring compression test has been widely accepted for estimating the interface friction coefficient, this method has never been used to attempt to estimate the coefficient of friction for ultrasonic assisted forming processes. There has been some conflicting evidence in the literature as to the effects of friction due to ultrasonic excitation with some studies reporting that friction was only temporarily reduced for the duration of superimposed ultrasonic excitation [2, 11, 19, 20] and did not affect the final deformation. The ultrasonic ring tests in this study tend to support this providing further evidence that ultrasonic excitation does not have a permanent effect on the deformation characteristics of the specimens and that ultrasonic ring tests produce very comparable FCCs to conventional ring tests for all the interface conditions studied here. Ring tests, therefore, can only show how the final deformation is affected and not how the interface condition is affected during ultrasonic excitation.

4.7 Surface Analysis

The quantitative assessment of the topographic features of surfaces is important for interpreting a wide variety of problems in surface contact. The mechanism of friction depends on the nature of the real contact between die and specimen interface and also upon the distributions, sizes and shapes of the asperities. Measurement of these features provides an essential insight into the contact friction.

There have been a few studies that observed the profile and texture of a surface prior to and after undergoing a process of ultrasonic deformation. The early work to observe topographic texture of the deformed surface of an aluminium wire after ultrasonic drawing was carried out by Pohlman [2]. In this study, by using high magnification images, Pohlman observed that the oxide layer on the wire surface was torn open when ultrasonic excitation was applied. By applying a slow drawing speed, eruption effects of ultrasonic excitation were noticed on the drawn surface. This observation suggests that the texture of a deformed surface under applied ultrasonic load is substantially influenced by the operational speed. A similar study of ultrasonic strip drawing was carried out by Seigert [6], who also agreed with Polman's findings that the smoothing effect of microstructure of the deformed surface is affected by the velocity of the drawing process.

In this present study, the surface texture of the deformed ring specimens was assessed by a roughness measurement and topographic evaluation. To evaluate the surface, two common surface evaluation procedures were carried out; (1) Surface roughness measurement using a 2D-profilometer and, (2) surface topographic imaging using scanning electron microscopy (SEM). It was expected that these measurement could provide some further evidence or explanations of the coefficients of friction measured in the LU and RU ring tests.

4.7.1 Profilometer

The use of a profilometer to assess surface roughness has been an established technique since the first instrument was invented for modern application by Taylor and Hobson in 1940. This stylus instrument, called Talysurf, is used in this study. A profilometer

consists of a stylus, mechanical system, electronic unit and a metering or recording device as the main components. During a measurement process, a stylus rests lightly on the surface and is traversed across it. The up and down movements of the stylus relative to a suitable mechanical datum are magnified and recorded by a metering device. The result of recorded and magnified measurements is presented into a two-dimensional graph that represents the profile of the traced surface, referred to as a profile graph [101].

The stylus is generally made of diamond with a pyramidal or conical shape with a very small flat or rounded tip. The stylus is connected to a mechanical system using a stiff material through a moving transducer. The mechanical system consists of a fixed transducer and mechanical devices to provide a reference surface measurement. The moving transducer provides the measuring surface signal and the fixed transducer generates a reference surface signal. The signal is amplified by an electrical unit into a presentable magnified profile graph. In order to gain an accurate surface profile interpretation, a few traces should be performed in one surface measurement. Also, slow recording speeds permit a higher magnification.

In most engineering applications, one of two parameters is usually used to define the texture of surfaces. These parameters are the R_a roughness value, and the R_q value [101]. The R_a value is defined as the arithmetic average value of the vertical deviation of the profile from the centre line, and the R_q value as the square root of the arithmetic mean of the square of this deviation. In mathematical form they can be written as

$$R_a = \frac{1}{n}\sum_{i=1}^{n}|Z_i| \tag{4.1}$$

and

$$R_q = \left[\frac{1}{n}\sum_{i=1}^{n}(Z_i)^2\right]^{\frac{1}{2}}. \tag{4.2}$$

Where n is the number of points on the centre-line at which the profile deviation z_i is measured as illustrated in Figure 4.11. The centre-line is taken as a line which divides the profile in such a way that the sums of the enclosed areas above and below it are

equal. These parameters are seen to be primarily concerned with the profile in the vertical direction only. These single numerical parameters are mainly useful for classifying surfaces of the same type which are produced by the same method. However in a modern profiler, others surface parameters such as slope, shape and size of asperities, and frequency and regularity of asperity occurrence can also be calculated [101, 102].

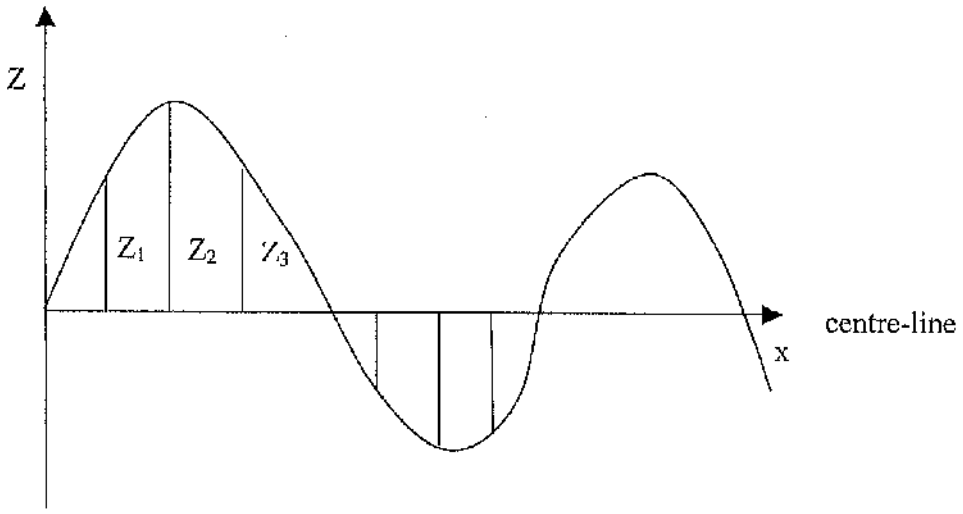

Figure 4.11: Graphic representation for surface roughness, R_a [101].

4.7.2 Scanning electron microscopy

A detailed examination of deformed specimens is vital to an investigation relating the process parameters to the behaviour of the contact surface. The application of SEM to workpieces from static [73, 79, 91] and ultrasonic [2, 6] deformation processes has been carried out previously to investigate contact surface parameters such as lubrication effects, asperities flattening, surface texture and roughness, which can be qualitatively characterised from SEM images. By understanding the surface features, the contact friction condition can be clarified.

The main components of an SEM unit consist of an electron gun, condenser and objective lenses, detector, display unit and vacuum system. Electrons from the gun are accelerated by a voltage and directed down the centre of an electron optical column consisting of two or three magnetic lenses. The electrons can only be emitted through a

vacuum environment and air trapped in the testing chamber must be pumped out by the vacuum unit prior to testing. The condenser lenses cause a fine electron beam to be focused onto the specimen surface. Scanning coils placed before the final lenses, or objective lenses, cause the electron spot to be scanned across the specimen surface in the form of a square raster. The electron beam incident on the specimen surface causes various phenomena, of which the emission of secondary electrons is the most commonly used. The emitted electrons strike the collector and the resulting current is amplified and used to modulate the brightness of a cathode ray tube (CRT). The image is built up from the different CRT brightnesses according to the signal received from the collector. The images are then recorded for processing [102].

4.7.3 Procedure for surface roughness measurement and SEM imaging

The deformed ring specimens from static and ultrasonic compression tests were cleaned with methanol and a soft cloth to remove the lubricants. Surface roughness measurements were carried out using a Form Talysurf profilometer. The stylus moves 3 mm horizontally across the surface at a speed of 10 mm/min. To preserve the accuracy of the measurement, three different lines were traced by the stylus for each surface. The profiles of the traces were plotted as a 2D graph to represent the profile of the measured surface. The roughness, R_a in the vertical direction was calculated using the analysis software. Three different values of R_a were subsequently calculated. The average, R_a was then considered to represent the roughness parameter for the entire surface. The above procedure was used for estimating a roughness value for all surfaces.

The same surface of the compressed ring specimens which was previously used for roughness measurement was then prepared for imaging by cleaning the surface using methanol. The cleaned surface was scanned using a Cambridge DS360 Leica SEM. For clarification, the images were magnified to x200. The acquired images were transferred from CRT display into the analysis software.

The measured roughness data were graphically presented using simple bar charts, to allow comparison of the roughness data for an undeformed surface with the data for deformed surfaces under static, LU and RU loading for the dry surface and four different lubricants. The SEM images were also used to compare the topographic

texture of the undeformed surface with the deformed surfaces under static and applied ultrasonic loads.

4.7.4 Results of surface roughness measurement and surface texture observation

Figure 4.12 shows a bar chart representing the average of roughness values, R_a, of the undeformed and deformed surfaces. Generally, the average roughness of all the deformed surfaces was lowered by static and ultrasonic loading during compression if compared with the undeformed surface. This can be explained by the flattening of the asperities due to high-pressure contact between the platens and specimen surfaces.

In the absence of lubricant, R_a was reduced by the greatest amount in all ring compression tests, followed by the liquid lubricants; oleic acid and Lubrodal. The use of grease and soft solid lubricants; Molyslip and PTFE film respectively, caused severe damage of the surface which gave a higher value of the average roughness, R_a, than the use of other lubricants or dry surface.

For the dry surface, the value of the roughness is almost identical for each compression, giving R_a = 0.2123 for static compression and followed by LU and RU compressions where R_a = 0.2138 and 0.2664 respectively. This data correlates with the topography texture as illustrated in Figure 4.13, where smoother texture is observed for static compression compared with LU and RU compressions.

The use of liquid lubricants; oleic acid and Lubrodal, has modified the surface texture, causing a notable reduction in roughness resulting in a smoother surface texture for each compression method compared with the undeformed surface. As illustrated in Figure 4.12, the roughness of the surfaces using Lubrodal show similar R_a values for each compression method, giving an R_a value from approximately 0.25 to 0.28. For the surfaces that deformed using oleic acid, a higher R_a value is measured under LU compression if compared with the R_a values for static and RU compressions. These roughness data seem to be well-correlated with the surface textures shown in Figure 4.14 and Figure 4.15 for oleic acid and Lubrodal respectively. As can be seen in Figure 4.15 (c), it is clear that a slight uneven surface is observed for LU compression with oleic acid, which agrees with the measured roughness data.

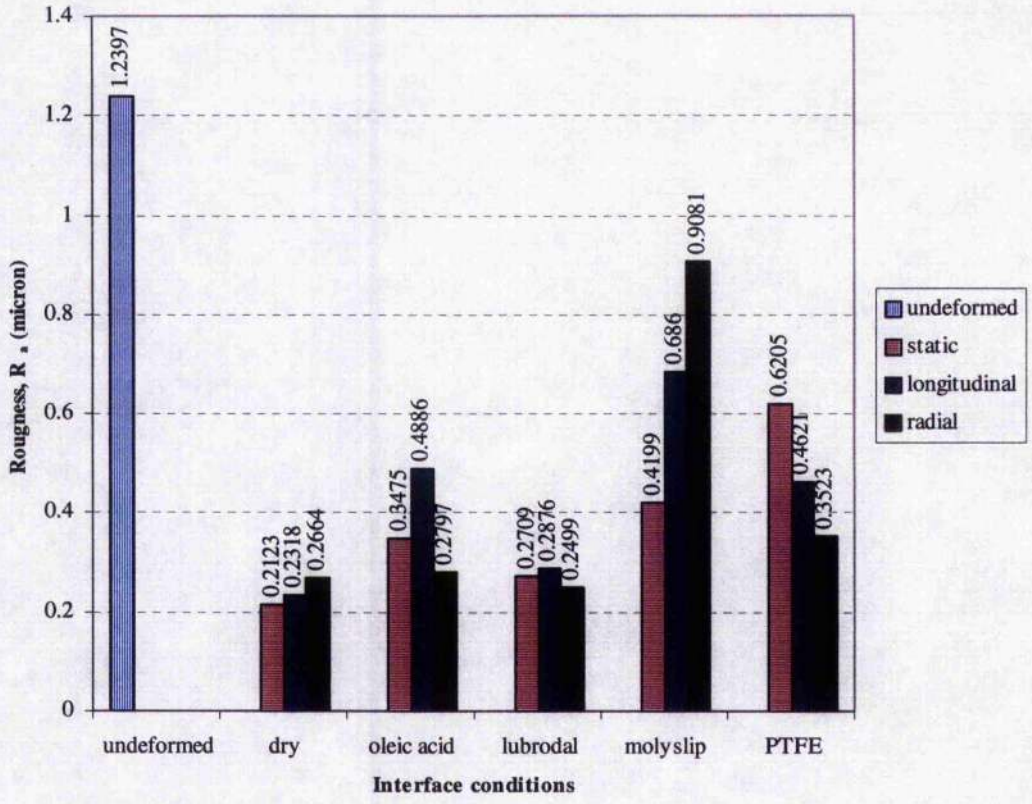

Figure 4.12: Average roughness, R_a.

Figure 4.16 shows the SEM images of the deformed surfaces using a semi-solid lubricant, Molyslip, for static, LU and RU compressions. Under static compression, the roughness was measured at a lower value and also a smooth surface texture is observed. For LU and RU compressions, a higher roughness value was measured and rougher surface texture is observed. This could be explained by the action of the ultrasonic load on the trapped lubricant, creating an alternating hydrostatic pressure on the surface during the deformation process, and subsequently deepening the valleys within the surface asperities.

The topographic images of the deformed surfaces using soft solid film (PTFE) are shown in Figure 4.17. By observing the SEM image for the static compression, this resulted in a rougher surface and a higher roughness value compared with the surface texture and roughness value for LU and RU compressions. By superimposing LU and RU excitation during compression, it is believed that the ultrasonic loading has removed parts of the PTFE layer, and then exposed the asperities. The continuous application of

ultrasonic excitation has led to a flattening of the exposed asperities. As a result, low R_a values were measured and better surface texture was observed for LU and RU compressions.

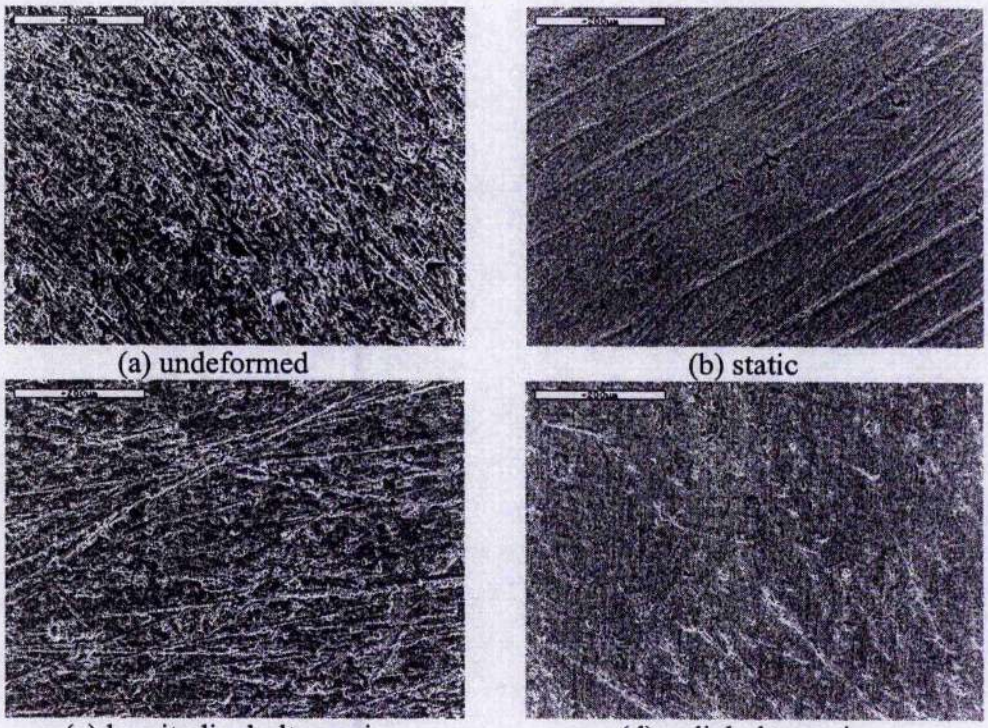

(a) undeformed (b) static

(c) longitudinal ultrasonic (d) radial ultrasonic

Figure 4.13: Dry interface, magnification x 200.

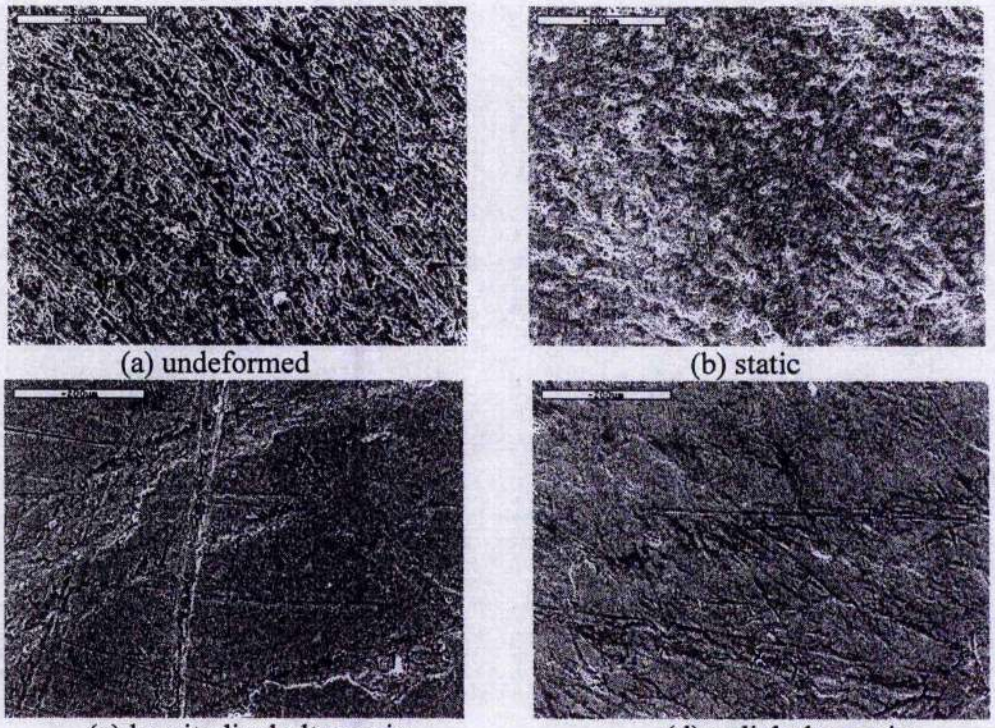

(a) undeformed (b) static

(c) longitudinal ultrasonic (d) radial ultrasonic

Figure 4.14: Oleic acid applied at interface, magnification x 200.

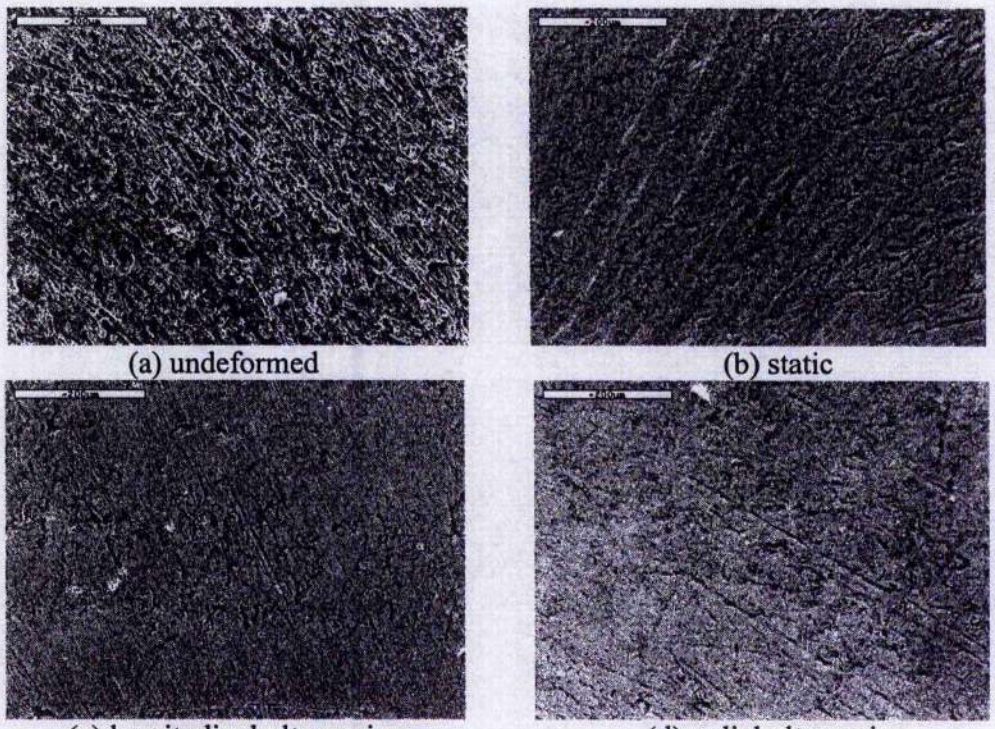

(a) undeformed (b) static

(c) longitudinal ultrasonic (d) radial ultrasonic

Figure 4.15: Lubrodal applied at interface, magnification x 200.

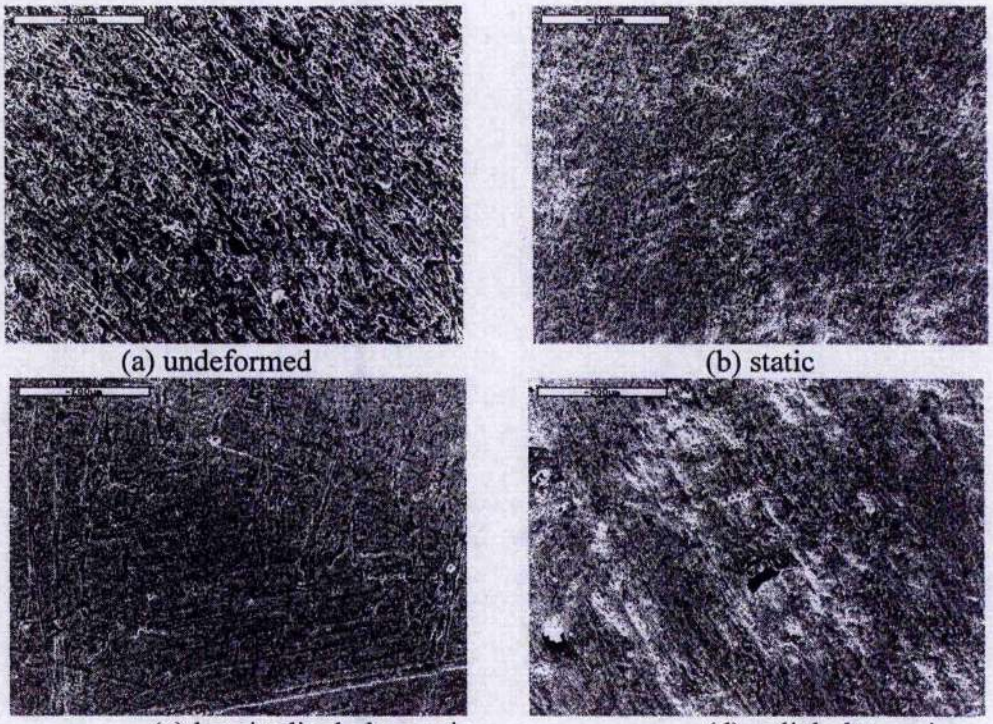

(a) undeformed (b) static

(c) longitudinal ultrasonic (d) radial ultrasonic

Figure 4.16: Molyslip applied at interface, magnification x 200.

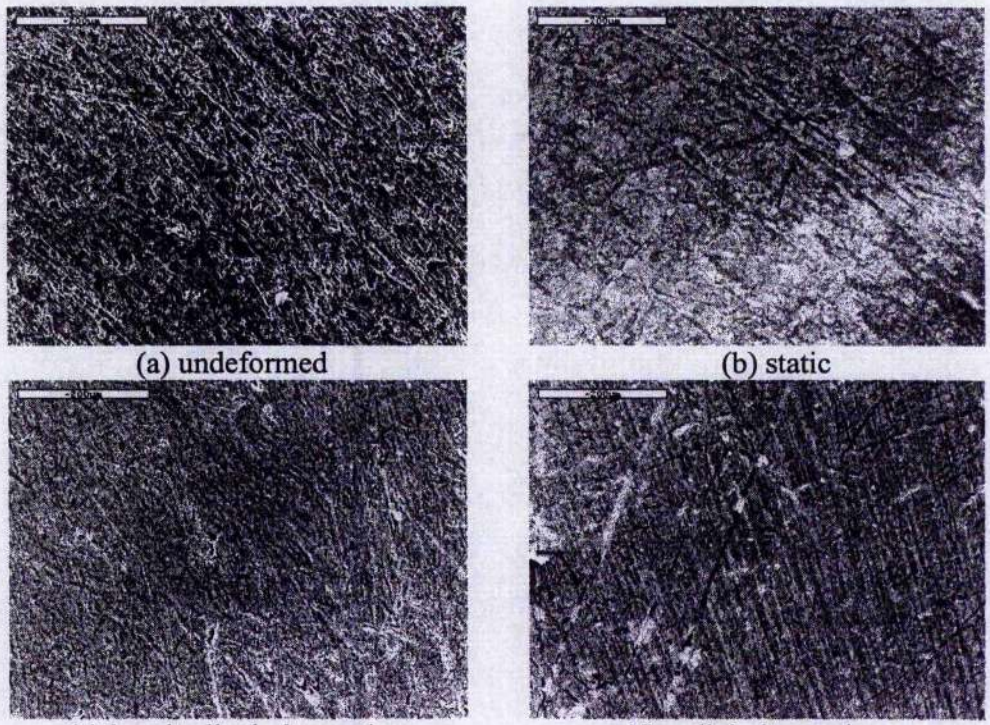

(a) undeformed (b) static

(c) longitudinal ultrasonic (d) radial ultrasonic

Figure 4.17: PTFE applied at interface, magnification x 200.

4.7.5 Correlation between surface profile and friction

To allow roughness data and friction data to be compared, Figure 4.18 plots the measured surface roughness, R_a, and estimated coefficient of friction, μ, for static, LU and RU compressions for dry and four different lubricated surfaces. The estimated friction coefficients for dry and, Molyslip and PTFE lubricated surfaces seem to be unrelated to their roughness values for each type of compression. For a dry surface, Figure 4.18 (a), although the roughness was measured at a low value for each compression method, the coefficient of friction was not reduced. On the other hand, for the surfaces which were deformed using Molyslip, Figure 4.18 (d), and PTFE, Figure 4.18 (e), the roughness of the surface was measured at a high value whereas the coefficient of friction was estimated at a low value for most compression methods.

The use of liquid lubricants, oleic acid, Figure 4.18 (b), and Lubrodal, Figure 4.18 (c), in most compression methods has effectively been to reduce both coefficient of friction and roughness value of the deformed surface. By comparing with the other compression methods, RU has effectively reduced the surface roughness for both lubricants, oleic acid and Lubrodal, however there has been no further reduction in the coefficient of friction under this compression method.

Generally, these data suggest that the coefficient of friction and the roughness of the deformed surfaces depend on the compression method applied; static, LU, or RU, and also the type and properties of the lubricants used at the die-specimen interface. However, there are some observations that may be suggested from the present investigation. (1) For a dry surface, the static, LU and RU compressions effectively reduce the roughness of the surface. By comparing with static compression the coefficient of friction is slightly reduced under RU compression, however there is no change in the coefficient of friction for LU compression. (2) By using oleic acid and Lubrodal, both the roughness of the surface and the coefficient of friction are reduced under static compression compared with a dry surface. Although the LU and RU compressions with these lubricants have reduced the roughness value further, the coefficient of fiction is slightly increased. (3) For the surfaces deformed using a semi-solid lubricant, Molyslip, and a soft film of PTFE, the coefficient of friction has been significantly reduced in particular for static compression followed by LU and RU

compressions. The LU and RU compressions have increased the roughness value of the surface deformed with Molyslip, however by using PTFE there has been some improvement of the deformed surfaces.

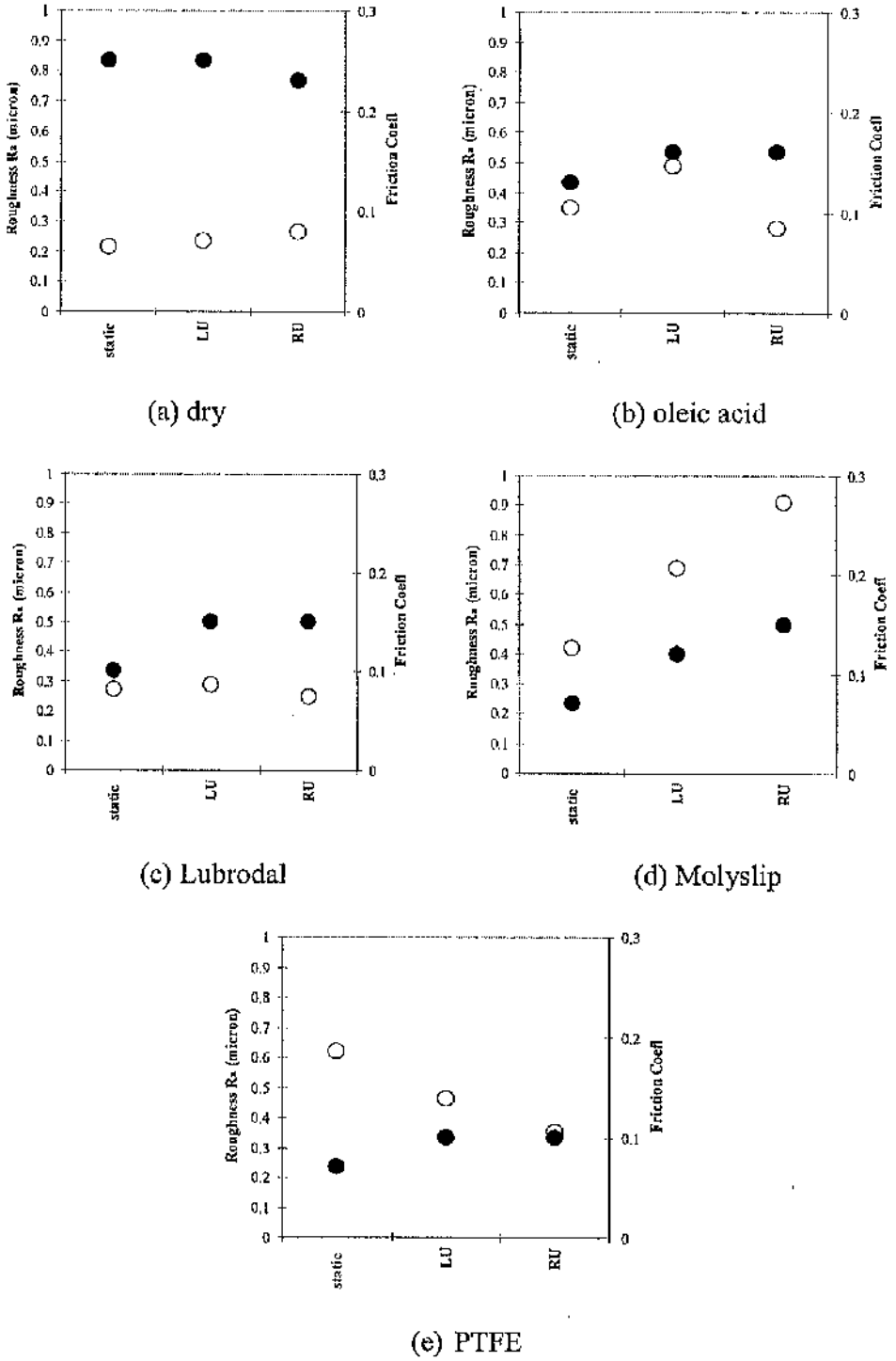

(a) dry

(b) oleic acid

(c) Lubrodal

(d) Molyslip

(e) PTFE

Figure 4.18: Average roughness, R_a (○) and coefficients of friction, μ (●) for static, LU and RU compressions..

4.8 Conclusions

The use of the ring test technique to estimate the coefficient of friction, μ, under different interface conditions for static, LU, and RU compressions was presented in this chapter. Finite element (FE) modelling was used to generate the friction calibration curves, FCCs. The coefficient of friction for each interface conditions for static, LU and RU ring tests was estimated by matching the measured friction data with the calculated FCC.

For static ring tests, it was found that the coefficient of friction for a dry surface was highest, followed by oleic acid, then Lubrodal. The lowest friction coefficient value was estimated for the surfaces that were applied with Molyslip or PTFE, with both lubricants giving the same friction coefficient value.

By comparing with static ring tests, it was found that there is no significant change in the coefficient of friction for the LU ring test for a dry surface. For the same surface condition, the coefficient of friction was slightly reduced for the RU ring test. However, for the lubricated surface conditions, the coefficient of friction for both LU and RU ring tests have shown a slight increase if compared with the static ring test. It is believed that if the change in coefficient of friction is temporary and only occurs during ultrasonic excitation, the ring tests only show how the final deformation is affected, and not how the interface condition is affected during ultrasonic compression. The final geometry of the ultrasonically deformed ring is very similar to the geometry of the statically deformed ring. This tends to support the evidence that any interface friction effects due to ultrasonic excitation are temporary and only evidenced during the excitation.

In an attempt to gain a better understanding of interface friction behaviour during static and ultrasonic compressions, the deformed surfaces have been evaluated using a profilometer and SEM for measuring roughness and observing topographic texture. The roughness of each surface has been well correlated with its surface texture. Generally, for all compression methods, a smoother surface was achieved by using dry and liquid lubricants and a rougher surface was presented by using Molyslip and PTFE. The application of the ultrasonic excitation during a compression test was effectively to reduce the surface roughness for dry and liquid lubricants. However for the surfaces that

were coated with Molyslip, the LU and RU loadings created an uneven surface texture. However a better surface texture was found by applying LU and RU for compression tests with PTFE.

The analysis of the correlation between roughness value and coefficient of friction of the deformed surface was carried out. It was found that the roughness and friction coefficient values for each surface depended on its deformation method and type of the lubricant used and there was no simple relationship. Generally, the roughness value seemed to be unrelated to the estimated friction coefficient value for a dry surface and for the surface that was coated with Molyslip and PTFE. For the dry surface, a low roughness value was measured and a high friction coefficient value was estimated for all compression methods. For Molyslip and PTFE, it was found that a high roughness value was measured and a low friction coefficient value was estimated for most compression methods.

For liquid lubricants; oleic acid and Lubrodal, the roughness and friction coefficient values seemed showed a more related trend for all compression methods. A better surface texture was found for any compression using these lubricants.

The reduced roughness value for some lubricants applied under static, LU and RU compressions could be explained by the asperities flattening. The uneven surface textures measured for static, LU and RU compressions were due to the physical and chemical actions of the lubricants and applied forces including hydrostatic pressure and partial preservation of asperities.

In conclusion, the present study would tend to suggest that the use of high viscosity lubricants in ultrasonic forming could not provide significant benefits over the use of low viscosity lubricants or no lubricant in terms of surface finish and reduction in the interface friction. In the absence of a lubricant or by using low viscosity lubricants, the surface finish of the deformed specimen can be improved for both static and ultrasonic compressions but there are no measurable improvements using high viscosity lubricants.

CHAPTER 5

STATIC AND ULTRASONIC COMPRESSION

5.1 Introduction

The main reason for using lubricants in metal forming processes is to reduce the interfacial friction between the tool and workpiece. The reduction of interface friction provides many benefits to the fabrication process and end product. For example, the process forming load can be lowered, tool life can be extended, and final product defects can be minimised. In current manufacturing processes involving metal forming, it is necessary to use lubricants that avoid or reduce environmental pollution. Dry and low viscosity lubricants have been used in metal working processes which contain reactive or non-reactive chemical additives that contribute to environmental pollution. Accordingly, some studies have been conducted to investigate the use of ultrasonic vibration as a non-chemical lubrication medium [32, 103].

Since Blaha and Langenecker [1] reported that the yield strength reduction was due to superimposed ultrasonic vibration in tensile testing of zinc crystals, many other similar studies have been carried out and several theories have been developed to explain the observed phenomena, including energy absorption due to moving dislocations [19], superposition effects of oscillating stress [3], reduction in internal friction [2], reduced material properties [12, 99], dynamic effects of vibrated tools [93], and reduction of interface friction [8-11].

A large number of investigations have observed that vibratory energy can reduce frictional forces. One publication [5] postulated five possible mechanisms that could improve the frictional condition under the influence of a vibratory load: (1) separation of surfaces and cyclic re-establishment of the lubricant film on the contacting surface, (2) friction force vector reversal due to movement of the tool, (3) heating of asperities

possibly reducing the shear strength, (4) pumping of lubricants to provide better lubrication conditions, and (5) cleaning effect which permits efficient bonding of the lubricant to the metals being deformed.

A study [27] of a wire drawing process with a low viscosity lubricant suggested that by superimposing ultrasonic vibration perpendicular to the wire movement direction the interface friction was significantly reduced compared with applying a parallel ultrasonic vibration.

The effects of ultrasonic vibration on friction during upsetting tests have been studied [8, 104] and it has been suggested that under an applied longitudinal ultrasonic load there is a reduction in interface friction. This effect has also been observed for applied radial mode ultrasonic vibrations. A recent study [104] of longitudinal and radial ultrasonic upsetting of plasticine reported that ultrasonic vibration significantly reduced the interface friction and the upsetting force due to a thermal reduction in the coefficient of friction.

In previous studies of ultrasonic metal forming, there have been attempts to investigate how the measured reduction in forming force can been attributed to friction reduction, material softening, thermal effects, or a combination of these effects [2, 12, 19, 20]. However, the lack of experimental facilities to measure the oscillatory stress has led to confusing data and lack of agreement in the published literature.

This study aims to investigate the stress-strain relationship when an oscillatory stress is superimposed on a static stress during ultrasonic compression tests of aluminium specimens under different interface friction conditions. As well as recording force-displacement data, from which the stress-strain relationship is derived, the vibration response of the dies and specimen, and the surface temperature are recorded. This allows any dynamic effects, such as resonance or amplitude variation to be investigated. Also, any measurable rise in temperature can be observed. Correspondingly, a series of FE models are developed to investigate the effects of changes in friction and material properties in simulations of ultrasonic compression tests, by comparing the stress-strain relationships derived from experiments and FE models.

5.2 Experimental Set-up and Test Procedures

In these experiments, aluminium cylindrical specimens were compressed between two platens. The lower platen consists of a tuned longitudinal mode slotted block horn, for tests which superimpose axial ultrasonic oscillation on the static deformation process, and a tuned radial mode cylindrical horn, for tests which superimpose radial oscillations on the static deformation process. For axial oscillations, the lower platen was a double-slotted block horn, tuned to a longitudinal mode at 20 kHz, providing a uniform nominal vibration peak amplitude of 10 μm on the platen surface. For radial ultrasonic excitation, the platen was a thick cylindrical horn, tuned to a radial mode at 20 kHz, giving a uniform nominal peak amplitude of 4 μm on the platen surface. Both horns were excited by a piezoelectric transducer driven by an ultrasonic generator. The ultrasonic system and the characterisation of these horns are described in detail in Chapter 3 and Chapter 4.

The upper die was connected to the cross-head of a Lloyd test machine which provided a constant cross-head speed of 5 mm/min for these experiments. A piezoelectric force transducer was used to measure the static-oscillatory force response during compression, and was mounted between the upper platen and the cross-head as shown in Figure 5.1 and Figure 5.2. A schematic of the radial ultrasonic compression test set-up is shown in Figure 4.4 (Chapter 4). The interface temperature was measured during ultrasonic compression between the top of the lower platen and the specimen surface, using a small thermocouple which was embedded in the specimen at the interface. The oscillatory displacement amplitude for longitudinal mode oscillation was measured during ultrasonic compression on the top surface of the block horn, on the side of the aluminium specimen, and on the bottom surface of the upper platen, using a 1D and 3D LDV. The recorded signals were acquired by Dataphysics signal acquisition hardware and software for data processing. The details of the components of the measurement system and their functions are described in Chapter 3.

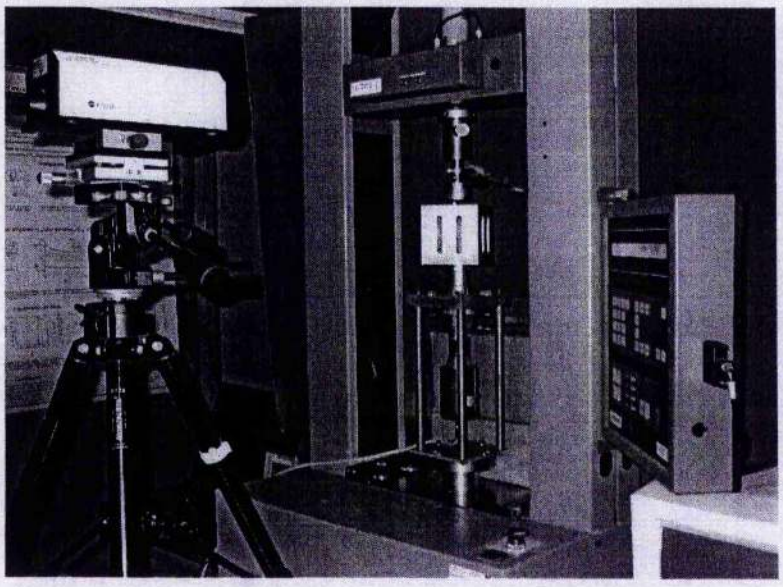

Figure 5.1: A photograph of the test set-up.

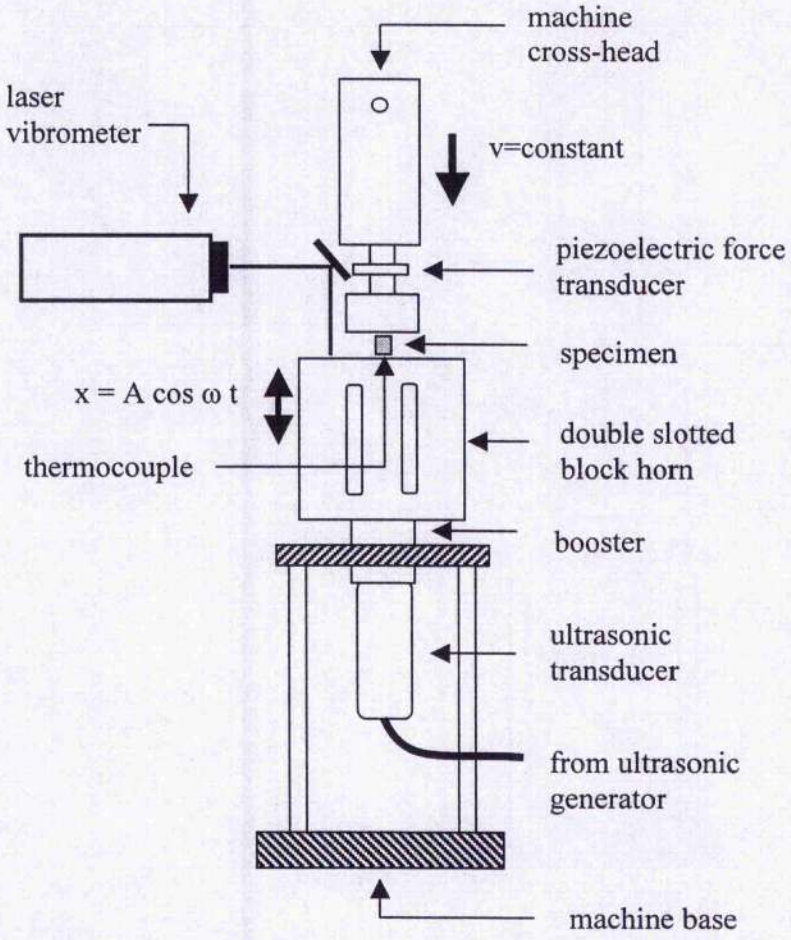

Figure 5.2: Schematic of the longitudinal ultrasonic compression test set-up.

5.2.1 Specimens and lubricants

Soft aluminium grade A1050 specimens were used in the upsetting tests. The cylindrical specimens, of 8 mm diameter and 8 mm height, giving an aspect ratio of 1, were machined from cylindrical bar. All specimen surfaces were polished using a high-grade abrasive paper (grit 1200) to provide a uniform surface roughness. The interface conditions between the specimen and dies were; dry, and lubricated by oleic acid, Lubrodal, and PTFE (Teflon). For modelling purposes, the coefficients of friction, μ, at the interfaces were estimated from static ring compression tests as described in Chapter 4, where for a dry surface $\mu = 0.25$, for oleic acid $\mu = 0.13$, for Lubrodal $\mu = 0.1$ and for PTFE $\mu = 0.07$. According to the ring tests, as described in Chpater 4, the estimated coefficient of friction for Molyslip was identical to the coefficient of friction for PTFE, $\mu = 0.07$ and therefore only PTFE was maintained for the present study. The physical, chemical and mechanical properties of the aluminium specimens were described in Chapter 3, and the physical and chemical properties of the lubricants were described in Chapter 4.

Prior to each compression test, the specimens and platens were cleaned with methanol and dried in air. Oleic acid and Lubrodal were brushed onto the surfaces, and a dry film of PTFE was prepared by spraying the suspension onto the surfaces and drying in air.

5.2.2 Static and longitudinal ultrasonic (LU) compression tests

A series of static and LU upsetting tests was performed at a constant cross-head speed of 5mm/min under dry and lubricated surface conditions. In the first experiments, under dry surface conditions, a cylindrical specimen was compressed conventionally in the Lloyds test machine, under static loading. Subsequently, for the ultrasonic compression tests, LU excitation was applied to the lower platen post-yield during plastic deformation. Two sets of ultrasonic compression tests were conducted. In the first set, the ultrasonic excitation was applied continuously, from the onset of plastic deformation to completion of the test. In the second set, LU excitation was applied for two short intervals during plastic deformation, with static compression continuing between these intervals when the ultrasonic excitation was discontinued. For the first interval, when

the specimen reached approximately 18 % of the original height, the LU excitation was applied for 6 seconds, then discontinued for 6 seconds to allow the specimen to continue to deform under static load, and subsequently, LU excitation was applied for another interval of 12 seconds. For both static and ultrasonic loading, the compression test was completed when the specimen reached 50% height reduction. These two sets of test procedures were repeated for three other series of experiments under the three different lubrication conditions. The static and ultrasonic force response data were recorded using a piezoelectric force transducer.

During the continuous application of LU vibration, the vibration displacement response on the top surface of the lower platen, on the side of the specimen, and on the bottom surface of the upper platen were measured by the LDVs, and the temperature was recorded using a thermocouple.

5.2.3 Radial ultrasonic (RU) compression tests

A series of RU upsetting tests was carried out using the same procedures as in LU compression tests, with the longitudinal block horn replaced by a radial-mode horn. In these experiments, the aluminium specimens were compressed under dry and the three lubricated surface conditions. Again the surface temperature for all interface conditions was measured using a thermocouple during the test with continuous ultrasonic excitation

5.3 Finite Element Methods

Finite element (FE) simulations were developed using the commercial finite element code, ABAQUS, with implicit solution. Half of the cylindrical specimen was meshed using 2D axi-symmetric 4-node elements. The upper and lower platens were assumed to be rigid bodies, modelled by an analytical rigid surface. The undeformed and deformed mesh profiles of the compression tests are shown in Figure 5.3. For modelling a compression process [104], a standard Coulombic friction model is considered and it is assumed that no relative motion occurs if the equivalent frictional stress, τ_e is less than critical stress, τ_0 which is proportional to the contact pressure, p, in the form;

$$\tau_c = \mu\, p, \tag{5.1}$$

where μ is the coefficient of friction. If the equivalent stress is at the critical stress ($\tau_e = \tau_c$), slip can occur. For solid cylindrical compression modelling, all nodal frictional forces are directed radially inwards to oppose the outward flow of material. Hence, using the Von Mises criterion, the maximum numerical friction coefficient value is $\mu_{max} = 0.577$. From the ring compression tests as described in Chapter 4, the coefficients of friction for dry and lubricated interfaces are below that of non-slip friction. For static compression simulations, a Coulombic coefficient of friction equal to 0.25 for dry, 0.13 for oleic acid, 0.1 for Lubrodal and 0.07 for PTFE, were used. The static and kinematic values of the coefficient of friction were assumed to be equal.

The specimen was deformed by controlling the upper platen with a constant velocity of 5 mm/min. The lower platen was fixed during static compression, and for static-ultrasonic compression a sinusoidal ultrasonic excitation was superimposed on the static motion by vibrating the lower platen such that the displacement of the lower platen is defined by $x = A\cos\omega t$, where A is the amplitude and ω is the circular frequency.

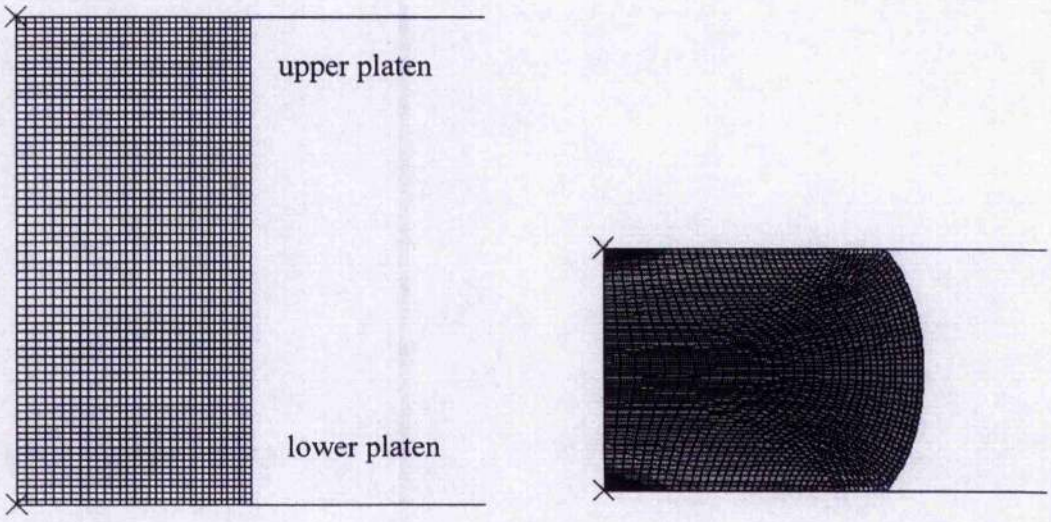

Figure 5.3: Original and deformed mesh profile of a cylindrical specimen for compression FE model.

5.3.1 Static compression simulation procedures

Initially, a series of static compression simulations was developed in order to validate the material model. The specimen was deformed using the same constant velocity of the upper platen of 5 mm/min as set in the experiments, while the lower platen was fixed. A stress-displacement analysis was implemented and a coefficient of friction of 0.25 was applied for the dry interface condition and the simulation was repeated for the coefficients of friction for the lubricated interface conditions. The simulations were stopped when the specimen reached 50 % reduction of its original height.

5.3.2 LU compression simulation procedures

The static-ultrasonic compression simulations were performed using the following procedure. Initially, the specimen was deformed under static loading by applying a constant velocity of 5 mm/min to the upper platen. By controlling the total time step, at 22 % reduction of the specimen height, ultrasonic excitation was superimposed on the lower platen during plastic deformation at a frequency of 20 kHz and longitudinal vibration amplitude of 10 μm. To allow for manageable computational time, the ultrasonic excitation was applied for 0.8 seconds in the FE models. Subsequently the model returned to its static loading condition before the simulation was stopped when the specimen was compressed to approximately 50 % of its original height.

For the second series of FE models, the effect of a change in the numerical value of the coefficient of friction during the interval of ultrasonic excitation was investigated. In this case, during static compression the coefficient of friction was set at 0.25 and, during ultrasonic excitation, the coefficient of friction was changed. Two different values were used; $\mu = 0$ for frictionless and $\mu = 0.15$. A friction value of 0.15 was chosen because it is consistent with reductions reported in previous studies. Maximum reductions in the coefficient of friction of 35 % and 40 % have typically been reported previously and the reduction to a value of 0.15 represents a 40 % reduction in coefficient of friction which was reported in a study of ultrasonic strip drawing [10].

For the third series of FE models, the combined effect of reduced material properties and a reduced interface friction coefficient were investigated. Based on a simulated

stress-strain relationship that has been derived from the measured mean oscillatory stress data in ultrasonic tension tests (Chapter 3), the reduction of plastic stress due to ultrasonic excitation has been calculated at 27 % of the original plastic stress giving a new yield stress of 44 MPa. This value is proposed to represent the softening effects of the material properties under ultrasonic loading, whilst the effects of a reduction in the interface friction condition during ultrasonic excitation was simulated by adjusting the interface friction coefficient from $\mu = 0.25$ during static compression to $\mu = 0.15$ during ultrasonic excitation.

5.3.3 RU compression simulation procedures

Similar procedures were applied to RU compression simulations. For the intervals of ultrasonic excitation, the frequency and vibration displacement amplitude were set such that the lower platen was excited by a radial mode vibration at a frequency of 20 kHz and peak amplitude of 4 μm.

The same series of simulations was then performed for RU compression models as for LU compression models described in the previous section.

5.4 Discussion of Static Compression Tests and Simulation Results

As well as for ring tests, upsetting of cylindrical specimens is another useful method for examining the friction between the die and specimen surfaces. Previous theoretical and experimental work in upsetting was reviewed by Kulkarni and Kalpakjian [59] and in a later study by Lee and Altan [63]. These suggested that upsetting tests provide a better explanation of the influence of friction on material flow in metal forming for low values of friction.

In this study stress-strain relationships for static compression tests under dry and lubricated surfaces were derived from load-displacement data. Figure 5.4 shows the stress-strain curves from static compression tests with different interface conditions. For the dry surface the flow stress is slightly higher than for the lubricated surfaces.

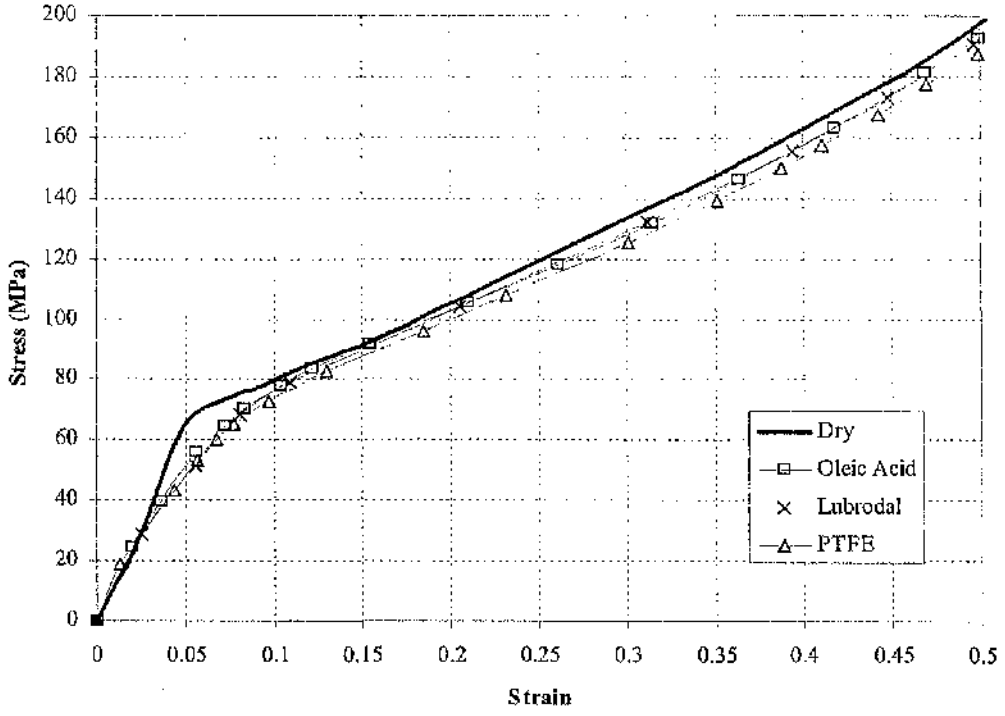

Figure 5.4: Static compression tests for dry and lubricated surfaces.

Figure 5.5 shows the stress-strain relationships from experimental and FE simulated static compression tests for cylindrical specimens with different interface conditions. Each curve demonstrates a unique stress-strain profile. The predicted stress-strain curve was calculated from the FE models, assuming a coefficient of friction as determined from the ring tests. Some deviation occurs for the elastic curves and yield points where the calculated data over predicts the elastic behaviour for the lubricated surfaces. This is because the material properties input to the FE models are based on static compression test and tension test data for a dry surface, and therefore a lowering of the elastic and yield stresses due to the lubrication effect are not accounted for in the material properties data. For the dry surface condition and the three lubricants used, close agreement is achieved between the experimental and FE stress-strain relationships in the plastic region. Consequently, it is believed that by combining the FE and experimental results of upsetting tests, incorporating controlled interface friction boundary conditions, this method could be adopted as an alternative to ring tests as an indicator of the coefficient of friction.

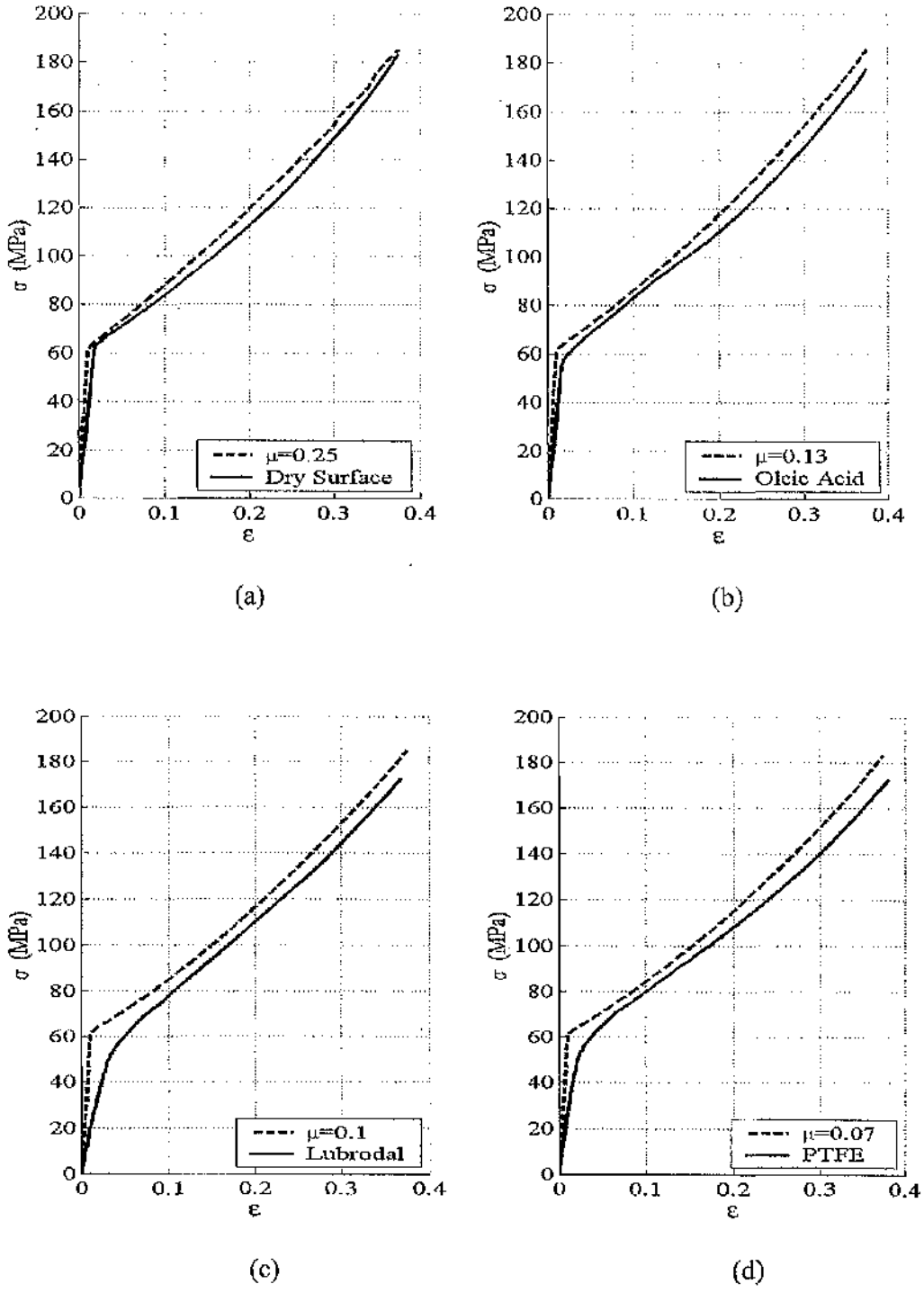

Figure 5.5: Comparison of FE (---) and experimental (—) stress-strain data for static compression with (a) dry surface, (b) oleic acid, (c) Lubrodal, (d) PTFE.

5.5 Discussion of LU Compression Test Results

The effects of longitudinal ultrasonic (LU) excitation on the stress-strain relationship for dry and lubricated contact conditions were investigated. Stress-strain curves were derived from the measured load-displacement and load-time data, which compares compression test data from a conventional static test with data from a test where ultrasonic excitation of the lower platen was applied during plastic deformation. Figure 5.6 (a) shows the stress-strain relationship for LU excitation continuously applied under a dry surface condition. For clarity, during applied ultrasonic excitation the paths of the maximum, mean and minimum oscillating stress are included in the figure, rather than the oscillations. The figure shows that the mean flow stress, and maximum and minimum oscillatory stresses are significantly reduced from the static stress at the onset of ultrasonic excitation and follow a path parallel to the static stress path.

Figure 5.6 (b) shows the stress-strain curves for static compression and for static-ultrasonic compression for two intervals of ultrasonic excitation of the lower platen during plastic deformation under dry surface conditions. In this test, ultrasonic excitation was applied for 6 seconds, then discontinued and after 6 seconds of continued static compression the ultrasonic excitation was applied again for 12 seconds. Comparing Figure 5.6 (a) with Figure 5.6 (b) the two figures can be overlaid, exhibiting exact correspondence between the paths of the maximum, mean and minimum oscillating stress during ultrasonic excitation intervals. This demonstrates that the effects of applied ultrasonic excitation do not depend on the duration of the interval of excitation or on the strain at which the ultrasonics is switched on or off.

For compression tests using the three lubricants, ultrasonic excitation was again applied to the lower platen continuously and then for two short intervals during plastic deformation. The results are shown in Figure 5.7. The static compression data is included in each figure and the ultrasonic oscillatory stress is again represented by maximum, mean, and minimum stress paths. Again, the mean flow stress, and maximum and minimum oscillatory stresses are significantly reduced at the onset of ultrasonic excitation and follow a path parallel to the static stress path. If the stress-strain curves for the lubricated surfaces are compared with the stress-strain curves for the dry surface in Figure 5.6, then it is observed that the oscillatory stress-strain

relationship is very similar in all cases. For example, the reduction in mean stress is 40 MPa at a strain of 0.22 and the peak-peak oscillatory stress amplitude is 24 MPa. Therefore, it can be concluded that the application of lubricants in the ultrasonic compression tests did not significantly modify the oscillatory stress behaviour from the dry surface contact behaviour.

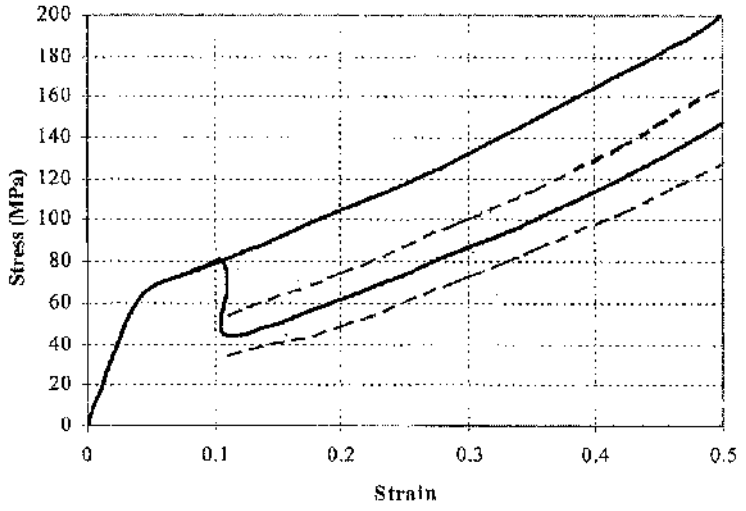

(a) Continuous ultrasonic excitation.

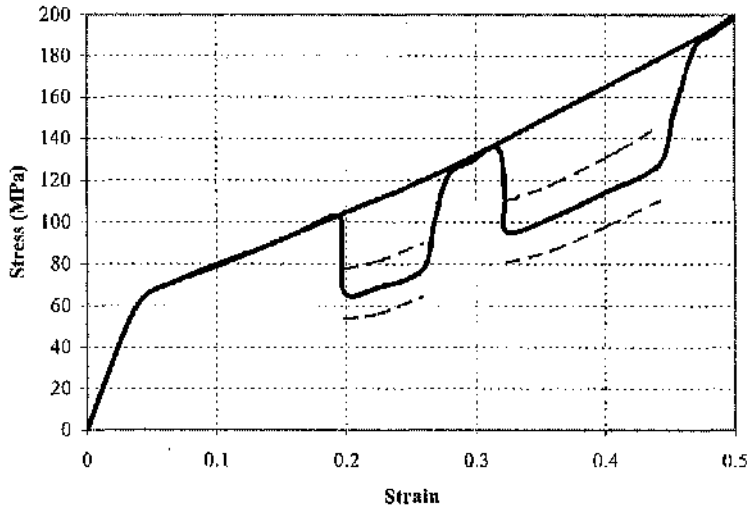

(b) Two intervals of ultrasonic excitation.

Figure 5.6: Measured static and ultrasonic compression test for dry surface, showing: — static and mean stress, ----- path of max. and min. oscillatory stress.

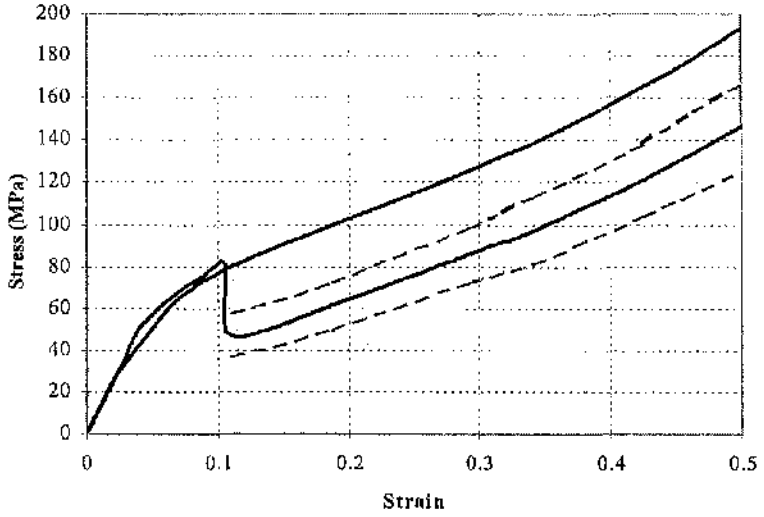

(i) Continuous ultrasonic excitation.

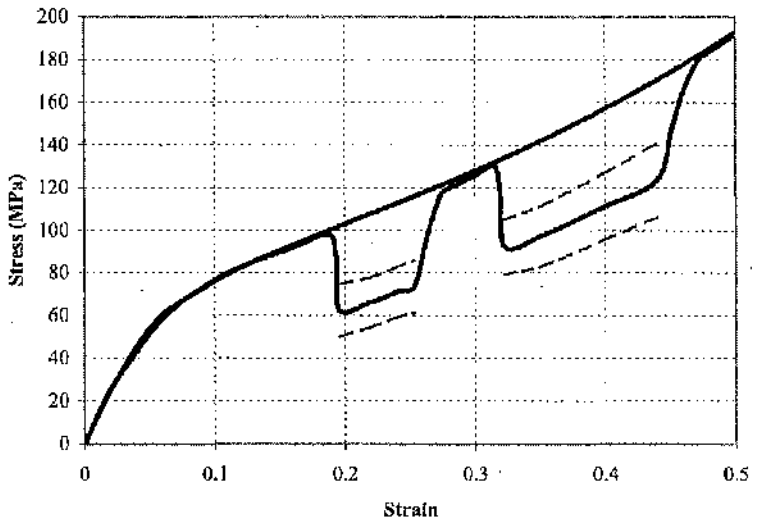

(ii) Two intervals of ultrasonic excitation.

Figure 5.7 (a): Measured static and ultrasonic compression test for oleic acid lubricated interface showing: — static and mean stress, ----- path of max. and min. oscillatory stress.

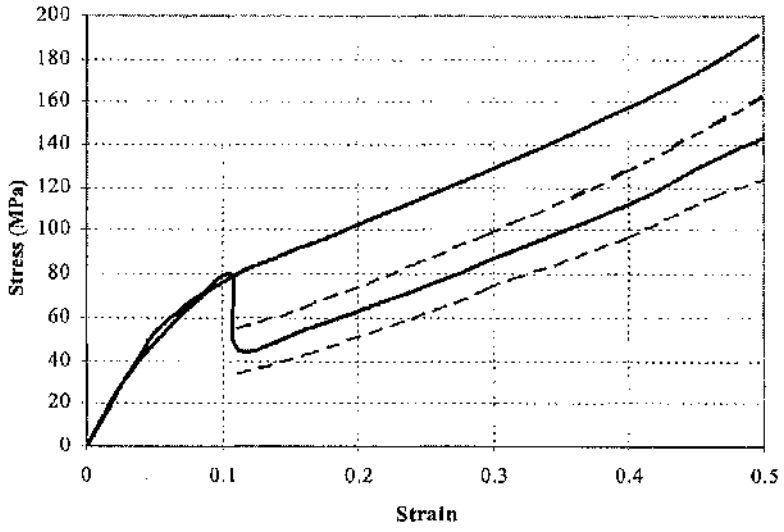

(i) Continuous ultrasonic excitation.

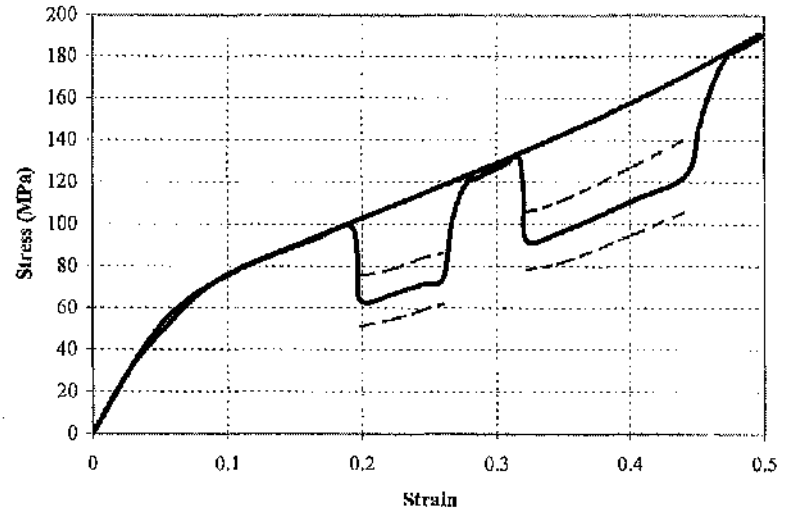

(ii) Two intervals of ultrasonic excitation.

Figure 5.7 (b): Measured static and ultrasonic compression test for Lubrodal lubricated interface showing: —— static and mean stress, ----- path of max. and min. oscillatory stress.

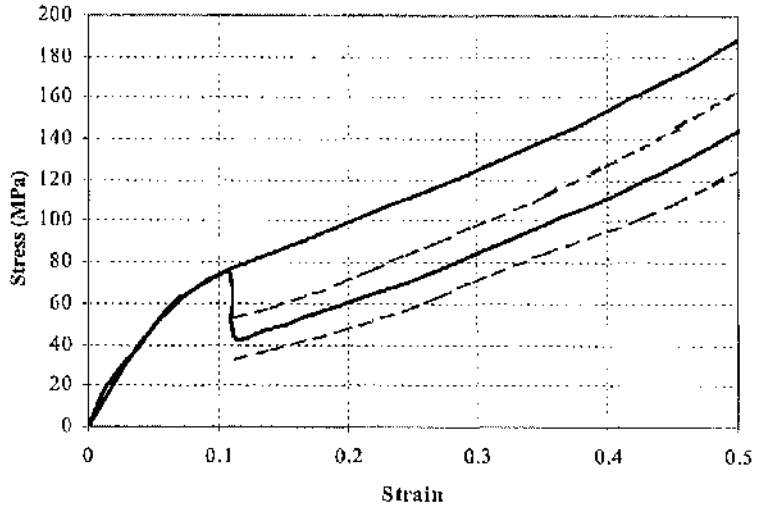

(i) Continuous ultrasonic excitation.

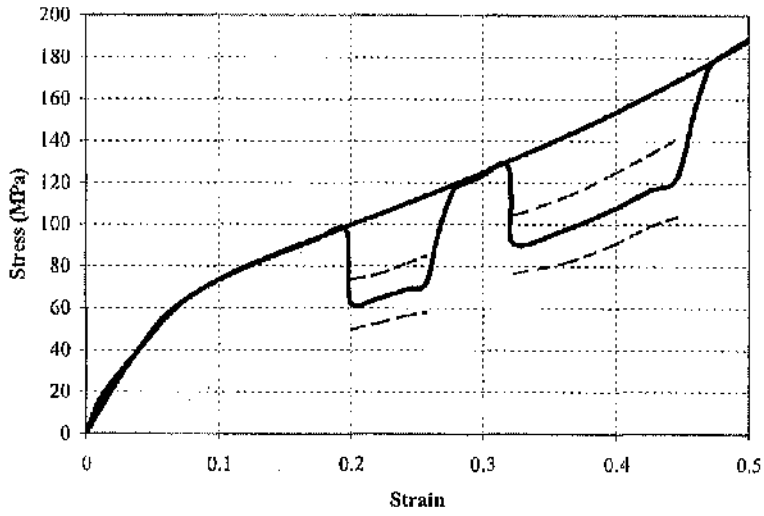

(ii) Two intervals of ultrasonic excitation.

Figure 5.7 (c): Measured static and ultrasonic compression test for PTFE lubricated interface showing: — static and mean stress, ----- path of max. and min. oscillatory stress.

However, it is also clear from Figure 5.6 and Figure 5.7 that the stress-strain relationships from compression tests do not satisfy the description of oscillatory stress superposition. There is a significant measured reduction in the path of the maximum oscillatory stress from the static stress. Also, the oscillatory stress amplitude is significantly higher for LU compression than for LU tension tests (Chapter 3).

In order to assess any response contributions due to machine dynamics throughout all the tests, the displacement amplitude response of the lower and upper platens was measured using laser vibrometers, on the top surface of the block, on the upper platen, and on a side of the specimen, as shown in Figure 5.8. For the compression tests reported here, the block horn was driven at a nominal constant longitudinal mode peak amplitude of 10 μm during ultrasonic compression. From Figure 5.8, the displacement vibration amplitude response of the upper platen increases linearly with specimen height reduction, but shows that little ultrasonic vibration is transmitted to the upper platen, with the amplitude increasing from 1.0 to 2.5 μm during compression. For the specimen, the displacement amplitude response measures a nearly linear decrease with specimen height reduction from 6.5 to 5.0 μm. It is clear that the ultrasonic system used in the compression experiments satisfied the requirement to deliver a constant nominal amplitude to the lower platen throughout the process and it is maintained at 10 μm. Hence, the flow stress reduction during LU compression tests was not attributable to any dynamic phenomena, such as resonance, of the ultrasonic system.

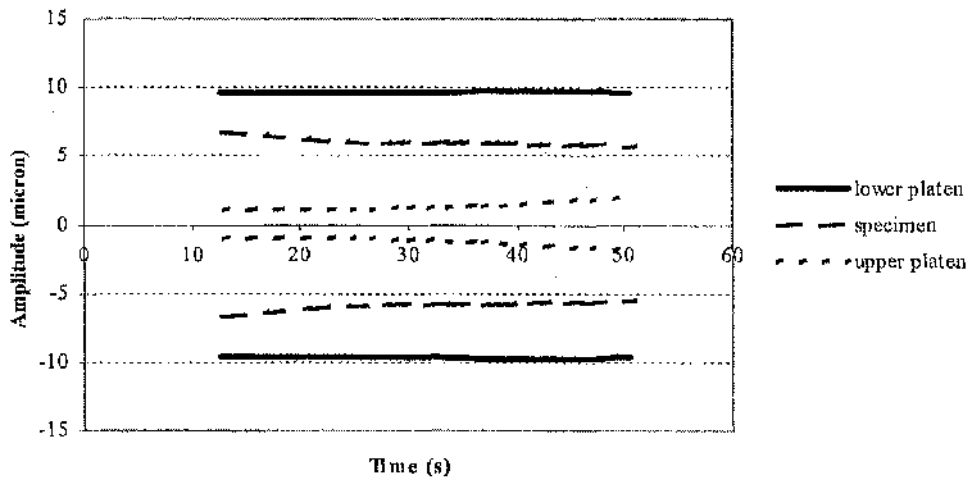

Figure 5.8: Amplitude response measured on lower platen, upper platen, and specimen during ultrasonic compression test.

Specimen temperature was also recorded for each interface condition, using an embedded thermocouple in the specimen at the interface of the lower platen. It can be seen from Figure 5.9 that during LU compression tests no significant rise in surface temperature was recorded. For the dry surface and three lubricated interfaces, when the specimen deformed to about half of the total height reduction, the temperature had increased from 18°C to a maximum of 24°C. Subsequently, when the specimen height reduced to 50% of the original height, the interface temperature had fallen again and was measured at 22°C. Similar results were reported by Izumi [12] for ultrasonic compression tests, and Konovalov [29] for ultrasonic tension tests for aluminium and other metals, where the bulk temperature of the metal specimen was not significantly increased by the ultrasonic energy. In the present investigation, no significant increase in surface temperature was recorded, therefore softening of the surface asperities due to an elevation in surface temperature could not be proposed as an explanation for the flow stress reduction during ultrasonic compression, as has been suggested in some previous studies [12, 20, 29].

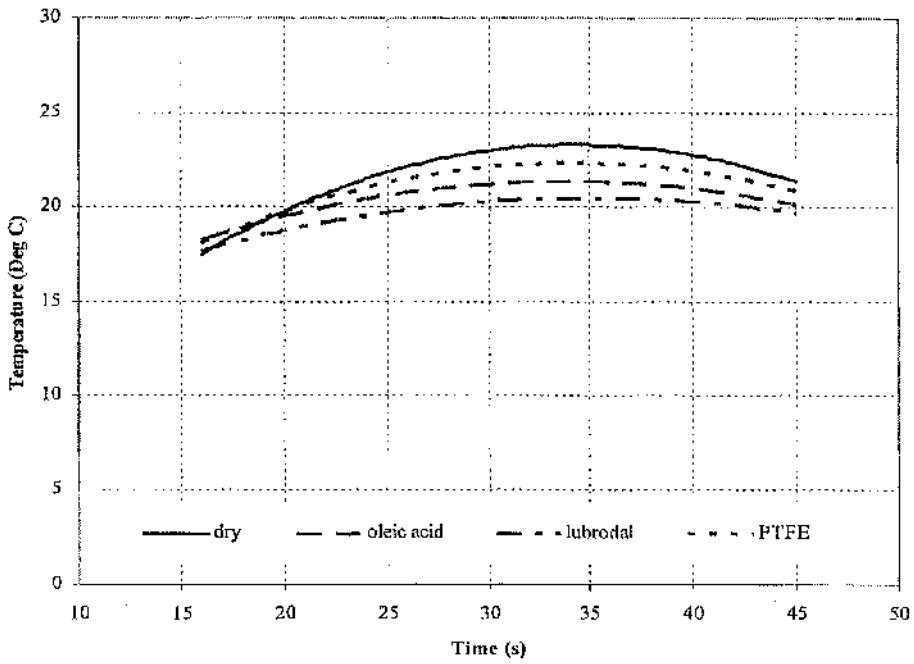

Figure 5.9: Temperature profile measured on the lower platen and specimen interface during LU compression test.

At the microscopic level, it has been claimed in previous studies that with a small increase in temperature ultrasonic energy could activate the process of migration and interaction of dislocations in local microvolumes, where the dislocation distribution formed into clusters [28]. It has also been suggested that under ultrasonic load, the local temperatures at the sites of different types of microscopic defects can be higher than the bulk temperature [28]. Although it is not possible to draw direct conclusions from comparison with these previous studies within the scope of this thesis, they may provide explanations of the effective material softening measured in the LU compression experiments which could be related to localised temperature effects on the microstructure.

5.6 Discussion on the Modification of FE models for LU Compression

The finite element (FE) models for compression were adjusted by including an effective material softening which was characterised for tension test modelling as described in Chapter 3. However, it is clear from comparison of the LU tension and compression test data of Chapter 3 and Figures 5.6 and 5.7, that the oscillatory stress response is quite different in tension and compression.

5.6.1 Adjusting material properties

For the compression model, the material properties during ultrasonic excitation input into the FE model are based on a stress-strain relationship that has been derived from the measured path of the mean oscillatory stress of the tension test experimental data (Chapter 3), providing a softer material model but with no effects of contact friction. Account has been taken of the differences in the stress-strain relationship for the aluminium specimens in tension and compression by only considering a low strain range (less than 0.3) in plastic deformation for the FE models, where tension and compression stress-strain data are in close agreement for the softer material model.

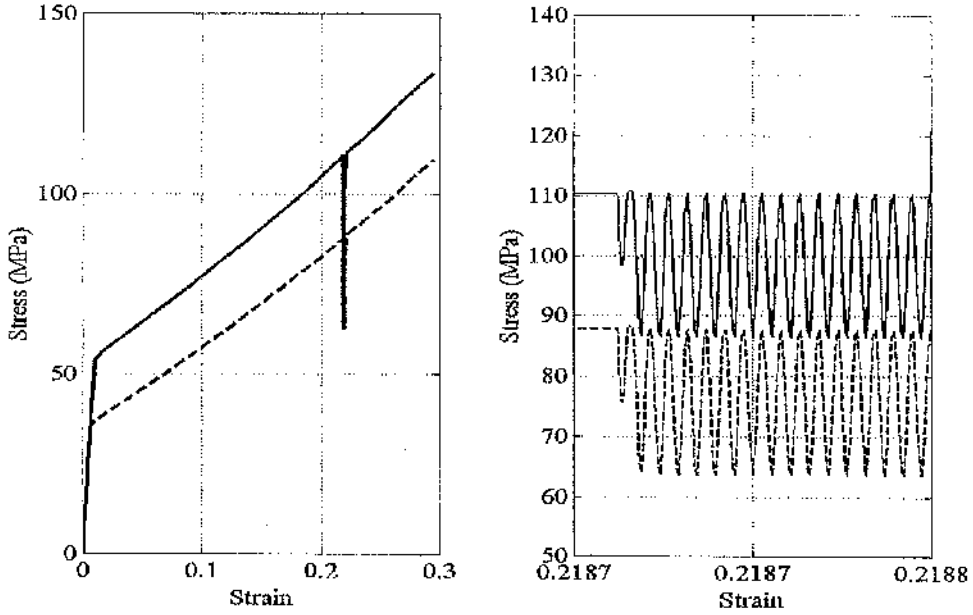

Figure 5.10: Compression FE model showing a short interval of superimposed LU excitation for: — original properties of material, and ----- softened properties of material.

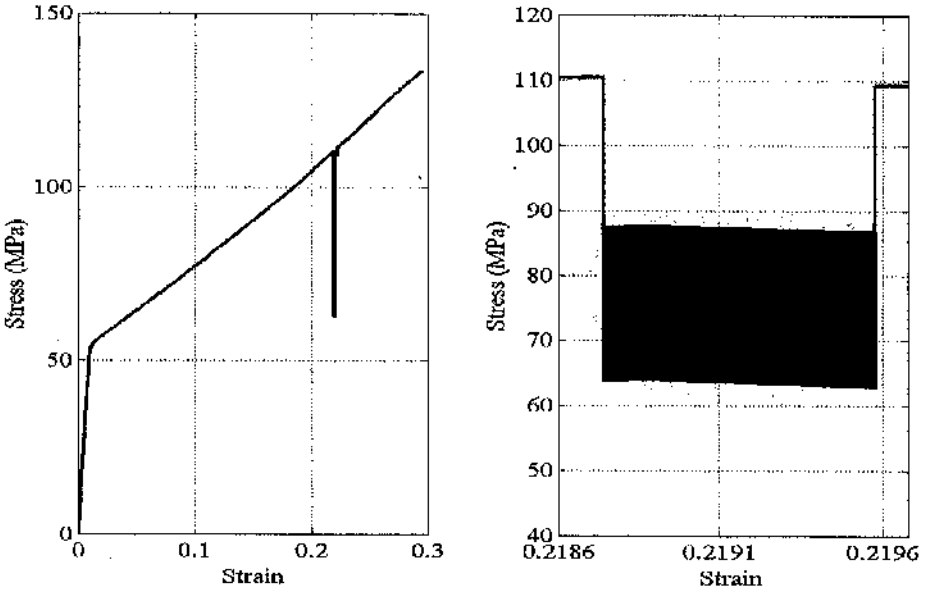

Figure 5.11: FE model showing the original material properties during static compression and softened material properties during ultrasonic compression.

For the compression test FE model, Figure 5.10 shows the predicted stress-strain relationships for the original and adjusted material properties, including a short interval of ultrasonic excitation of the lower platen. In Figure 5.11, the original aluminium material properties were modelled for static compression and then the softened material properties were used as the material model during static-ultrasonic compression. The coefficient of friction of $\mu = 0.25$ was kept constant. From the FE data, with adjusted material properties, for superimposing ultrasonic excitation at a strain of 0.218 the mean stress is reduced by 35 MPa and the peak-peak oscillatory stress amplitude is 24 MPa. It is clear that the oscillatory stress amplitude from experimental and FE data is the same, at 24 MPa, but agreement is not so close for the mean stress reduction, which exhibits a 5 MPa difference. It is possible that a more realistic representation of the compression test data could be modelled by combining a temporary adjustment in material properties with a temporary adjustment in the friction contact condition during ultrasonic excitation.

5.6.2 Adjusting the coefficient of friction

Initially, an investigation of the effects of only adjusting the coefficient of friction in the FE compression test simulation was conducted in order to determine whether the measured reduction in maximum oscillatory stress could be explained purely in terms of a temporary change in the coefficient of friction during the intervals of ultrasonic excitation of the lower platen. Previous studies [5, 12] have suggested that improved friction conditions at the specimen-platen interface mainly contribute to the measured reduction in mean forming load. These findings have been largely unsubstantiated due to the lack of measurement of the oscillatory force response. Therefore, in this study, an FE model was developed by adopting an interface friction coefficient of $\mu = 0.25$, representing a dry surface condition, for static compression and then changing this to a friction free contact by setting $\mu = 0$ during static-ultrasonic compression.

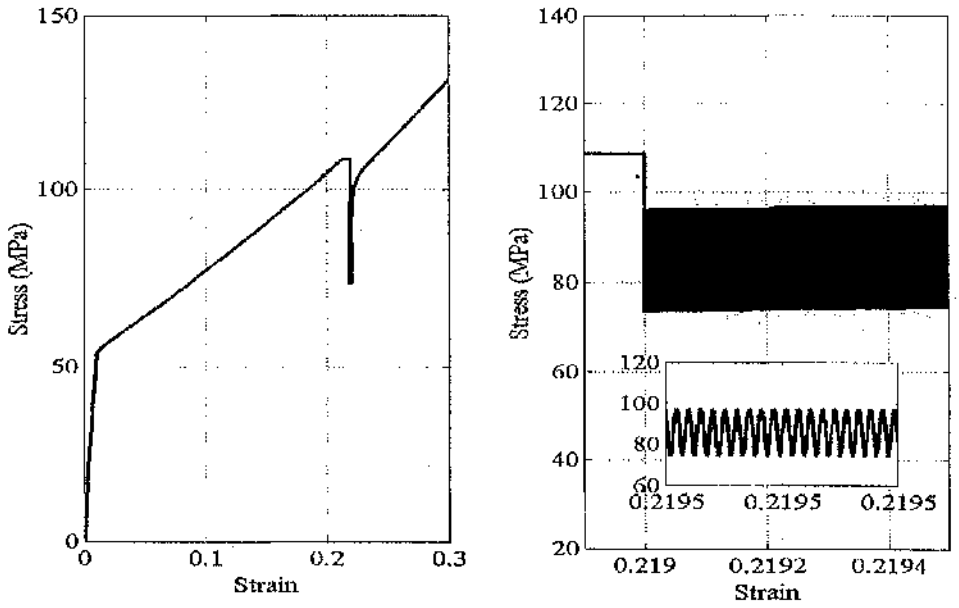

Figure 5.12: FE model data showing an interval of ultrasonic excitation, with a friction coefficient $\mu = 0.25$ during static compression adjusted to friction free, $\mu = 0$, for ultrasonic compression (using original material properties data).

The model effectively changes the boundary condition from a dry surface to a friction free condition. In Figure 5.12, the numerical stress-strain data is shown and it can be seen that by temporarily reducing the coefficient of friction to zero during the interval of LU excitation of the lower platen, the paths of the mean, maximum and minimum oscillatory stress are all reduced, departing from the stress superposition model and in common with the experimental stress-strain data. However, there are significant differences between the measured stress-strain data and the FE predictions. Firstly, the FE model predicts a reduction in the mean oscillatory stress of 22 MPa from the static stress. However, the experimental results measure a reduction of 40 MPa in the mean oscillatory stress. Further, a reduction in the coefficient of friction to zero leads to a reduction in the paths of the maximum, mean and minimum oscillatory stress, and the calculated oscillatory stress amplitude is exactly the same as for the stress superposition model, estimating a peak-peak amplitude of 24 MPa for both contact models. This would suggest that a temporary reduction in the coefficient of friction cannot solely explain the experimental results.

5.6.3 Combined effects of adjusted material properties and friction

A compression test FE model was developed which combined the effects of adjusting the material properties with an adjustment in the coefficient of friction. The original material properties for aluminium and a coefficient of friction of 0.25 were used for static compression. For intervals of LU excitation, the softened material properties and a coefficient of friction of 0.15 were adopted. The coefficient of friction of 0.15 was chosen to provide an estimate that, combined with the softened material properties validated by the tension test model, would result in a reduction in the mean oscillatory stress comparable with the experimental data. The resulting predicted stress-strain curve is plotted in Figure 5.13. For superimposing ultrasonic excitation at a strain of 0.219, the mean stress is reduced by 38 MPa and the peak-peak oscillatory stress amplitude is 24 MPa. These results show that a close correlation between experiment and FE model data for static-ultrasonic compression is achievable by modelling the effects of superimposed ultrasonic excitation as a combination of a temporary reduction in the coefficient of friction and an adjustment of the material properties to match the path of the mean stress-strain data from an ultrasonic tension test.

In this case, the combination of a reduction in the coefficient of friction and the adjusted material properties has been chosen so that the same softer material is adopted for ultrasonic tension and compression models. This assumes that the difference between tension and compression data is the issue of the contact friction condition. However, the same reduction in mean oscillatory stress, of 40 MPa and the same oscillatory stress amplitude, of 24 MPa, is achievable in the compression model by adjusting the material properties further to adopt an even softer material model and maintaining the coefficient of friction at 0.25. This may also offer a valid explanation of the experimental data as the improved coupling of ultrasonic energy into a compression specimen compared to a tension specimen could have a more significant effect on the specimen material, especially if these effects are localised. Clearly, these issues can only be addressed by developing an understanding of the microstructural response of this soft grade aluminium to the applied ultrasonic excitation.

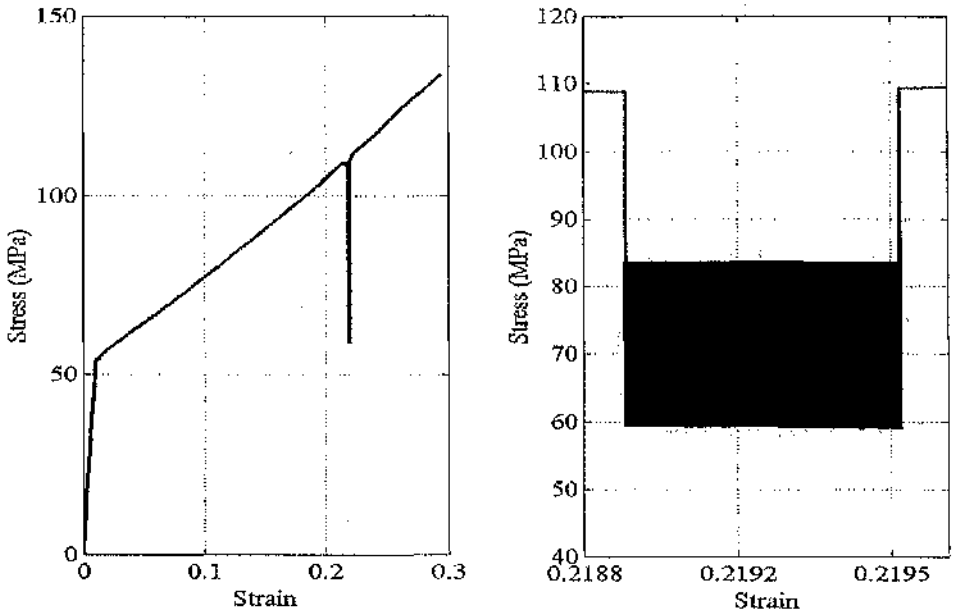

Figure 5.13: FE model showing an interval of ultrasonic excitation for the combined effects of a change in material properties and a change in friction coefficient from μ = 0.25 to μ = 0.15 for ultrasonic compression.

5.7 Discussion of RU Compression Test Results

The effects of applying a radial mode ultrasonic vibration during the compression process are investigated. Again, the mean, maximum, and minimum paths are plotted to represent the oscillatory stress and, for comparison, the conventional static stress data are included in the figures. Figures 5.14 and 5.15 illustrate the consistent results for continuous and two interval RU excitation applied to the lower platen during plastic deformation under different lubrication conditions. In general, the onset of ultrasonic excitation results in an immediate drop in the mean, maximum and minimum oscillatory stress from the static stress and they follow a path parallel to the static stress path. By comparing the continuous ultrasonic excitation, Figure 5.14 (a) or Figures 5.15 (i), with two intervals of ultrasonic excitation, Figure 5.14 (b) or Figures 5.15(ii), during compression for dry and lubricated surfaces, the two can again be overlaid, exhibiting exact correspondence between the paths of the maximum, mean and minimum oscillating stress during ultrasonic excitation intervals.

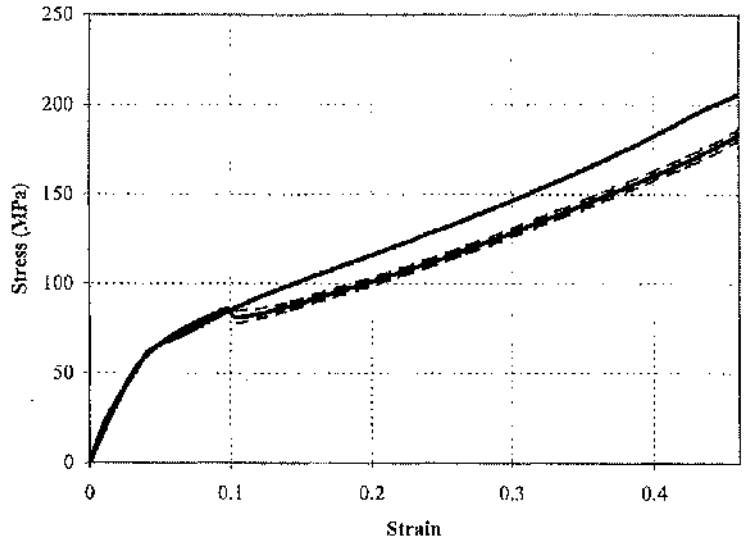

(a) Continuous ultrasonic excitation.

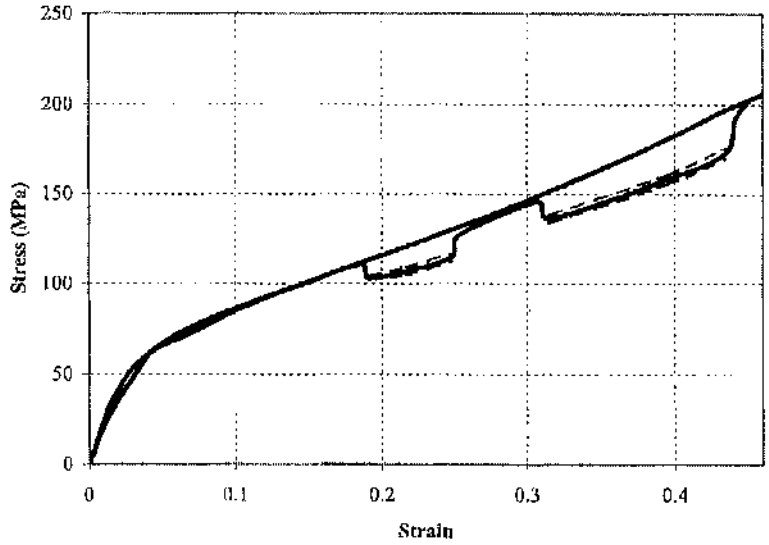

(b) Two intervals of ultrasonic excitation.

Figure 5.14: Measured static and RU compression test for dry surface showing: — static and mean stress, ----- path of max. and min. oscillatory stress.

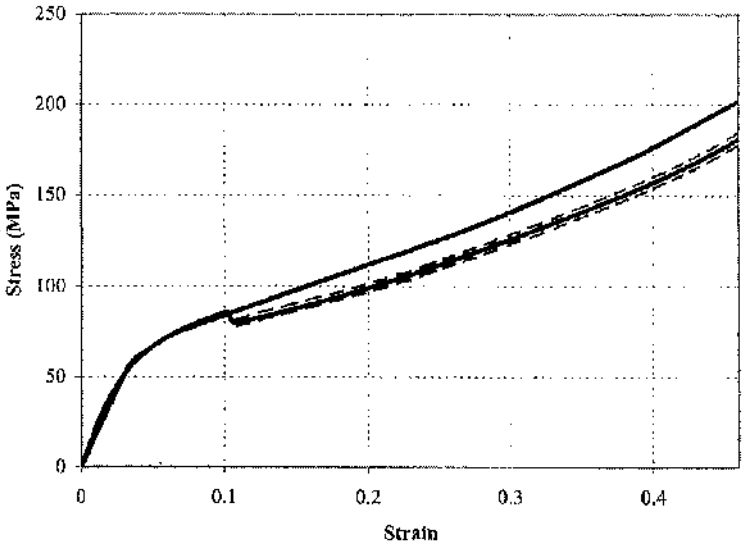

(i) Continuous ultrasonic excitation.

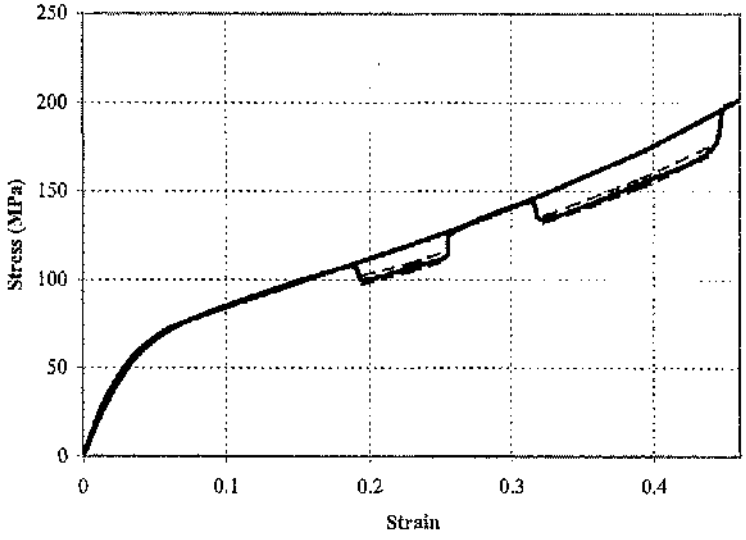

(ii) Two intervals of ultrasonic excitation.

Figure 5.15 (a): Measured static and RU compression test for oleic acid lubricated surface showing: — static and mean stress, ----- path of max. and min. oscillatory stress.

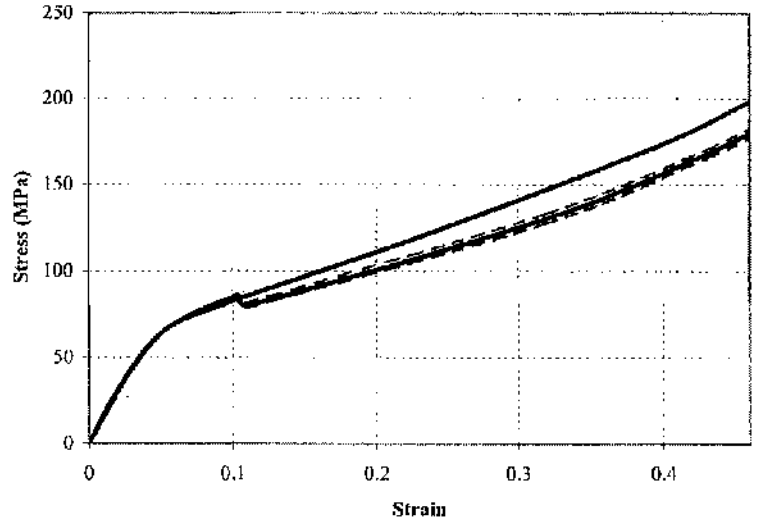

(i) Continuous ultrasonic excitation.

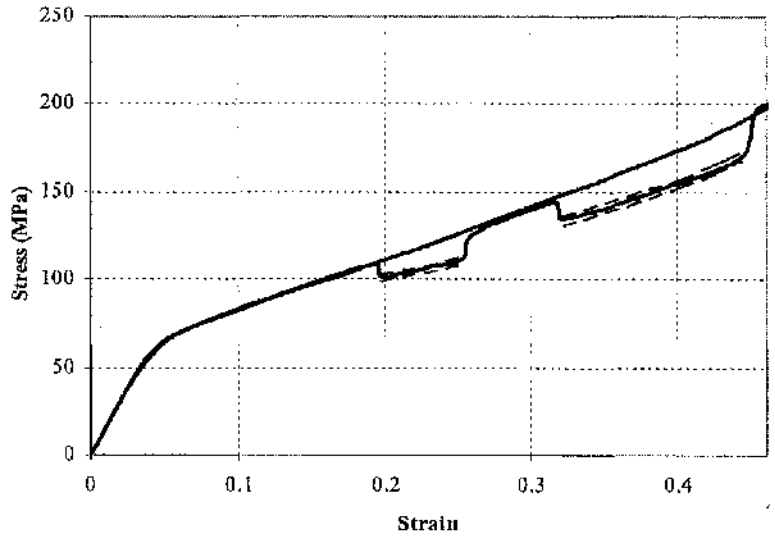

(ii) Two intervals of ultrasonic excitation.

Figure 5.15 (b): Measured static and RU compression test for Lubrodal lubricated surface showing: — static and mean stress, ----- path of max. and min. oscillatory stress.

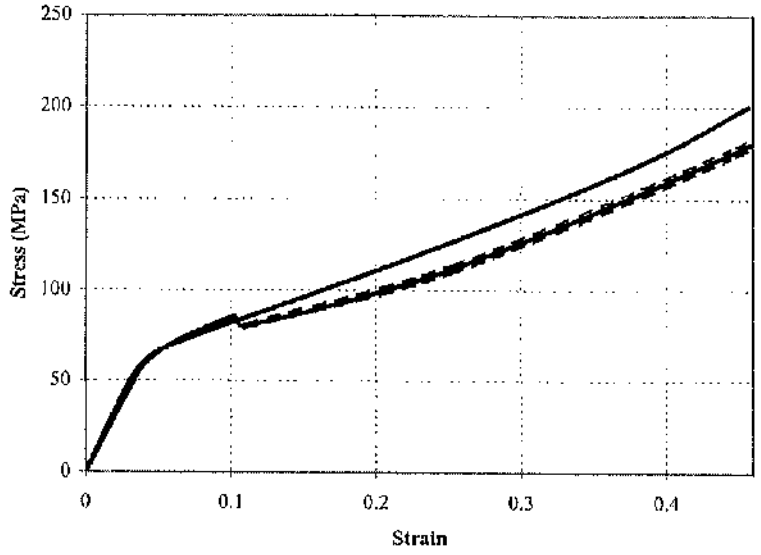

(i) Continuous ultrasonic excitation.

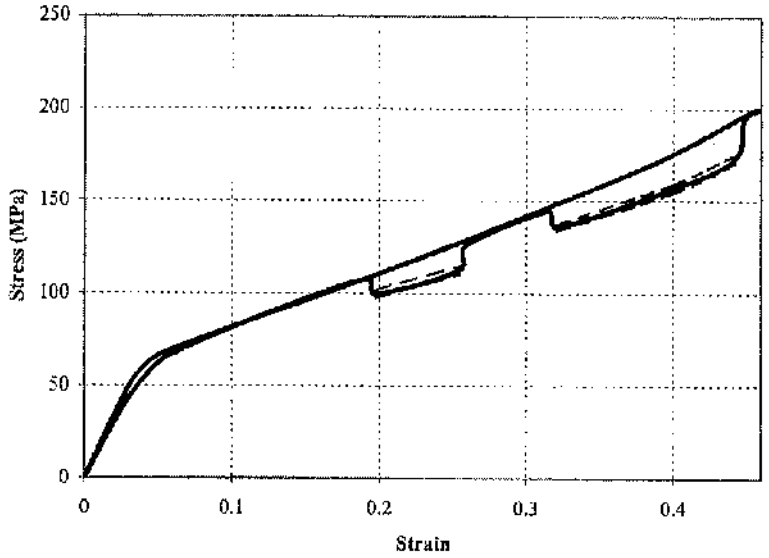

(ii) Two intervals of ultrasonic excitation.

Figure 5.15 (c): Measured static and RU compression test for PTFE lubricated surface showing: — static and mean stress, ----- path of max. and min. oscillatory stress.

If the stress-strain curves for RU compression under lubricated conditions are compared with the stress-strain curves for the dry surface, with $\mu = 0.25$, the oscillatory stress-strain relationship is very similar in all cases. For example, the reduction in mean stress is 9 MPa at a strain of 0.22 and the peak-peak oscillatory stress amplitude is 4 MPa. Again, it can be suggested that the application of lubricants in the RU compression tests did not significantly modify the oscillatory stress behaviour from the dry surface contact.

Under all interface conditions, the mean stress reductions and peak-peak oscillatory stress amplitudes for RU compression are less than the mean stress and peak-peak oscillatory stress amplitudes for LU compression. Some of the difference is accounted for by the different vibration amplitudes used in longitudinal and radial mode ultrasonic tests, since for classic oscillatory stress superposition the oscillatory stress amplitude and hence the mean oscillatory stress are dependent on the amplitude of the applied ultrasonic vibration. However, this factor does not account for the size of the discrepancy between the oscillatory stress amplitudes and mean stress reductions for longitudinal and radial ultrasonic compression. This suggests that the coupling effects of the co-axial static load and vibration displacement of the lower platen on the specimen in LU compression provided a greater effect on the material deformation. For RU compression, the oscillation direction is normal to the static loading axis and therefore does not result in an enhanced physical coupling of ultrasonic energy into the specimen. Intuitively, RU compression is more likely to affect the interface friction condition.

A previous study suggested that the reduction of yield stress under applied radial ultrasonic excitation was due to a rise in bulk temperature and a reduction in interface friction [14]. Similar results were recently reported by Huang [104] for plasticine specimens compressed under radial ultrasonic excitation. For the aluminium specimens in the present study, there is no significant temperature increase measured during RU compression for dry and lubricated contact surfaces. Figure 5.16 illustrates the profiles of the interface temperature. As the specimen deformed to half of its total height reduction, the maximum temperature recorded was 25°C for the surface lubricated with PTFE, and the temperature gradually decreased to 20°C as the specimen fully deformed

to the total height reduction. For the surfaces which were lubricated with Lubrodal and oleic acid, there was no measurable change in temperature.

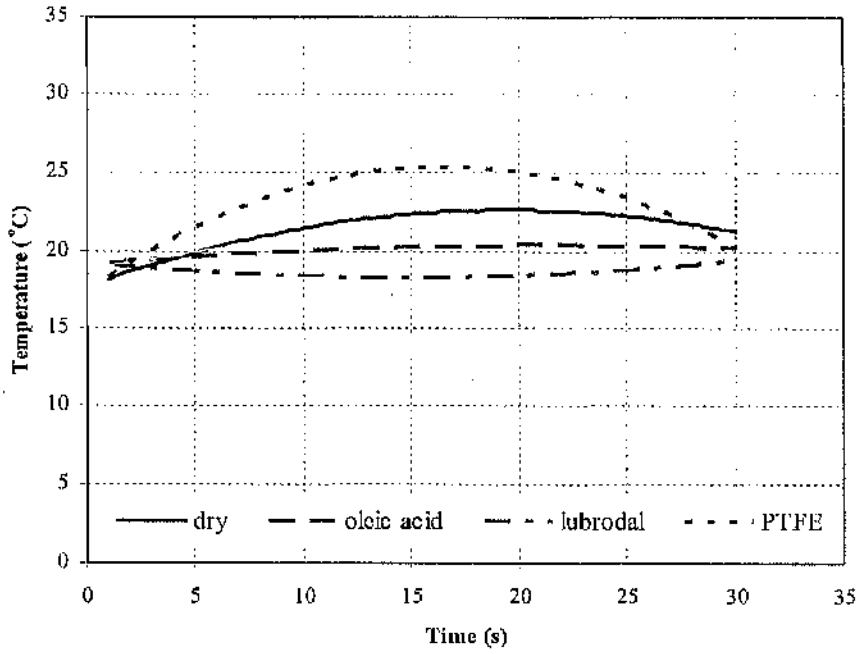

Figure 5.16: Temperature profile measured on the lower platen and specimen interface during RU compression test.

5.8 Discussion of FE Model Results for RU Compression

In some previous investigations, radial ultrasonic excitation has been applied in the study of a wire drawing process. In most cases, the application of ultrasonic excitation onto the drawing die, giving a tangential oscillation relative to the specimen motion, reduced the drawing force and it was suggested that this reduction was caused by a reduction in interface friction [9, 24]. Since the oscillatory stress was not measured, there were conflicting interpretations of the measured data and of the possible factors that could reduce the mean stress. It was not known whether a change in friction or stress superposition effects or both caused the reduction in mean stress. Since there are no previous investigations reporting RU compression of metals, the experimental data cannot be compared with any previous similar experimental results.

In an attempt to simulate the experimental data with FE models, initially the numerical effects on stress-strain behaviour were examined when a constant dry interface friction coefficient, $\mu = 0.25$, was applied during static and ultrasonic excitation intervals. Figure 5.17 shows the calculated stress-strain curve for static and RU intervals for $\mu = 0.25$. At the onset of RU excitation, the mean oscillatory stress reduced by approximately 4 MPa from the static stress, whereas the measured reduction was 9 MPa in the experiments. At a strain of 0.2188, the peak-peak oscillatory stress amplitude is 3 MPa which agrees quite well with the 4 MPa peak-peak stress amplitude measured in the RU compression experiments. It can be observed in the FE data in Figure 5.17, that unlike LU compression simulations, RU simulations calculate a drop in the maximum oscillatory stress from the static stress for a constant coefficient of friction for static and RU compressions and this does not fit with the classic oscillatory stress superposition definition described in Chapter 3. For radial mode ultrasonic excitation, the friction force and excitation force are co-axial and the ultrasonic excitation force modifies the friction force vector cyclically. It is therefore expected that the friction force is modified even though the coefficient of friction is constant and that this accounts for the drop in maximum oscillatory stress from the static stress in RU compression simulations under a constant interface friction coefficient.

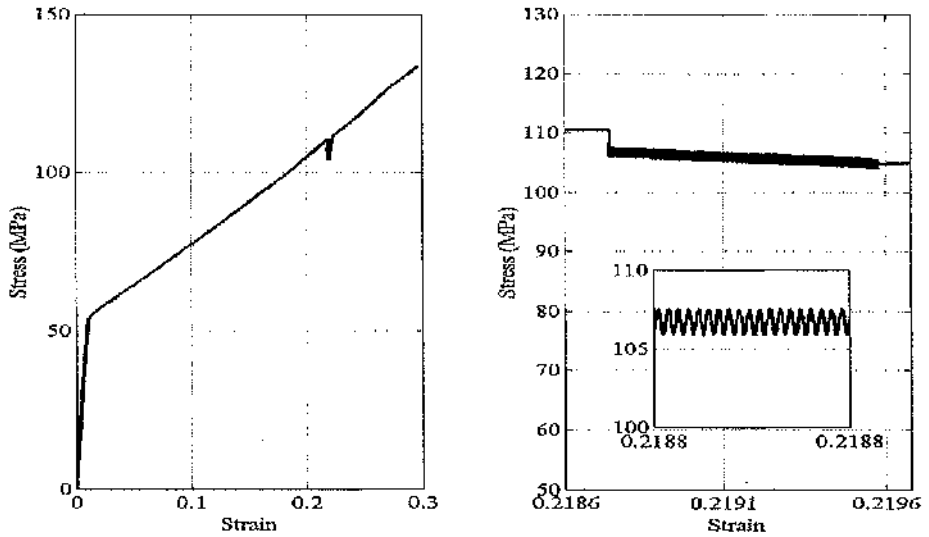

Figure 5.17: FE model showing an interval of RU excitation for a constant coefficient of friction $\mu = 0.25$, inset shows zoomed view of oscillatory stress amplitude.

The investigation using the FE model continued by changing the interface friction coefficient from dry to a friction free condition, $\mu = 0$. Figure 5.18 plots a compression test simulation with $\mu = 0$ throughout, and with an interval of ultrasonic excitation (which cannot be seen in the main figure but it is visible in the zoomed inset). During the interval of RU excitation there is no measurable change in the mean stress and no significant peak-peak stress amplitude was calculated. Figure 5.19, compares the two previous figures, illustrating how the oscillatory stress amplitude for $\mu = 0$ is extremely small and therefore not visible in the figure. Figure 5.19 also shows that the difference between the static stress and mean oscillatory stress at a strain of 0.219 for $\mu = 0.25$ is 6 MPa, which is less than the measured mean reduction of 9 MPa when RU was superimposed on the static load during compression.

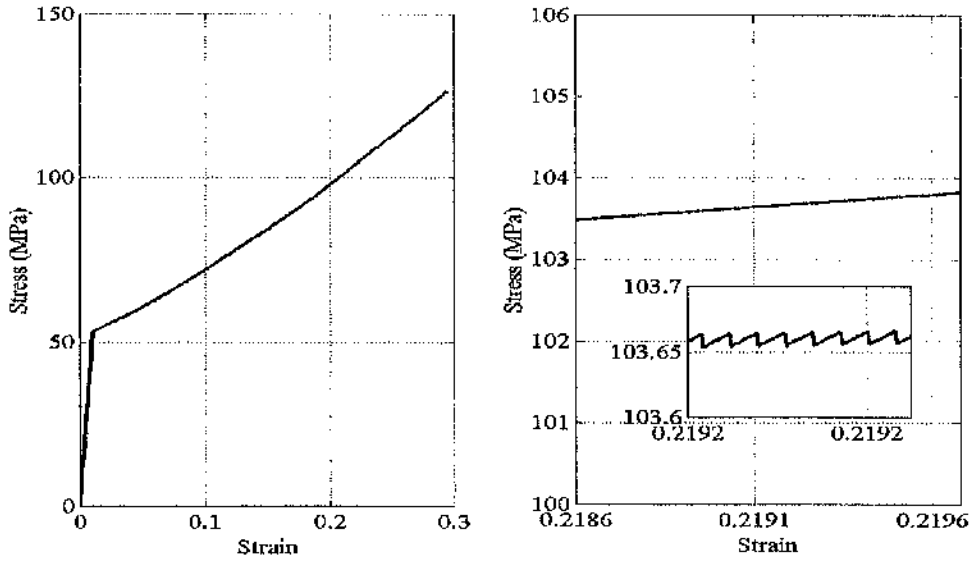

Figure 5.18: FE model showing an interval of RU excitation for zero friction, $\mu = 0$, inset shows zoomed in view of oscillatory stress amplitude.

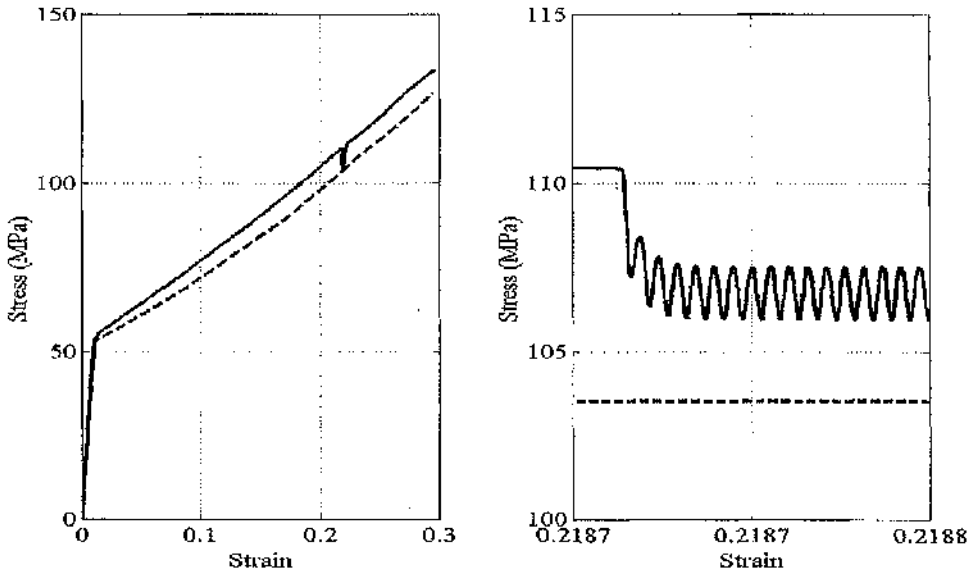

Figure 5.19: Combining Figure 5.17 and 5.18 for RU excitation, showing — for μ = 0.25, ---- for μ = 0, left shows zoomed in view of oscillatory stress amplitude (which is too small to be visible for μ = 0).

The above models do not satisfactorily represent the experimental results of the mean flow stress reduction under applied RU excitation during compression tests. The FE model was therefore developed by adjusting the coefficient of friction from a value which represents a dry surface to a friction free surface during RU excitation. Figure 5.20 illustrates the numerical effects on the stress-strain relationship. By changing the numerical friction coefficient from μ = 0.25 for a dry surface to a frictionless surface, μ = 0, during applied RU excitation, the mean oscillatory stress is now significantly reduced from the static stress. For applying ultrasonic excitation at a strain of 0.219, the mean stress is reduced by 15 MPa from the static stress but there is no measurable peak-peak oscillatory stress amplitude. For a friction free contact there is no resistance to sliding and no friction force, and the force in the radial direction at the contact surface is only due to the ultrasonic excitation force. The calculated oscillatory force response is therefore of very low amplitude, leading to a low oscillatory stress amplitude in the calculated stress-strain relationship. This is not a practically realisable test configuration.

There are dissimilarities between the FE model data and the experimental results. Firstly, the measured reduction in the mean stress from static to RU excitation is 9 MPa, for all surface conditions, however the FE model predicted 15 MPa. The peak-peak stress amplitude from the RU compression experiments was consistently 4 MPa, for all surface conditions, whereas the FE model predicts a peak-peak oscillatory stress amplitude of only 0.01 MPa.

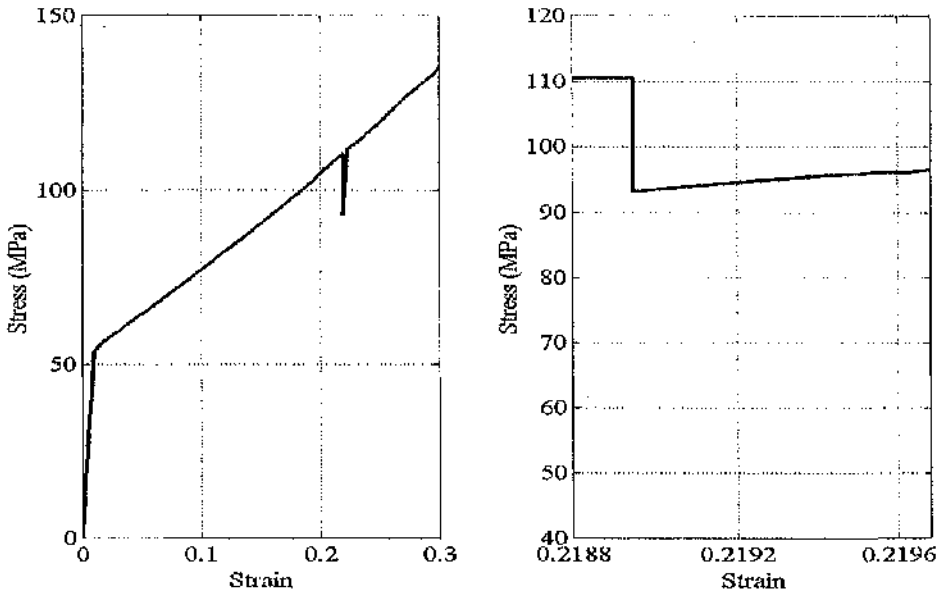

Figure 5.20: FE model showing an interval of RU excitation for friction coefficient μ = 0.25 for static compression and change to friction free, μ = 0 for ultrasonic compression, left expanded scale of ultrasonic stress interval.

Another FE model was developed, where the coefficient of friction was maintained at μ = 0.25 during static compression, and was changed to μ = 0.15 during the ultrasonic compression interval. From the calculated stress-strain relationship, as illustrated in Figure 5.21, a close agreement is now achieved with the measured stress-strain data under dry and lubricated surface conditions. The reduction in mean stress which was measured from the experiments is identical to the reduction which is predicted by the FE model. At a strain of approximately 0.22 the mean stress is reduced by 9 MPa from the static stress. The measured peak-peak stress amplitude at the same strain value is 4 MPa from experimental results and predicted at 3 MPa from simulation data. This result agrees with previous studies [10, 24, 93] which claim that the interface friction can be reduced if the specimen is subjected to a radial ultrasonic excitation during a static

deformation process. From the present investigation, however, it can be concluded that during RU compression, the interface friction coefficient is reduced to the same value under dry and lubricated surfaces and the use of lubricants does not further improve the interface friction under RU compression.

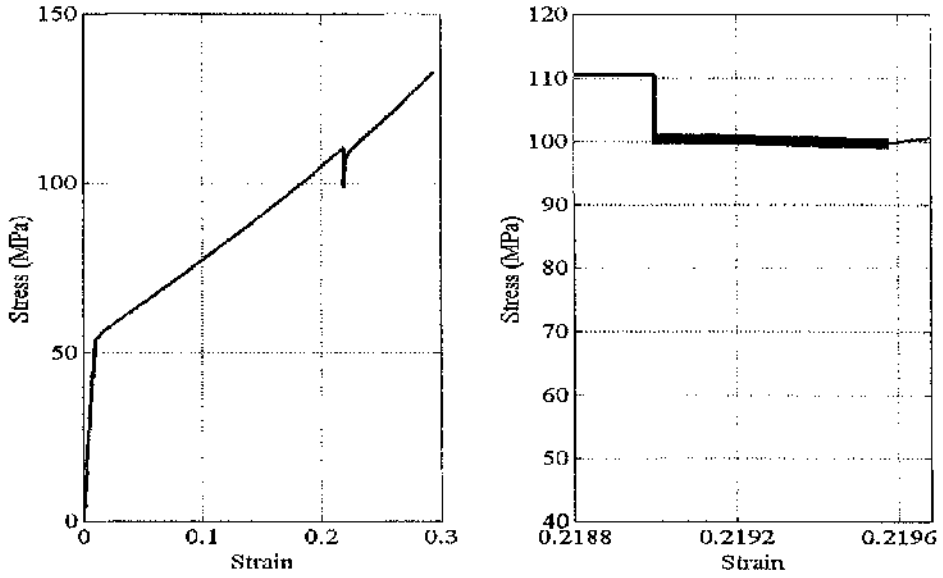

Figure 5.21: FE model showing an interval of RU excitation for friction coefficient μ = 0.25 for static compression and μ = 0.15 for ultrasonic compression.

5.9 Conclusions

The effects of the application of ultrasonic excitation in compression tests have been investigated. During plastic deformation, longitudinal and radial mode ultrasonic oscillations were superimposed on the lower platen, where dry and different lubricated surface conditions were applied. Finite element models were developed to investigate numerically the material and friction effects of ultrasonically assisted compression. The FE models were improved by modifying material and frictional parameters during ultrasonic compression. This provided a realistic prediction of the material and frictional behaviour for LU and RU compressions.

By considering the experimental and simulation results of tensile tests described in Chapter 3, with the modification of material and friction parameters of the compression

models, it can be concluded that the reduction in the oscillatory stress during LU compression is dominated by a softening mechanism of the material and coupling effects of the LU excitation response. Under dry surface conditions, it is concluded that the interface friction coefficient is reduced during LU compression, however the reduction in the friction coefficient was not sufficient to result in the significant measured change in the mean stress. It is therefore also concluded that the material is effectively softened during LU compression. To clarify the softening mechanism, further investigation is required into localised temperature and dynamic behaviours of the microstructure of the material.

An investigation into RU compression was carried out and it is concluded that the changes in the stress-strain relationship during RU compression can be accounted for by changes in the interface friction during RU compression. In the present study of the compression tests, RU excitation effectively reduced the coefficient of friction from a dry surface of 0.25 to a value of 0.15. It is also concluded that there is no effective material softening during RU compression.

The differences between the effects of LU and RU compression support experimental evidence that ultrasonic vibrations couple well into material specimens in compression when the compression axis and excitation axis coincide. The positive coupling in LU compression tests result in an effective material softening and changes in the interface friction condition, whereas the RU compressions alter the interface friction condition.

The application of lubricants on the die-specimen interface has not significantly modified the mean stress or oscillatory stress amplitude from the dry surface for both LU and RU compression tests.

CHAPTER 6

FINITE ELEMENT MODELLING OF ULTRASONIC EXTRUSION AND DIE-NECKING

6.1 Introduction

Since the work of Blaha and Langenecker in 1955 [1], researchers have carried out investigations into the effects of applying ultrasonic excitation to metals undergoing elastic and plastic deformations [2, 10, 19-21, 47, 103]. Experiments have been conducted under various conditions from pure tension and compression, to complex metalworking operations such as wire and strip drawing [9, 10], extrusion [25], and sheet-metal forming [105, 106]. The reported benefits of applying ultrasonic vibrations to tools include a reduction in forming load, an increase in achievable deformation and improvement in the product quality. These benefits have been attributed to volume effects and surface effects as described in Chapter 2. However, quantitative evaluations of the benefits have not previously been reported.

Friction at the die-billet interface, particularly for severe metal forming processes such as extrusion and sheet metal forming, significantly influences the forming load and quality of the final products. The use of lubricant in a severe metal forming process is a common procedure in order to improve the forming process. It has been reported that the use of a dry lubricant in the extrusion of aluminium effectively reduces the extrusion pressure compared to other types of lubricants [107, 108]. In sheet metal forming processes, when two metals are in sliding contact under pressure, as in deep drawing operations, galling or pressure welding of the tools and work metal is likely. When extreme galling occurs, the drawing force increases and becomes unevenly distributed causing fracture of the workpiece. To overcome these contact surface problems, lubricant is used based on the ability to prevent galling, wrinkling, buckling, and tearing during the deep drawing process. There are problems regarding the use of lubricants

however. These include the difficulty of removing it from the finished parts, the possibility for chemical reactions taking place at a certain load and temperature, and some high viscosity lubricants contain non-degradable materials which can cause environmental pollution [32, 109]. Accordingly, by utilising ultrasonic vibration in the forming process, it has been suggested that the application of a high viscosity lubricant in wire drawing can be avoided [32]. Also, by applying ultrasonic vibration, the interface friction in wire drawing [6, 9] and extrusion [25] are reduced, and the wrinkling of drawn cups in the deep drawing process is eliminated [108].

In a wire drawing process, radial mode ultrasonic excitation of the drawing die reduced the drawing force more than an applied axial mode ultrasonic vibration [32, 47]. In addition, the effect of ultrasonics in lowering the extrusion and drawing forces decreased as the extrusion speed or drawing rate increased for both radial and axial ultrasonic vibration [10, 25, 32]. It was claimed that by superimposing the ultrasonic excitation parallel to the drawing direction the interface friction coefficient was reduced by more than 30% compared to conventional drawing [6, 9]. The reduction was attributed to a friction force vector reversal mechanism causing intermittent metal-tool contact every cycle in the deformed area.

A study of the effects of ultrasonic excitation on sheet-metal forming was carried out by Jimma et al [105]. By ultrasonically vibrating the blank-holder and the die plate in a deep drawing process, the limiting drawing ratio was increased. By applying a radial mode ultrasonic excitation, the flange tears and wrinkles during drawing were also diminished. The authors agreed that the improvement in increasing the limiting drawing ratio and reducing defects during ultrasonic drawing was due to a reduction in the deformation resistance and friction as previously suggested by Blaha and Langenecker [1], which is known as Blaha's effect.

This chapter investigates the effects of the application of ultrasonic excitation in two metal forming processes: the extrusion of a cylindrical bar and die-necking of a hollow thin metal cylinder. During extrusion and necking processes, the frictional effects at the die-workpiece interface may contribute substantially to the overall load required to induce plastic deformation. In most cases, minimising friction is beneficial as it reduces

the force and energy required for a given operation. Reducing the stresses imposed on the tooling contributes to longer tool life and increased quality of the finished products.

Buckling in extrusion and sheet-metal forming can be prevented by lubricating the interface of the die and workpiece. However, perfectly lubricated surfaces are difficult to achieve because high pressure contact between the die and workpiece surfaces during deformation breaks the lubricant film. Hence, the application of ultrasonic vibration has been proposed to reduce the forming force in the extrusion process [25] and to reduce buckling in sheet metal forming [105, 106]. Although the beneficial effects obtained in previous studies were attributed to a reduction in friction, measurement of the oscillatory forces and the magnitude and mechanism of reduced interface friction due to ultrasonic vibration were not presented.

Therefore, in an attempt to determine a quantitative evaluation of the beneficial effects of ultrasonic excitation in the extrusion and die-necking operations, the investigations in this present study were carried out using numerical analysis. By utilising FE methods in the present study, a detailed investigation of the load and buckling data for different interface boundary conditions during ultrasonic forming can be carried out. In the static and ultrasonic models, the effects of friction on the extrusion load were investigated when radial and axial ultrasonic vibrations were applied to the die. The prediction of material buckling during necking of thin cylinders was carried out under static and ultrasonic load. In these models it was assumed that the ultrasonic excitation reduced the interface friction coefficients. Some previous investigations of the application of FE modelling in metal forming processes have reported close agreement between FE results and measured data for conventional extrusion [41, 42, 96] and for ultrasonic drawing [47]. This allows this current study to draw comparisons between the numerical models developed and published experimental data and the FE models are therefore verified by comparing the calculated results with the measured data of previous studies of ultrasonic extrusion [25] and ultrasonic die-necking [106].

6.2 FE Modelling of Ultrasonic Extrusion

This section describes a numerical analysis of the application of ultrasonic excitation during an extrusion process. The experimental work on ultrasonic extrusion was carried out by Petukhow et al in 1973 [25]. By applying ultrasonic vibration to the punch and container, the authors claimed that the extrusion force was significantly reduced. Also, it was reported that the effectiveness of ultrasonic extrusion in reducing the extrusion force decreased as the extrusion speed increased. This study claimed that the reduction in extrusion force was related to a reduction in friction.

A series of FE models was developed to simulate the extrusion process under ultrasonic excitation. Based on the previous experimental work by Murakawa [32] and a previous numerical study of radial and axial ultrasonic wire drawing [47], the current FE models could be verified using the formulation for critical drawing speed, V_c [32, 47]. These experimental and numerical studies suggested that applying radial or axial ultrasonic vibration in a drawing process is only effective below a critical speed, V_c. The critical speeds for radial and axial ultrasonic excitation are given by the equations,

$$V_c = 2\pi af \tag{6.1}$$

for axial ultrasonic excitation and,

$$V_c = \frac{2\pi af}{\tan\alpha} \tag{6.2}$$

for radial ultrasonic excitation, where a is the vibration amplitude, f is the ultrasonic frequency and α is the die half angle.

A numerical investigation of ultrasonic drawing using FE methods was carried out by Hayashi et al [47]. These models were well validated by comparing with a prior experimental study of ultrasonic wire drawing [32]. The modelling and experimental results of these studies agreed that a reduction in drawing force can only be achieved when the drawing speed is below the critical speed for axial or radial ultrasonic

excitation. Since extrusion is a reverse process of drawing [110], a similar observation was reported by Petukhow [25] where the effectiveness of applying ultrasonic vibration in an extrusion process was increased at a lower speed.

In this study, static and ultrasonic extrusion models were developed. By specifying interface friction coefficients, the extrusion force for static and ultrasonic loads were predicted. Subsequently, the effects of extrusion speed were investigated by calculating the extrusion force during applied radial and axial ultrasonic excitation under different extrusion speeds. Subsequently, an investigation into the modification of the interface boundary condition was carried out and the predicted data were analysed by comparing with the previously published experimental results. Figure 6.1 shows a schematic of the ultrasonic extrusion model.

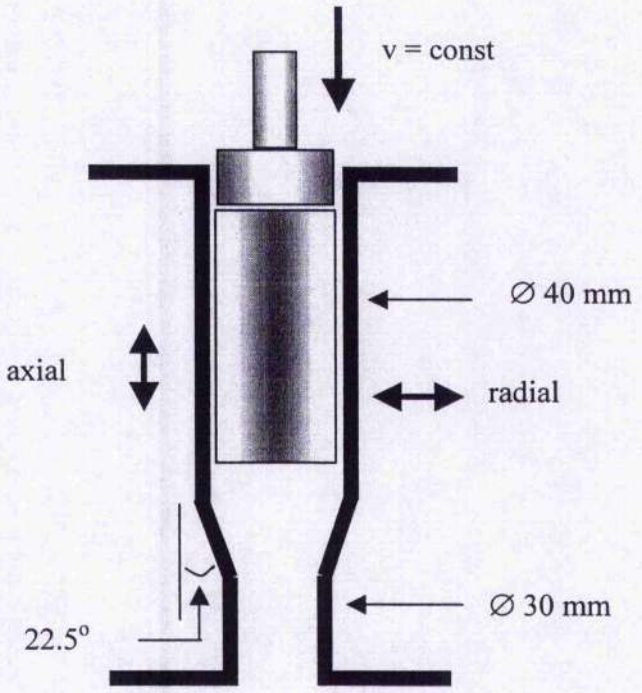

Figure 6.1: Problem description of the ultrasonic extrusion model.

6.2.1 Modelling procedure

Finite element (FE) simulations were developed using ABAQUS with implicit solution. Half of the extrusion billet was modelled using axi-symmetric 4-node elements, taking

advantage of symmetry. A fine uniform mesh was used for the billet to ensure a sufficiently accurate analysis for severe material deformation with a complex contact condition. The punch and die were assumed to be rigid bodies, modelled by an analytical rigid surface. The deformed and undeformed mesh profiles of the extrusion process are shown in Figure 6.2. The material properties used in the model are for aluminium, derived from the static compression tests as described in Chapter 5.

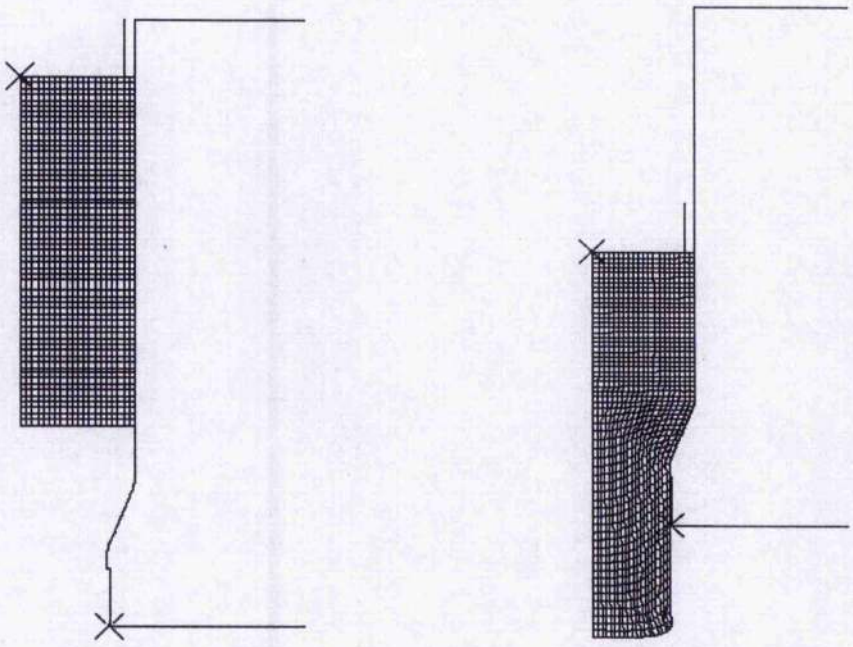

(a) Original (b) Deformed

Figure 6.2: Element meshes of the billet for extrusion model.

The die and billet geometry used was based on a previous numerical study of extrusion by Long et al [41], giving the initial billet diameter 40 mm, die diameter 3 0mm, providing a extrusion reduction of 43.8 % and die half angle, $\alpha = 22.5^{\circ}$. For a smooth transition for the billet to approach the die, the billet was located at a distance of 5 mm from the die opening. A static extrusion force was applied by a constant velocity of the plunger.

To investigate the numerical effects of the interface friction during static and ultrasonic extrusion, the following procedures were carried out. In the first series of models, the billet was extruded under static load by giving the plunger a constant velocity of 10 mm/s, and a constant die-billet interface friction coefficient of 0.1 was used throughout the process. These static modelling procedures were repeated for two other constant interface friction coefficients, $\mu = 0.05$, and $\mu = 0$. The simulations were completed when the plunger achieved a displacement of 40 mm. The predicted relationships between extrusion force and plunger displacement for different friction coefficients were derived from the FE data.

In the second series of models, radial and axial ultrasonic vibrations were applied for the entire extrusion process. As described earlier, the reduction of extrusion force was significantly affected by the extrusion speed and the ultrasonic vibration mode used. By assuming that extrusion is a reversal of the drawing process [110], the current FE models could be verified by observing the mean of the oscillatory force calculated for various extrusion speeds. This could be achieved when radial and axial ultrasonic excitation was superimposed for speeds ranging from below to above the critical speed.

Radial and axial ultrasonic excitation were superimposed on the die at a frequency of 20 kHz and an amplitude of 3 μm, giving critical speeds of 910 mm/s and 377 mm/s for radial and axial ultrasonic excitation respectively. Therefore, the extrusion speeds set in the FE models were 380 mm/s, 1000 mm/s and 3000 mm/s for radial mode excitation and 300 mm/s, 500 mm/s and 1000 mm/s for axial mode excitation. A constant interface friction coefficient, $\mu = 0.05$, was used in these models.

The effects of interface friction during radial and axial ultrasonic extrusion were numerically investigated in the third series of models. For the first set of simulations, constant coefficients of friction, $\mu = 0.1$, 0.05 and 0 were used throughout the static and ultrasonic intervals. Initially, the material was allowed to deform under static load by defining a constant velocity of the plunger at 10 mm/s. Subsequently a radial or axial ultrasonic excitation was superimposed on the die when the plunger was displaced a distance of 25 mm. To allow for manageable computational time, the ultrasonic excitation was applied for a short interval at a frequency of 20 kHz and amplitude 3 μm.

Subsequent models were then created where the coefficient of friction of $\mu = 0.1$ used during static deformation was changed to $\mu = 0.05$ and 0 at the onset of radial or axial ultrasonic excitation. When the ultrasonic excitation was discontinued, the material was further deformed under static load. The static-ultrasonic extrusion process was completed when the plunger was displaced 30 mm. The numerical force-displacement curves and stress contours were derived from the FE model results.

6.2.2 Effect of friction on static extrusion

Figure 6.3 shows the force-displacement curves for the static extrusion models with different interface friction coefficients. Each curve demonstrates a unique profile. The FE model predicts that the extrusion force in the elastic and plastic region is significantly reduced as the friction coefficient is reduced to friction-free. This implies that the use of proper lubricants that reduce the die-billet interface friction could significantly reduce the extrusion force throughout the process.

Previously, Tan et al [108] carried out a similar experimental study of a forward extrusion of aluminium and steel using soap and Molybdenum disulphide (MoS_2) as lubricants. It was reported that the use of soap, effectively to reduce interface friction, significantly reduced the absolute extrusion pressure compared to MoS_2. By comparing with Tan's experimental results, the current FE models also predict that the extrusion force is substantially reduced by reducing the interface friction coefficient.

Some waviness of the force-displacement curve can be observed in Figure 6.3. This is caused by the high deformation of some elements during extrusion and has been smoothed by ensuring a fine mesh in the vicinity of high deformations. The waviness can be further smoothed by remeshing in high deformation zones but this additional computational time is not deemed necessary in this study as the effects of ultrasonic excitation are readily calculated by the current FE mesh.

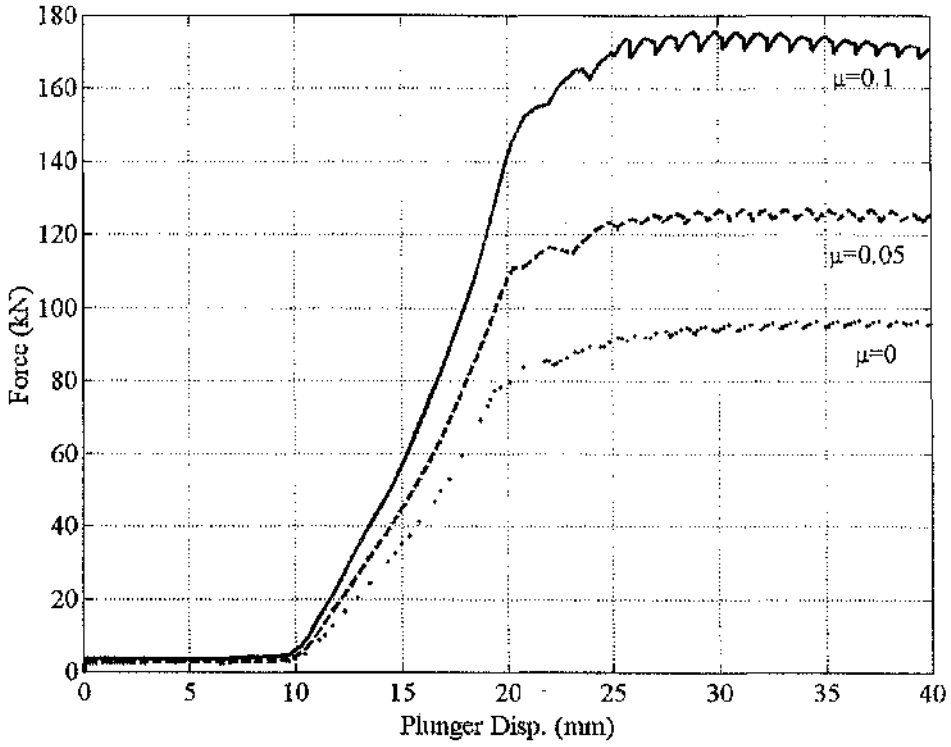

Figure 6.3: Predicted extrusion force versus plunger displacement for different interface friction coefficients.

Figure 6.4 shows the calculated von Mises stress distribution of the statically extruded billet at a plunger displacement of 40 mm with different interface friction coefficients. From the figures, for all cases the maximum stress is concentrated on the billet outer layer at the transition of the die opening. As can be seen in Figure 6.4 (a), for $\mu = 0.1$, the maximum stress is calculated at 130.7 MPa and for $\mu = 0$ as in Figure 6.4 (c), the maximum stress is predicted at 127.0 MPa. These FE results would tend to suggest that reduced stress in the deformed billet in the extrusion of aluminium is substantially attributed to the reduction in friction at the die-billet interface.

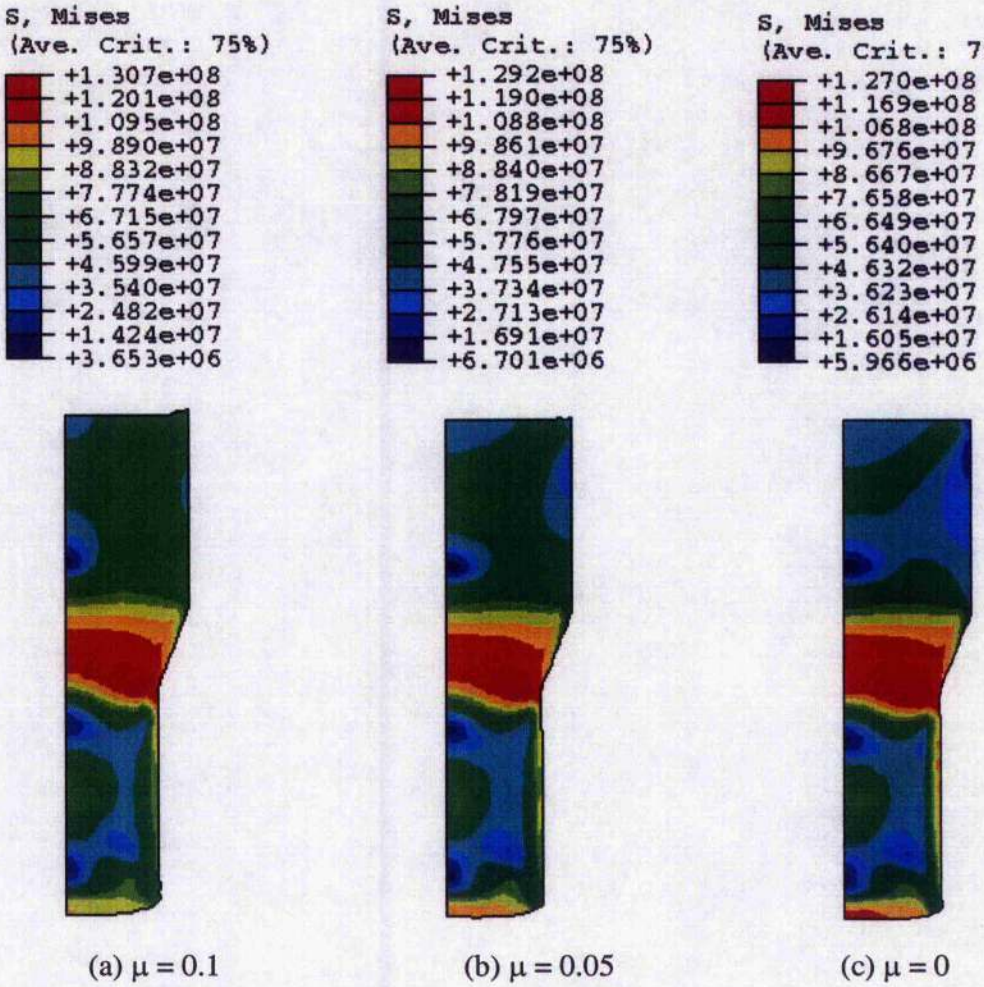

(a) $\mu = 0.1$ (b) $\mu = 0.05$ (c) $\mu = 0$

Figure 6.4: Stress distribution in static extrusion FE models.

6.2.3 Effects of speed in ultrasonic extrusion

In an attempt to validate the present FE models, the effect of the extrusion speed during superimposed ultrasonic vibration on the die was investigated and compared with results from a previous study [47]. The radial and axial ultrasonic excitations were continuously applied in these FE models.

Figure 6.5 shows the calculated extrusion force for three different extrusion speeds for radial ultrasonic excitation. Some cycles of the ultrasonic oscillatory force are shown in the figure in an expanded axis for clarity and it can be seen in these graphs that the oscillatory force is superimposed on the low frequency waviness calculated for the static

load for reasons described earlier. For the extrusion speed of 380 mm/s, which is below the critical speed for radial ultrasonic excitation, at a plunger displacement of 28.2 mm, the predicted mean extrusion force is 122.0 kN and the magnitude of the peak-peak oscillatory force is 2.3 kN, as illustrated in Figure 6.5 (a). In Figure 6.5 (b) and (c), for the same plunger displacement the mean forces were higher and the magnitude of the peak-peak oscillatory forces were reduced for the higher extrusion speeds. The mean force for an extrusion speed of 1000 mm/s was 122.8 kN and increased to 123.0 kN when the extrusion speed was increased to 3000 mm/s, which are higher than critical speed, whilst the magnitude of the peak-peak oscillatory force reduced from 1.5 kN to 0.5 kN for the 1000 mm/s and 3000 mm/s cases respectively. In these simulations, the calculated force-displacement data are consistent with oscillatory stress superposition and in this case the maximum oscillatory force is equal to the static force. In most previous studies only the mean force was measured and it was assumed that the bigger the reduction in mean force, the greater the benefit of ultrasonic vibrations. It is difficult to argue that there is any real load benefit from oscillatory stress superposition since the maximum oscillatory load and static load are equal. However, the calculated data agree with previous studies that the achievable mean force reduction is greatest when the extrusion speed is below the critical speed.

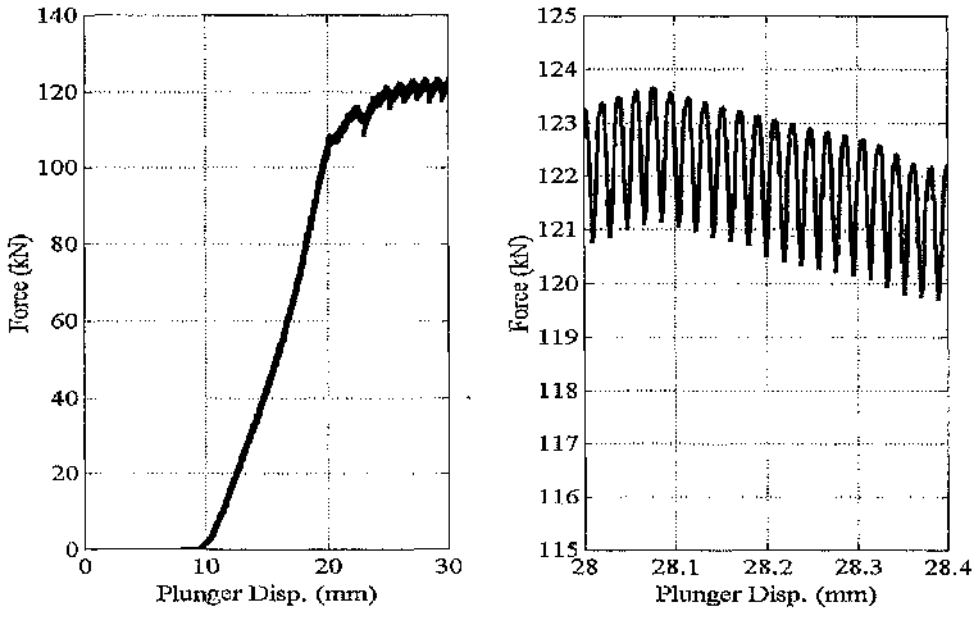

(a) Extrusion speed = 380 mm/s (below critical speed), left enlarged scale of the ultrasonic oscillatory force.

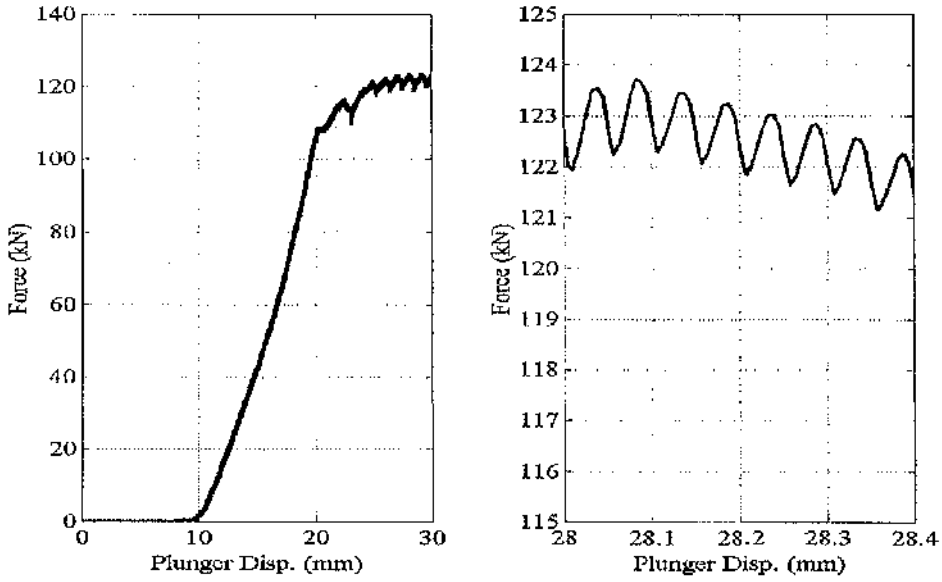

(b) Extrusion speed = 1000 mm/s (close to critical speed), left enlarged scale of the oscillatory force.

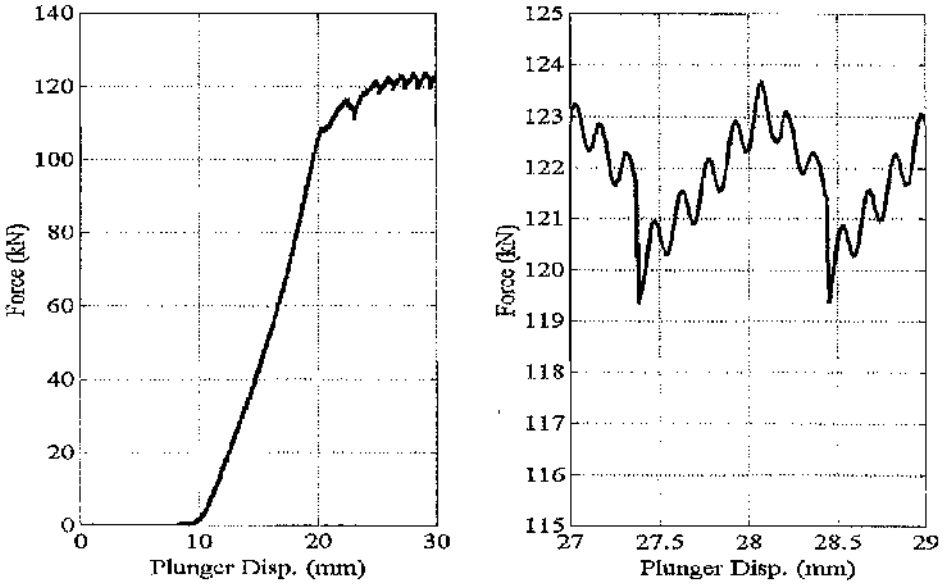

(c) Extrusion speed = 3000 mm/s (higher than critical speed), left enlarged scale of the oscillatory force.

Figure 6.5: Oscillatory extrusion force for radial ultrasonic extrusion model with a constant interface friction coefficient, $\mu = 0.05$.

The above analysis procedure for radial ultrasonic extrusion was repeated for axial ultrasonic extrusion. Figure 6.6 illustrates the force-displacement curves for different extrusion speeds for axial ultrasonic extrusion. As can be seen in Figure 6.6 (a), at a plunger displacement of 28.2 mm and an extrusion speed below the critical speed for axial ultrasonic excitation, the mean extrusion force was calculated at 122.6 kN and the peak-peak oscillatory force amplitude was 0.25 kN. By increasing the extrusion speed above the critical speed, 500 mm/s and 1000 mm/s, as illustrated in Figure 6.6 (b) and (c) respectively, there was no difference in calculated mean force for these specified speeds. Both cases predicted the mean force at 123.2 kN for the same plunger displacement. The peak-peak oscillatory forces for both extrusion speeds seem to be negligible for axial ultrasonic extrusion.

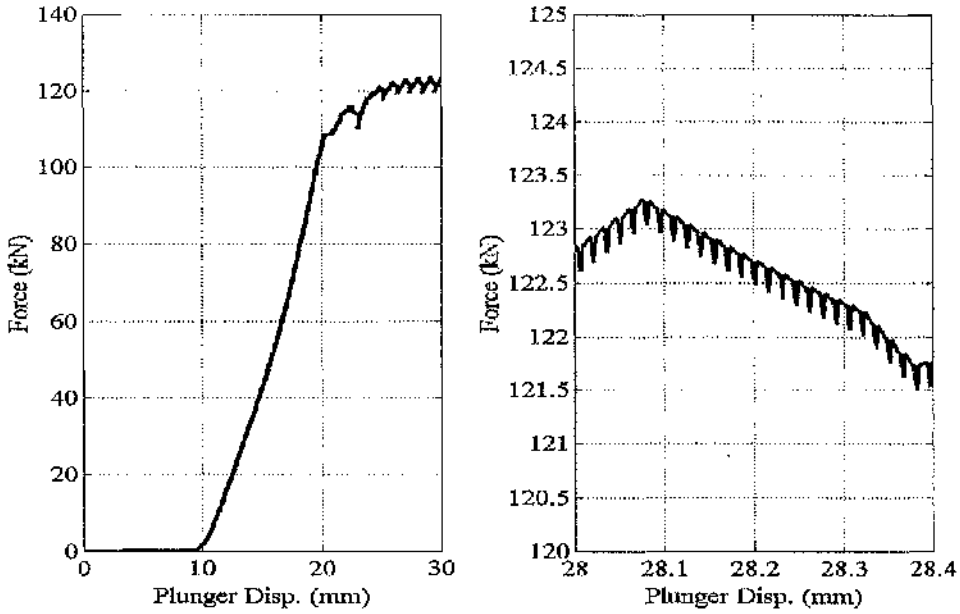

(a) Extrusion speed = 300 mm/s (below critical speed), left enlarged scale of the oscillatory force.

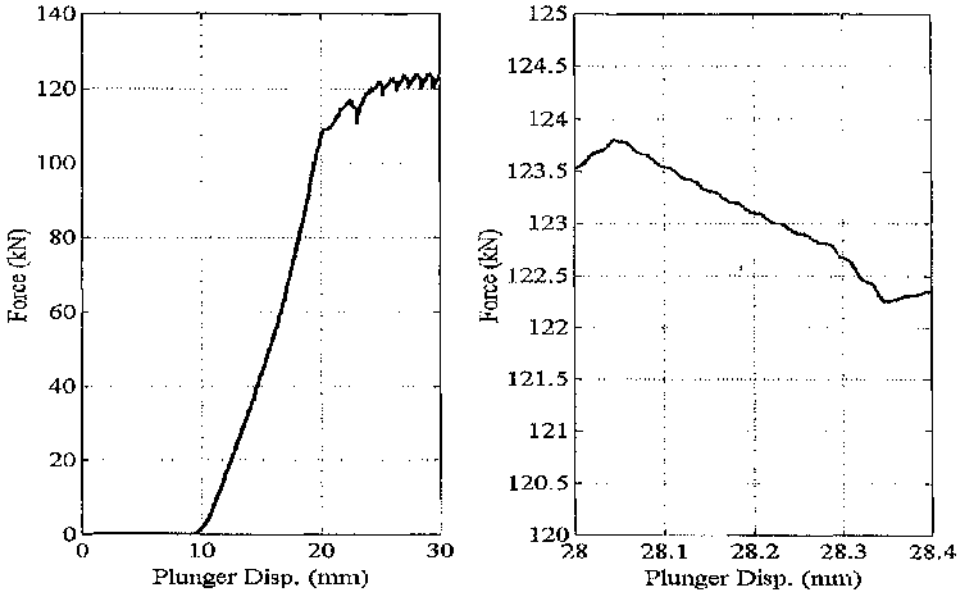

(b) Extrusion speed = 500 mm/s (slightly greater than critical speed), left enlarged scale of the oscillatory force.

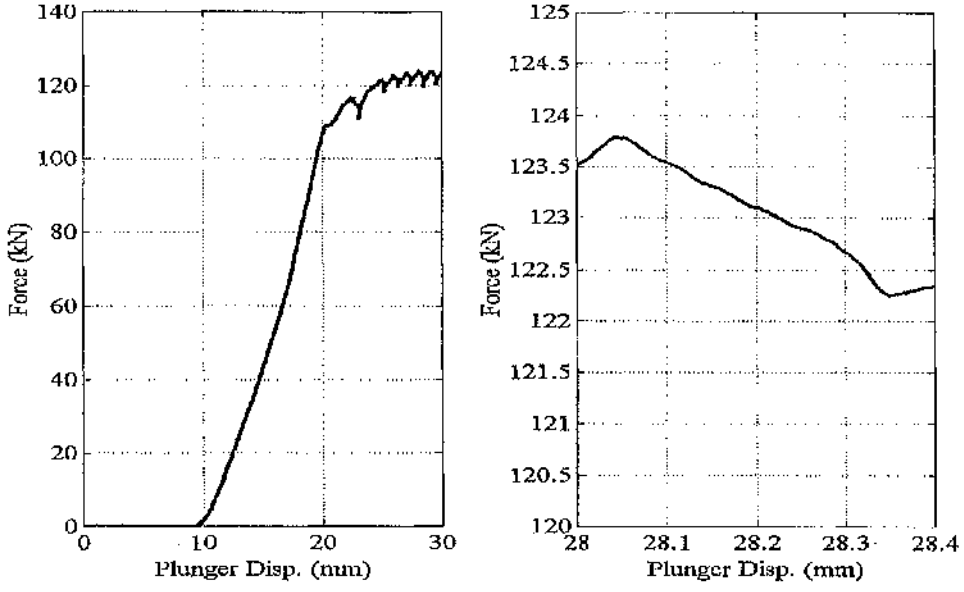

(c) Extrusion speed = 1000 mm/s (higher than critical speed), left enlarged scale of the oscillatory force.

Figure 6.6: Oscillatory extrusion force for axial ultrasonic extrusion model with a constant interface friction coefficient, $\mu = 0.05$.

The above FE results for radial and axial ultrasonic extrusions suggest that the calculated oscillatory forces substantially depend on the extrusion speed. For an extrusion speed below the critical speed, the magnitude of the peak-peak oscillatory force for both radial and axial ultrasonic excitation is highest. However, these values gradually decrease when the extrusion speed is increased to the critical speed or higher than the critical speed. This implies that, at speeds above the critical speed, the effectiveness of applying the normal and tangential ultrasonic excitations is reduced, and consequently the drop in the mean oscillatory force calculated due to the ultrasonic load is negligible. By comparing Figure 6.5 and Figure 6.6, in terms of a reduction in the mean oscillatory force compared with the static force, radial ultrasonic vibration is more effective than axial ultrasonic vibration for speeds below the critical speed.

According to a previous experimental study of ultrasonic wire drawing [32], the average drawing force was measured and the relationship between the drawing speed and drawing force was plotted for radial and axial ultrasonic drawing. The experimental results of Murakawa's study [32] are reproduced as illustrated in Figure 6.7. These studies concluded that the effectiveness of superimposing radial or axial ultrasonic vibrations during the wire drawing process was significantly affected by the drawing speed. The feasibility of using FE methods to quantify the mean load reduction during ultrasonic drawing clarified the dependence of the peak-peak oscillatory force on the drawing speed [47].

The FE results of the current extrusion models are presented in Figure 6.8 in a similar format to the experimental data from wire drawing experiments in Figure 6.7 [32]. Figure 6.8 shows the relationship between the mean extrusion force and extrusion speed for static, radial and axial ultrasonic extrusion. By comparing the experimental data for ultrasonic drawing (Figure 6.7) with the FE results for ultrasonic extrusion (Figure 6.8), it is clear that a very similar force-speed trend is achieved in both cases and that equations 6.1 and 6.2, for estimating the critical drawing speeds, can also be used to estimate the critical speed for radial and axial ultrasonic extrusion processes.

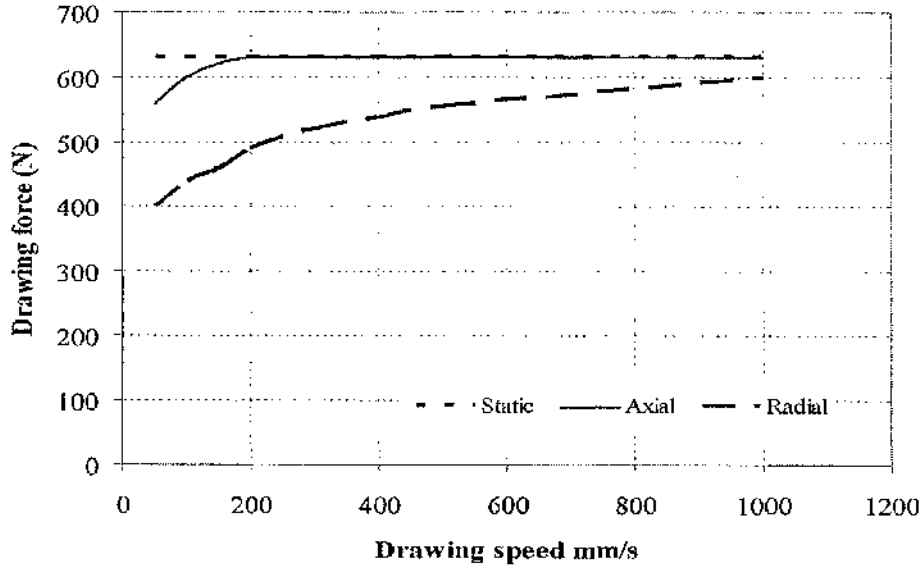

Figure 6.7: Reproduced data of Murakawa's experimental results [32] of ultrasonic wire drawing.

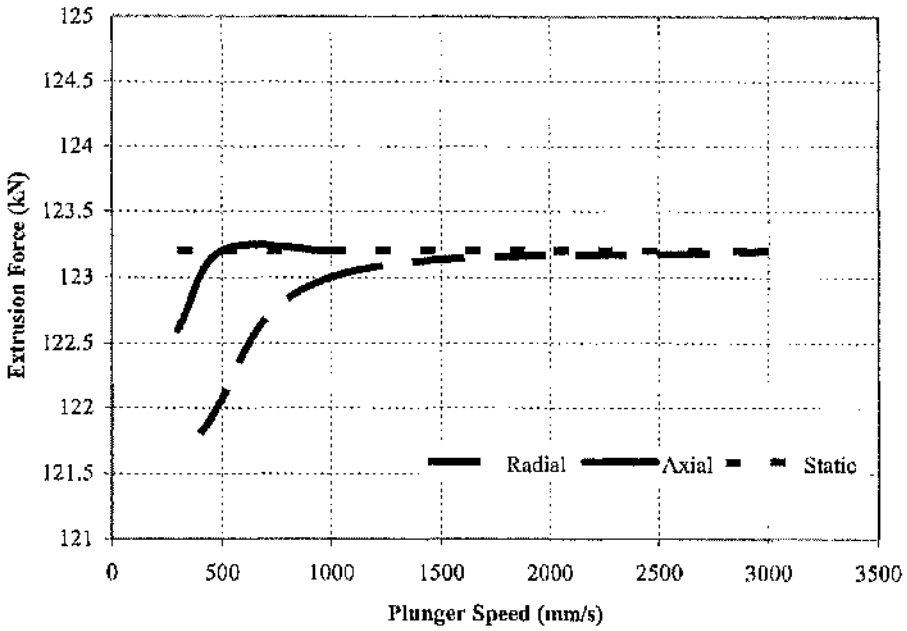

Figure 6.8: Relationship between calculated extrusion forces and extrusion speeds using FE models.

Figure 6.9 shows the stress contours of the extruded billet under radial and axial ultrasonic excitations. At a similar extrusion speed, the calculated maximum value of the mean oscillatory stress of the extruded part with applied radial ultrasonic vibration is 126.0 MPa and with applied axial ultrasonic vibration is 128.4 MPa, which is 2.4 MPa higher than radial ultrasonic extrusion. This FE data calculates that radial ultrasonic excitation can reduce the mean stress more than axial ultrasonic excitation for the extrusion process.

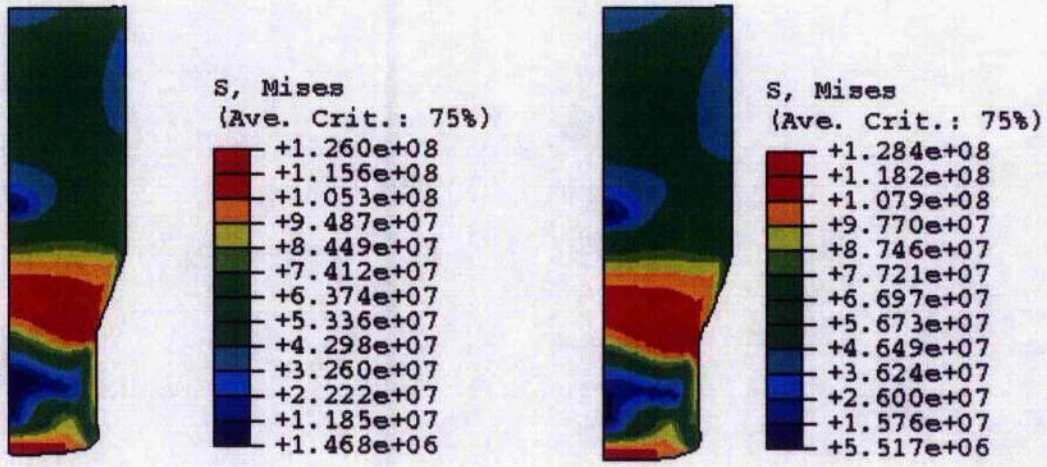

(a) Radial mode extrusion (b) Axial mode extrusion

Figure 6.9: Mean stress contours from ultrasonic extrusion model for extrusion speed below the critical speed.

6.2.4 Effects of adjusting friction in ultrasonic extrusion

In order to investigate the effects of superimposed radial and axial ultrasonic excitation on the extrusion process numerically, the FE models initially used constant coefficients of friction, $\mu = 0$ (friction free), $\mu = 0.05$, $\mu = 0.1$, during static and ultrasonic intervals. As described in the previous section, the maximum effect of the superimposed ultrasonic excitation can only be achieved by maintaining the speed of the plunger below the critical speed. Therefore, in these models, the speed of the plunger was set at a constant speed of 10 mm/s. Figure 6.10 and Figure 6.11 show the predicted force-

displacement relationships for static and a short ultrasonic excitation interval applied in radial and axial modes.

The paths of the static force-displacement curves for each coefficient of friction used exactly duplicated the predicted force-displacement curves for static models from Figure 6.3. For the ultrasonic interval, the effect is merely the superposition of an oscillatory force on the static force as described by Nevill [3] and Kirchner [4]. As can be seen in Figure 6.10 and 6.11 in the expanded part, it is clear that the FE data agrees with the earlier models [4] and the path of maximum oscillatory force follows the path of the static force, with a reduction in the mean force. Once ultrasonic excitation is discontinued, the force-displacement returns elastically to the static curve.

The magnitude of the predicted peak-peak oscillatory force for radial and axial ultrasonic excitation depends on the interface boundary condition specified and is found to be higher for a high surface friction coefficient compared with a low surface friction coefficient. By comparing Figure 6.10 and Figure 6.11, it is clear that for all interface conditions the radial ultrasonic load calculated higher peak-peak oscillatory forces than for the axial ultrasonic load. These peak-peak oscillatory forces for radial and axial ultrasonic load with different surface friction coefficients are summarised in Table 6.1. Accordingly, the models would tend to suggest that the die-billet interface boundary condition effectively changes the magnitude of the peak-peak oscillatory force during ultrasonic extrusion.

Table 6.1: Peak-peak oscillatory force for radial and axial ultrasonic extrusion.

Coefficient of friction	Radial ultrasonic extrusion peak-peak force (kN)	Axial ultrasonic extrusion peak-peak force (kN)
$\mu = 0.1$	5.0	3.5
$\mu = 0.05$	3.0	2.5
$\mu = 0$	2.0	0.5

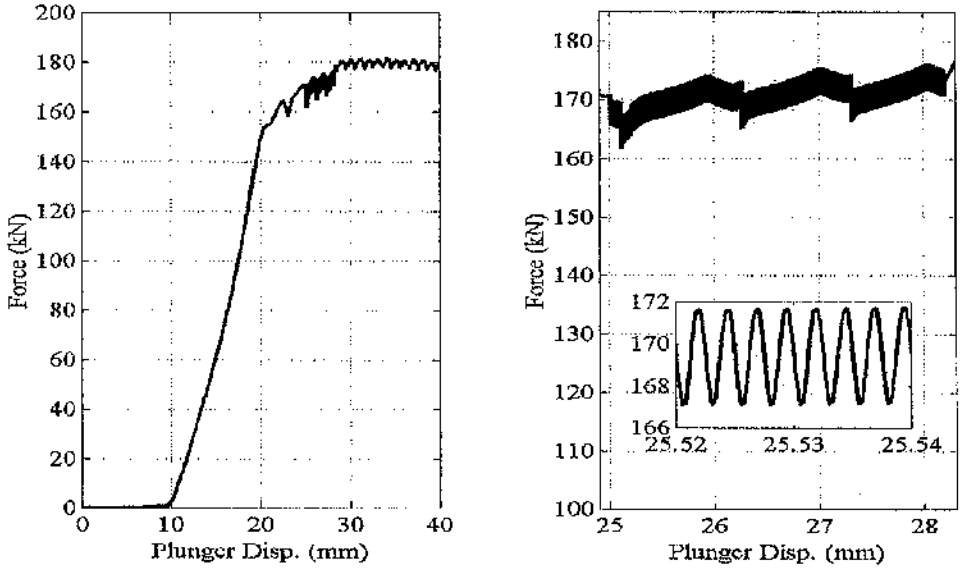

(a) Constant coefficient of friction, μ = 0.1, during static and ultrasonic intervals.

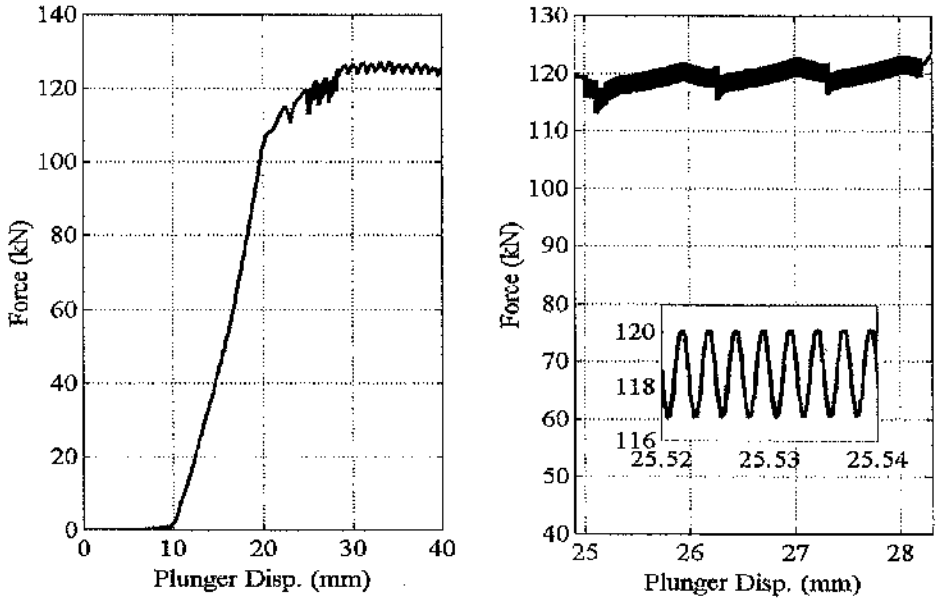

(b) Constant coefficient of friction, μ = 0.05, during static and ultrasonic intervals.

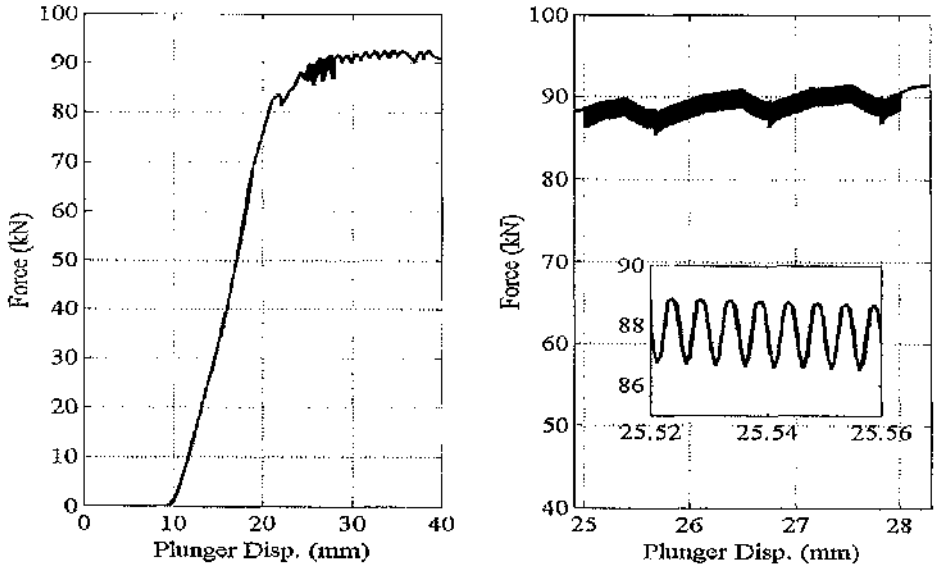

(c) Frictionless interface, $\mu = 0$, during static and ultrasonic intervals.

Figure 6.10: Radial ultrasonic excitation superimposed for a short interval during plastic deformation, left inset figures show expanded scales of the oscillatory force.

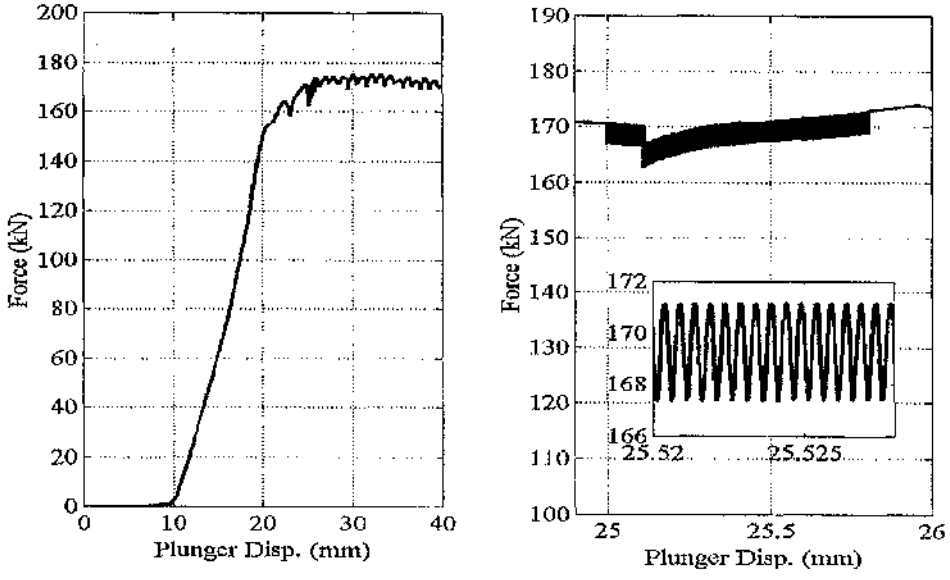

(a) Constant coefficient of friction, $\mu = 0.1$, during static and ultrasonic intervals.

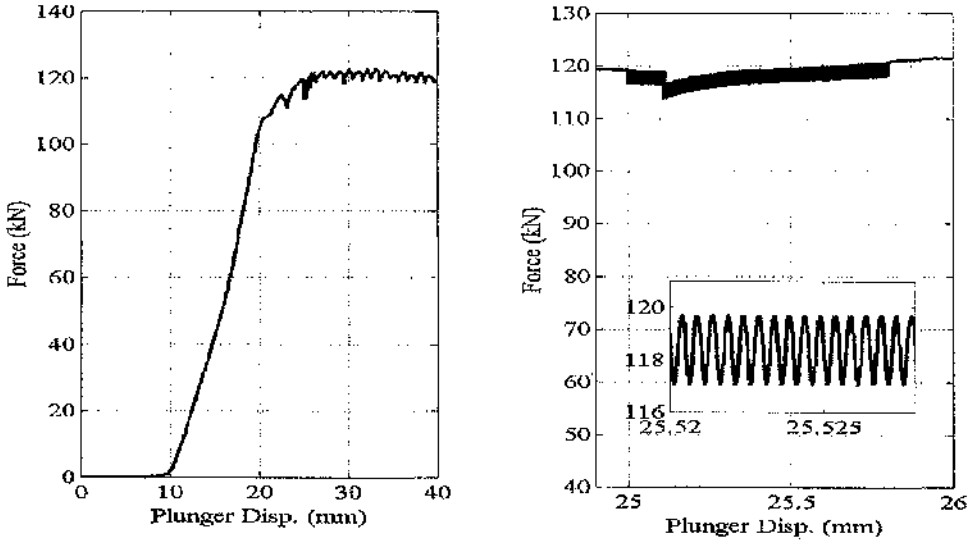

(b) Constant coefficient of friction, $\mu = 0.1$, during static and ultrasonic intervals.

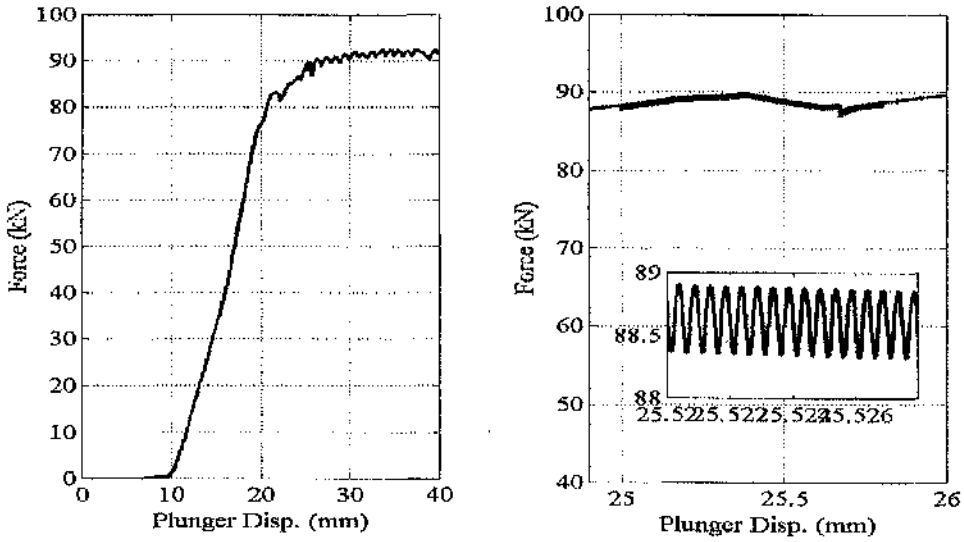

(c) Frictionless interface, $\mu = 0$, during static and ultrasonic intervals.

Figure 6.11: Axial ultrasonic excitation superimposed for a short interval during plastic deformation, left inset figures show expanded scales of the oscillatory force.

An investigation of the effects of adjusting the coefficient of friction in the FE extrusion model was performed in order to determine if the measured reduction of mean oscillatory force of Petukhow's study [25] could be explained in term of a temporary change in the coefficient of friction during applied ultrasonic excitation. In Petukhow's study, the extrusion force was measured when an axial ultrasonic excitation was superimposed on the die during extrusion of aluminium. This paper reported that by applying an ultrasonic load, the extrusion force was lowered by 35% from the static force. However this result was not accompanied by an explanation due to difficulties of real-time measurement of the oscillatory force response. Also, Petukhow did not clearly define whether the force reduction was attributed to a reduction in friction, to material softening or to a combination of both effects. Previous investigations of ultrasonic strip drawing [10] and ultrasonic wire drawing [9] suggested that by superimposing either radial or axial ultrasonic excitation on metal strip drawing, and by superimposing axial ultrasonic vibrations on wire drawing, the interface coefficient of friction was significantly reduced in both cases. Rozner [10] reported that a maximum of 40% reduction in the coefficient of friction could be achieved during both radial and axial ultrasonic strip drawing, whilst Susan [9] claimed that the coefficient of friction was lowered by at least 30% during axial ultrasonic wire drawing.

On the basis of Petukhow's experiments, where 35% of the force was reduced during ultrasonic extrusion, the current models were created in an attempt to quantify the friction coefficient which could result in that reduced force. This was achieved by assuming the ultrasonic excitation effectively modifies the interface friction coefficient to a reduction of between 30% and 40% as suggested by Rozner [10] and Susan [9]. For example, if $\mu = 0.1$ during static intervals, then it would be changed to $\mu = 0.07$ (30% reduction) and then $\mu = 0.05$ (50% reduction) during ultrasonic intervals. Also, the effect of changing the coefficient of friction, $\mu = 0.1$, during static load to a frictionless interface, $\mu = 0$, during ultrasonic load was also investigated.

Figure 6.12 and 6.13 show the numerical force-displacement data for the radial and axial ultrasonic extrusion simulations. These figures show how the models effectively change the boundary condition from the friction condition for static extrusion to the reduced and friction free conditions during the ultrasonic interval. In the expanded parts of the figures, it is clear that the paths of the maximum, mean and minimum oscillatory

force are all reduced, departing from the stress superposition model and in common with the experimental stress-strain data [2, 10]. The mean force reductions due to modification of the interface friction during ultrasonic excitation of the extrusion models are presented in Table 6.2.

Table 6.2: Mean force reduction due to the reduction of interface friction during ultrasonic extrusion.

Reduction of μ from 0.1 to	Radial mode		Axial mode	
	Force reduction		Force reduction	
	(kN)	%	(kN)	%
μ = 0.07 (30%)	27.5	16.7	27.5	16.4
μ = 0.05 (50%)	43.0	25.6	43.5	25.9
μ = 0.0 (100%)	77.0	45.8	76.5	45.5

However, these models only address the issue of interface friction. Therefore some deviation is observed between the measured force data of Petukhow's work and the FE model results. By assuming the ultrasonic excitation significantly reduces the coefficient of friction, say by 50% which is significantly higher than the commonly quoted maximum of 35-40 %, the FE model predicts the mean forces were reduced by 25.6% for radial and 25.9% for axial ultrasonic loading. However, Petukhow reported a 35% reduction in the mean force from the static drawing force. This would indicate that friction effects alone are not sufficient to explain the measured mean force reductions and that an effective material softening may be occurring also, as described in Chapter 3.

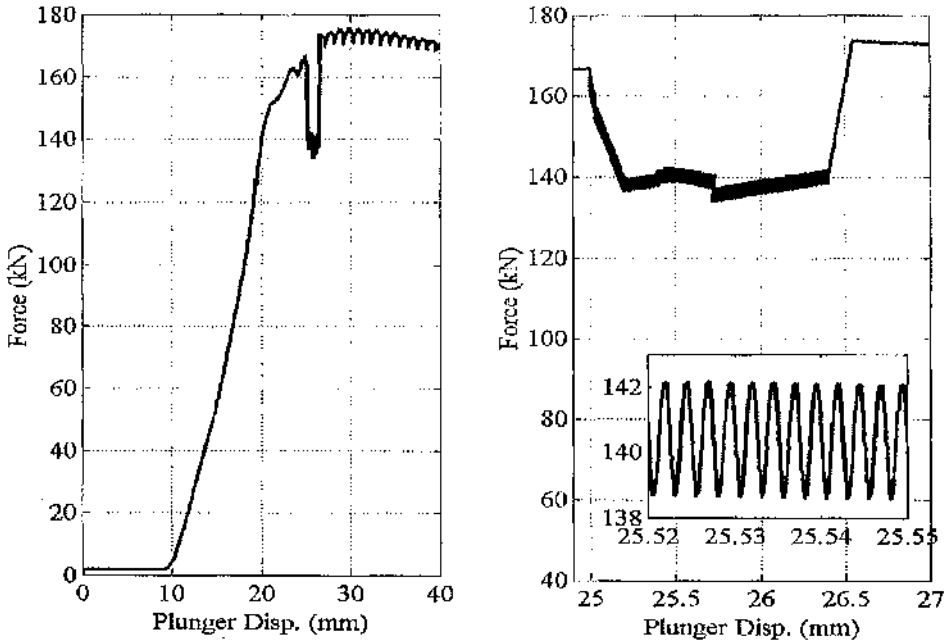

(a) $\mu = 0.1$ during static intervals, changed to $\mu = 0.07$ during ultrasonic interval.

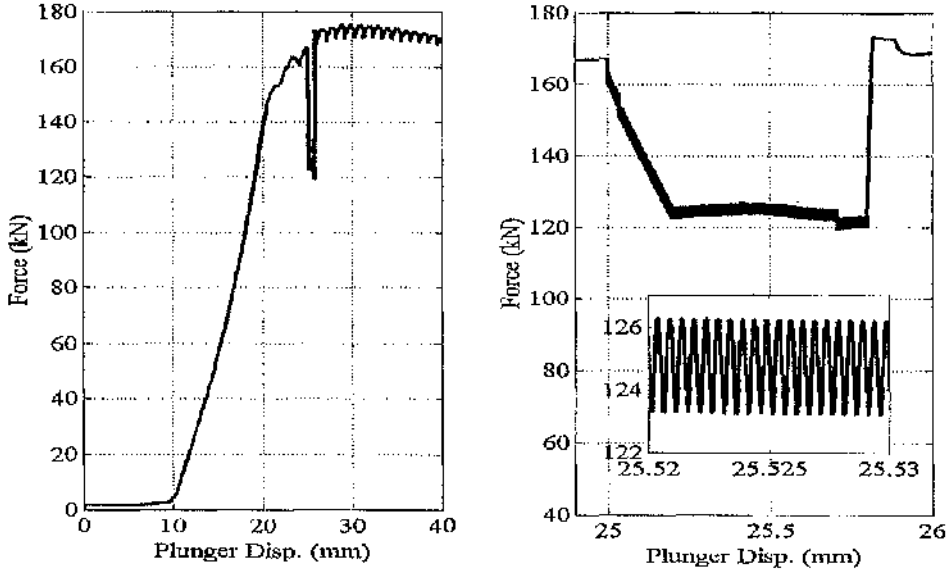

(b) $\mu = 0.1$ during static intervals, changed to $\mu = 0.05$ during ultrasonic interval.

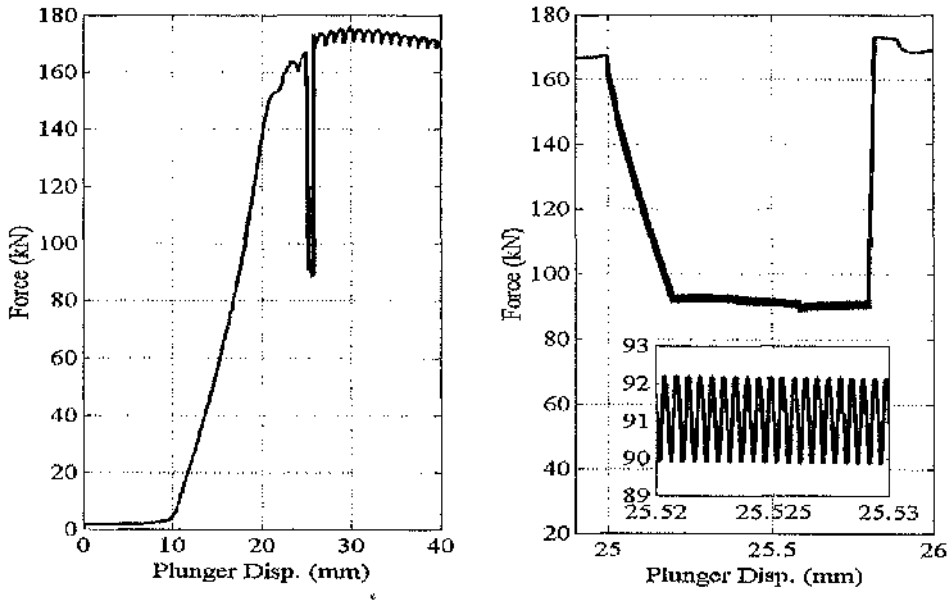

(c) $\mu = 0.1$ during static intervals, changed to $\mu = 0$ during ultrasonic interval.

Figure 6.12: Predicted force – displacement data for static and superimposed radial ultrasonic excitation, left inset figures show expanded scale of oscillatory force.

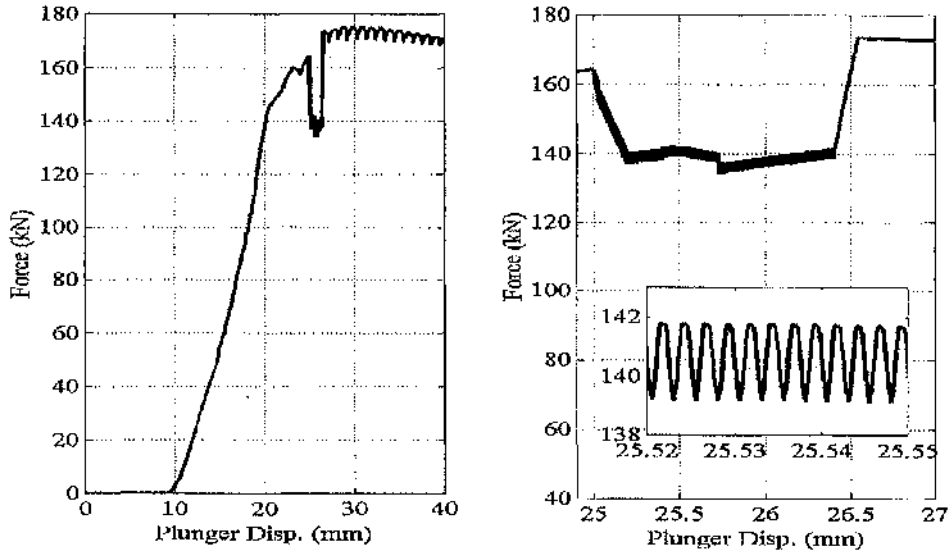

(a) $\mu = 0.1$ during static intervals, changed to $\mu = 0.07$ during ultrasonic interval.

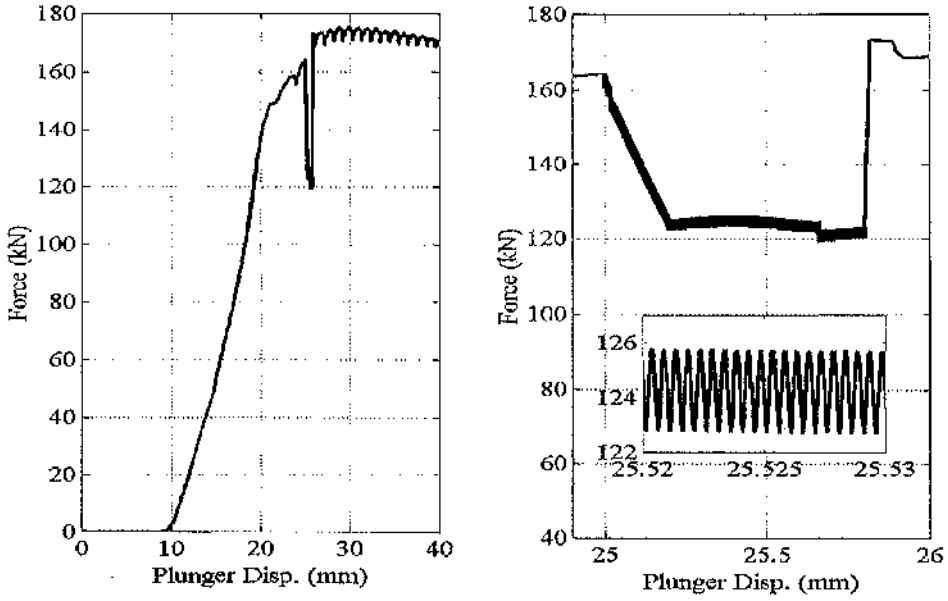

(b) $\mu = 0.1$ during static intervals, changed to $\mu = 0.05$ during ultrasonic interval.

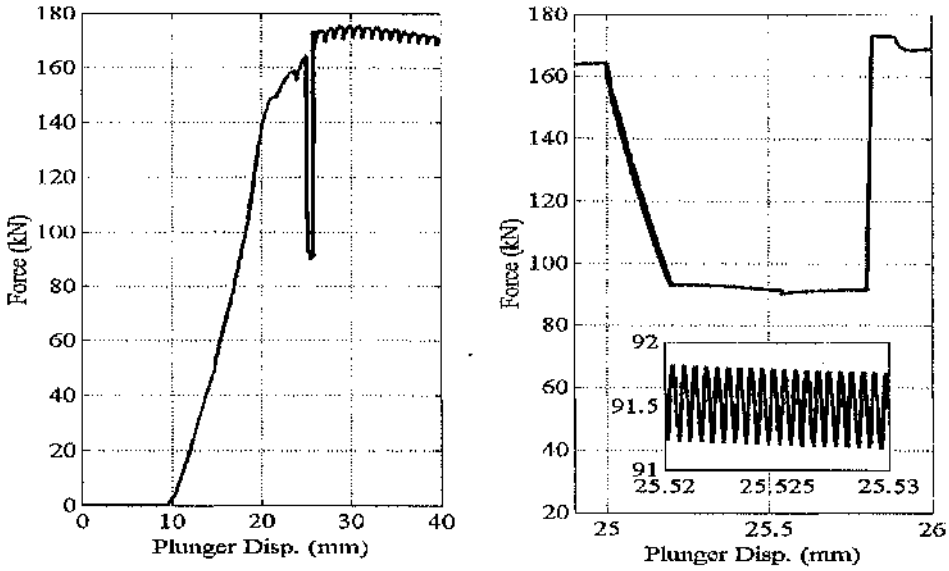

(c) $\mu = 0.1$ during static intervals, changed to $\mu = 0$ during ultrasonic interval.

Figure 6.13: Predicted force – displacement data for static and superimposed axial ultrasonic excitation, left inset figures show expanded scale of oscillatory force.

6.3 FE Modelling of Die-Necking under Superimposed Ultrasonic Excitation

A conventional design of thin hollow cylindrical can comprises three components; a cone, a cylindrical body and a base dome. The main purpose of the cone is to bridge the gap between the body of the can and the closure assembly, which may be a nozzle or cap. A new design for an aerosol can was proposed by Cheers [106], who suggested that manufacturing aerosol cans without cones would provide material and cost savings. This was achieved by necking and curling the top part of the cylinder into a smaller diameter which could accept the nozzle assembly. To achieve the required diameter reduction without buckling of the can body, the process involved several gradual diameter reduction stages, which was time consuming and increased the cost by requiring multiple reduction dies.

In order to solve this problem, the use of ultrasonic vibrations was proposed to assist in the necking of a thin cylinder in one die-stage for manufacture of aerosol cans. For tinplate cans, a 2 mm increase in diameter reduction in one pass was achieved by using a radial mode ultrasonic die. The effective increase in the formability of the cylinder under ultrasonic load was attributed to a reduction of deformation resistance and an improvement in interface friction [106]. However, quantitative experimental data to support the proposed benefits of ultrasonics were not reported.

This section describes a numerical analysis of the effects of interface friction on the static and ultrasonic die-necking of a thin hollow cylinder, based on the experimental study by Cheers [106]. Static and ultrasonic necking processes were simulated by finite element models. The geometry of the die and the dimensions of the thin cylinder were estimated from the Cheers study. Ultrasonic excitation was superimposed on the die during the necking process prior to buckling in the radial direction. Figure 6.14 illustrates the arrangement of die and thin cylinder and a problem description for the FE model.

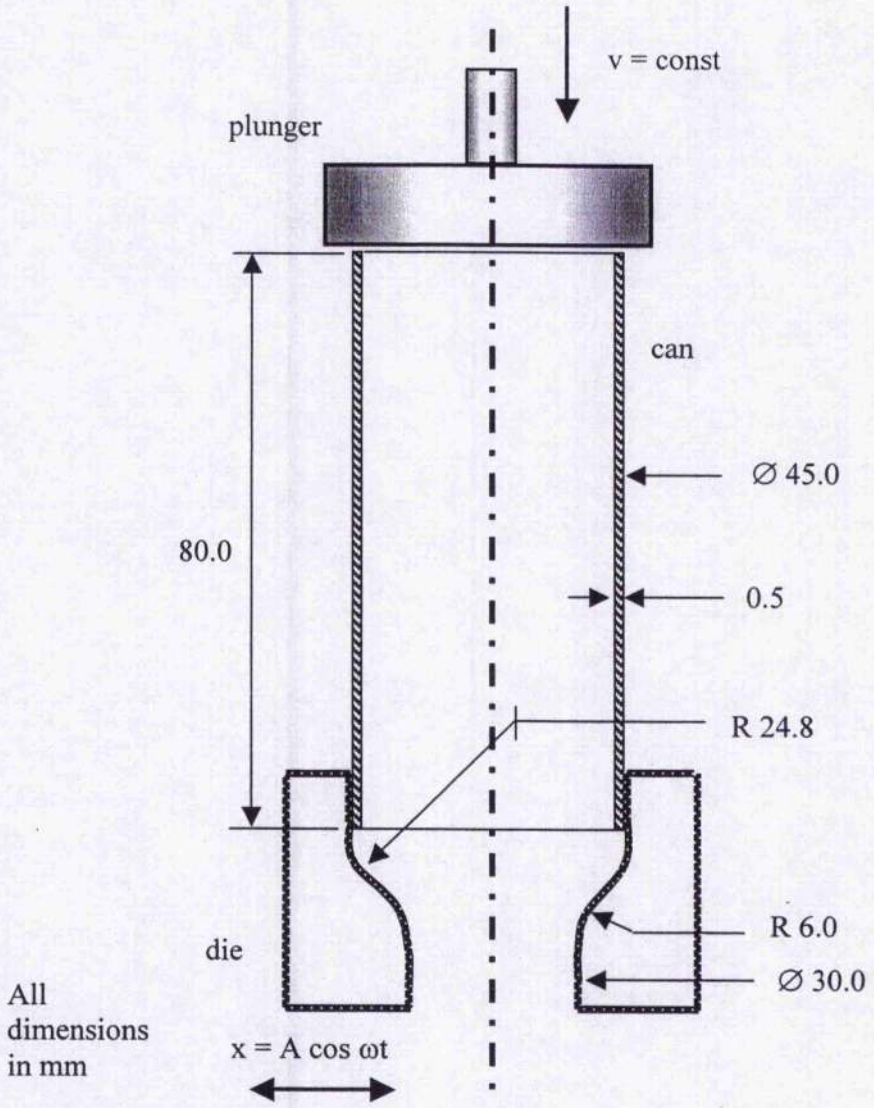

Figure 6.14: Problem description for hollow thin cylinder die-necking process, dimensions in mm.

6.3.1 FE modelling procedure

Finite element simulations were used to model the static and ultrasonic necking processes. Half of the cylinder was meshed using 2D axi-symmetric 4-node elements. The die is assumed to be rigid since it may be regarded as much stiffer than the thin cylinder. The deformed and undeformed mesh profiles are shown in Figure 6.15. The material properties used in the model were that of aluminium, derived from static

compression tests as described in Chapter 5. The necking process was simulated under static conditions, with the plunger displaced at a constant velocity of 300 mm/s. As no process speed was reported by Cheers, 300 mm/s was selected for the FE models as it is well below the critical speed for radial ultrasonic vibration. The ultrasonic excitation was superimposed on the process by vibrating the die in the radial direction at a frequency of 20 kHz and an amplitude of 3 μm. The amplitude was selected to provide a converged solution within manageable computational time.

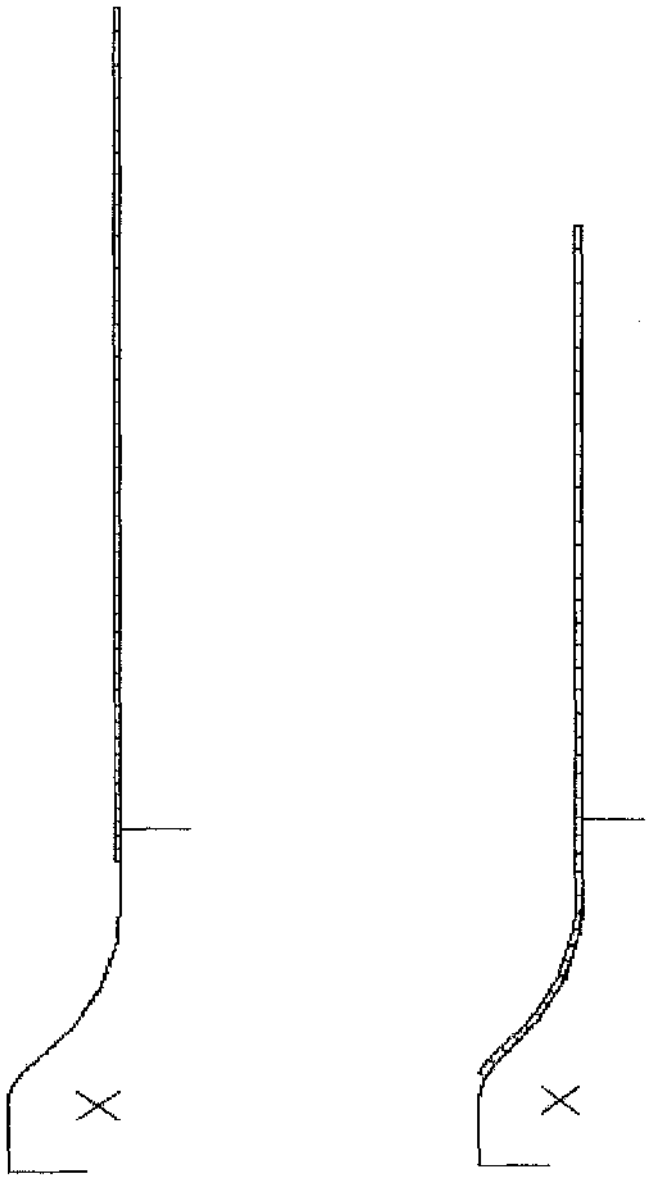

Figure 6.15: Undeformed and deformed mesh profile of thin cylinder die-necking.

In the first series of FE models, the necking force for static and ultrasonic necking was predicted for different interface boundary conditions using an implicit solution. By including a stabilise option in the FE simulation, the model continuously proceeded without buckling and the necking force could therefore be calculated for ideal necking condition. For the static necking model, constant coefficients of friction, μ = 0.1, 0.07, 0.05, 0.03 and 0 were used throughout the necking process. For ultrasonic necking, constant coefficients of friction, μ = 0.05 and μ = 0, were used during static and ultrasonic intervals. To allow for manageable computing time whilst ensuring the effects of friction at the interface could be evaluated, the ultrasonic excitation was applied for a short interval at a plunger displacement of Δl = 20.4 mm. To investigate the effects of a change in the coefficient of friction numerically, subsequent models were created where a coefficient of friction of 0.1 was used during static intervals and changed to 0.05 and 0 (friction free) at the onset of ultrasonic excitation. For both static and ultrasonic loading, the simulation was completed when the plunger displaced Δl = 22.5 mm. The predicted necking force-plunger displacement curves were derived from the FE data.

An investigation into the buckling of the thin cylinder body was carried out using FE models during the necking process using an explicit solution. In these models, buckling of the hollow cylinder body was allowed to occur and ultrasonic excitation was superimposed on the die prior to buckling.

To determine the plunger displacement, Δl, prior to buckling, the necking process was modelled under static loading conditions. A constant interface friction coefficient of 0.1 was used and very small time increments were applied in the simulation. The total time prior to buckling, the total time required to initiate buckling, and the total time for several stages of post buckling were recorded so that several plunger displacements, Δl, prior to buckling, during and post buckling, could be calculated.

To investigate the effects of static and ultrasonic necking processes for different interface friction coefficients on the buckling profile of the can body, subsequent models were created where constant coefficients of friction of 0.1, 0.07, 0.05, 0.03 and 0 were used during static and ultrasonic necking. For the ultrasonic models, the ultrasonic excitation was superimposed on the die prior to buckling at a plunger

displacement Δl = 20.4 mm as previously calculated from the static simulation. The radial displacement of the die defined for the necking simulation is as illustrated in Figure 6.16. The simulations were completed when Δl was 21.4 mm. The buckling profiles of the necked thin cylinder were plotted from the field data of the FE models.

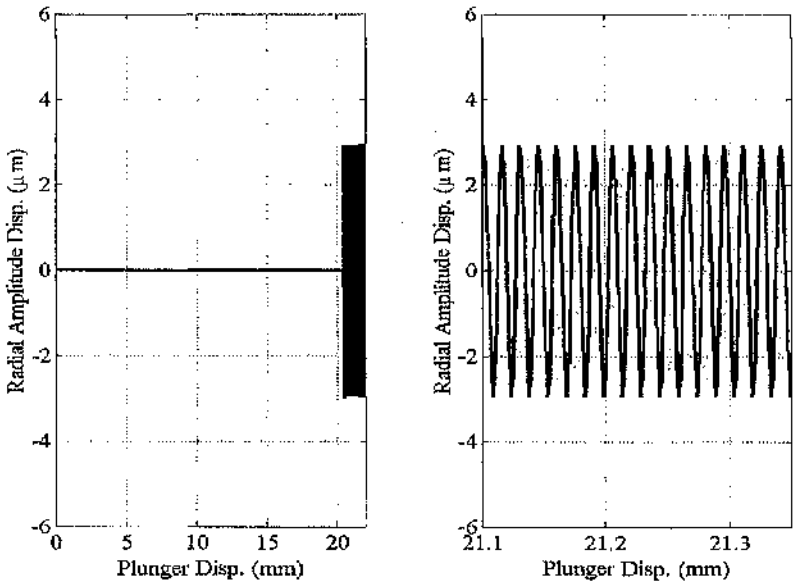

(a) (b)

Figure 6.16: (a) Die displacement profile in radial direction, (b) enlarged scale of the ultrasonic oscillations.

6.3.2 Discussion of the predicted necking force

Figure 6.17 illustrates the numerical necking force-plunger displacement profiles from the static FE model under different interface friction coefficients. Each curve demonstrates a unique force-displacement profile. It is clear that the interface friction condition effectively changes the necking force required and for the highest coefficient of friction given, μ = 0.1, the necking force is higher than for the lower friction coefficients as the plunger displacement, Δl, increases. These FE results agree with the experimental results of Cheers [106] which reported that the necking force is significantly reduced for lower coefficients of friction.

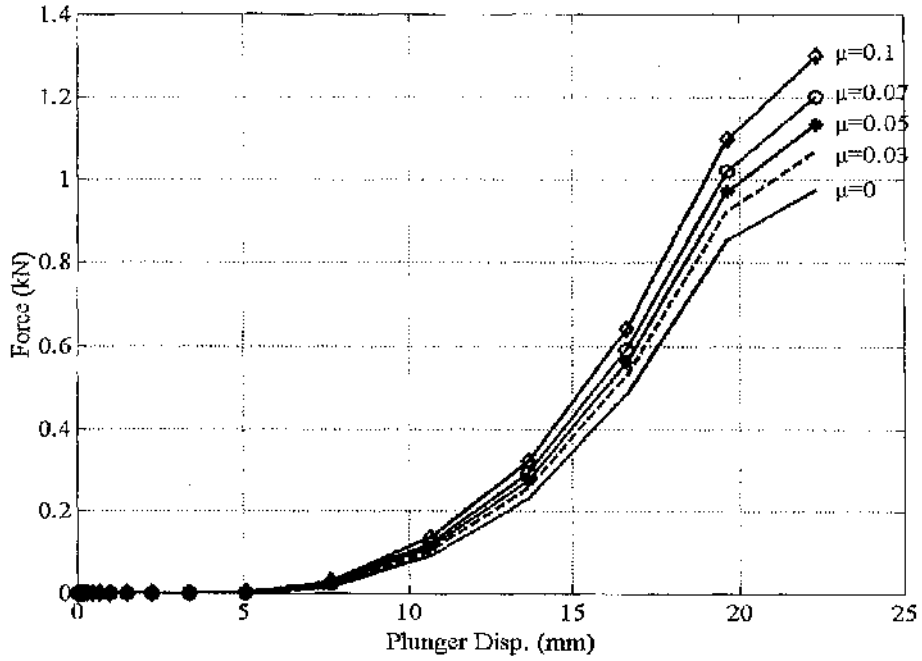

Figure 6.17: Static necking forces for different interface friction coefficients.

Figure 6.18 shows the necking force-displacement curves for static and superimposed ultrasonic necking of the hollow cylinder for two different coefficients of friction, μ = 0.05 and μ = 0, which were constant during the static and ultrasonic intervals. In the expanded part of the figure, it can be clearly seen that the FE model agrees with the stress superposition model and the maximum oscillatory force follows the path of the static force for both interface friction conditions. Subsequently, the models were developed to include an interface friction coefficient of 0.1 during static necking, which was changed to μ = 0.05 and μ = 0 during ultrasonic necking. As can be seen in Figure 6.19 and Figure 6.20, the model essentially changes the trend of the necking force from increasing during static loading to decreasing during ultrasonic loading. The FE model therefore predicts that ultrasonic excitation reduces the necking force if the interface friction is effectively reduced by the application of radial mode ultrasonic excitation. This calculated data agrees with a previously published experimental study [106] which reported that by superimposing a radial ultrasonic excitation on the die the mean necking force was significantly reduced, in this case to 35 to 45 % of the static force.

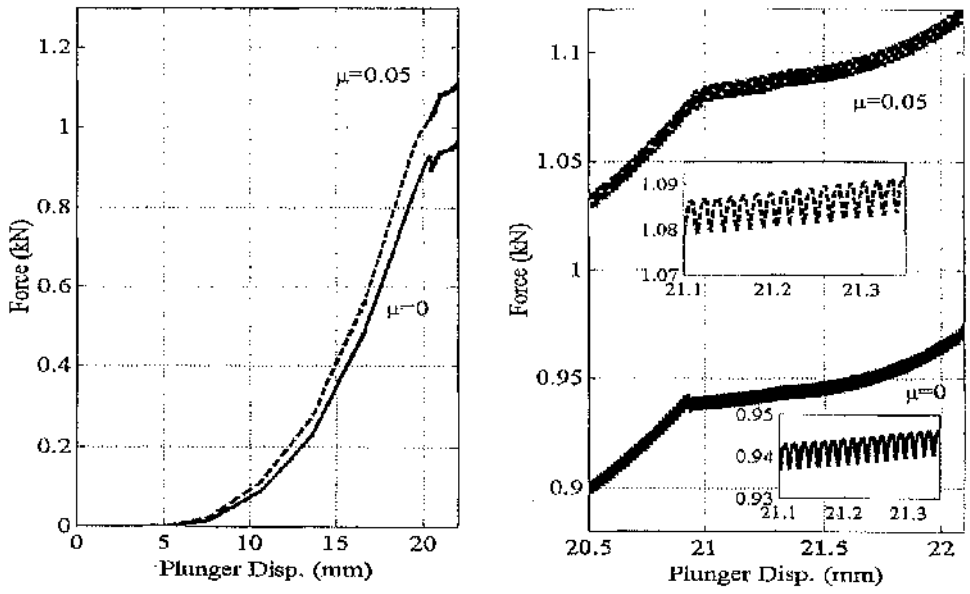

Figure 6.18: (a) Constant coefficients of friction, $\mu = 0$ and $\mu = 0.05$ applied during static and ultrasonic necking, (b) expanded scales of the oscillatory forces.

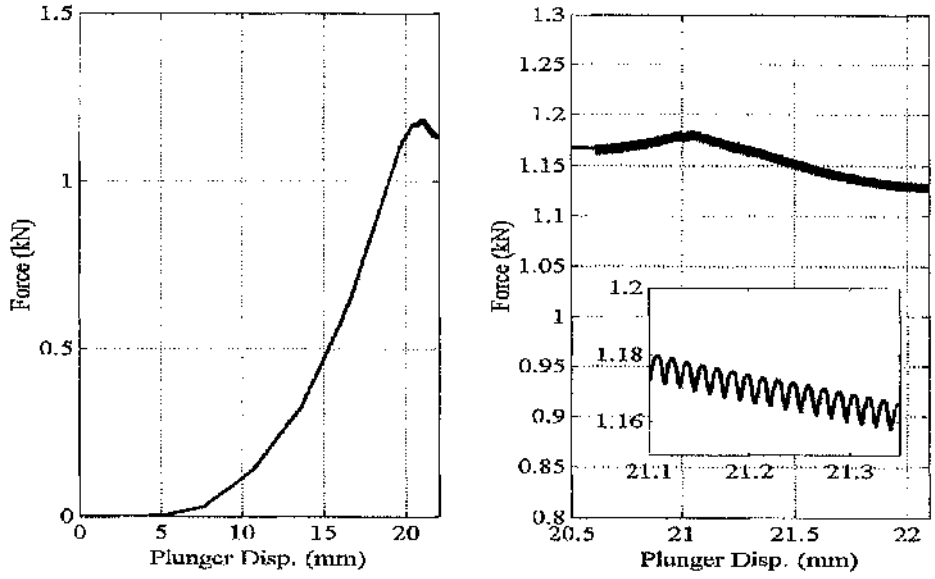

Figure 6.19: (a) Coefficient of friction $\mu = 0.1$ during static load, changed to $\mu = 0.05$ during ultrasonic load, (b) expanded scales of the oscillatory forces.

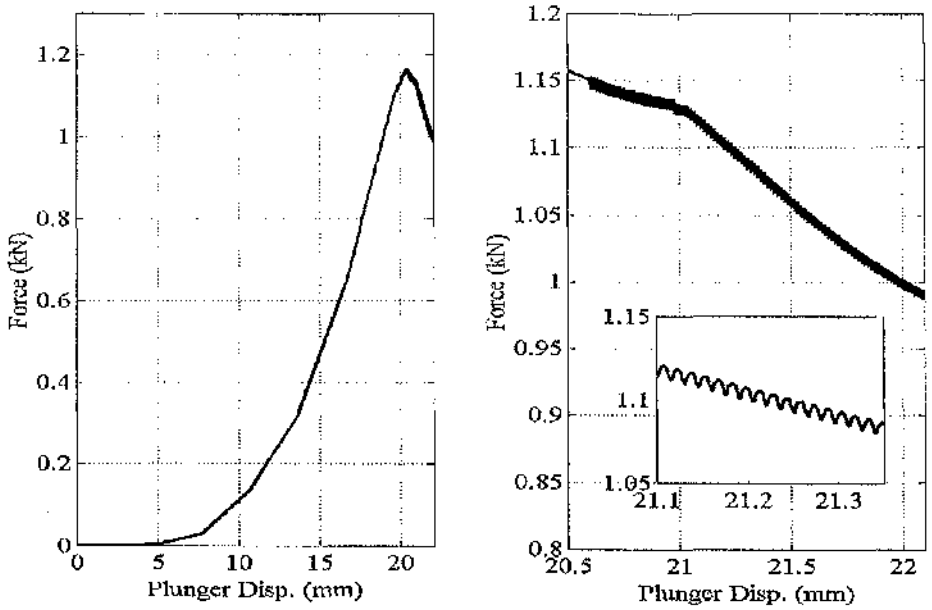

Figure 6.20: (a) Coefficient of friction $\mu = 0.1$ during static load, changed to $\mu = 0$ during ultrasonic load, (b) expanded scales of the oscillatory forces.

6.3.3 Discussion of the effects of friction on buckling

The sequence of Δl prior to buckling, during buckling and post buckling were predicted using the static deformation model, by applying a constant speed of the plunger and using a constant coefficient of friction, $\mu = 0.1$ throughout the necking process. Figure 6.21 shows the sequence of the buckling profile for the cylinder body for static necking. The models predicted that at a plunger displacement of 20.4 mm the cylinder was about to buckle, at $\Delta l = 20.7$ mm the cylinder started to buckle, the cylinder progressively distorted at $\Delta l = 21.0$ mm, and the modelling process was stopped at $\Delta l = 21.4$ mm when the cylinder was severely distorted.

In order to investigate the effects the different interface boundary conditions and superimposed ultrasonic excitation during the necking process, the interface friction coefficients were set, $\mu = 0.1$, 0.07, 0.05, 0.03, and 0 (frictionless) during the static and static-ultrasonic necking process. To allow for manageable computational time, the ultrasonic excitation was applied to the die after the plunger displaced $\Delta l = 20.4$ mm, or at the point the cylinder is about to buckle as predicted in the static models.

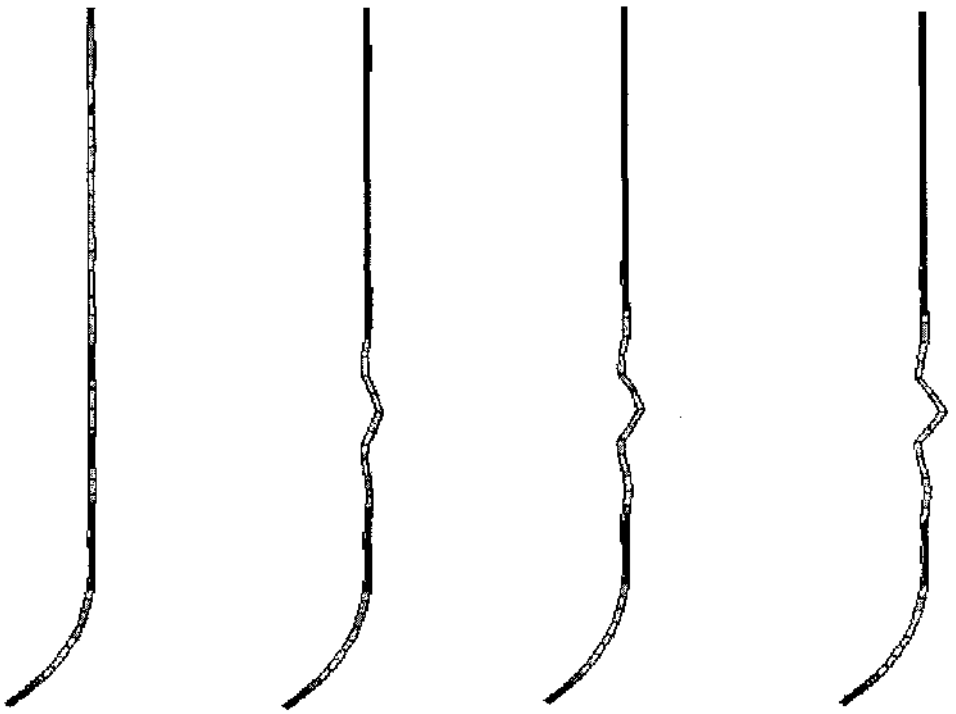

(a) Δl = 20.4 mm (b) Δl = 20.7 mm (c) Δl = 21.0 mm (d) Δl = 21.4 mm

Figure 6.21: The sequences of buckling profiles of the cylinder as the plunger is displaced during static necking for the interface friction coefficient $\mu = 0.1$.

Figure 6.22 shows the predicted buckling profile of the cylinder for a constant interface friction coefficient, $\mu = 0.1$ during both static necking as illustrated in Figure 6.22 (a) and static-ultrasonic necking as illustrated in Figure 6.22 (b). As can be seen in the figures, for a coefficient of friction of $\mu = 0.1$, the models predict that there is no change in the buckling profile for static and for ultrasonic necking.

By using a slightly lower coefficient of friction value of 0.07 for static and for ultrasonic necking modelling, a noticeable effect of ultrasonic excitation on the buckling profile was calculated. Figure 6.23 (a) and (b) illustrate the buckling profiles for static and ultrasonic necking respectively, where a constant coefficient of friction of $\mu = 0.07$ was used throughout the process. These figures show that for a lower coefficient of friction the distortion of the cylinder is considerable improved from the model with $\mu = 0.1$. However, in this case by superimposing ultrasonic excitation prior to buckling a

measurable improvement in the distortion of the cylinder is calculated than for static necking.

The buckling profile is improved further as the friction coefficient value is furtther reduced and in each case, Figures 6.24 to 6.26, ultrasonic necking achieves less distortion of the cylinder that static necking. The FE models predict that the buckling of the can body was nearly eliminated when ultrasonic excitation was superimposed on the die with an interface friction coefficient of 0.05 (Figure 6.24) and is eliminated, Figure 6.25 and 6.26, for friction coefficient values of 0.03 and 0.

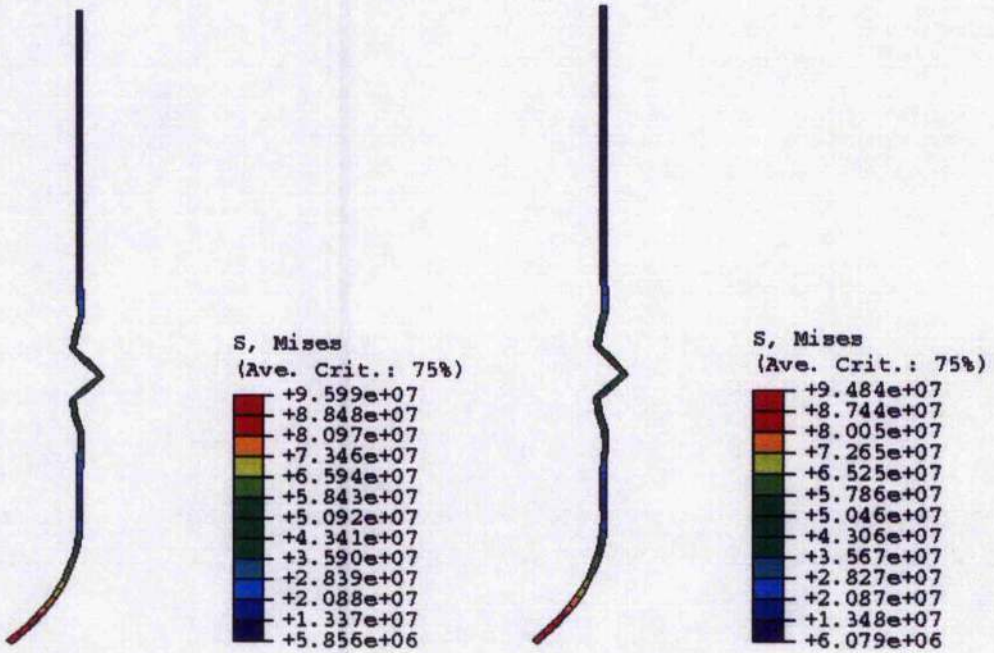

(a) (b)

Figure 6.22: Stress contours and deformation profile of cylinder for a constant coefficient of friction, $\mu = 0.1$ during (a) static and (b) static-ultrasonic necking.

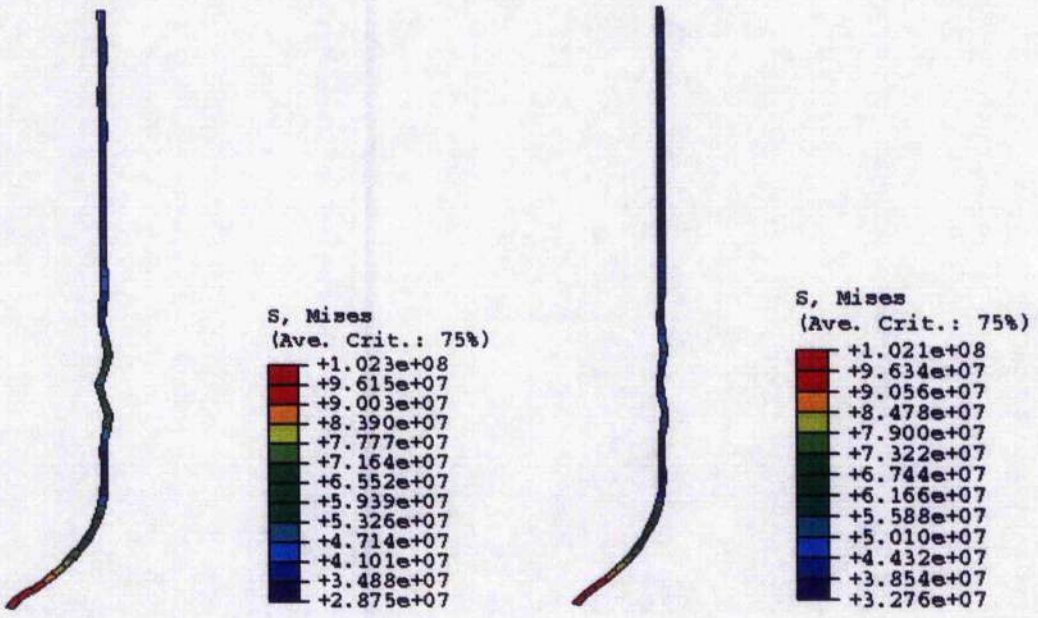

(a) (b)

Figure 6.23: Stress contours and deformation profile of cylinder for (a) constant coefficient of friction, $\mu = 0.07$ during (a) static and (b) static-ultrasonic necking.

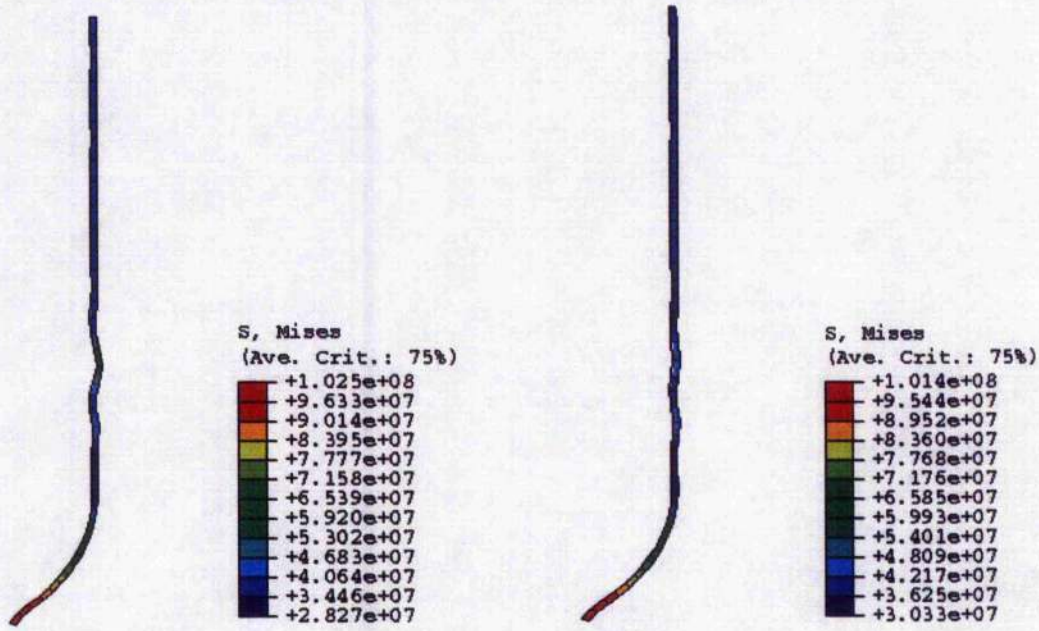

(a) (b)

Figure 6.24: Stress contours and deformation profile of cylinder for (a) constant coefficient of friction, $\mu = 0.05$ during (a) static and (b) static-ultrasonic necking.

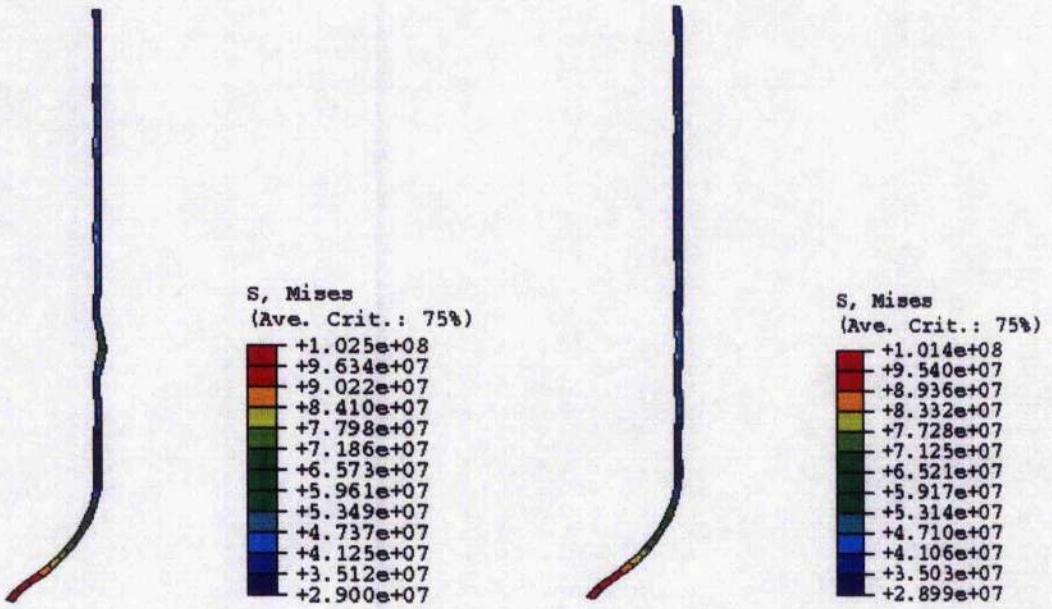

(a) (b)

Figure 6.25: Stress contours and deformation profile of cylinder for (a) constant coefficient of friction, $\mu = 0.03$ during (a) static and (b) static-ultrasonic necking.

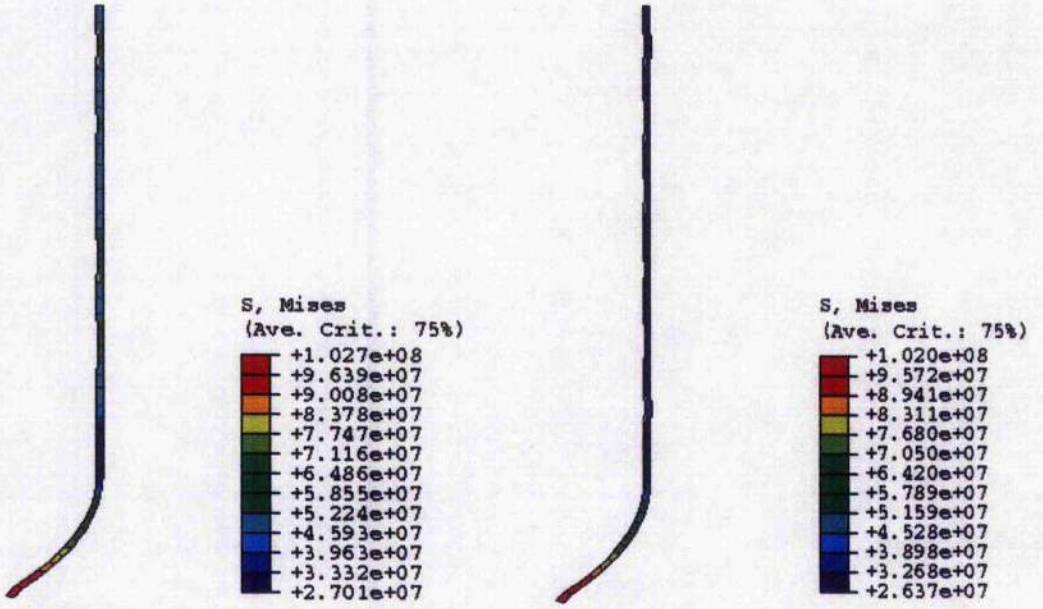

(a) (b)

Figure 6.26: Stress contours and deformation profile of cylinder for (a) constant coefficient of friction, $\mu = 0$ (frictionless) during (a) static and (b) static-ultrasonic necking.

According to Cheers [106], by superimposing radial ultrasonic excitation during the necking of tinplate aerosol cans the interface friction was reduced by 60%. By radial mode ultrasonic excitation of the die, Cheers proposed that a reduction in interface friction was responsible for achieving a further 2 mm diameter reduction of the can without buckling. In the present study, FE models were created for an aluminium thin hollow cylinder with the same geometry as the tinplate cylinder of Cheers' study. In these models a reduction in the coefficient of friction from $\mu = 0.1$ during static loading to $\mu = 0.03$ during ultrasonic loading, which represents a 70% reduction in the interface friction coefficient, was required in order to eliminate buckling. Although these results cannot be compared directly with Cheers' experiments, since the cylinder body material is different, the reported friction reduction is of a similar magnitude and supports the predictions of the FE model data that ultrasonic excitation effectively reduces the interface friction during radial mode ultrasonic necking.

6.4 Conclusions

In this chapter, finite element (FE) simulations of ultrasonic extrusion and ultrasonic die-necking of a thin hollow cylinder have been developed. The models have been used to simulate static loading and also then to predict the effect of interface friction under ultrasonic loading. Radial and axial ultrasonic modes were superimposed on the static load in the extrusion model and only radial ultrasonic excitation was applied in the die-necking model.

The extrusion models were validated against a previous experimental study of ultrasonic wire drawing. As was reported in previous experimental studies of wire drawing and extrusion, the FE models predicted that a reduction of the extrusion force under applied ultrasonic excitation can only be achieved by specifying an extrusion speed below the critical speed of the ultrasonic vibration velocity. By reducing the interface friction coefficient during ultrasonic loading, the model successfully lowered the extrusion force. However, by comparing the calculated extrusion force reduction with the previous experimental results, a reduction in friction alone did not account for the measured force reduction which was 10% greater that the FE prediction. Therefore, as previously described in Chapter 2, it is possible that an effective material softening also contributes to the reduced extrusion force.

The FE model of die-necking enabled an investigation into the effects of interface friction on the buckling profile. By reducing the coefficient of friction during ultrasonic loading, the buckling profile was calculated and showed that by applying ultrasonic excitation with a reduced interface friction coefficient, the models effectively displaced the can body 1 mm further in the axial direction without buckling. A similar result was previously reported in an experimental study of ultrasonic necking of a tinplate thin hollow cylinder, where a further 2 mm of diameter reduction was achieved without buckling for ultrasonic loading compared to static loading.

In conclusion, the FE models developed in the present study are an accurate representation of extrusion and die-necking and provide useful insights into the numerical effects of interface friction under static and ultrasonic loading. It is also possible that ultrasonic loading effectively softens the material properties of the workpieces, as reported in Chapters 4 and 5, but this has not been investigated here.

CHAPTER 7

CONCLUSIONS

7.1 Conclusions

This thesis has presented experimental and finite element (FE) analyses of static and ultrasonic forming of aluminium. Aluminium specimens were fabricated into standard specimen geometries to allow the material to be deformed using laboratory scale test equipment. The responses of the aluminium specimens and the interface friction effects under different modes of deformation and different friction conditions have been investigated, allowing characterisation of the oscillatory stress response during superimposed ultrasonic excitation. This study used uniaxial tension, and ring and cylindrical specimen compression tests to establish insights into the effects of ultrasonic excitation during these standard tests. By using FE models to simulate the experiments, it was found that effective material softening, oscillatory stress superposition, and an effective reduction in the coefficient of friction were the main contributing factors to the measured reductions in the mean and maximum oscillatory forming load from the static load. The knowledge gained from these investigations were subsequently used to develop finite element models of two ultrasonic forming operations; extrusion and thin cylinder necking.

A test rig was designed to accommodate the ultrasonic excitation system, specimens, platens and measurement instruments in the Lloyds test machine. The test rig needed to satisfy the requirements of supporting the high forming loads, minimising vibration transmission to the support structure and, for the ultrasonically excited platen, of maintaining a constant vibration amplitude and amplitude uniformity on the platen output surface throughout the tests. The lower platen in all tests consisted of an ultrasonic horn tuned to 20 kHz and three horns were required for the tests; a longitudinal mode block horn and a radial mode cylindrical horn for compression tests,

and a longitudinal mode conical horn for tension tests. Initially the design of the horn relied on FE models to predict the modal frequencies and mode shapes. Models were validated by experimental modal analysis, using LDVs, and updated to achieve the required ultrasonic vibration mode at the tuned frequency of 20 kHz. The vibration response of the ultrasonic system, specimen and upper platen used in the experiments was monitored using a 2D and 3D LDV to measure the vibration amplitude during the tests and to verify that the ultrasonic horns delivered a constant vibration amplitude to the contact surface with the specimen. A piezoelectric force transducer was used to measure the static and oscillatory force response during all tests, and signals were acquired using DataPhysics data acquisition and post-processing hardware and software. The test rig proved to be very successful in meeting the test requirements and allowing highly repeatable measurements to be achieved.

A series of static and ultrasonic tension tests were conducted using standard aluminium specimens. Measurement of the static force-displacement response provided knowledge of the static deformation history. From these tests material properties data were derived and subsequently used in the FE models. The oscillatory stress-stain curve measured when ultrasonic excitation was applied to the specimen was initially compared to the classic description of oscillatory stress superposition, where the path of the maximum stress follows the path of the static stress curve and the mean oscillatory stress path is parallel to, but reduced from, the static stress path. However, the stress-strain relationship derived from the measurement data of the ultrasonic tension tests showed a departure from this classic superposition description, exhibiting a temporary reduction in the maximum, mean and minimum oscillatory stress from the path of the static stress-strain curve. The effect of ultrasonic excitation in tension tests was successfully simulated in FE models by a temporary softening of the material during the intervals of ultrasonic excitation. By matching the temporarily reduced plastic response material properties to the path of the mean oscillatory stress in the measured ultrasonic tension test stress-strain data, and by maintaining the original material properties for aluminium during static loading, the measured stress-strain relationship gave very close agreement to the FE data for the entire static and ultrasonic tension test. By matching the FE models and experiments in this way, it was possible to conclude that for tension tests, where there is no influence from an interface condition, the application of ultrasonic excitation to the lower platen results in an effective temporary softening of the plastic

material properties and, when the ultrasonic excitation is discontinued, there is elastic recovery back to the static stress-strain relationship. The measurement of the oscillatory response has, for the first time, provided a complete experimental characterisation of ultrasonic tension tests and shown conclusively that oscillatory stress superposition does not wholly account for the measured reduction in mean forming force.

Initially to investigate the effects of friction in ultrasonic metal forming, static, longitudinal ultrasonic and radial ultrasonic ring tests were conducted for a variety of different lubricants. The coefficients of friction for dry and lubricated surfaces were first estimated from static ring tests and by generating friction calibration curves using FE models. Ultrasonic ring tests were then conducted and the friction coefficients were estimated by again matching the measured friction data with the FE generated friction calibration curves. For the dry surface, it was found that the coefficients of friction from the longitudinal and radial ultrasonic tests were identical to the coefficient of friction for static tests. However, under lubricated surfaces, the coefficients of friction for the ultrasonic tests tended to be slightly higher than the coefficient of friction for static ring test. By conducting these ring tests and also by using specimen surface analysis measurements, it was demonstrated that any change in the interface friction condition during ultrasonic excitation can only be temporary and the effects are not measurable by analysis of the specimen after ultrasonic excitation is discontinued.

The effects of friction in ultrasonic metal forming were further investigated by conducting static, and longitudinal mode and radial mode ultrasonic compression tests. For the longitudinal mode ultrasonic compression tests of cylindrical specimens, it was possible to simulate the measured stress-strain data in FE models by combining a temporary softening of material properties, as adopted for the ultrasonic tension test simulations, with a temporary adjustment in the coefficient of friction at the die-specimen interface during intervals of ultrasonic excitation. The same oscillatory stress-strain behaviour, for longitudinal mode ultrasonic compression, could also be simulated by a further softening of the specimen material and no adjustment in the friction condition during intervals of longitudinal ultrasonic excitation. Both simulations offer explanations of the measured data: the case for a reduction in the coefficient of friction has been well supported in published literature, and any material softening effects could be expected to be enhanced in compression tests where the vibration axis and

compression axis are collinear, as this provides the best configuration for coupling ultrasonic energy into the specimen. It was also shown that the initial contact friction condition had an insignificant effect on the measured stress-strain data during ultrasonic compression. Previous studies have argued that ultrasonic energy is not absorbed to cause excitation of dislocations at such low ultrasonic frequencies and that dislocation absorption is in the 100 MHz region and that therefore effective material softening is not a valid explanation of the effects. Also, no bulk temperature rise was recorded for aluminium in this or previous studies. However, in all these previous studies, the oscillatory stress has not been measured and therefore the arguments have largely been based on very incomplete data. It is clear from this study that the measurements presented for longitudinal ultrasonic compression require the whole issue of the effects of ultrasonic vibrations on bulk properties of metals to be readdressed and that it is not sufficient to explain the effects only in terms of stress superposition and surface effects.

Similarly, in the radial mode ultrasonic compression tests of cylindrical specimens, there was no bulk temperature rise recorded throughout the tests. In this case, by superimposing radial ultrasonic excitation on static compression, the resulting measured mean stress and maximum stress reductions were much smaller than for longitudinal mode ultrasonic compression. It was possible to simulate these tests using FE models only by an adjustment in the interface friction, by reducing the coefficient of friction. These results suggest that ultrasonically vibrating the die in a direction parallel to the material flow direction, ie. in the sliding direction, effectively reduces friction at the die-specimen interface but does not affect the material properties of the specimen. This would also be consistent with the fact that radial mode vibrations do not provide very effective coupling of the ultrasonic energy into the deforming specimen. As for the ring tests, assessment of the deformed specimen surfaces was conducted using a surface profilometer and SEM. As before, it was not possible to relate the specimen surface condition at the end of the test to any temporary change in the interface friction condition during ultrasonic excitation. Again, the classic oscillatory stress superposition definition is not sufficient to explain the effects of ultrasonic excitation on compression tests of aluminium.

FE models were developed to simulate the processes of ultrasonic extrusion and die-necking of a thin cylinder. Based on previous experimental studies of ultrasonic wire

drawing and ultrasonic necking of aerosol cans, the experimental evidence provided valuable verifications for the FE models. By adjusting the coefficient of friction from a higher value during static loading to a lower value during ultrasonic loading, the models have successfully shown that the extrusion force can be reduced and buckling of the cylinder can be eliminated. The models can also easily be adjusted in the future to investigate material softening effects and can be used to simulate real industrial metal forming processes.

7.2 Innovations

Innovations in this research are as follows:

- This study has provided detailed measurements of the oscillatory response during ultrasonic tension and compression tests, including characterisations of the maximum, mean, and minimum paths of the oscillatory stress. Such data, which have not been included in any previous studies, provide a better insight into the benefits of the application of ultrasonic excitation in metal forming in terms of material effects, surface friction, and oscillatory stress superposition.

- The present study has introduced the use of the ring compression technique to estimate the permanent effects on the interface friction coefficient of ultrasonic excitation. By deriving friction calibration curves from FE models and the test data, it is possible to investigate these friction effects. These tests clarified that any beneficial reduction in the coefficient of friction during ultrasonic excitation is temporary and does not affect the friction coefficient derived at stages throughout the ring deformation procedure.

- The use of various different lubricants in the study of ultrasonic compression tests was introduced for the first time. It could therefore be determined in this study that the effective reduction in the coefficient of friction at the die-specimen interface does not depend significantly on the original interface condition and also that the final specimen surface condition after ultrasonic compression does not significantly depend on the original interface condition.

- This study has allowed, for the first time, a direct comparison of ultrasonic forming where there is no effect from interfacial friction, in the form of tension tests, with forming where the interface condition plays a role in the stress-strain response, in the form of compression tests. By measuring the oscillatory force response, the study has also allowed direct comparison with FE model data for the first time.

- Novel FE models of ultrasonic extrusion and thin cylinder die-necking have been developed, showing how industrial ultrasonic metal forming processes can be successfully simulated.

7.3 Future Work

Although it has been postulated that, at low ultrasonic frequencies, a reduction in the mean flow stress due to preferential absorption of ultrasonic energy at dislocations can not be explained by resonance, this present study provides evidence that ultrasonic energy temporarily softens aluminium specimens. Therefore, it is suggested that this softening mechanism needs to be investigated at a microstructural level in order to determine a physical explanation.

A possible way forward for investigating changes in the friction coefficient would be to adapt the ring compression test procedure to perform real-time measurement of the ring geometry during the ultrasonic test.

In the present study, the specimens used were not tuned to the excitation frequency. Although maintaining specimen resonance during deformation is not straightforward, it is believed that by comparing the stress-strain relationship of tuned and non-tuned specimens during ultrasonic tension and compression tests, maximising the ultrasonic energy into the specimen via resonance would provide additional knowledge of the material and friction effects.

Verification of the surface friction and material effects should be conducted by using other specimen materials, including materials such as copper where significant bulk temperature rises have been reported in previous studies.

APPENDIX A

LIST OF PUBLICATIONS

1. Lucas, M., Daud, Y., Ultrasonic compression tests on aluminium, Ultrasonics Industries Association Symposium, Las Vegas, USA, March (2005).

2. Daud, Y., Lucas, M., Huang, Z., Superimposed ultrasonic oscillations in compression tests of aluminium, World Congress in Ultrasonic Merged with Ultrasonics International, Beijing, China, August-September (2005).

3. Lucas, M., Daud., Y., Huang, Z., Ultrasonic compression tests on aluminium, British Society for Strain Measurement International conference on Advances in Experimental Mechanics, Southampton, UK, September (2005).

4. Daud, Y., Lucas, M., Huang, Z., Ultrasonic compression tests on aluminium, Applied Mechanics and Materials, Vol.3-4 (2005), 99-104.

5. Daud, Y., Lucas, M., Huang, Z., Superimposed ultrasonic oscillations in compression tests of aluminium, Ultrasonics 2006 (in press).

6. Daud, Y., Lucas, M., Huang, Z., Modelling the effects of superimposed ultrasonic vibrations on tension and compression tests of aluminium, Journal of Materials Processing Technology (under review).

APPENDIX B

EXAMPLES OF ABAQUS INPUT FILES

B.1 Tension Model Input Data

```
** MATERIALS
**
*Material, name=aluminium
*Elastic
 69e+09, 0.33
*Plastic
 60e+06,  0.
  66e+06,  0.01
  71e+06,  0.02
  74e+06,  0.03
  78e+06,  0.05
  79e+06,  0.06
  81e+06,  0.1
  82e+06,  0.125
  83.5e+06,  0.25
  84e+06,  0.375
  84.2e+06,  0.5
**
** INTERACTION PROPERTIES
**
*Surface Interaction, name=IntProp-1
1.,
*Friction
0.,
**
** BOUNDARY CONDITIONS
**
** Name: bottom Type: Displacement/Rotation
*Boundary
_PickedSet86, 1
_PickedSet86, 6
_PickedSet87, 1
_PickedSet87, 6
** Name: xsymm Type: Symmetry/Antisymmetry/Encastre
*Boundary
_PickedSet78, XSYMM
**
** INTERACTIONS
**
** Interaction: Int-1
*Contact Pair, interaction=IntProp-1
_PickedSurf75, Part-3-1.RigidSurface_
** Interaction: Int-2
```

```
*Contact Pair, interaction=IntProp-1
_PickedSurf77, Part-2-1.RigidSurface_
** ----------------------------------------------------------------
**
** STEP: Step-1
**
*Step, name=Step-1, Inc=1000
*Static
1e-05, 21., 1e-05, 5.
**
** BOUNDARY CONDITIONS
**
** Name: top Type: Velocity/Angular velocity
*Boundary, type=VELOCITY
_PickedSet87, 2, 2, 8.333e-05
*Boundary
_PickedSet86, 2
**
** OUTPUT REQUESTS
**
*Restart, write, frequency=1
**
** FIELD OUTPUT: F-Output-1
**
*Output, field, variable=PRESELECT
**
** HISTORY OUTPUT: H-Output-1
**
*Output, history
*NODE OUTPUT, NSET=_PickedSet87
U2, RF2
*El Print, freq=999999
*Node Print, freq=999999
*End Step
```

B.1.1 Restart procedure to define longitudinal ultrasonic vibration

```
*HEADING
**
**
**CONTINUE ANALYSIS
**
*AMPLITUDE, NAME=SINE, DEFINITION=PERIODIC, VALUE=ABSOLUTE, TIME=STEP
TIME
1, 125663.706, 0., 0.
0., -10.0E-6
**
**
*RESTART, READ, STEP=1, END STEP, WRITE, FREQ=10
**
**
*STEP, INC=10000, AMPLITUDE=RAMP
*STATIC
1.0E-12, 0.02, 1.0E-12, 6.25E-6
*BOUNDARY, TYPE=VELOCITY
_PickedSet87, 2, 2, 8.333E-5
*BOUNDARY, TYPE=DISPLACEMENT, AMPLITUDE=SINE
_PickedSet86, 2, 2
*END STEP
```

B.2 Compression Model Input Data

```
*HEADING
**
**ultrasonic assisted compression on axis symmetry aluminium cylinder
specimen between two rigid platens
**under different friction condition
**
**units: m,N,s,v=5.00mm/min (8.333e-5m/s)
**
*INCLUDE, INPUT=cylinder.inp
**
**
**rigid surface
**
*NODE, NSET=RNODE
8999, 0., 0.008
9999, 0., 0.
*SURFACE, TYPE=SEGMENT, NAME=TDSURF
START, 0.008, 0.008
LINE,  0.0, 0.008
*RIGID BODY, ANALYTICAL SURFACE=TDSURF, REF NODE=8999
*SURFACE, TYPE=SEGMENT, NAME=BDSURF
START, 0.0, 0.
LINE, 0.008, 0.
*RIGID BODY, ANALYTICAL SURFACE=BDSURF, REF NODE=9999
**
**surface definition
**
*SURFACE, NAME=TWSURF, TYPE=ELEMENT
TOS, S2
TOP, S3
*SURFACE, NAME=BWSURF, TYPE=ELEMENT
BOT, S1
BOS, S2
**
**contact definition
**
*CONTACT PAIR, INTERACTION=ROUGH
TWSURF, TDSURF
BWSURF, BDSURF
**
**contact bahaviour
**
*SURFACE INTERACTION, NAME=ROUGH
*FRICTION
0.25
**
**material definition
**
*SOLID SECTION, ELSET=SAMPEL, MATERIAL=ALUMINIUM
*MATERIAL, NAME=ALUMINIUM
*ELASTIC
69.E9,0.33
*PLASTIC
60.E6,0.
79.E6,0.125
95.E6,0.25
106.E6,0.375
114.E6,0.5
```

```
132.E6,1.0
135.E6,2.0
*BOUNDARY
SYMM, XSYMM
8999, 1
RNODE, 6
**
**
*RESTART, WRITE, FREQ=100
**
**step 1, upper die move down
**
*STEP, INC=1000, AMPLITUDE=RAMP, NLGEOM
*STATIC
1.0E-10, 21, 1.0E-10, 1.0
*CONTROLS, ANALYSIS=DISCONTINUOUS
*BOUNDARY
9999, 1, 2
*BOUNDARY, TYPE=VELOCITY
8999, 2, 2, -8.333E-5
**
**output
**
*MONITOR, NODE=8999, DOF=2
*OUTPUT, FIELD, VARIABLE=PRESELECT
*OUTPUT, HISTORY
*NODE OUTPUT, NSET=RNODE
U2, RF2
*END STEP
```

B.2.1 Restart procedure to define longitudinal ultrasonic vibration

```
*HEADING
**
**continue analysis
**
**ultrasonic amplitude definition
**
*AMPLITUDE, NAME=SINE, DEFINITION=PERIODIC, VALUE=ABSOLUTE, TIME=STEP
TIME
1, 125663.706, 0., 0.
0., -10.0E-6
*RESTART, READ, STEP=1, END STEP, WRITE, FREQ=100
**************************************
*STEP,INC=10000, AMPLITUDE=RAMP, NLGEOM
*STATIC
1.0E-12, 0.015, 1.0E-12, 6.25E-6
*CONTROLS, ANALYSIS=DISCONTINUOUS
*BOUNDARY, TYPE=VELOCITY
8999, 2, 2, -8.333E-5
*BOUNDARY, TYPE=DISPLACEMENT, AMPLITUDE=SINE
9999, 2, 2
*END STEP
```

B.2.2 Restart procedure to define radial ultrasonic vibration

```
*HEADING
**
**continue analysis
**
**ultrasonic amplitude definition
**
*AMPLITUDE, NAME=SINE, DEFINITION=PERIODIC, VALUE=ABSOLUTE, TIME=STEP
TIME
1, 125663.706, 0., 0.
0., -4.0E-6
*RESTART, READ, STEP=1, END STEP, WRITE, FREQ=100
************************************
*STEP,INC=10000, AMPLITUDE=RAMP, NLGEOM
*STATIC
1.0E-12, 0.02, 1.0E-12, 6.25E-6
*CONTROLS, ANALYSIS=DISCONTINUOUS
*BOUNDARY, TYPE=VELOCITY
8999, 2, 2, -8.333E-5
*BOUNDARY, TYPE=DISPLACEMENT, AMPLITUDE=SINE
9999, 1, 1
*END STEP
```

B.2.3 Restart procedure to define radial ultrasonic vibration and change in the coefficient of friction

```
*HEADING
**
**continue analysis
**
**ultrasonic amplitude definition
**
*AMPLITUDE, NAME=SINE, DEFINITION=PERIODIC, VALUE=ABSOLUTE, TIME=STEP
TIME
1, 125663.706, 0., 0.
0., -4.0E-6
*RESTART, READ, STEP=1, END STEP, WRITE, FREQ=100
************************************
*STEP,INC=10000, AMPLITUDE=RAMP, NLGEOM
*STATIC
1.0E-10, 0.02, 1.0E-10, 6.25E-6
*CONTROLS, ANALYSIS=DISCONTINUOUS
*CHANGE FRICTION, INTERACTION=ROUGH
*FRICTION
0.15
*BOUNDARY, TYPE=VELOCITY
8999, 2, 2, -8.333E-5
*BOUNDARY, TYPE=DISPLACEMENT, AMPLITUDE=SINE
9999, 1, 1
*END STEP
```

REFERENCES

[1] Blaha, F., Langenecker, B., Tensile deformation of zinc crystal under ultrasonic vibration, Naturwissenschaften, Vol. 42 (1955), 556.

[2] Pohlman, R. and Lehfeldt, E., Influence of ultrasonic vibration on metallic friction, Ultrasonics, Vol.4 (1966), 178-185.

[3] Nevill, G.E., Brotzen, F.R., Effect of vibrations on the yield strength of a low-carbon steel, First Technical Report, The Rice Institute, Solid States Science Division, Air Force Office of Scientific Research, ARDC, Washington, Technical Document No. AFOSR-TN-57-170 (1957).

[4] Kirchner, H.O.K., Kromp, W.K., Prinz, F.B. and Trimmel, P., Plastic deformation under simultaneous and unidirectional loading at low and ultrasonic frequencies, Materials Science and Engineering, Vol.68 (1984-1985), 197-206.

[5] Winsper, C.E., Dawson, G.R. and Sansome, D.H., An introduction to the mechanics of oscillatory metalworking, Metals and Materials (1970), 158-162.

[6] Siegert, K. and Ulmer, J., Influencing the friction in metal forming processes by superimposing ultrasonic waves, Annals of the CIRP, Vol.50 (2001), 195-200.

[7] Kristoffy, I., Metal forming with vibrated tools, Trans. ASME, Journal of Engineering for Industry (November 1969), 1168-1174.

[8] Perotti, G., An experiment on the use of ultrasonic vibrations in cold upsetting, Annals of the CIRP, Vol.22 (1978), 195-197.

[9] Susan, M. and Bujoreanu, L.G., The metal-tool contact friction at the ultrasonic vibration drawing of ball-bearing steels wires, Revesita De Metalurgia (Madrid), Vol.35, No.6 (1999), 379-383.

[10] Rozner, A.G., Effect of ultrasonic vibration on coefficient of friction during strip drawing, The Journal of the Acoustical Society of America, Vol.49, No.5 (1970), 1368-1371.

[11] Huang, Z., Lucas, M. and Adams, M.J., Influence of ultrasonics on upsetting of a model paste, Ultrasonics, Vol. 40 (2002), 43-48.

[12] Izumi, O., Oyama, K. and Suzuki, Y., Effects of Superimposed Ultrasonic vibration on compressive deformation of metals, Trans. Japanese Institute of Metals, Vol.7 (1966), 162-167.

[13] Dawson, G.R., Winsper, C.E. and Sansome, D.H., Application of high and low frequency oscillations to the plastic deformation of metals, Metal Forming (1970), 234-238.

[14] Eaves, E.A., Smith, A.W., Waterhouse, W.J. and Sansome, D.H., Review of the application of ultrasonic vibrations to deforming metals, Ultrasonics, Vol.13 (1975), 162-170.

[15] Frederick, J.R., Ultrasonic Engineering, John Wiley & Son, United State of America, 1965.

[16] Goldman, R., Ultrasonic Technology, Reinhold Publishing Corporation, New York, 1662.

[17] Cracknell, M.F., Cracknell, A.P., Applications of ultrasonics, Contemporary Physics, Vol.17, No.1 (1976), 13-44.

[18] Abramov, O.V., High Intensity Ultrasonics – Theory and Industrial Applications, Gordon and Breach Science Publisher, Singapore, 1998.

[19] Langenecker, B., Effects of Ultrasound on Deformation Characteristics of Metals, IEEE Transaction on Sonics and Ultrasonics, Vol.13, No.1 (1966), 1-8.

[20] Izumi, O., Oyama, K. and Suzuki, Y., On the superimposing of ultrasonic vibration during compressive deformation of metals, Trans. Japanese Institute of Metals, Vol.7 (1966), 158-162.

[21] Winsper, C.E. and Sansome, D.H., A review of the application of oscillatory energy to metals deforming plasticity, 8th International MTDR Conference, Manchester, 1967, 1359-1360.

[22] Schmid, E., Plasticity of insonated metals, Trans. Japanese Inst. Metals, Vol.9 (1968), 798-804.

[23] Lee, D., Sata, T., Backofen., W. A., The reduction of compressive deformation resistance by cyclic loading, Journal of The Institute of Metals, Vol.93 (1964-65), 418-422.

[24] Siegert, K. and Mock, A., Wire drawing with ultrasonically oscillating dies, Journal of Materials Processing Technology, Vol.60 (1996), 657-660.

[25] Petukhow, V. I., Abramov. O.V., Zubko, A.M., Manegin, Yu V., Extrusion of aluminium in an ultrasonic filed, Light Metal Age, Vol. 31 (1973), 6-8.

[26] Sansome D.H., Ultrasonic Techniques, Edited by Beadle, J.D., Chapter 21,Metal Forming Production Engineering Series, Macmillan Engineering Evaluation, 1971.

[27] Winsper, C.E., Sansome, D.H., The superposition of longitudinal sonic oscillations on the wire drawing process, Proc. Instn. Mech. Engrs., Vol.183 (1968-69), 545-562.

[28] Smirnov, O.M., Orlov., L.G., Usikov., M.P., Influence of alternating stresses of ultrasonic frequency on the formation of the dislocation structure of iron in tension, Physics of Metals and Metallography (Fiz. Metal. Metalloved.), Vol.68 (1989), 129-132.

[29] Konovalov, E. G., Skripnichenko, A. L., The effect of ultrasonic vibrations on the tensile properties of metals, Russian Engineering Journal, Vol.4 (1965), 31-32.

[30] Fridman, H.D. and Levesque, P., Reduction of static friction by sonic vibration, Journal of Applied Physics, Vol.30, No.30 (1959), 1572-1575.

[31] Skare, T. and Stahl, J.E., Static and dynamic friction processes under influence of external vibrations, Wear, Vol.154 (1992), 177-192.

[32] Murakawa, M., Jin, M., The utility of radially and ultrasonically vibrated dies in the wire drawing process, Journal of Materials Processing Technology, Vol.113 (2001), 81-86.

[33] Hung, J.C., The influence of ultrasonic-vibration on hot upsetting of aluminium alloy, Ultrasonics, Vol.43 (2005), 692-698.

[34] Severdenko, V.P., Petrenko, V.V, Effect of ultrasonic vibrations on the efficiency of lubricants in the closed upsetting of carbon steel, Fiz Khim Mat, Vol.6 (1970), 7.

[35] Neppiras, E.A., Ultrasonic machining and forming, Ultrasonics, October-December (1964), 167-173.

[36] Mitrofanov, A.V., Babitsky, V.I. and Silbershmidt, V.V., Finite element simulation of ultrasonically assisted turning, Computational Materials Science, Vol.28 (2003), 645-653.

[37] Parrini, L., New methodology for the design of advanced ultrasonic transducer for welding devices, IEEE Ultrasonics Symposium, 2000, 699-703.

[38] Inal, K., Wu, P.D., and Neale, K.W., Large strain behaviour of aluminium sheets subjected to in-plane simple shear, Modelling and Simulation in Materials Science and Engineering, Vol.10 (2002), 237-252.

[39], Nakamura, T., Bay, N., Zhang, Z.L., FEM simulation of friction testing method based on combined forward rod-backward can extrusion, Transactions of the ASME: Journal of Tribology, Vol.119 (1997), 501-506.

[40] Nakamura, T., Bay, N., Zhang, Z.L., FEM simulation of a friction testing method based on combined forward conical can-backward straight can extrusion, Transactions of the ASME: Journal of Tribology, Vol.120 (1998), 716-723.

[41] Long, H., Balendra, R., FE simulation of the influence of thermal and elastic effects on the accuracy of cold-extruded components, Journal of Materials processing Technology, Vol.84 (1998) 247-260

[42] Long, H., Balendra, R., Evaluation of elasticity and temperature effects on the dimensional accuracy of back-extruded components using finite element simulation, Journal of Materials Processing Technology, Vol.80-81 (1998) 665-670.

[43] Wang, S.P., Choudhry, S. and Werthemeir, T.B., Comparison between the static implicit and dynamic explicit methods for FEM simulation of sheet forming processes, White papers of the MARC Corporation, 1997.

[44] Lee,W.B., and To, S., Computer modelling of the effect of rolling schedule on the plastic anisotropy of cold-rolled aluminium sheets, Journal of Materials Processing Technology, Vol.48 (1995), 173-178.

[45] Baltov, A.I. and Nedev, A.G., An Approach to the modelling of contact friction during rolling, Journal of Materials Processing Technology, Vol.53 (1995), 695-711.

[46] Huang, Z., Lucas, M. and Adams, M.J., Modelling wall boundary conditions in elasto-viscoplastic material forming process, Journal of Materials Processing Technology, Vol.107 (2000), 267-275.

[47] Hayashi, M., Jin, M., Thipprakmas, S., et. al., Simulation of ultrasonic-vibration drawing using the finite element method (FEM), Journal of Materials Processing Technology, Vol.140 (2003), 30-35.

[48] Wu, J.Z., et. al., Simulation of Mechanical Response of Fingertip to Dynamic Loading, Medical Engineering and Physics, Vol.24 (2002), 253-264.

[49] Cardoni, A., and Lucas, M., Enhanced vibration performance of ultrasonic block horns, Ultrasonics, Vol.40 (2002), 365-369.

[50] Lucas, M., Vibration sensitivity in the design of ultrasonic forming dies, Ultrasonics, Vol.34 (1996) 35-41.

[51] Lucas, M., and Chapman, G., Design of ultrasonically assisted radial dies by validated finite element methods, Ultrasonics International 93 Conference Proceedings, 1993, 707-710.

[52] Chapman, G.M., Lucas, M., Frequency analysis of an ultrasonically exited thick cylinder, International Journal of Mechanical Sciences, Vol.32, No.3 (1990), 205-214.

[53] Lucas, M., The application of vibration analysis techniques to the development of an ultrasonically assisted die forming process, PhD Thesis, Loughborough University of Technology, 1992.

[54] Huang, Z., Lucas, M. and Adams, M.J., Wedge indentation of an elasto-viscoplastic material, The 3rd International Conference on Experimental Mechanics, Beijing, China, 2001.

[55] Van Rooyen, G.T. and Backofen, W.A., A study of interface friction in plastic compression, Int. J. Mech. Sci., Vol.1 (1960), 1-27.

[56] Wagener, H.W. and Wolf, J., Coefficient of friction in cold extrusion, Journal of Materials Processing Technology, Vol.44 (1994), 283-291.

[57] Shen, G., Vedhanayagam, A., Kropp, et. al., A method for evaluating friction using a backward extrusion-type forging, Journal of Materials Processing Technology, Vol.33 (1992), 109-123.

[58] Han, S.S., The influence of tool geometry on friction behaviour in sheet metal forming, Journal of Materials Processing Technology, Vol.63 (1997), 129-133.

[59] Kulkarni, K. M., Kalpakjian, S., A study of barrelling as an example of free deformation in plastic working, ASME Journal of Engineering for Industry, Vol.91 (1969), 743-754.

[60] Tan X., Comparison of friction models in bulk metal forming, Tribology International, Vol.35 (2002), 385-393.

[61] Persson, B.N.J., Sliding friction, Surface Science Reports, Vol.33 (1999), 83-119.

[62] Schroeder, W. and Webster, D.A., Press-forging thin section: Effect of friction, area, and thickness on pressure required, Journal of Applied Mechanics, Vol.1 (1949), 289-294.

[63] Lee, C.H., Altan, T., Influence of metal flow stress and friction upon metal flow in upset forging of rings and cylinders, Transaction of the ASME, Journal of Engineering for Industry, Vol.94 (1972), 775-782.

[64] Kunogi, M., A new method of cold extrusion, Journal of the Scientific Research Institute, Vol.50, No.1437 (1956), 215-246.

[65] Male, A.T. and Cockcroft, M.G., A Method for the determination of the coefficient of friction of metals under condition of bulk plastic deformation, Journal of the Institute of Metals, Vol.93 (1964-65), 38-46.

[66] Tabor, D., Friction – The present state of our understanding, Journal of Lubrication Technology, Vol.103 (1981), 169-179.

[67] Chang, W.R., Etsion, I. and Bogy, D.B., Static friction coefficient model for metallic rough surfaces, Journal of Tribology, Vol.110 (1988), 57-63.

[68] Petersen, S.B., Martins, P.A.F., Bay, N., Friction in bulk metal forming: a general friction model vs the law of constant friction, Journal of Materials processing Technology, Vol.66 (1997), 186-194.

[69] Huang, Z., The Application of oscillation to the deformation of an elasto-viscoplastic material, PhD Thesis, Faculty of Engineering, University of Glasgow, 2000.

[70] Chakrabarty, J., Theory of Plasticity, McGraw-Hill Inc., United States of America, 1987.

[71] Wanheim, T., Friction at high normal pressure, Wear, Vol.25 (1973), 225-244.

[72] Chodnikiewicz, K., Petersen, S.B., Balendra, R., Martins, P.A.F., Loading of forming presses by the upsetting of oblique specimens, Journal of Materials processing Technology, Vol.68 (1997), 13-18.

[73] Rao, K.P., Wei, J.J., Performance of a new dry lubricant in the forming of aluminium alloy sheets, Wear, Vol.249 (2001), 86-93.

[74] Pearsall, G.W., Backofen, W.A., Frictional boundary conditions in plastic compression, Transaction of the ASME, Journal of Engineering for Industry, Vol.85 (1963), 68-76.

[75] Male, A.T., Variations in friction coefficients of metals during compressive deformation, Journal of The Institute of Metals, Vol.94 (1966), 121-125.

[76] Butler, L.H., The effects of lubricants on the surface appearance of aluminium after plastic deformation, Metallurgia, Vol.53 (1957), 63-66.

[77] Butler, L.H., The effect of interposed lubricant on the surface deformation of metals during plastic working, Journal of the Institute of Metals, Vol.88 (1959-60), 337-343.

[78] Fukui, S., Ohi, T., Kudo, H., et. al., Some aspects of friction in metal-strip drawing, Int. J. Mech. Sci., Vol.4 (1962), 297-312.

[79] Rasp, W. and Wichern, C.M., Effects of surface-topography directionality and lubrication condition on frictional behaviour during plastic deformation, Journal of Materials Processing Technology, Vol.125-126 (2002), 379-386.

[80] Carpick, R.W., Ogletree, D.F. and Salmeron, M., A general equation for fitting contact area and friction vs load measurements, Journal of Colloid and Interface Science, Vol.211 (1999), 395-400.

[81] Male, A. T., Depierre, V., The validity of mathematical solutions for determining friction from the ring compression test, Trans. ASME-Journal of Lubrication Technology, July (1970), 389-397.

[82] DePierre, V., Gurney, F., A method for determination of constant and varying friction factors during ring compression tests, Transaction of ASME, Journal of Lubrication Technology, Vol.96 (1974), 482-488.

[83] Hartley, P., Sturgess, C.E.N., Rowe, G.W., Friction in finite element analyses of metal forming processes, Int. J. Mech. Sci., Vol.21 (1979), 301-311.

[84] Sofuoglu, H. and Rasty, J., On the measurement of friction coefficient utilizing the ring compression test, Tribology International, Vol.32 (1999), 327-335.

[85] Rudkins, N.T., Hartley, P. and Petty, D., Friction modelling and experimental observations in hot ring compression tests, Journal of Materials Processing Technology, Vol.60 (1996), 349-353.

[86] Wang, J-P., A new evaluation to friction analysis for the ring test, International Journal of Machine Tools & Manufacture, Vol.41 (2001), 311-324.

[87] Sofuoglu, H. and Gedikli, H., Determination of friction coefficient encountered in large deformation processes, Tribology International, Vol.35 (2002), 27-34.

[88] Carter, W.T. Jr., Lee, D., A finite element analysis of cylinder and ring compression and its experimental verification, Computational Structure, Vol. 21 (1985), 1-19.

[89] Wang, F., Lenard, J.G., An experimental study of interfacial friction-hot ring compression, Journal of Engineering Materials and Technology, Vol.144 (1992), 13-18.

[90] Male, A.T., Determination of coefficients of friction during compressive deformation, Proc. Instn. Mech. Engrs., Vol.182 (1967-68), 64-67.

[91] Hu, Z.M., Dean, T.A., A study of surface topography, friction and lubrication in metal forming, International Journal of Machine Tools & Manufacture, Vol.40 (2000), 1637-1649.

[92] Kempe, W., Kroner, K., Dislocation damping of aluminium single crystals at room temperature, Zeitschrift fur Metallkunde, Vol. 47, No.5 (1956), 302.

[93] Astashev, V.K., Influence of high frequency vibration on plastic deformation processes, Soviet Machine Science (Mashinovedenie), No.2 (1983), 1-9.

[94] Metals Handbooks, Volume 2: Properties and Selection: Nonferrous Alloys and Pure Metals, 9th Edition, American Society for Metals, Metal Park, Ohio 44073, 1979.

[95] Callister, W.D., Materials Science and Engineering – An Introduction, 5th Edition, John Wiley & Sons, Inc., USA, 2000.

[96] Li, L., Zhou, J., and Duszczyk, J., Prediction of temperature evolution during the extrusion of 7075 aluminium alloy at various ram speeds by means 3D FEM simulation, Journal of Materials processing Technology, Vol.145 (2004), 360-370.

[97] Zhou, J., Li, L., and Duszczyk, J., 3D FEM simulation of the whole cycle of aluminium extrusion throughout the transient state and the steady state using the updated Lagrangian approach, Journal of Materials processing Technology, Vol.134 (2003), 383-397.

[98] British Standard Method for Tensile testing of metals, British Standard Institution, BS 18 : 1987.

[99] Nerubai, M.S., Effect of ultrasonic vibration on the mechanical properties of difficult-to-deform materials, (Metallovedenie i Termicheskaya Obrabotka Metallov), Metals Science and Heat Treatment, Vol.29 (1987), 254-258.

[100] Abaqus Standard User's manual, Version 6.3, Hibbit, Karlsson & Sorensen, Inc., USA, 2002

[101] Halling, J., Principles of Tribology, The Macmillan Press Ltd., Great Britain, 1975.

[102] Kane, F., Graydon, Larrabee, G.B., Characterization of solid surfaces, Plenum Press, London, 1974.

[103] Murakawa, M., Kaewtatip, P., Jin, M., Improving ironing performance using dies subjected to ultrasonic radial vibration, Technical Paper – Society of Manufacturing Engineers. MF, No.MF99-153 (1999), 1-6.

[104] Huang, Z., Lucas, M., Adams, M.J., Study of ultrasonic upsetting under radial and longitudinal die vibration, Materials Science Forum, Vol.440-441 (2003), 389-396.

[105] Jimma, T., Kasuga, Y., Iwaki, N., et al, An application of ultrasonic vibration to the deep drawing process, Journal of Materials Processing Technology, Vol.80-81 (1998), 406-412.

[106] Cheers, C.F., Ultrasonically assisted die necking, Metal Box Technical Record No. TR0814 (1985).

[107] Tabata, T., Masaki, S., Hosokawa, K., Effects of type of lubricant in cold extrusion of sintered performs, Transactions of the ASME: Journal of Engineering Materials and Technology, Vol.105 (1983), 138-131.

[108] Tan, X., Bay, N. and Zhang, W., Friction measurement and modelling in forward rod extrusion tests, Proc. Instn Mech. Engrs, Part J: Journal of Engineering Tribology, Vol.217 (2003), 71-82.

[109] Metals Handbooks, Volume 14: Forming and Forging, American Society for Metals, Metal Park, 9th Ed., Ohio 44073, 1979.

[110] Kalpakjian, S., Manufacturing Processes for Engineering Materials, 3rd Ed, Addison Wesley, USA, 1997.